

## ABSTRACT

Title of Dissertation: DESIGN AND SYNTHESIS OF GLYCOCONJUGATES FOR ELUCIDATING THE BIOLOGICAL FUNCTIONS OF GLYCANS

Thomas Connor Donahue, Doctor of Philosophy, 2023

Title and Dissertation directed by: Professor Lai-Xi Wang, Department of Chemistry and Biochemistry

Glycosylation is a prevalent post-translational modification referring to the attachment of glycans or sugars to proteins. Glycosylation has significant impacts on a protein's structure and function, and the glycans themselves can also be recognized by carbohydrate-binding proteins to enact new functions that may improve the efficacy and half-life of protein-based therapeutics. However, the mammalian glycan biosynthesis pathway produces extraordinarily diverse and heterogeneous glycans, making glycan function and recognition challenging to characterize. My research focuses on the development of tools to probe glycan function, evaluate protein-glycan interactions, and leverage the known glycan specificities of carbohydrate-binding proteins for therapeutic indications and includes three major research projects. The first project was to evaluate the immunogenicity of natural N-glycans aiming to raise N-glycan specific antibodies. For the purpose, a series of N-glycan-based immunogens were prepared from five common human N-glycan structures and chemically conjugated to a bacteriophage Q $\beta$  carrier protein as an adjuvant, and the conjugates were used as immunogens for immunization in mice. Analysis of the immune response revealed that most of the antibodies elicited by all N-glycan conjugates unexpectedly targeted the conserved chitobiose core, giving cross-reactive antibodies. Importantly, terminal sialylation and linker chemistry were found to have significant effects on the titer and specificity of the elicited antibodies. This study outlines significant challenges to

raising selective N-glycan-specific antibodies and provides important guidelines for the further optimization of N-glycan-based immunogens towards the development of selective N-glycan-specific monoclonal antibodies as probes for studying glycan functions.

The second project was focused on application of cationic vesicles as synthetic scaffolds for the multivalent display of N-glycans to probe protein-glycan interactions. A general platform was developed allowing for multivalent display of various N-glycans on cationic vesicles. It was found that the N-glycan-coated vesicles had high affinities for several plant and mammalian lectins. Furthermore, vesicles were prepared that displayed more than one glycan structure simultaneously. These well-defined vesicles were employed to recapitulate diverse glycan-coated surfaces as mimics of the mammalian glycocalyx and provided valuable insights into lectin recognition of glycan ligands in such complex environments. Indeed, for the vesicles displaying two unique N-glycan structures simultaneously, the presence of an unrelated glycan structure was found to significantly impact lectin binding to its cognate glycan ligand. Thus, N-glycan-coated cationic vesicles have great potential as tools for characterizing complex protein-glycan interactions and elucidating glycan function.

The third project explored the chemoenzymatic method developed by our lab for constructing site-specific antibody-glycan conjugates as next-generation Lysosome Targeting-Antibody Chimeras (LYTACs). These site-specific conjugates were used in evaluating optimal glycan ligands for targeted lysosomal degradation of clinically relevant protein targets. Several natural and synthetic glycan ligands containing terminal galactose or N-acetylgalactosamine (GalNAc) were attached to monoclonal antibodies and evaluated in cell-based binding and protein-degradation assays. Interesting new trends in glycan ligand binding were discovered, and natural triantennary N-glycans were reported for the first time to be effective ligands for

lysosomal delivery of target proteins. Antibody conjugates containing synthetic tri-GalNAc or natural triantennary N-glycan ligands were found to significantly degrade extracellular human PCSK9, a well-validated therapeutic target for treating high cholesterol. Additional experiments indicated that targeted degradation of PCSK9 may be a promising new therapeutic strategy for lowering cholesterol, and this strategy could easily be adapted for the targeted degradation of other extracellular disease-associated proteins. In summary, these studies present methodologies for producing diverse glycoconjugates as valuable tools for elucidating glycan function and intervening in disease.

DESIGN AND SYNTHESIS OF GLYCOCONJUGATES FOR ELUCIDATING THE  
BIOLOGICAL FUNCTIONS OF GLYCANS

by

Thomas Connor Donahue

Dissertation submitted to the Faculty of the Graduate School of the  
University of Maryland, College Park, in partial fulfillment  
of the requirements for the degree of  
Doctor of Philosophy  
2023

Advisory Committee:

Professor Lai-Xi Wang, Chair  
Professor Kwaku Dayie  
Professor Philip DeShong  
Professor Paul Paukstelis  
Professor Xiaoping Zhu

©Copyright by  
Thomas Connor Donahue  
2023

## Acknowledgements

I would like to first thank my thesis advisor, Dr. Lai-Xi Wang, for his mentoring and support during my PhD research. You have taught me many valuable things, including how to carefully design experiments and how to extract meaningful information from experimental failures. Ultimately, you have helped me to become an independent scientist able to design and execute my own projects.

Special thanks to my wife Emmy, without your care and support none of this would have been possible. I would also like to express my gratitude to my friends and family, especially to baby Elena, to whom this work is dedicated.

I am very grateful to the current and past members of the Wang group for their contributions to my research, especially to Dr. Guanghui Zong, who has been a great co-mentor and friend. You have been a very supportive lab mate, and I would not have accomplished much without your help and guidance. I also thank Dr. Qiang Yang, Dr. Xin Tong, Dr. Roushu Zhang, Dr. Sunaina Prabhu, Dr. Yuanwei Dai, Dr. Xiao Zhang, Dr. Chong Ou, Dr. Chao Li, Dr. Kun Huang, Grace Lunde, Darnell Harris, Margaryta Gomozkova, Helena Yun, Natasha Owitipana, Nikolai Tolstoy, and Emilie Liang.

I also want to thank my committee members, Dr. Kwaku Dayie, Dr. Philip DeShong, Dr. Paul Paukstelis, Dr. Peter Nemes, and Dr. Xiaoping Zhu. Thank you for your constructive criticism and guidance during my PhD studies.

Finally, I would like to thank all my collaborators including Dr. Jeffery Gildersleeve, Nicholas O'Brien, Dr. George Lewis, and Robin Flinko. Many thanks to the facility managers of the NMR and MS instruments for training me and helping make this research possible.

## Table of Contents

Acknowledgements .....	ii
Table of Contents .....	iv
List of Schemes .....	v
List of Tables .....	vi
List of Figures .....	vii
List of Abbreviations .....	ix
Chapter 1: Introduction .....	1
1.1 Biological importance of glycans .....	1
1.2 Biosynthesis of N-glycans .....	5
1.3 Features of carbohydrate-protein interactions .....	7
1.3.1 Multivalent interactions .....	8
1.4 Leveraging glycobiology for therapeutic development .....	11
Chapter 2: Synthesis and Immunological Study of N-Glycan-Bacteriophage Q $\beta$ Conjugates Reveal Dominant Antibody Responses to the Conserved Chitobiose Core .....	16
2.1 Introduction .....	16
2.2 Results and discussion .....	20
2.3 Conclusion .....	39
2.4 Experimental procedures .....	39
2.5 Supporting information .....	57
Chapter 3: Cationic Vesicles as a Facile Scaffold to Display Natural N-Glycan Ligands for Probing Multivalent Carbohydrate-Lectin Interactions .....	69
2.1 Introduction .....	69
2.2 Results and discussion .....	71
2.3 Conclusion .....	88
2.4 Experimental procedures .....	89
2.5 Supporting information .....	104
Chapter 4: Synthetic Site-Specific Antibody-Ligand Conjugates Promote Degradation of Extracellular Human PCSK9 Mediated by the Liver Asialoglycoprotein Receptor .....	114
2.1 Introduction .....	114
2.2 Results and discussion .....	118
2.3 Conclusion .....	136
2.4 Experimental procedures .....	137
2.5 Supporting information .....	152
Chapter 5: Conclusions and Future Directions .....	186
Literature Cited .....	190

## List of Schemes

Scheme 2.1. Synthesis of chemically functionalized N-glycans for bioconjugation .....	22
Scheme 2.2. Synthesis of N-glycan-Q $\beta$ conjugates .....	24
Scheme 3.1. Synthesis of N-glycolipids carrying lipid chains of different lengths .....	72
Scheme 3.2. Assembly of N-glycan coated cationic vesicles .....	73
Scheme 4.1. Synthesis of ligands for the human asialoglycoprotein receptor .....	121
Scheme 4.2. Synthesis of site-specific antibody-ligand conjugates by the chemoenzymatic method .....	124

List of Tables

Table 2.1. Average glycan loading of N-glycan-Q $\beta$  immunogens ..... 26

Table 2.2. Glycan-specific IgG antibody titers of mouse antisera ..... 29

Table 2.3. Glycan-specific IgM antibody titers of mouse antisera ..... 30

Table 3.1. Hydrodynamic diameter and polydispersity index of cationic vesicles ..... 76

Table 4.1. All antibodies used in western blotting and testing LYTAC function ..... 151

## List of Figures

Figure 1.1. Cartoon structures of major glycan classes .....	2
Figure 1.2. Glycoconjugates of the glycocalyx .....	4
Figure 1.3. N-glycan biosynthesis in mammals .....	7
Figure 1.4. Major mechanisms of multivalent protein-glycan binding .....	9
Figure 1.5. Structure of human IgG1 and associated glycoforms .....	12
Figure 2.1. SDS-PAGE of reduced N-glycan-Q $\beta$ conjugates .....	25
Figure 2.2. MALDI-TOF-MS of N-glycan-BSA conjugate coating antigens .....	27
Figure 2.3. Binding of mouse antisera to glycan microarray .....	32
Figure 2.4. Epitope mapping of glycan specificity by ELISA .....	35
Figure 2.5. Binding of mouse antisera to SARS-CoV-2 spike protein .....	37
Figure 3.1. N-glycolipid incorporation in cationic vesicles .....	75
Figure 3.2. Endo-CC glycan release experiments on N-glycan coated vesicles .....	78
Figure 3.3. Microplate inhibition assay with N-glycan coated vesicles .....	81
Figure 3.4. Comparison of PSA and HPLC-based N-glycolipid incorporation assays .....	84
Figure 3.5. N-glycolipid incorporation in hetero-multivalent vesicles quantified by HPLC .....	86
Figure 3.6. Microplate inhibition assays with hetero-multivalent vesicles .....	88
Figure 4.1. Cholesterol regulation in human hepatocytes .....	118
Figure 4.2. PCSK9 protein secretion by HepG2 cells under different culture conditions .....	125
Figure 4.3. Binding of LYTACs to cell-surface ASGPR by flow cytometry .....	126
Figure 4.4. PCSK9 degradation by Alirocumab-based LYTACs .....	130
Figure 4.5. PCSK9 degradation by Alirocumab-based LYTACs at different time points .....	130
Figure 4.6. Western blotting of total cellular LDLR after LYTAC treatment .....	132
Figure 4.7. EGFR degradation by Cetuximab-based LYTACs .....	133
Figure 4.8. EGFR degradation by Cetuximab-based LYTACs at different time points .....	136
Figure 4.9. LC-ESI-MS analysis of IdeS treated native Alirocumab .....	152
Figure 4.10. LC-ESI-MS analysis of IdeS treated GNF-Alirocumab .....	153
Figure 4.11. LC-ESI-MS analysis of IdeS treated G3F-Alirocumab .....	154

Figure 4.12. LC-ESI-MS analysis of IdeS treated di-N <sub>3</sub> -S2G2-Alirocumab .....	155
Figure 4.13. LC-ESI-MS analysis of IdeS treated di-N <sub>3</sub> -Man-Alirocumab .....	156
Figure 4.14. LC-ESI-MS analysis of IdeS treated G2 click-Alirocumab .....	157
Figure 4.15. LC-ESI-MS analysis of IdeS treated G3 click-Alirocumab .....	158
Figure 4.16. LC-ESI-MS analysis of IdeS treated tri-GalNAc-S2G2-Alirocumab .....	159
Figure 4.17. LC-ESI-MS analysis of IdeS treated tri-GalNAc-Man-Alirocumab .....	160
Figure 4.18. LC-ESI-MS analysis of IdeS treated native Cetuximab .....	161
Figure 4.19. LC-ESI-MS analysis of IdeS treated GNF-Cetuximab .....	162
Figure 4.20. LC-ESI-MS analysis of IdeS treated G3F-Cetuximab .....	163
Figure 4.21. LC-ESI-MS analysis of IdeS treated di-N <sub>3</sub> -S2G2-Cetuximab .....	164
Figure 4.22. LC-ESI-MS analysis of IdeS treated G2 click-Cetuximab .....	165
Figure 4.23. LC-ESI-MS analysis of IdeS treated G3 click-Cetuximab .....	166
Figure 4.24. LC-ESI-MS analysis of IdeS treated tri-GalNAc-S2G2-Cetuximab .....	167
Figure 4.25. MALDI-TOF-MS of asialofetuin .....	168
Figure 4.26. MALDI-TOF-MS of native Alirocumab .....	169
Figure 4.27. MALDI-TOF-MS of G3F-Alirocumab .....	170
Figure 4.28. MALDI-TOF-MS of G2 click-Alirocumab .....	171
Figure 4.29. MALDI-TOF-MS of G3 click-Alirocumab .....	172
Figure 4.30. MALDI-TOF-MS of tri-GalNAc-S2G2-Alirocumab .....	173
Figure 4.31. MALDI-TOF-MS of tri-GalNAc-Man-Alirocumab .....	174
Figure 4.32. MALDI-TOF-MS of biotinylated asialofetuin .....	175
Figure 4.33. MALDI-TOF-MS of biotinylated native Alirocumab .....	176
Figure 4.34. MALDI-TOF-MS of biotinylated G3F-Alirocumab .....	177
Figure 4.35. MALDI-TOF-MS of biotinylated G2 click-Alirocumab .....	178
Figure 4.36. MALDI-TOF-MS of biotinylated G3 click-Alirocumab .....	179
Figure 4.37. MALDI-TOF-MS of biotinylated tri-GalNAc-S2G2-Alirocumab .....	180
Figure 4.38. MALDI-TOF-MS of biotinylated tri-GalNAc-Man-Alirocumab .....	181

## List of Abbreviations

ADCC	Antibody-dependent cellular cytotoxicity
BCA	Bicinchoninic acid assay
BgaA	<i>Alkalophilic bacillus</i> $\beta$ 1,4-galactosidase
CDC	Complement-dependent cytotoxicity
CTAT	Cetyltrimethylammonium tosylate
CuAAC	Copper catalyzed azide-alkyne cycloaddition
DBCO	Dibenzylcyclooctyne
DC-SIGN	Dendritic cell-specific ICAM-grabbing non-integrin
DHB	2,5-dihydroxybenzoic acid
<i>E. coli</i>	<i>Escherichia coli</i>
ELISA	Enzyme-linked immunosorbent assay
EMEM	Eagle's minimum essential media
ESI	Electrospray ionization
Fc	Fragment crystallizable region
FcRn	Neonatal Fc receptor
FPLC	Fast protein liquid chromatography
GlcNAc	<i>N</i> -acetylglucosamine
HATU	Hexafluorophosphate azabenzotriazole tetramethyl uronium
HER-2	Human epidermal growth factor receptor 2
HIV	Human immunodeficiency virus
HPLC	High performance liquid chromatography
HRP	Horseradish peroxidase
IdeS	IgG- degrading enzyme of <i>Streptococcus pyogenes</i>
IgG	Immunoglobulin G
IgM	Immunoglobulin M
LC-ESI-MS	Liquid chromatography-electrospray ionization- mass spectrometry
LDL-C	Low density lipoprotein- cholesterol
M6P	Mannose-6-phosphate
MALDI-TOF MS	Matrix-assisted laser desorption ionization- time of flight mass spectrometry
MvNA	<i>Micromonospora viridifaciens</i> $\alpha$ 2,6-neuraminidase (sialidase)
MWCO	Molecular weight cut-off

NHS	N-hydroxysuccinimide
NMR	Nuclear magnetic resonance
PDL-1	Programmed cell death ligand 1
PEG	Polyethylene glycol
PGC	Porous Graphitic Carbon
PSA	Phenol-sulfuric acid assay
RIPA	Radioimmunoprecipitation assay buffer
SARS-CoV-2	Severe acute respiratory syndrome coronavirus 2
SDBS	Sodium dodecylbenzenesulfonate
SDS-PAGE	Sodium dodecyl sulfate–polyacrylamide gel electrophoresis
TFA	Trifluoroacetic acid
TLC	Thin layer chromatography

## Chapter 1: Introduction

### *1.1. Biological importance of glycans*

Glycosylation is a type of post-translational modification (PTM) referring to the covalent attachment of a carbohydrate or glycan to a biomolecule such as a protein, lipid, or nucleic acid.<sup>1</sup>

<sup>2</sup> Glycosylation is one of the most common PTMs observed in proteins, with several studies suggesting that greater than 50% of the human proteome is glycosylated.<sup>3</sup> As such, glycans constitute a significant portion of the molecules in the cell microenvironment and make important contributions to cell biology. Glycans contribute to processes like cell signaling, motility, metabolism, and immunology.<sup>1</sup>

Protein glycosylation can be divided into two classes, O-glycosylation and N-glycosylation, with each referring to the type of linkage between the glycan and the protein amino acid side chain. O-linked glycans are generally short glycans attached to the hydroxyl group sidechain of a serine or threonine amino acid. N-linked glycans on the other hand, are typically larger and are attached to proteins via the nitrogen atom of the amide side chain in an asparagine residue. N-glycosylation initiates in the Endoplasmic Reticulum (ER) and is matured in the Golgi apparatus, while typical O-glycosylation (except O-GlcNAc glycosylation) occurs in the latter. N-glycans are added to proteins containing the consensus sequence N-X-S/T (where X is any amino acid except proline), but there is no known consensus sequence for O-glycosylation.<sup>4</sup>

N-glycans are the most abundant class of protein glycosylation and can be further categorized into complex, high-mannose, or hybrid type depending on the nature of the modification to the three-mannose core common to all N-glycan structures (Figure 1.1). Addition

of N-acetylglucosamine (GlcNAc) to the  $\alpha(1,3)$ - and  $\alpha(1,6)$ -mannose arms results in complex type N-glycans that can be further modified by the addition of  $\beta(1,4)$ -galactose and  $\alpha(2,3)$ - or  $\alpha(2,6)$ -N-acetylneuraminic acid (sialic acid) to the nonreducing end. High-mannose N-glycans are further elaborated by the addition of mannose residues to the three-mannose core. Lastly, modification of the  $\alpha(1,3)$ -mannose arm with GlcNAc and the  $\alpha(1,6)$ -mannose arm with mannose results in the hybrid type N-glycan (Figure 1.1).<sup>4</sup>

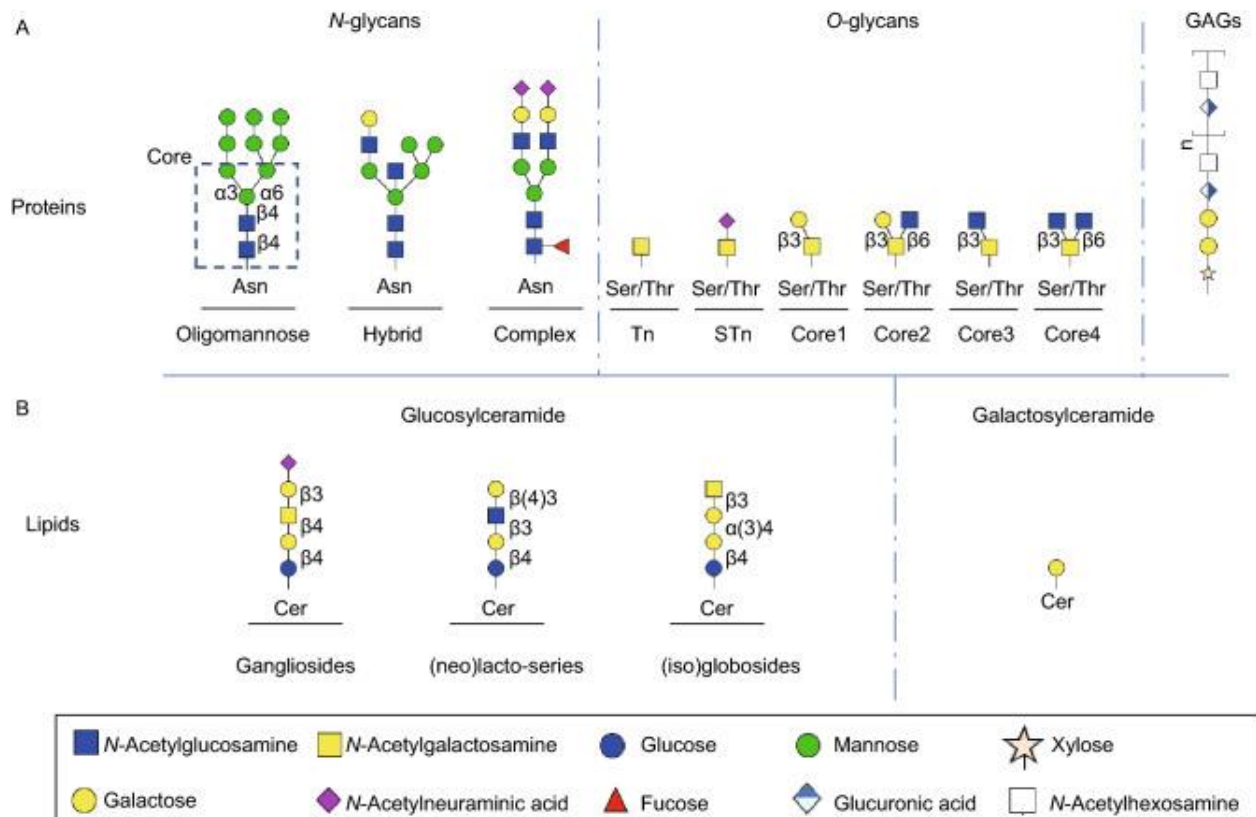


**Figure 1.1.** Cartoon representations of major mammalian glycan families including A) N-glycans, O-glycans, glycosaminoglycans (GAGs), and B) various glycolipids. Figure taken from publication by Zhang, et al.<sup>5</sup>

As mentioned previously, N-glycans contribute to several biological processes of the cell (Figure 1.2). Generally, N-glycosylation has a positive impact on protein stability by increasing

solubility, thermal stability, and protease resistance.<sup>1,4</sup> Moreover, the N-glycans themselves can be recognized by carbohydrate-binding proteins (i.e. lectins or glycan-specific antibodies) with a preference for specific glycan structures to enact a particular function. For example, highly sialylated complex-type N-glycans are known to engage sialic acid-binding immunoglobulin (Ig)-like lectin (Siglec) receptors on the surface of immune cells which contain cytosolic Immunoreceptor Tyrosine-based Inhibitory Motifs (ITIMs) able to recruit phosphatase enzymes for inhibition of immunoreceptor signaling.<sup>6</sup> Several human Siglec receptors exist, each with a distinct sialic acid linkage specificity [i.e.  $\alpha(2,3)$ ,  $\alpha(2,6)$ , or  $\alpha(2,8)$ ] and typically expressed on the surface of immune cells where they function to establish a threshold for immune tolerance and response to foreign antigens.<sup>7</sup> Several sialylated and fucosylated N-glycans are also recognized by human selectins, a group of carbohydrate-binding protein receptors expressed on the surface of endothelial cells that facilitate immune cell transport and migration to sites of inflammation.<sup>8</sup>

Removal of terminal sialic acid exposes  $\beta(1,4)$ -galactose residues which can interact with many galactose-specific carbohydrate-binding proteins including the asialoglycoprotein receptor (ASGPR) and the human galectins. The asialoglycoprotein receptor is a liver-specific membrane-bound receptor with particularly high affinity for tri- and tetra-antennary complex type  $\beta$ -galactosides.<sup>9</sup> This receptor is involved in galactosyl homeostasis by the endocytosis of asialoglycoproteins and their delivery to the lysosome, an intracellular organelle containing hydrolytic enzymes such as proteases and glycosidases responsible for the degradation of glycoproteins and other molecules.<sup>10</sup> Indeed, this receptor has been leveraged for the delivery of several therapeutics directly to the liver.<sup>11</sup> The human galectins on the other hand, are soluble extracellular proteins secreted by epithelial and immune cells, they are important regulators of cell signaling, endocytosis, and even apoptosis.<sup>12</sup> Galectins are typically oligomeric proteins and

are known to form intermolecular lattices between glycoproteins containing terminal  $\beta$ -galactose or *N*-acetylgalactosamine (GalNAc). These formed intermolecular lattices can directly affect the organization of glycosylated signaling receptors on the cell surface to promote/ inhibit receptor crosslinking and activation.<sup>12-14</sup> Galactose-bearing human IgG is also known to bind and recruit components of the complement system resulting in formation of a membrane-attack-complex and the killing of target cells such as bacteria.<sup>15</sup>

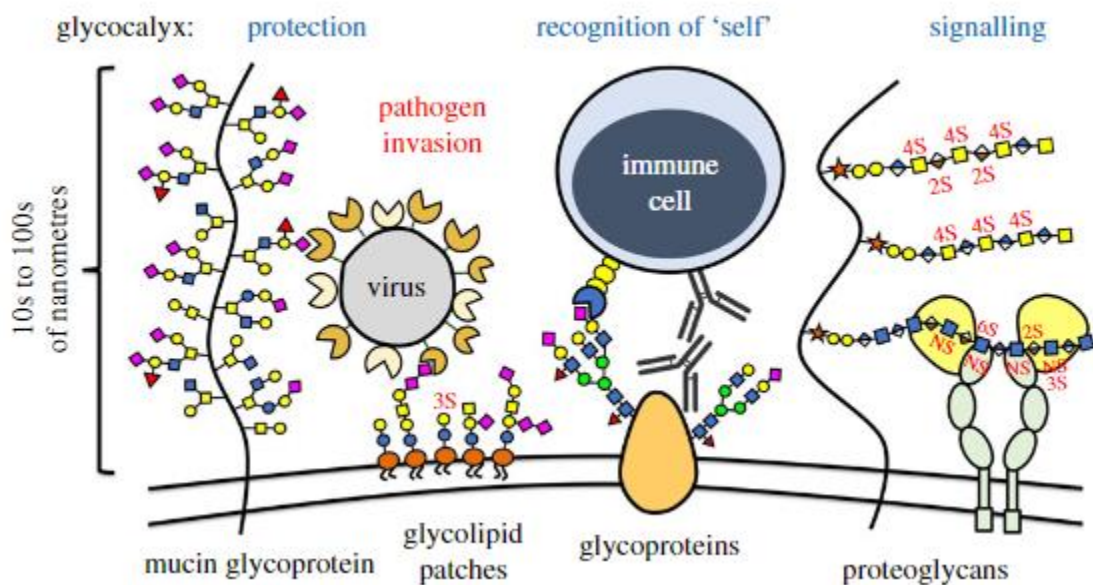


**Figure 1.2.** Glycoconjugates of the glycocalyx are recognized by carbohydrate binding proteins to mediate various biological processes. Figure taken from a publication by Purcell, et al.<sup>16</sup>

Glycoproteins with low galactose content have terminal GlcNAc exposed on their *N*-glycan chains, this epitope can be recognized by immunoreceptors such as DC-SIGN expressed on antigen presenting cells to mediate pro-inflammatory responses and antigen uptake/presentation.<sup>17, 18</sup> High-mannose type *N*-glycans are also recognized by DC-SIGN, as well as the Mannose Receptor (MR) of macrophages which is used in the phagocytosis of pathogens as well as antigen processing and presentation.<sup>19</sup> Phosphorylated high-mannose *N*-glycans are ligands of

the cation-independent mannose-6-phosphate receptor (CI-M6PR), a receptor responsible for sorting glycosylated hydrolytic enzymes to the lysosome, and the principal target of enzyme replacement therapies for the treatment of lysosomal storage disorders.<sup>20</sup> Several other carbohydrate-binding receptors with distinct specificities and functions exist, however, the above examples serve to illustrate the diverse biological functions of glycans and the profound impact that glycosylation can have on protein fate. My research focuses on the design and synthesis of glycoconjugates for elucidating the function of various human N-glycans and informing the design of more efficacious vaccines and glyco-therapeutics.

### *1.2. Biosynthesis of N-glycans*

Newly synthesized proteins are *N*-glycosylated on the asparagine sidechain of the N-X-S/T sequon through a multi-step process beginning in the endoplasmic reticulum (ER) and ending in the Golgi apparatus (Figure 1.3).<sup>21</sup> N-acetylglucosamine (GlcNAc) is first transferred to the membrane anchored lipid carrier dolichol phosphate (Dol-P) with uridine diphosphate N-acetylglucosamine as the donor (UDP-GlcNAc) to make GlcNAc-P-P-Dol. Monosaccharides are then added sequentially from their respective sugar nucleotide donors by the action of several glycosyltransferase enzymes to produce Man<sub>5</sub>GlcNAc<sub>2</sub>-P-P-Dol. The Man<sub>5</sub>GlcNAc<sub>2</sub>-P-P-Dol glycolipid is then flipped to the lumen of the ER and more monosaccharides are transferred to form the Glc<sub>3</sub>Man<sub>9</sub>GlcNAc<sub>2</sub>-P-P-Dol intermediate, which is then transferred to the glycosylation sequon of the nascent polypeptide by action of the oligosaccharyltransferase (OST) enzyme. The terminal glucose residues are trimmed by glucosidases to give the Glc<sub>1</sub>Man<sub>9</sub>GlcNAc<sub>2</sub> glycan which is then utilized to perform protein folding and quality control by several chaperone proteins. Incorrectly folded proteins are degraded, while correctly folded proteins are trimmed

further at the *N*-glycan terminus to give  $\text{Man}_9\text{GlcNAc}_2$  and transported to the Golgi for further processing. High-mannose *N*-glycans are not modified further, however, sequential trimming by  $\alpha$ -mannosidase enzymes followed by transfer of GlcNAc monosaccharides to the trimannose core by GnT (N-acetylglucosaminyl transferase) enzymes gives complex-type *N*-glycans containing up to four antenna that can be further decorated by galactose and sialic acid.<sup>21</sup> The structures of the *N*-glycan end-products depend on the extent of processing by glycosidase and glycosyltransferase enzymes as dictated by factors such as accessibility of the glycan, availability of sugar-nucleotide pools, and glycosidase/ glycosyltransferase expression levels.<sup>21</sup>

<sup>22</sup> The various monosaccharide structures available, their different regio- and stereo-chemical linkages, as well as their functionalization by phosphate, sulfate, and acetyl groups, gives rise to tremendous diversity in glycan structure. Furthermore, differences in glycan processing due to factors outlined above, results in heterogenous glycan structures that can be asymmetrically decorated by various monosaccharides on their nonreducing ends. Moreover, several diseases including various cancers and immune disorders are known to affect the expression of glycan processing enzymes, often resulting in unique glycan structures that can be leveraged as disease biomarkers for diagnostics, as therapeutic targets, and for vaccine development.<sup>22</sup>

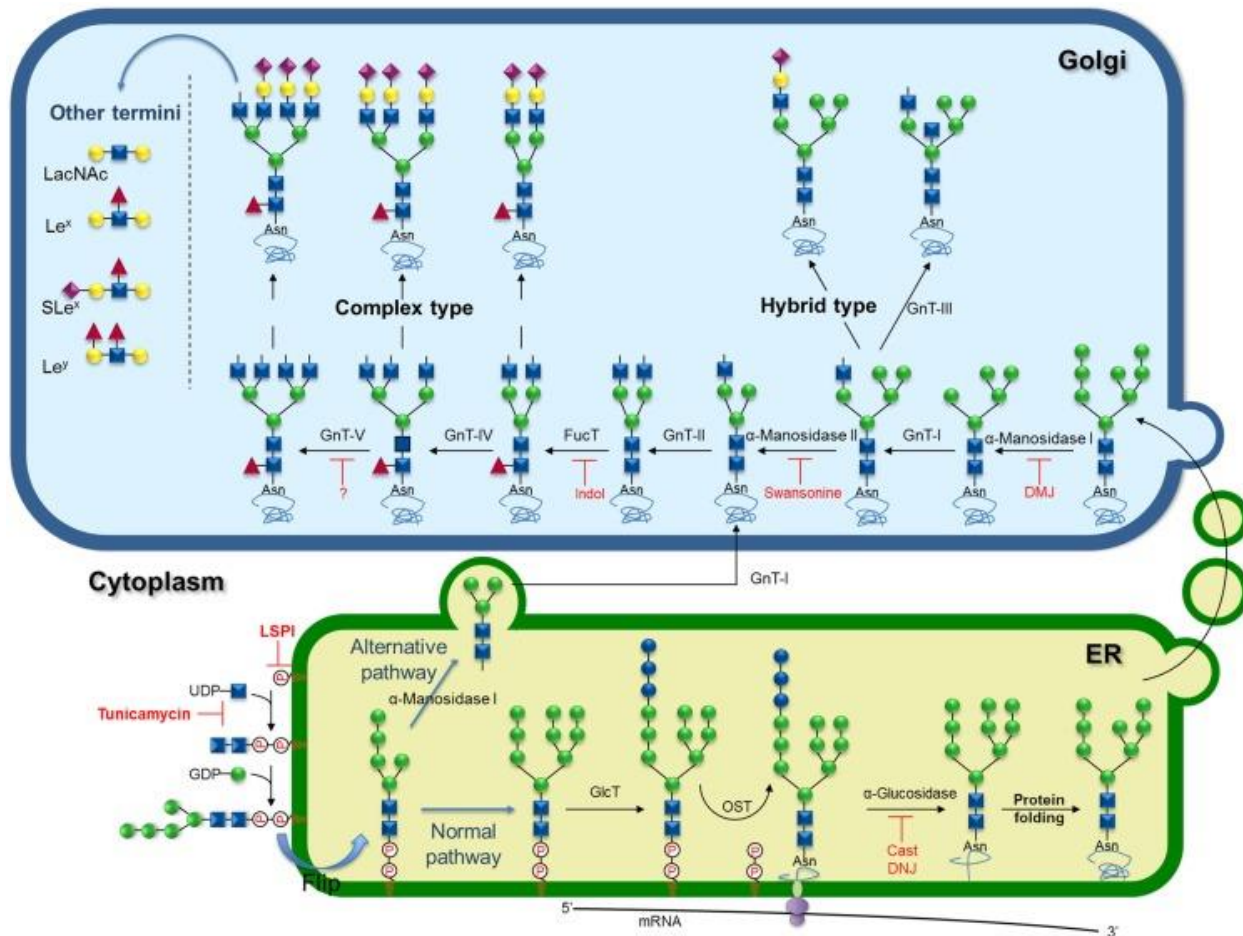


**Figure 1.3.** N-glycan biosynthesis in mammals. Figure taken from a publication by Santos, et al.<sup>21</sup>

### 1.3. Features of carbohydrate-protein interactions

The tremendous diversity and heterogeneity in N-glycan structure means that carbohydrate binding proteins must be able to bind and distinguish effectively between related structures and glycan isomers (glycoforms). Carbohydrate-binding proteins and lectins predominantly employ amino acids with aromatic and hydrogen-bonding compatible sidechains in their carbohydrate-binding sites.<sup>23</sup> Aromatic amino acids can engage in CH- $\pi$  interactions between the electropositive C-H bonds of the sugar ring and electron-rich  $\pi$ -bonds of the aromatic rings, this effect is most common for glucose, GlcNAc, galactose, fucose, and mannose monosaccharides

containing axial C-H bonds. Several carbohydrate-binding proteins and enzymes also employ metal cofactors such as calcium in the binding pocket, coordinated primarily by the carboxylate groups of aspartic acid or glutamic acid, to make interactions with the free hydroxyl groups of the glycan and withdraw electron density to reinforce the aforementioned CH- $\pi$  interactions. Polar amino acids such as aspartic acid, asparagine, and glutamine can engage in hydrogen bonding interactions with the free hydroxyl groups on the sugar, and charged amino acids can form salt bridges with charged functional groups on the glycan (i.e. carboxylate, phosphate, sulfate, and amino groups). Importantly, acetylated sugars can participate in hydrophobic interactions between the acetyl methyl group and aliphatic amino acids of the binding domain to increase the binding affinity of the interaction.<sup>23-25</sup>

Carbohydrate-binding proteins typically have shallow binding pockets and make few hydrophobic contacts, but leverage many of the structural features mentioned above for enhanced specificity to the glycan ligand. Furthermore, GBPs recognize several monosaccharides in a glycan for enhanced specificity, making unique contacts with motifs in each monosaccharide, such as bifurcated hydrogen bonds with the cis-diols of mannose and galactose.<sup>26</sup> Apart from the common trends in amino acid sequence, there are several conserved structural motifs in GBP secondary structure. Many carbohydrate-binding proteins employ  $\beta$ -sandwich,  $\beta$ -trefoil,  $\beta$ -helix, or V-set domain folds in their binding domains with  $\alpha$ -helices being less common.<sup>6, 27, 28</sup> The main driving forces for protein-glycan interactions are hydrogen-bonding and electronic forces that drive CH- $\pi$  interactions.

### *1.3.1. Multivalent interactions*

Protein interactions with monosaccharides or individual oligosaccharides are typically weak and transient with  $K_D$ 's in the  $10^{-4}$ - $10^{-3}$  M range, however, Nature makes use of multivalency

(display of several sugar ligands on a single surface) to enhance the apparent affinity and lifetime of the interaction ( $K_D = 10^{-9}$ - $10^{-6}$  M). This effect is analogous to Velcro patches, which make use of several weakly interacting Velcro filaments to achieve strong surface adhesion. Multivalency enhances the apparent binding affinity by lowering the rate of dissociation by a variety of mechanisms including statistical rebinding, chelate effect, receptor clustering, and steric shielding (Figure 1.4).<sup>29-31</sup> To enable the investigation of these complex multivalent binding events, chemical biologists have developed glycoengineering strategies, as well as several multivalent glycomimetic probes that consist of a synthetic scaffold presenting multiple copies of the glycan ligand. Several synthetic scaffolds have been used, including dendrimers, liposomes, metal nanoparticles, and cyclodextrin. These multivalent glycomimetics have provided valuable insight into GBP function and have been used as imaging probes, inhibitors of pathogenic lectins, and drug delivery vehicles.<sup>32</sup>

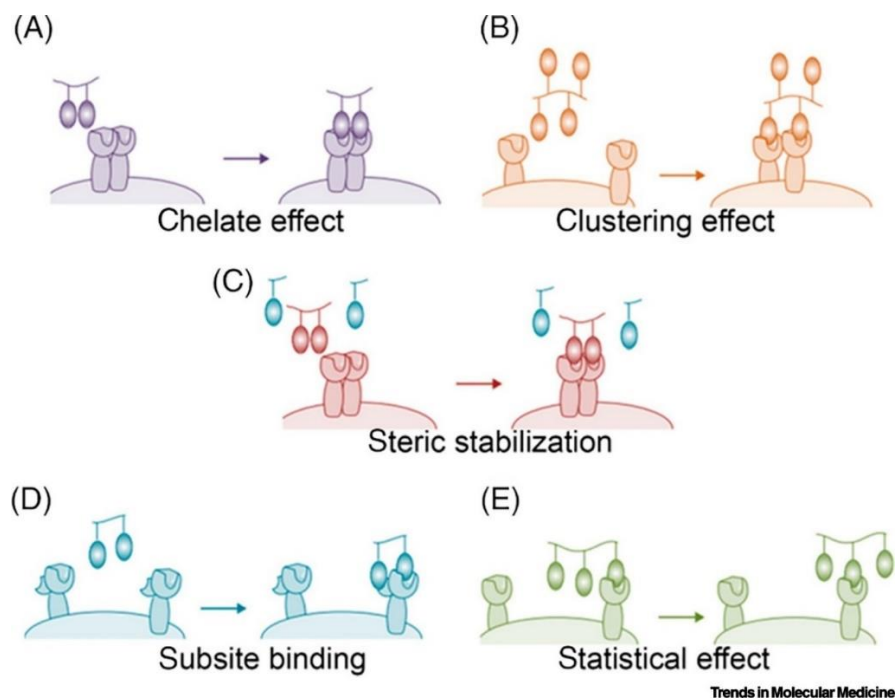


**Figure 1.4.** Major mechanisms of multivalent protein-glycan binding for enhanced affinity. Glycan ligands are depicted as colored ovals, carbohydrate-binding protein receptors are

represented by colored shapes with binding pockets. Figure taken from a publication by Bohmer, et al.<sup>29</sup>

Multivalent binding also significantly increases specificity of glycan recognition, for example, L-selectin recognizes its natural ligand sialyl Lewis X and binds to 6-sulfo-sialyl Lewis X with only a 3-fold enhancement in binding affinity. However, when a glycopolymer containing several sialyl Lewis X units is compared to a glycopolymer containing 6-sulfo-sialyl Lewis X, a 10,000-fold binding enhancement is observed towards the 6-sulfo-sialyl Lewis X polymers.<sup>33</sup> This intriguing result illustrates that small differences in binding affinity are amplified by multivalent display. However, cells display diverse glycan structures on their surfaces simultaneously, and multivalent glycomimetics bearing multiple copies of the same glycan structure do not faithfully mimic the cell microenvironment. Indeed, much of what we know about protein-glycan interactions comes from studies on a protein binding to a single glycan structure or multivalent presentations of that same structure. The influence of unrelated glycans on a lectin's recognition of the cognate ligand is poorly understood, and such studies are challenged by the large diversity in glycan structure, and the relatively low abundance of specific glycoforms. Reports exploring this phenomenon are limited, however, and interesting discoveries have been made indicating that unrelated glycan structures in the cellular microenvironment can have modular effects on the ability of a carbohydrate-binding protein to bind its cognate ligand (i.e. enhance or diminish).<sup>34-36</sup> Nevertheless, improved glycomimetics and precision-glycoengineering strategies are required to better understand the impacts of a heterogeneous glycosylation landscape on protein function and inform the design of therapeutics targeting these pathways.

#### 1.4. Leveraging glycobiology for therapeutic development

The development of prophylactic vaccines using *pneumococcus* capsular polysaccharides in the early 1940's represents one of the most notable glycan-based therapies in modern medical history.<sup>37</sup> Since then, glycan-based vaccines have been developed against a variety of pathogens including other strains of bacteria, pathogenic fungi, and various cancers.<sup>38-40</sup> These vaccines make use of unusual glycan structures displayed by disease cells to elicit an immunogenic response culminating in protective cellular and humoral immunity. Due to the weak immunogenicity of glycans, however, a carrier protein or adjuvant is commonly used in the immunization to encourage the activation of helper T cells which are integral for the propagation of an immune response by the adaptive immune system.<sup>41</sup> Activated helper T cells are then able to promote the proliferation of antibody-producing B cells against foreign glycan structures. Monoclonal glycan-specific antibodies have been proven to be successful therapies against various malignant cancers, with several glycan-specific antibodies in the pipeline for FDA approval.<sup>42-44</sup>

Therapeutic glycoproteins and glycoconjugates have also been leveraged for the treatment of disease. Prominent examples include mannose-6-phosphate (M6P)-modified hydrolases for the treatment of lysosomal storage disorders. Lysosomal storage disorders are caused by defective sorting of hydrolytic enzymes to the lysosome where they mediate the breakdown of cellular metabolites and waste, resulting in the accumulation of undigested waste products in the lysosome and the manifestation of symptoms such as muscular dystrophy or neurological disorders.<sup>45</sup> Enzymes are normally sorted to the lysosome by lysosome-targeting receptor CI-M6PR which recognizes high-mannose N-glycans containing a mannose-6-phosphate. Intravenous infusion of fresh enzyme containing this glycan (Enzyme Replacement

Therapy) has been demonstrated to significantly reduce and in some cases temporarily cure symptoms of lysosomal storage disorders like Pompe disease and Gaucher disease.<sup>45</sup>

Additionally, existing protein-based therapies including erythropoietin (EPO) and insulin have demonstrated longer half-lives and efficacy when glycosylated.<sup>46-48</sup>

Several revolutionary discoveries have also been made in the case of human monoclonal IgG antibodies, which contain a conserved N-glycosylation site on Asn-297 that is fucosylated at the chitobiose core (Figure 1.5). When fucose is removed, up to a 100-fold enhancement in affinity is observed between the antibody Fc and the Fc $\gamma$ R2 receptor, resulting in a remarkable >50-fold increase in antibody-dependent cellular cytotoxicity (ADCC) and target cell killing.<sup>49, 50</sup> Intravenous immunoglobulin (IVIG), a mixture of human polyclonal IgG's commonly used as a treatment for autoimmune disorders and in people suffering from immunodeficiencies, has been demonstrated to have anti-inflammatory properties mediated primarily by the sialylated glycans of the Fc domains.<sup>51, 52</sup> These exciting findings have spurred great interest in the glycoengineering of antibodies and other glycoproteins for enhanced therapeutic efficacy.

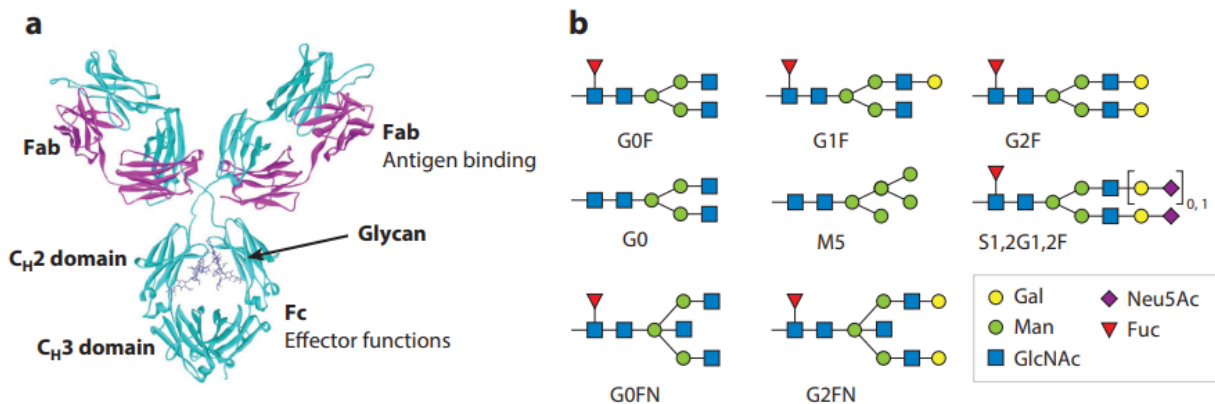


**Figure 1.5.** Structure of *a*) human IgG1 and *b*) common N-glycan structures found on the conserved glycosylation site at Asn297. Figure taken from a publication by Wang, et al.<sup>53</sup>

Glycoengineering is typically accomplished by employing genetic, metabolic, chemical, or chemoenzymatic methods. Genetic methods involve knock-in or knock-out of specific glycosyltransferase/ glycosidase -encoding genes of the glycosylation pathway to control the glycosylation end-products. However, genetic manipulation is labor-intensive, some glycosyltransferase enzymes cannot be knocked out without compromising cell viability, and it is challenging to obtain complete homogeneity in glycan structure.<sup>54-56</sup> In metabolic engineering, chemical inhibitors or derivatives of natural monosaccharides are used to modify the glycan biosynthesis pathway of live cells to obtain the desired glycan structures. While less laborious than the genetic methods, metabolic engineering is generally less efficient at preparing glycoproteins with the desired glycoforms, since in many cases inhibition of glycan processing enzymes is reversible and not complete.<sup>55</sup> Chemical methods involve the total synthesis of the glycan structure followed by attachment to the protein backbone by chemical conjugation using synthetic linkers or by chemoenzymatic methods. Chemical methods can be time-consuming and expensive, as they typically require several synthetic steps with careful regio- and stereo-chemical control. However, total chemical synthesis gives well-defined and homogenous glycan products that can be used for detailed studies on glycan function.<sup>57</sup> Lastly, chemoenzymatic methods involve enzyme-catalyzed glycan synthesis and modification *in vitro*, the glycan substrates can either be synthesized completely enzymatically by the sequential transfer of monosaccharides to a protein acceptor or synthesized separately and transferred enzymatically *en bloc*. An approach introduced by Lai-Xi Wang and others involves the chemical synthesis of an activated glycan donor or its isolation from a natural source, followed by transfer of the glycan structure *en bloc* to a protein acceptor using mutant endoglycosidase enzymes.<sup>54</sup> This process is typically done in two steps, first deglycosylation of the glycoprotein's heterogenous glycans is

done with a wild-type endoglycosidase enzyme to yield the deglycosylated protein bearing the reducing GlcNAc at each glycosylation site. Next, mutant endoglycosidase enzymes devoid of hydrolytic activity, but replete with glycan transfer activity, are used in the presence of activated sugar-oxazoline donors to transfer structurally well-defined glycans to the sites of GlcNAc-modification on the protein giving glycoproteins with homogenous glycan structures.<sup>54</sup> These strategies have been used extensively for exploring glycan function and for preparing glycotherapeutics with improved efficacy.

Genetic knock-down of FUT8 (the sole fucosyltransferase responsible for core-fucosylation in mammals) with lentiviral shRNA or knock-out by zinc-finger nucleases have been successful approaches for obtaining glycoproteins and monoclonal antibodies with little to no fucose content.<sup>58, 59</sup> Metabolic engineering with fluoro-fucose analogues and chemoenzymatic engineering strategies using endoglycosidase mutants have also been promising.<sup>60, 61</sup> The chemoenzymatic method has also been leveraged to install highly sialylated glycans on the Fc regions of IVIG, which may translate to enhanced anti-inflammatory activities.<sup>61</sup> Total chemical synthesis of chemically modified natural glycans, such as azide-modified disaccharides followed by chemoenzymatic transfer to the conserved N-glycosylation site of human IgG has enabled the site-specific click conjugation of several therapeutic cargoes such as cytotoxic drugs for cell-specific killing or fluorophores for imaging.<sup>62</sup> Furthermore, chemical conjugation of glycan structures to synthetic scaffolds or proteins has given several useful multivalent glycomimetics with application as viral entry inhibitors, drug delivery vehicles, immune modulators, and vaccines.<sup>63</sup> Moreover, these tools have enabled the interrogation of the natural ligands for various carbohydrate-binding proteins and assigning functions to putative carbohydrate-binding proteins.<sup>64, 65</sup> These few notable examples illustrate the impact that glycans can have on the

biological function of proteins, and how glycoprotein-based therapeutics can be further improved by glycoengineering. In these next chapters, I will make use of chemical synthesis and chemoenzymatic glycoengineering strategies to investigate the biological functions of several human N-glycans and leverage them for therapeutic functions.

## Chapter 2: Synthesis and Immunological Study of N-Glycan-Bacteriophage Q $\beta$ Conjugates Reveal Dominant Antibody Responses to the Conserved Chitobiose Core.

Part of this work was published in *Bioconjugate Chemistry*.<sup>66</sup>

Donahue, T. C.; Zong, G.; O'Brien, N. A.; Ou, C.; Gildersleeve, J. C.; Wang, L. X., Synthesis and Immunological Study of N-Glycan-Bacteriophage Q $\beta$  Conjugates Reveal Dominant Antibody Responses to the Conserved Chitobiose Core. *Bioconjug. Chem.*, **2022**, *33* (7), 1350-1362.

L.X.W. conceived the idea and supervised the research; T.C.D. and L.X.W. designed the experiments; T.C.D performed the experiments; G. Z. and C. O. assisted in chemical synthesis and data analysis; N. O. and J. C. G. performed the glycan microarray analysis; T.C.D. and L.X.W. analyzed the data and wrote the manuscript; all co-authors contributed to the revision of the manuscript.

### **2.1 INTRODUCTION**

Glycans are ubiquitous molecules of the cell and are known to play a crucial part in protein signaling, cell-mediated immunity, and cell migration.<sup>12, 67</sup> Carbohydrate-binding proteins with distinct glycan structural specificities such as lectins and glycan-specific antibodies have long been used as valuable tools for functional studies involving glycans.<sup>68</sup> In particular, glycan-specific antibodies are usually of excellent specificity for the target glycans and have found applications in the diagnosis and treatment of diseases such as autoimmune and infectious diseases, and cancer.<sup>69-75</sup> On the other hand, targeting pathogen- or cancer-specific carbohydrate antigens constitutes an important approach for vaccine design.<sup>76-78</sup>

N-Glycosylation, the attachment of an oligosaccharide to the amide side chain of an asparagine residue in proteins, is a major posttranslational modification of proteins found in eukaryotic systems. The corresponding N-glycans can be categorized in three major forms, including high-mannose type, complex type, and hybrid type. While some hypersialylated multi-

antennary complex-type and truncated N-glycans are associated with diseases such as autoimmunity and cancer, very few N-glycan specific antibodies have been characterized.<sup>68, 79, 80</sup> A notable exception is the identification of a new class of glycan-dependent broadly neutralizing antibodies against HIV-1 in recent years. These include antibody 2G12 that recognizes a unique High-mannose N-glycan cluster on HIV-1 gp120,<sup>81</sup> and the PGT series antibodies (PG9, PGT128, PGT121, and 10-1074) that recognize conserved N-glycans and a peptide region located in the V1V2 and V3 domains of HIV-1 gp120.<sup>82-89</sup> Other reported N-glycan specific antibodies include those targeting the paucimannose  $\text{Man}_3\text{GlcNAc}_2$  and the desialylated tetra-antennary complex-type N-glycans, but with poor affinity or specificity.<sup>68</sup>

One of the major challenges facing the development of glycan-specific antibodies is the low immunogenicity of carbohydrate antigens, primarily due to activation of a helper T cell-independent immunological pathway.<sup>41, 90</sup> Several approaches have been undertaken to generate new glycan-specific monoclonal antibodies. In an elegant approach by Pancer and coworkers, evolutionarily distant lamprey were chosen as animal models to raise monoclonal single chain Variable Lymphocyte Receptors (VLRs) or lambodies against a variety of tumor-associated carbohydrate antigens.<sup>91</sup> Lamprey do not have the same cell-surface glycan structures as higher vertebrates, and were demonstrated to elicit strong immune responses against otherwise universal mammalian glycans. Expanding on this approach, Cummings and co-workers have leveraged whole cell immunization and yeast surface-display libraries to select lamprey B cells with specificity towards cell surface glycans, and obtained an array of useful monoclonal VLRs against several terminal epitopes of cell surface glycans.<sup>92, 93</sup> However, heterogeneity in the cell surface glycome of the whole cell vaccine makes it difficult to obtain antibodies specific for low-abundance glycans, and isolating glycan-specific antibodies from infected patients is not possible

for the non-disease associated carbohydrates. In these situations, antibodies produced by immunization with semisynthetic immunogens can still be an advantageous strategy to achieve monoclonal antibodies with narrow specificity.

To improve glycan immunogenicity, synthetic neoglycoconjugate immunogens composed of glycan antigens conjugated to an immunogenic carrier protein are employed to enhance MHC-II type presentation by helper T cells and to activate B cell proliferation.<sup>94, 95</sup> Several carrier proteins and adjuvants have been shown to be effective in eliciting high titers of carbohydrate-specific IgG antibodies, including CRM197 (a non-toxic mutant of diphtheria toxin), the tetanus toxoid protein, and the virus-like nanoparticle, bacteriophage Q $\beta$ .<sup>38</sup> Bacteriophage Q $\beta$  is a virus-like nanoparticle that consists of 180 protein subunits per particle. The protein subunits encapsulate bacterial RNA which can also act as an adjuvant.<sup>96</sup> There are several advantages for using Q $\beta$  as a platform for the design of epitope-based vaccines.<sup>97, 98</sup> The rigid and highly repetitive surface pattern permits highly ordered display of multiple copies of glycopeptide epitopes. Q $\beta$  has been shown to be particularly effective as a carrier protein for glycan antigens due to its highly ordered arrangement of free lysines available for bioconjugation which promotes B-cell receptor crosslinking, and helper T cell epitopes that facilitate helper T cell recruitment.<sup>90, 99-101</sup>

Early attempts to generate N-glycan-specific antibodies using N-glycan containing glycoconjugates as immunogens have focused on generating 2G12-like broadly neutralizing antibodies (bNAbs) that recognize the high-mannose patch of HIV gp120, but they were met with limited success.<sup>102</sup> Immunization with tetravalent galactoside-based Man9-GlcNAc<sub>2</sub> clusters conjugated to keyhole limpet hemocyanin (KLH), elicited antibodies that react strongly towards the immunogen's maleimide linker with relatively low titers of glycan-specific antibodies that

are only weakly cross-reactive with HIV gp120.<sup>103</sup> In other reports, immunization with Man9-glycopeptides or Man9-BSA conjugates appear to produce high glycan-specific antibody titers with weak affinity for recombinant HIV gp120.<sup>104, 105</sup> However, the glycan specificity has not been fully characterized. Rabbits immunized with Man9-Q $\beta$  conjugates mounted strong glycan-specific immune responses, but antisera were found to target mannose linkages of the three-mannose core structures and do not cross-react with the HIV envelope glycoprotein gp120.<sup>106</sup> More recently, Krauss and co-workers demonstrated that oligomannose glycopeptide conjugates as mimics of the 2G12 epitope elicit antibodies targeting the oligomannose core instead of the external mannose moieties, probably due to  $\alpha$ -mannosidase-catalyzed trimming of the outer mannose residues.<sup>107, 108</sup> On the other hand, we designed and synthesized self-adjuvant three-component immunogens that consist of the HIV-1 V3 glycopeptide epitopes carrying one or two N-glycans, a universal T-helper epitope P30, and a lipopeptide (Pam<sub>3</sub>CSK<sub>4</sub>) ligand of Toll-like receptor 2 for stimulating immune response.<sup>109-112</sup> It has been shown that the synthetic three-component glycopeptide immunogens can elicit glycan-dependent antibodies. Moreover, the induced antibodies have exhibited broad recognition of several HIV-1 gp120s across clades.<sup>109-112</sup> Despite these developments, raising N-glycan specific antibodies through immunization remains a challenging task that merits continuous efforts.

To address the general lack of consensus in immunogen design and to inform future N-glycan-specific antibody development, we describe in this paper the design and synthesis of a set of N-glycan-Q $\beta$  immunogens bearing five different human N-glycans and two different chemical linkers. Our mouse immunization studies showed that the N-glycan-Q $\beta$  conjugates raised significant IgG antibodies that recognize N-glycans but, surprisingly, most of the glycan-dependent antibodies were directed to the chitobiose core and were nonspecific for respective N-

glycan structures. We also found that the linkers affected antibody specificity and sialylation of the N-glycans significantly suppressed glycan-dependent immune response. During this work, Wong and co-workers reported the immunization of CRM197-based glycoconjugates bearing hybrid-type or truncated high-mannose type N-glycans and found that most of the IgG antibodies responses were directed to the chitobiose core regardless of the nature of N-glycans.<sup>113</sup>

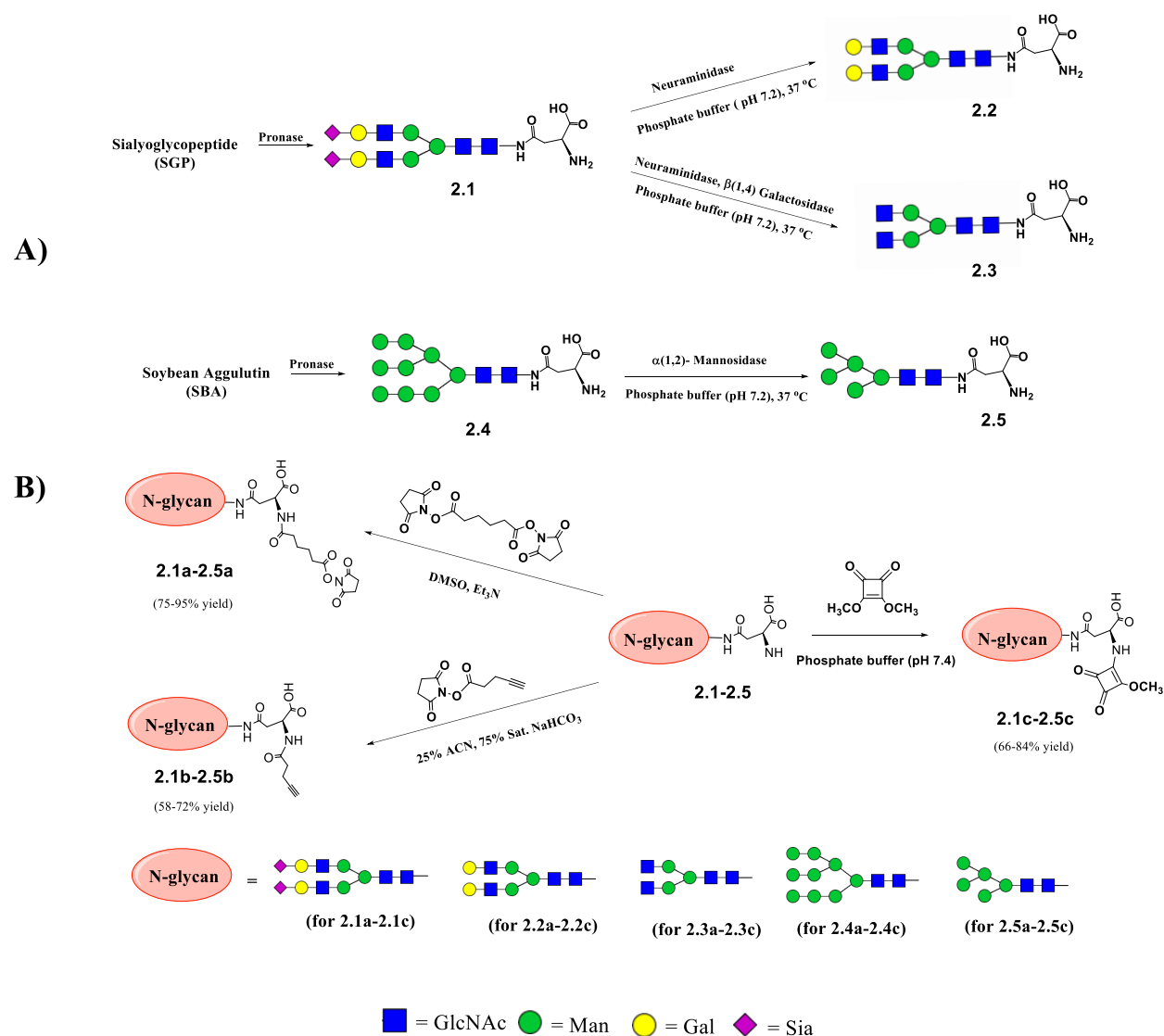
## **2.2 RESULTS AND DISCUSSION**

**Semisynthesis of tagged N-glycans.** To avoid the cumbersome synthetic procedures commonly involved in the total chemical synthesis of mammalian N-glycans, we used a top-down chemoenzymatic approach for quick access to different N-glycan structures by sequential enzymatic trimming of two readily available natural N-glycans. Thus, the asparagine (Asn)-linked sialylated biantennary N-glycan (S2G2-GlcNAc<sub>2</sub>-Asn, **2.1**) was synthesized by protease digestion of a sialoglycopeptide (SGP) obtained from chicken egg yolks.<sup>114-116</sup> Then, **2.1** was subjected to exoglycosidase trimming by an  $\alpha(2, 6/8)$ -neuraminidase and a  $\beta(1,4)$ -galactosidase to afford the truncated complex type N-glycans, S0G2-GlcNAc<sub>2</sub>-Asn (**2.2**) and S0G0-GlcNAc<sub>2</sub>-Asn (**2.3**), respectively. The high-mannose type N-glycan, Man<sub>9</sub>GlcNAc<sub>2</sub>-Asn (**2.4**) was obtained from protease digestion of soybean agglutinin followed by gel filtration chromatography.<sup>117</sup> Trimming of **2.4** with  $\alpha(1,2)$ -mannosidase gave the Man<sub>5</sub>GlcNAc<sub>2</sub>-Asn (**2.5**)<sup>118</sup> (Scheme 2.1).

The N-glycans were then functionalized at the free amino group of the asparagine to install reactive handles. First, we sought to functionalize the N-glycans with a linker carrying an N-hydroxy-succinimide activated ester for protein conjugation. For this purpose, each Asn-linked glycan (**2.1-2.5**) was reacted with an excess (10 mol. equiv.) of N-hydroxy-dissuccinimidyl adipate in anhydrous DMSO in the presence of triethylamine (Scheme 2.1). After 2 h, the

reaction was complete as judged by LC-MS analysis. Initial attempts to purify the activated N-glycans by reverse-phase HPLC and water-chloroform extractions failed, as the NHS-activated ester was labile and was readily hydrolyzed to the free carboxylic acid during the procedures. The purification of the products was achieved by lyophilization of the reaction mixture to give a dry film, followed by washing thoroughly with chloroform to afford the glycan mono-NHS esters (**2.1a-2.5a**) in reasonable purity and good overall yields ( $\geq 90\%$ ).

Next, we synthesized the alkyne-tagged glycans (**2.1b-2.5b**), which would enable click conjugation with an azido-modified carrier protein. Thus, N-glycans **2.1-2.5** were reacted with 4-pentynoic acid NHS ester (3 mol. equiv.) in a solvent system of 25% acetonitrile and 75% sat.  $\text{NaHCO}_3$  at room temperature, then the crude mixture was desalted on a Sepharose G15 column and finally purified by reverse-phase HPLC to obtain **2.1b-2.5b** in moderate yields (58-72%). We also synthesized squaric acid-functionalized N-glycans, which would allow direct coupling with free amino groups on a carrier protein. Thus, N-glycans **2.1-2.5** were reacted with an excess (20 mol. equiv.) of 3,4-dimethoxy-3-cyclobutene-1,2-dione at 37 °C in a phosphate buffer to give the glycan-Asn-squaric acid monoamides (**2.1c-2.5c**), which were purified by gel filtration to obtain the respective products in good yields (66-84%) (Scheme 2.1). Functionalized N-glycans with alkyne or mono-NHS handles were ready for coupling with bacteriophage Q $\beta$  to prepare the glycoconjugate immunogens, respectively. On the other hand, N-glycan-squaric acid monoamides (**2.1c-2.5c**) could be coupled to another carrier protein such as bovine serum albumin (BSA) and used as coating antigens for measuring glycan-specific antibody titers.

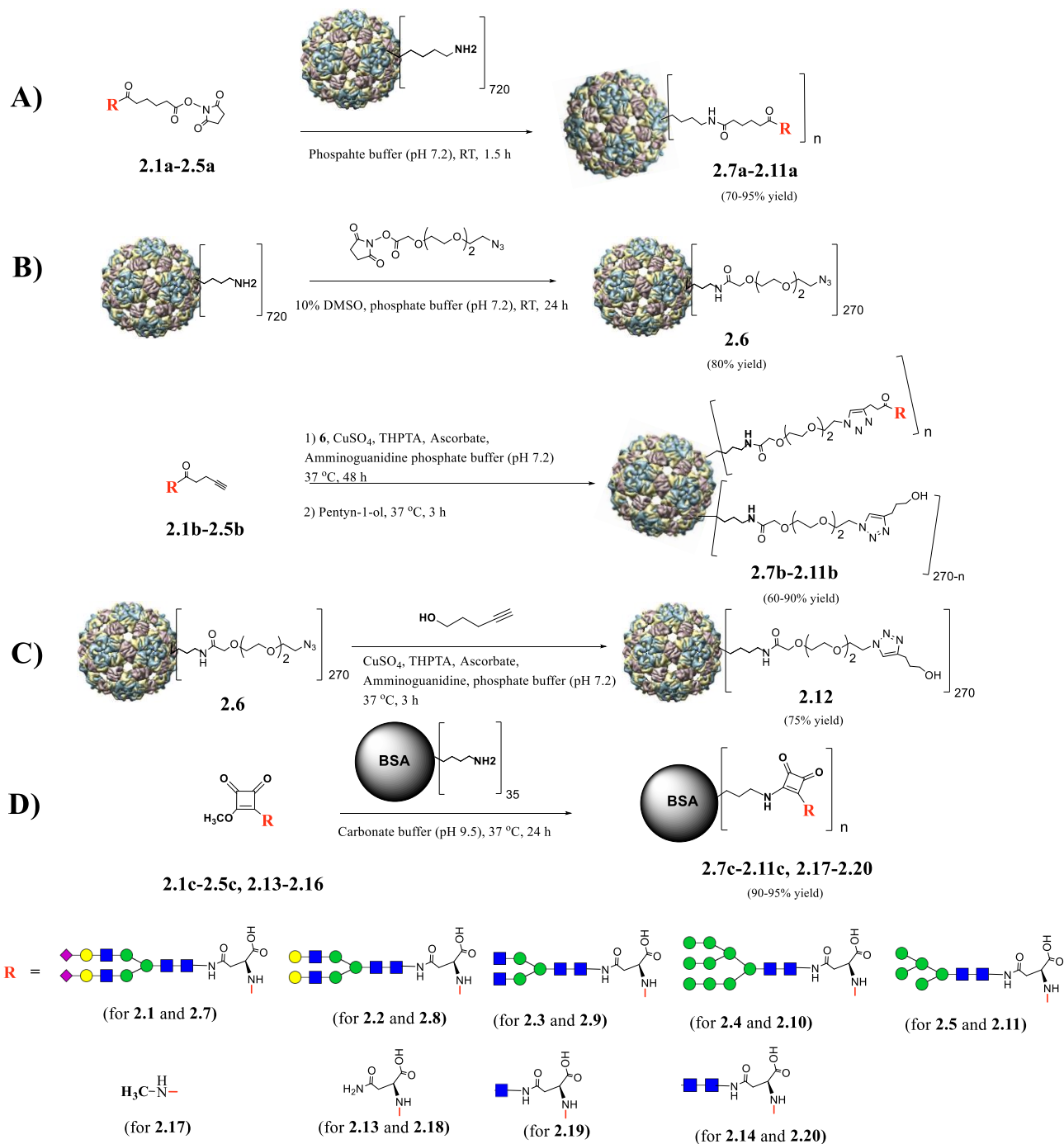


**Scheme 2.1.** A) Synthesis of different N-glycans through enzymatic trimming of the N-glycan precursors. B) Functionalization of the N-glycans with mono-NHS, alkyne, or squaric acid monoamide tags.

**Synthesis of N-glycan-Q $\beta$  immunogens and N-glycan-BSA coating antigens.** With the activated N-glycans (**2.1a-2.5a** and **2.1b-2.5b**) in hand, we prepared two types of N-glycan-Q $\beta$  conjugates as immunogens, which differ in their linker structures. The synthesis is summarized in Scheme 2.2. Reaction of glycan mono-NHS esters **2.1a-2.5a** with bacteriophage Q $\beta$  (8 mol.

*equiv.* of N-glycan per Q $\beta$  subunit) in phosphate buffer (pH 7.4) gave the N-glycan-Q $\beta$  conjugates (**2.7a-2.11a**), respectively. It was found that a relatively high concentration of Q $\beta$  was important for efficient coupling with mono-NHS esters **2.1a-2.5a**, as hydrolysis of the NHS-activated N-glycans became significant over the course of the coupling reaction. The reaction progress was monitored by MALDI-TOF MS. The final glycan loading, or the average number of glycans conjugated to the Q $\beta$  particle, was estimated by SDS-PAGE analysis of the Q $\beta$  subunits after reduction of conjugates **2.7a-2.11a** by  $\beta$ -mercaptoethanol reducing agent. The SDS-PAGE analysis of the reduced **2.7a-2.11a** indicated a mixture of the Q $\beta$  subunits carrying mainly 0, 1, and 2 N-glycans (Figure 2.1A). Quantitative analysis of the SDS-PAGE band density by Bio-Rad ImageLab software suggested that the glycan loading ranged from 135 to 181 per nanoparticle (i.e., per 180 Q $\beta$  subunits) for the glycoconjugates **2.7a-2.11a** (Table 2.1).

For the conjugation with the alkyne-functionalized N-glycans (**2.1b-2.5b**), azide moieties were first installed on the Q $\beta$  particle to enable a copper-catalyzed azide-alkyne cycloaddition (CuAAC) reaction with the carrier protein. Thus, wild-type Q $\beta$  was acylated with 16 equivalents of the azido-(PEG)<sub>2</sub>-NHS ester in a phosphate buffer (pH 7.4), following our previously reported procedure,<sup>119</sup> giving the azido-Q $\beta$  conjugate (**2.6**) bearing an average of 270 azide groups. After purification of conjugate **2.6** by dialysis, the triazole linked glycan-Q $\beta$  conjugates (**2.7b-2.11b**) were synthesized by reaction of **2.6** with the alkyne-functionalized N-glycans (**2.1b-2.5b**) (8 *mol. equiv.* of N-glycan per Q $\beta$  subunit), following a modified procedure described by Finn and co-workers.<sup>120</sup> The click reaction was monitored by MALDI-TOF MS analysis. After 48 h at 37°C, the N-glycan Q $\beta$  conjugates had reached a suitable glycan loading as assessed by SDS-PAGE (Figure 2.1B) analysis of the reduced Q $\beta$  subunits. The glycan loading of conjugates **2.7b-2.11b** was found to range from 137 to 168 per Q $\beta$  particle (Table 2.1). Thus, the average number of N-



**Scheme 2.2.** A) Synthesis of N-glycan-Q $\beta$  conjugates bearing adipic acid (**2.7a-2.11a**) linkers. B) Acylation of WT-Q $\beta$  with NHS-(PEG)<sub>2</sub>-N<sub>3</sub> to prepare azido-functionalized Q $\beta$  conjugate (**2.6**) and click conjugation of alkyne-tagged glycans to prepare N-glycan-Q $\beta$  conjugates with triazole linkers (**2.7b-2.11b**) C) CuAAC of conjugate **2.6** with pentyn-1-ol to afford control immunogen **2.12**. D) Synthesis of N-glycan-BSA squaric acid bisamide coating antigens **2.7c-2.11c** for ELISA experiments.

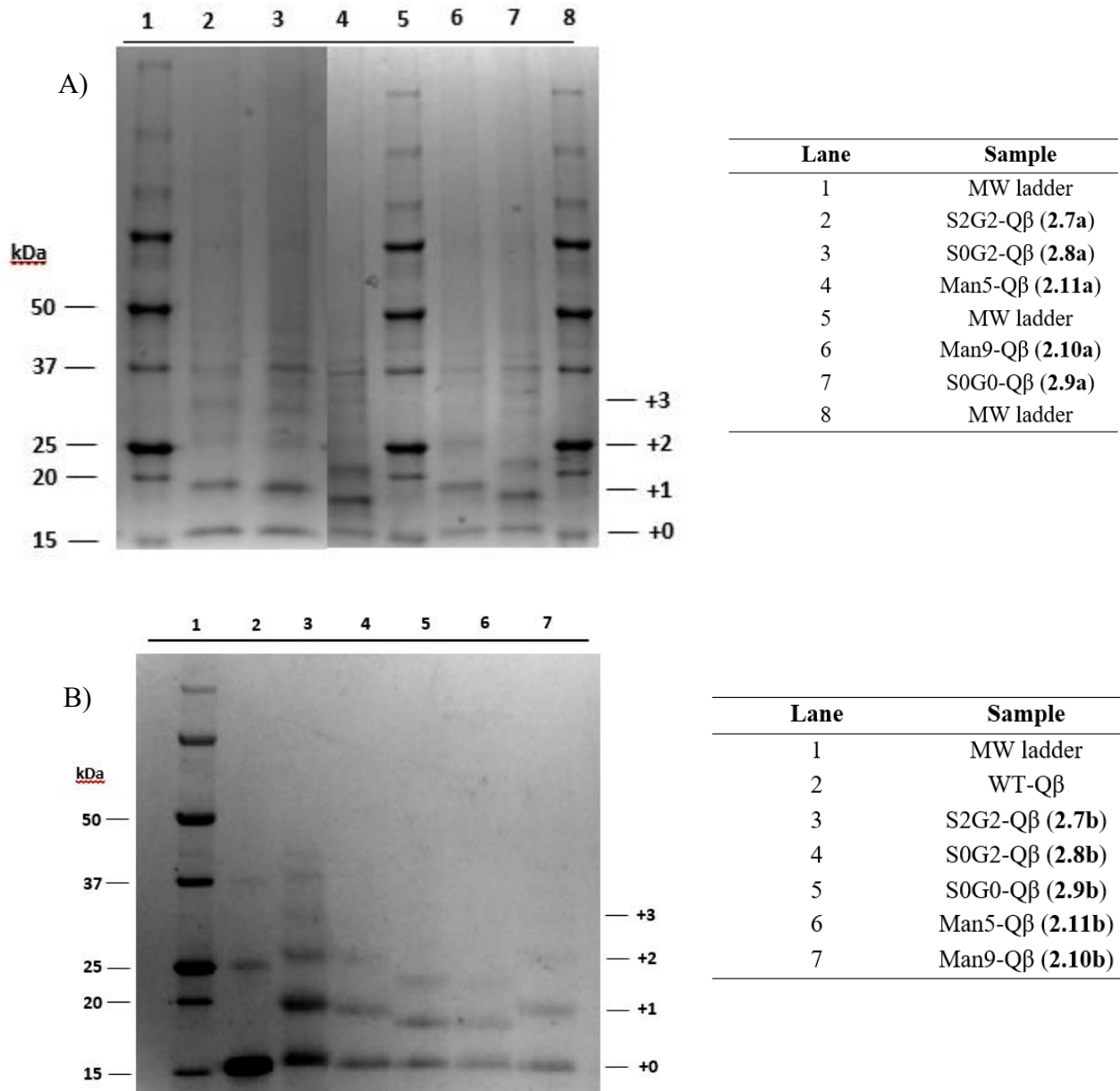


**Figure 2.1.** SDS-PAGE of the reduced *A*) N-glycan-adipoyl-Q $\beta$  (**2.7a-2.11a**), and *B*) N-glycan-triazole-Q $\beta$  conjugates (**2.7b-2.11b**). Panel A is a composite of two gels. Numerical values on the right margin indicate the degree of conjugation, with either zero, one, two, or three N-glycan units.

glycans conjugated to both sets of immunogens, **2.7a-2.11a** and **2.7b-2.11b**, were comparable so that any significant difference in immune response could be attributed to the chemical linker employed for bioconjugation.

To enable analysis of glycan-specific antibody titers in mouse serum after immunization, we synthesized the corresponding N-glycan-BSA conjugates (**2.7c-2.11c**) using a squaric acid linker. Importantly, these conjugates contain a carrier protein and a linker different from the immunogens (**2.7a-2.11a** and **2.7b-2.11b**). As a result, these glycoconjugates would be suitable as coating antigens to detect antibody responses specifically for the respective glycans without cross reactivity to the carrier protein or linker. Thus, BSA was reacted with the glycan-Asn-squaric acid monoamides (**2.1c-2.5c**), respectively, in a carbonate buffer (pH 9.5) (60 *mol. equiv.* of the glycan-Asn-squaric acid monoamide per BSA) at 37 °C for 18 h. The glycan loading of N-glycan-BSA conjugates (**2.7c-2.11c**) was determined by MALDI-TOF MS analysis by taking the observed mass difference between the N-glycan-BSA conjugates and free BSA divided by the mass of the corresponding N-glycan-Asn-squaric acid monoamide (**2.1c-2.5c**). This gave an average glycan loading ranging from 8 to 10 N-glycans per BSA for the resulting glycoconjugates (**2.7c-2.11c**) (Figure 2.2). These data are comparable to previous reports using the squaric acid ester method for conjugation of oligosaccharides of similar size to BSA.<sup>118, 121</sup>

**Table 2.1.** The linkers and average glycan loading of the synthetic N-glycan-Q $\beta$  conjugate immunogens.

Q $\beta$ conjugates	R	Linker	Loading (n)
WT-Q $\beta$	-	-	-
<b>2.12</b>	-OH	triazole	270
<b>2.7a</b>	S2G2-GlcNAc <sub>2</sub>	adipic acid	148
<b>2.8a</b>	S0G2-GlcNAc <sub>2</sub>	adipic acid	135
<b>2.9a</b>	S0G0-GlcNAc <sub>2</sub>	adipic acid	144
<b>2.10a</b>	Man <sub>9</sub> -GlcNAc <sub>2</sub>	adipic acid	168
<b>2.11a</b>	Man <sub>5</sub> -GlcNAc <sub>2</sub>	adipic acid	181

<b>2.7b</b>	S2G2-GlcNAc <sub>2</sub>	triazole	168
<b>2.8b</b>	S0G2-GlcNAc <sub>2</sub>	triazole	137
<b>2.9b</b>	S0G0-GlcNAc <sub>2</sub>	triazole	133
<b>2.10b</b>	Man <sub>9</sub> -GlcNAc <sub>2</sub>	triazole	164
<b>2.11b</b>	Man <sub>5</sub> -GlcNAc <sub>2</sub>	triazole	139

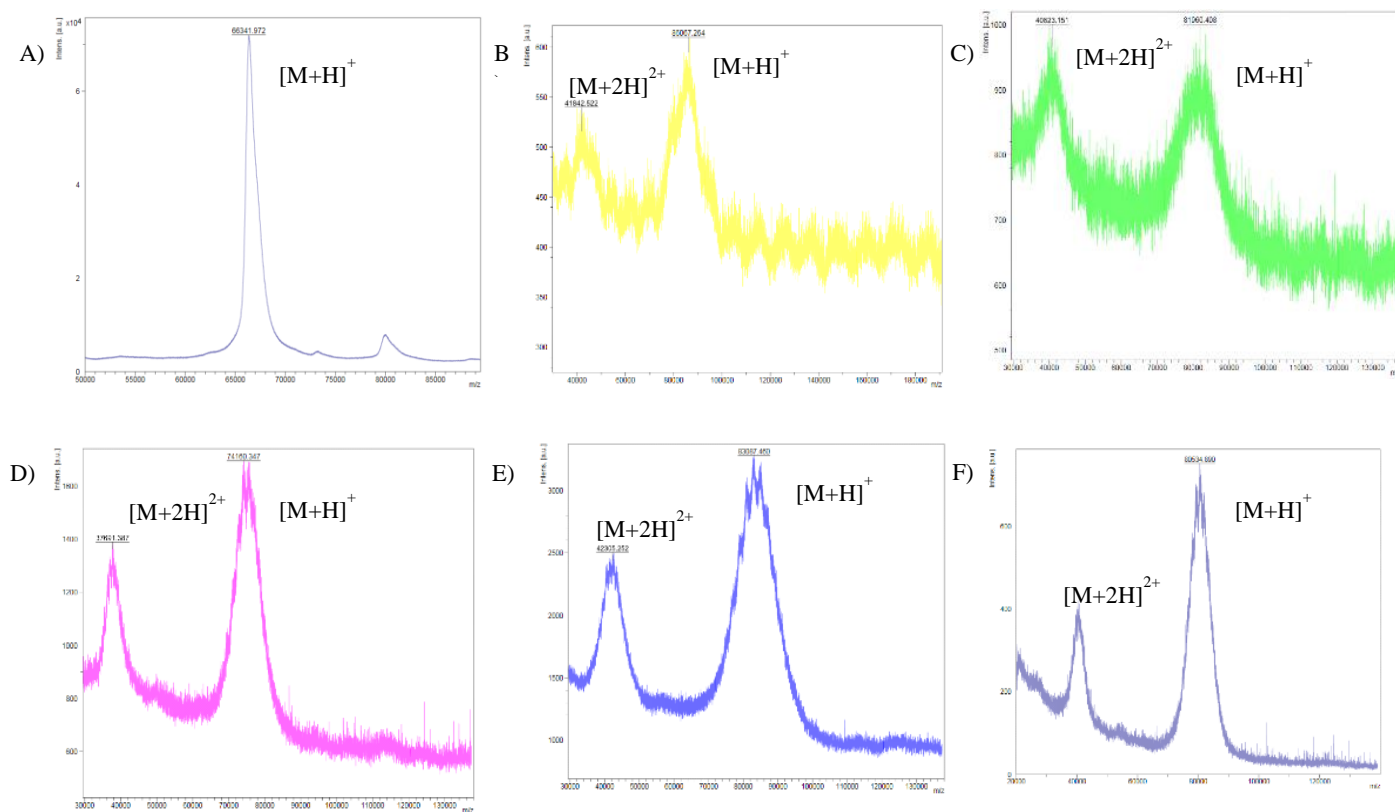


**Figure 2.2.** MALDI-TOF MS of commercial BSA and the glycan-BSA conjugates (**2.7c-2.11c**). A, commercial BSA; B, **2.7c** with 8 N-glycans on average; C, **2.8c** with 8 N-glycans on average; D, **2.9c** with 9.5 N-glycans on average; E, **2.10c** with 8.5 N-glycans on average; F, **2.11c** with 10 N-glycans on average.

**Mouse immunization and glycan-specific antibody titers.** Female C57BL/6 mice were immunized subcutaneously with the adipoyl-linked glycan-Q $\beta$  conjugates (**2.7a-2.11a**; groups 3-7) and the triazole-linked glycan-Q $\beta$  conjugates (**2.7b-2.11b**; groups 8-12), as emulsions in complete Freund's adjuvant on day 0, with booster injections on days 14 and 28 in incomplete

Freund's adjuvant. Wild-type Q $\beta$  (group 1) and triazole-Q $\beta$  (**2.12**; group 2) were included as controls to facilitate identification of non-specific immune responses. Blood samples were collected on days 0, 7, and 35 and glycan-specific antibody titers were evaluated on pooled serum samples of each group against N-glycan-BSA conjugates **2.7c-2.11c** relative to the day 0 pre-bleed. The results were summarized in Table 2.2. As expected, the controls (groups 1 and 2) showed only marginal glycan cross-reactive responses with end-point titers of 720 and 260, respectively. Encouragingly, significant anti-glycan responses were detected in all groups immunized with glycan-Q $\beta$  immunogens. However, low N-glycan-specific antibody titers were observed in groups that received immunogens carrying sialylated N-glycans (S2G2 complex-type N-glycan, **2.7a** and **2.7b**). This result might be partially explained by the fact that sialylated natural N-glycans induce immune tolerance via siglec-sialic acid interactions.<sup>6, 122</sup> Notably, the day 35 titers induced by glycan-Q $\beta$  immunogens containing adipic acid linkers (conjugates **2.7a-2.11a**; groups 4-7) were significantly higher than those found for the triazole-linked glycan-Q $\beta$  immunogens (**2.7b-2.11b**; groups 9-12). These results appear to be consistent with previous reports on similar linker structures which suggest that the immunogenic triazole linker reduces immune responses to glycan antigens, while the less immunogenic linkers such as the adipoyl moiety induce higher titers of glycan-dependent antibodies.<sup>123-125</sup> Interestingly, the glycan-specific antibody titers induced by immunogens carrying smaller N-glycans were higher than those carrying larger N-glycans, with antibody titers against S0G0-Q $\beta$  (**2.9a**; group 5) and Man5-Q $\beta$  (**2.11a**; group 7) being the highest. The day 7 titers also follow this trend for groups 3-7 (Table 2.2). The Man5-adipoyl-Q $\beta$  conjugate (**2.11a**; group 7) was found to be the most immunogenic, giving an excellent titer that is comparable to antibody levels previously reported for glycopeptide immunogens.<sup>110, 126</sup> The high immune response against conjugate **2.11a** as

compared to the other glycan immunogens or conjugate **2.11b** may reflect an immune response mounted against a core glycan epitope accessible on the flexible adipic acid linked conjugate (**2.11a**).

**Table 2.2.** IgG antibody titers determined by ELISA experiments<sup>a)</sup>

Group	Immunogen	R	Linker	Day 7 titer	Day 35 titer	Anti-triazole titer
1	WT-Q $\beta$	-	-	-	720 <sup>b</sup>	-
2	<b>2.12</b>	-OH	triazole	-	260 <sup>b</sup>	3200
3	<b>2.7a</b>	S2G2-GlcNAc <sub>2</sub>	adipic acid	< 50	800	-
4	<b>2.8a</b>	S0G2-GlcNAc <sub>2</sub>	adipic acid	50	12800	-
5	<b>2.9a</b>	S0G0-GlcNAc <sub>2</sub>	adipic acid	200	12800	-
6	<b>2.10a</b>	Man9-GlcNAc <sub>2</sub>	adipic acid	800	12800	-
7	<b>2.11a</b>	Man5-GlcNAc <sub>2</sub>	adipic acid	3200	102400	-
8	<b>2.7b</b>	S2G2-GlcNAc <sub>2</sub>	triazole	100	1600	12800
9	<b>2.8b</b>	S0G2-GlcNAc <sub>2</sub>	triazole	50	800	25600
10	<b>2.9b</b>	S0G0-GlcNAc <sub>2</sub>	triazole	400	3200	800
11	<b>2.10b</b>	Man9-GlcNAc <sub>2</sub>	triazole	1600	3200	12800
12	<b>2.11b</b>	Man5-GlcNAc <sub>2</sub>	triazole	< 50	1600	1600

<sup>a)</sup> Glycan-specific antibody titers for days 7 and 35 were determined by ELISA against the respective N-glycan-BSA conjugates (**2.7c-2.11c**) carrying the same N-glycan. Anti-triazole titers were determined for day 35 antisera against the triazole-BSA conjugate (**2.13**).

<sup>b)</sup> Antibody titer is an average titer against the respective N-glycan-BSA coating antigens (**2.7c-2.11c**).

In contrast, low endpoint titers were observed for groups of mice immunized with the triazole-linked N-glycan-Q $\beta$  immunogens (**2.7b-2.11b**; groups 8-12) and no obvious pattern in glycan-specific titers was found (Table 2.2). In most cases, high anti-triazole titers were observed. However, there was no correlation between anti-triazole titer and N-glycan response, suggesting that the triazole linkage was not solely responsible for the low immunogenicity but might instead be limiting the repertoire of anti-glycan antibodies as reported for mucin-specific antibodies elsewhere.<sup>124</sup> N-glycan-specific IgM antibody titers were also measured and found to

be much lower than the corresponding IgG antibody titers (Table 2.3), indicating successful class-switching induced by the Q $\beta$  carrier protein.

**Table 2.3.** Glycan-specific IgM titers of groups 3-12 measured on day 35 against N-glycan-BSA coating antigens **2.7c-2.11c**.

Group	Immunogen	Glycan (R)	Linker	IgM titer
1	WT-Q $\beta$	-	-	-
2	<b>2.12</b>	-OH	triazole	-
3	<b>2.7a</b>	S2G2-GlcNAc <sub>2</sub>	adipic acid	200
4	<b>2.8a</b>	S0G2-GlcNAc <sub>2</sub>	adipic acid	800
5	<b>2.9a</b>	S0G0-GlcNAc <sub>2</sub>	adipic acid	800
6	<b>2.10a</b>	Man9-GlcNAc <sub>2</sub>	adipic acid	1600
7	<b>2.11a</b>	Man5-GlcNAc <sub>2</sub>	adipic acid	6400
8	<b>2.7b</b>	S2G2-GlcNAc <sub>2</sub>	triazole	3200
9	<b>2.8b</b>	S0G2-GlcNAc <sub>2</sub>	triazole	1600
10	<b>2.9b</b>	S0G0-GlcNAc <sub>2</sub>	triazole	1600
11	<b>2.10b</b>	Man9-GlcNAc <sub>2</sub>	triazole	800
12	<b>2.11b</b>	Man5-GlcNAc <sub>2</sub>	triazole	800

**Glycan microarray characterization of anti-glycan specificity.** The glycan-specificity of mouse polyclonal antisera was determined by glycan microarray containing diverse glycan structures immobilized to an NHS-activated glass slide. Immobilized glycans included various N-glycan isoforms conjugated to BSA by reductive amination, which results in reduction of the first N-acetylglucosamine (GlcNAc) moiety of the N-glycan structures (Fig. 2.3A). As expected, no significant binding was observed by either of the control groups (groups 1 and 2) to the target glycan ligands, except for group 2 antisera which bound strongly to ligands containing a triazole linkage (structure 13, Figure 2.3B). To our surprise, the antisera did not show any significant binding to the N-glycans containing S2G2-GlcNAc<sub>1</sub>, S0G2-GlcNAc<sub>1</sub>, G0-GlcNAc<sub>1</sub>, Man9-GlcNAc<sub>1</sub>, and Man5-GlcNAc<sub>1</sub> immobilized in the glycan array (structures 1-7, Figure 2.3B). Some binding was observed to small oligosaccharide fragments of N-glycans, but none to the

larger structures. For example, an apparent binding was observed towards a mannose- $\alpha(1,6)$ -mannose BSA conjugated disaccharide containing a 5-carbon alkyl diamide linker (structure 6, Figure 2.3A) by antisera from N-glycan-adipoyl-Q $\beta$  (**2.7a-2.11a**) immunized mice (groups 3-7). The data imply that the antisera from these groups might recognize the  $\alpha(1,6)$ -mannose linkage of the core mannose structure common to all N-glycan immunogens. However, the results require further verification. Interestingly, antisera from mice immunized with conjugate **2.10a** (Man9-adipoyl-Q $\beta$ , group 6) showed strong binding toward mannose structure 7 and also bound ligands containing similar mannose linkages, suggesting that the antisera from this group could recognize branched structures on the  $\alpha(1,6)$ -mannose arm such as those containing  $\alpha(1,3)$  and  $\alpha(1,6)$  mannose linkages. In contrast, no binding towards reduced N-glycans or  $\alpha(1,6)$ -mannose structures was observed by group 8-12 antisera elicited by N-glycan-triazole-Q $\beta$  immunogens **2.7b-2.11b** (structures 1-6, Figure 2.3B), suggesting that immunogens **2.7a-2.11a** elicit immune responses against more diverse glycan epitopes when compared to immunogens **2.7b-2.11b**.

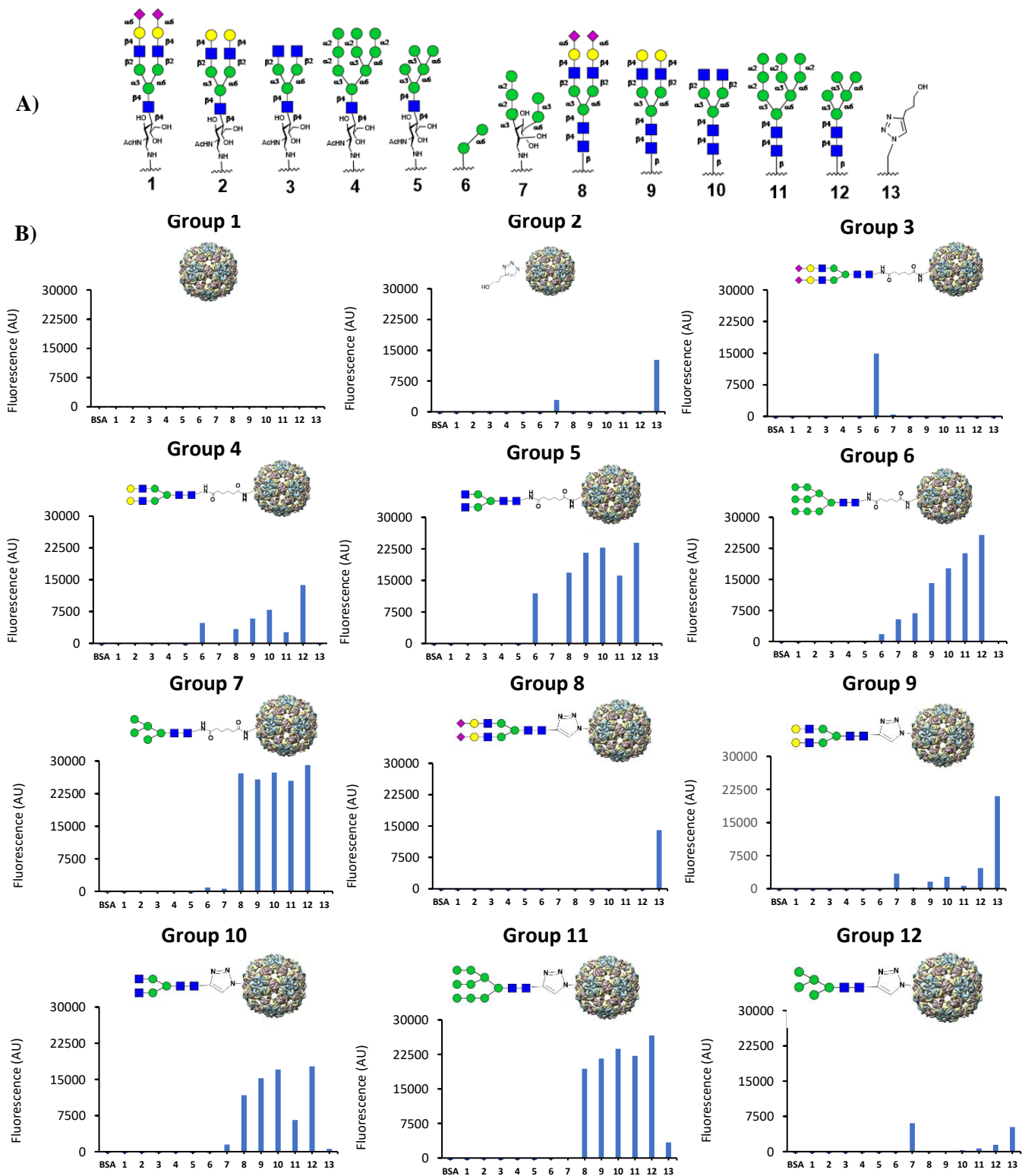


**Figure 2.3.** A) Structures of relevant glycan antigens immobilized on glycan microarray. Antigens 1-5 are N-glycans immobilized by reductive amination, antigens 6 and 7 are synthetic mannose structures, antigens 8-12 are N-glycan antigens with the reducing GlcNAc intact. Antigen 13 is a control ligand for testing binding to the triazole linker. B)

Binding of pooled antisera of six mice from groups 1-12 to antigens 1-13 on glycan microarray. Numerical values on x-axis represent coating antigens from panel A, abbreviated structures of N-glycan-Q $\beta$  immunogens are included above each graph. Fluorescent signal recorded as Raw Fluorescence Units (RFU).

A key difference between the ELISA and glycan microarray assay was the structures of the captured glycan antigens. The glycan microarray experiments were conducted using N-glycan-BSA conjugates prepared by reductive amination, a coupling method that destroys the pyranose structure of the first GlcNAc at the reducing end, giving a ring-opened secondary amine (structures 1-5, Figure 2.3A). However, the coating antigens used for ELISA (N-glycan-BSA conjugates **2.7c-2.11c**) keep the native Asn-linked N-glycans structures intact (structures 8-12, Figure 2.3A). The apparent difference in antibody responses as measured by ELISA using intact N-glycan coating antigens and glycan array with N-glycan coating antigens lacking the first GlcNAc moiety, strongly suggest that the reducing-end GlcNAc structure of the N-glycans could be an essential immune determinant for mounting antibody responses against N-glycans.

To evaluate this hypothesis, we also printed the intact Asn-linked N-glycans on microarray slides (structures 8-12, Figure 2.3A) and performed the glycan array analysis. We found that the antisera from mice immunized with the adipoyl-linked glycan-Q $\beta$  conjugates (**2.8a-2.11a**; groups 4-7) all raised robust and strong antibody responses that recognize the intact N-glycans without apparent specificity. In addition, the antisera from the mice immunized with the triazole-linked glycan-Q $\beta$  conjugates (**2.8b-2.11b**; groups 9-12) also demonstrated binding to the intact N-glycans printed on the slides, but with much lower affinity (Figure 2.3B). Consistent with the ELISA data, antisera from mice (groups 3 and 8) immunized with the sialylated N-glycan-Q $\beta$  conjugates (**2.7a** and **2.7b**) failed to raise significant antibody responses capable of recognizing the N-glycans on the slides. Interestingly, however, antisera from groups 4-6 and groups 9-11 showed a similar pattern of N-glycan recognition, where the observed binding signal

was incrementally higher for truncated N-glycans within each respective complex-type and high-mannose N-glycan class. In other words, the binding signal of pooled serum samples from groups 4-6 or groups 9-11 to the immobilized N-glycan-BSA conjugates increased incrementally when comparing S2G2 to the shorter S0G0 complex-type N-glycan antigens and when comparing Man9 to the smaller Man5 high-mannose N-glycan. This pattern in N-glycan recognition may correlate with increased accessibility to a structure on the reducing end as the N-glycan becomes smaller.

**Epitope mapping of antisera specificity.** To further elucidate the epitope of the glycan specific antibodies, we synthesized BSA conjugates bearing discrete and overlapping structural units common to the reducing end of the N-glycan immunogens. Specifically, BSA conjugates bearing the asparagine moiety (**2.18**), the reducing end GlcNAc (**2.19**), and the chitobiose core (**2.20**) were designed as coating antigens for ELISA (Fig. 2.4A). A BSA conjugate bearing the methylamine-capped squaric acid linker (**2.17**) was also prepared to exclude the possibility that the squaric acid linker was the source of antibody cross-reactivity. BSA conjugates bearing squaric acid, asparagine, and chitobiose were prepared by *de novo* synthesis, whereas the reducing GlcNAc-containing BSA conjugate (**2.19**) was prepared by endoglycosidase digestion of Man5-BSA conjugate **2.11c** with wild-type Endo-CC enzyme from *Coprinopsis cinerea*.<sup>127</sup> Antisera from mice immunized with N-glycan-Q $\beta$  conjugates (groups 3-12) showed minimal binding to coating antigen **2.17** with methylamine-capped squaric acid linker, demonstrating that robust binding was not due to cross-reactivity to the squaric acid linker (Fig. 2.4B).

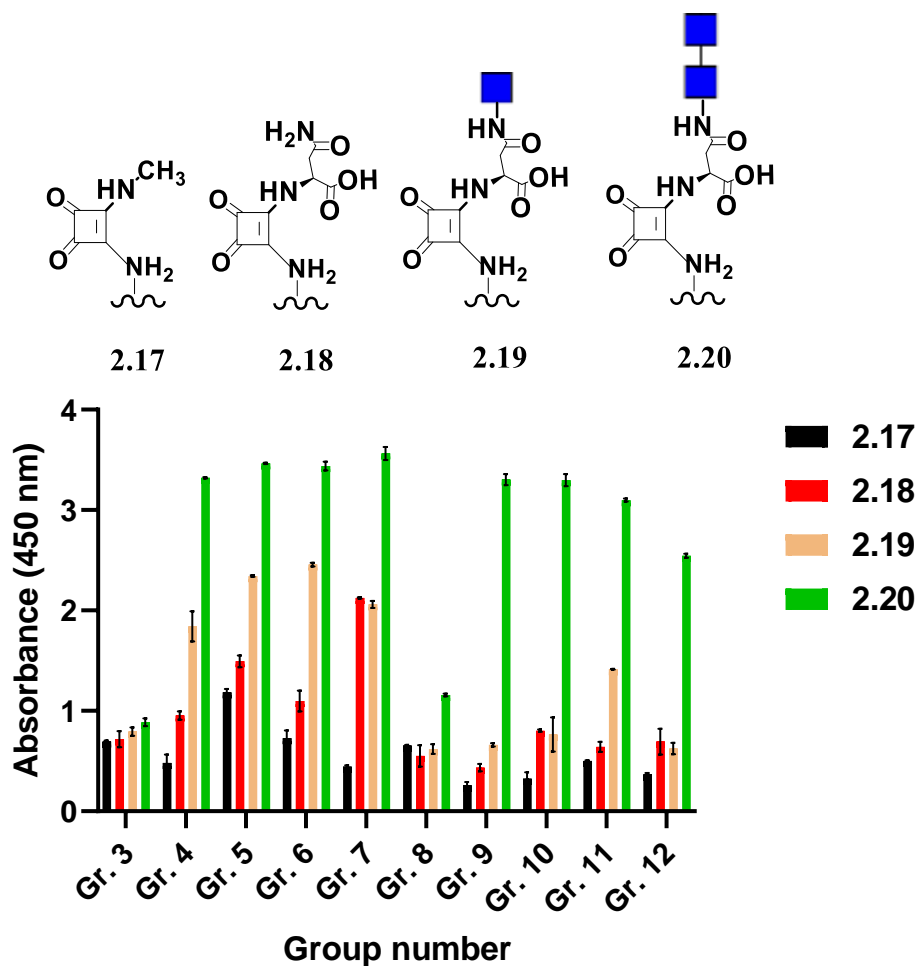


**Figure 2.4.** A) Structures of relevant antigens coated on ELISA plate. B) Binding of pooled antisera of six mice from groups 3-12 to epitopes representing the reducing end of N-glycan immunogens. Numerical values on y-axis are absorbance intensities representative of antisera binding at a 1:200 dilution, antisera from each group were tested in duplicate.

Furthermore, most of the groups showed little binding towards the asparagine amino acid conjugate (2.18), indicating that the asparagine amino acid backbone was not an important epitope for the observed antibody response. One exception was the Man5-adipoyl-Q $\beta$  immunogen (2.11a; group 7) which elicited antibodies with strong cross-reactivity to the Asn structure, partially explaining the high antibody titer observed for this group. Interestingly, a

significant increase in antibody binding was observed towards coating antigen **2.19** bearing the reducing end GlcNAc for groups 4-6. The results suggest that the reducing GlcNAc was a predominant structure responsible for raising the glycan-specific antibody response. However, no significant increase in binding towards this coating antigen was observed for group 7, indicating that the reducing GlcNAc is not an important epitope for antibodies raised by immunogen **2.11a** (Man5-adipoyl-Q $\beta$ ). In contrast, little to no increase in binding was observed towards this same coating antigen by antibodies from N-glycan-triazole-Q $\beta$  immunized groups (groups 8-12), except for the group 11 mice immunized with Man9-triazole-Q $\beta$ . These results clearly show a difference in the specificity of antibodies elicited by N-glycan immunogens prepared with different linker chemistries and suggest that linker chemistry can affect the immunogenicity of nearby structures such as the reducing end GlcNAc.

Lastly, binding of mouse antisera was evaluated against BSA coating antigens bearing the chitobiose core (**2.20**). Strong binding to the chitobiose moiety was observed for all antisera elicited by the N-glycan-Q $\beta$  immunogens (**2.8a-2.11a** and **2.8b-2.11b**; groups 4-7 and 9-12), including those containing different high-mannose and complex type N-glycans. This trend did not hold true for the sialylated N-glycan-Q $\beta$  immunogens (**2.7a** and **2.7b**; groups 3 and 8), however, and can be attributed to their low immunogenicity. These results clearly suggest that the chitobiose core of the N-glycans is an immunodominant epitope that raises antibodies cross-reactive to different N-glycans that carry this moiety. Furthermore, weak but significant binding to SARS-CoV-2 spike protein was observed for antisera from groups 4-6 by ELISA (Figure 2.5), with antibodies from groups 5 and 6 displaying the strongest binding. The reason for the observed differences in binding of SARS-CoV-2 spike protein despite their comparable specificity is not known but may reflect differences in antibody titers to more accessible glycan

epitopes such as the innermost reducing GlcNAc, or the  $\alpha(1,6)$ -mannose arm. Additionally, the affinity of the raised antibodies is not known and could be an important factor affecting the recognition of glycoproteins like the SARS-CoV-2 spike. Nevertheless, this result demonstrates that the elicited chitobiose-specific antibodies can also recognize natural glycoproteins.

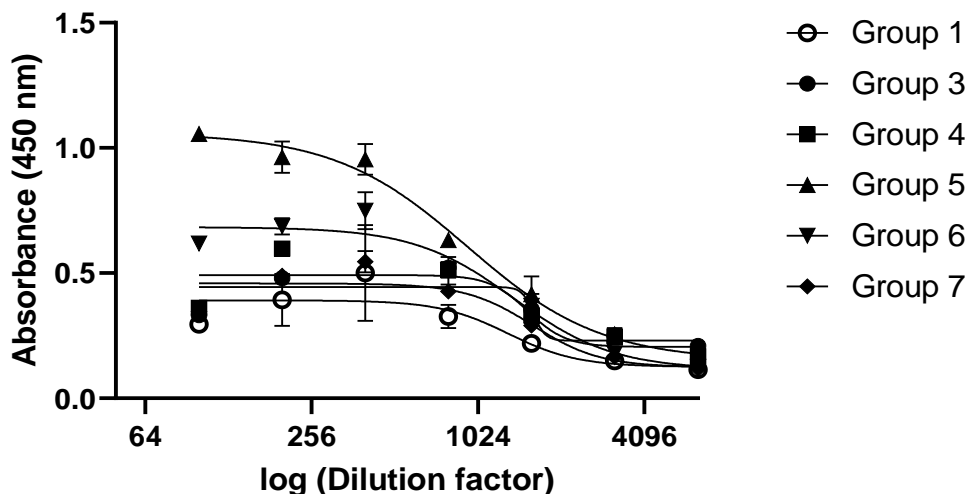


**Figure 2-5.** Binding curves for serial dilutions of antisera from groups 1 and 3-7 against a SARS-CoV-2 spike protein coating antigen.

Recently, Wong and co-workers have reported a similar observation when they attempted to raise hybrid N-glycan-specific antibodies against HIV-1 glycoproteins.<sup>113</sup> They have found that mice immunized with CRM197-based glycoconjugates bearing hybrid-type or truncated high-mannose type N-glycans elicit IgG antibodies that are directed mainly to the chitobiose core and are nonspecific for the N-glycans carried by the immunogens. The authors have further shown that the polyclonal antibodies raised with a chitobiose-CRM197 conjugate could equally recognize complex-type and high-mannose N-glycans by a glycan microarray analysis. Our results are consistent with their findings and provide further information on the binding specificities of N-glycan-specific antibodies. In addition to the findings of immunodominance of

the chitobiose core, we also found that immunogens containing the sialylated N-glycan were poorly immunogenic in comparison with the immunogens carrying high-mannose type or truncated complex type N-glycans. Furthermore, the N-glycan-Q $\beta$  immunogens with adipoyl linker were found to elicit much higher titers of the glycan-dependent antibodies than the corresponding triazole-linked N-glycan-Q $\beta$  conjugates.

In a related study, Krauss and co-workers have shown that 2G12 epitope mimics consisting of oligomannose glycopeptide conjugates, which lack the chitobiose core, elicit antibodies targeting the glycan core instead of the external mannose moieties.<sup>107, 108</sup> The immune response to the mannose core is attributed partially to the fact that endogenous  $\alpha$ -mannosidases trim the outer mannose residues in the immunogens during the immunization.<sup>107, 108</sup> More recently, Ye and co-workers have reported the synthesis and mouse immunization of the CRM197 conjugates of the Man5 core and its fluorinated derivatives that lack the chitobiose core.<sup>128</sup> They have shown that the Man5-CRM197 conjugate failed to raise any measurable glycan-specific antibody responses; the fluorinated Man5-CRM197 conjugates stimulate moderate Man5-dependent antibody responses but they do not show any cross-reactivity toward native HIV-1 gp120 expressing natural Man5GlcNAc<sub>2</sub> epitope. The immune dominance of the chitobiose core as well as the immune tolerance of the extended N-glycan structures, as observed in the present and other related studies, poses a challenge to raise N-glycan specific antibodies through conventional glycoconjugate vaccine design and immunization. It should be noted that in these synthetic glycoconjugate immunogens, the chitobiose moiety of the N-glycans is protruding out through the linkers, making it more accessible and recognizable to the immune system, while the chitobiose moiety of natural N-glycans in the context of glycoproteins is “buried” within the glycoprotein structure and is likely much less accessible. This structural

difference may partially explain the immunodominance of the chitobiose moiety in the “artificial” synthetic glycoconjugate immunogens. Further comparative studies are required to clarify this point.

### **2.3 CONCLUSION**

We report here a facile and selective modification of the Asn-linked N-glycans at the asparagine moiety with chemically compatible handles that allow site-specific bioconjugation to bacteriophage Q $\beta$  or other carrier proteins to make glyco-immunogens or coating antigens. Our immunization studies with the synthetic N-glycan- Q $\beta$  conjugates reveal unexpected antibody responses that were directed largely to the chitobiose core regardless of the N-glycan structures included in the immunogens. Furthermore, we demonstrate that the sialylated N-glycans are much less immunogenic than the high-mannose type or truncated complex type N-glycans. The immune dominance of the chitobiose core of natural N-glycans coupled with the immune tolerance of the extended natural N-glycan structures, may partially explain why very few antibodies have been characterized that are specific for different natural N-glycans. The robust immunogenicity of the chitobiose core also poses a challenge in vaccine design aiming to raise glycan-specific antibodies such as the broadly neutralizing antibodies against HIV-1. One possible solution is to modify the chitobiose core to reduce its immunodominance or to selectively modify the outer monosaccharide moieties to make them more immunogenic and raise antibodies that can specifically recognize the respective natural N-glycoforms.

### **2.4 MATERIALS AND METHODS**

**Materials:** The biantennary complex-type containing sialoglycoprotein (SGP) was prepared from dried hen’s egg yolk following the reported procedure.<sup>115</sup> The high mannose

containing glycoprotein soybean agglutinin was prepared from soybean flour following a previously reported method.<sup>118</sup> *Vibrio cholerae* neuraminidase, Bgaa  $\beta(1,4)$ -galactosidase, and  $\alpha(1,2)$ -mannosidase were overexpressed in *E. coli* BL21(DE3) cells following our previously reported procedure.<sup>118</sup> 1-Ethyl-3-(3-dimethylaminopropyl)carbodiimide (EDC) was purchased from Oakwood Chemical. 10 KDa MWCO spin filters were purchased from Merck. High binding polystyrene 96-well ELISA plates were purchased from Santa Cruz Biotechnology, Inc. All other materials were purchased from Sigma Aldrich unless stated otherwise and used as received.

**General Methods:** Analytical RP-HPLC was performed on a Waters 626 HPLC instrument with a Symmetry 300 C18 column (5.0  $\mu\text{m}$ , 4.6 $\times$ 250 mm). Analytical reverse-phase HPLC was conducted on all alkyne-functionalized glycans using an isocratic gradient of 100% milli-Q water containing 0.1% trifluoroacetic acid as mobile phase A and a flow rate of 1 mL/min, with dual UV detection at 214 nm and 280 nm. Preparative HPLC was performed on a Waters 600 HPLC instrument with preparative reverse-phase C18 column (Waters Symmetry 300, 19 $\times$ 300 mm) and dual UV detection at 214 nm and 280 nm, and at a flow rate of 10 mL/min for all purifications. NMR spectra were measured with Bruker AV III HD NanoBay 400 MHz NMR spectrometer and the chemical shifts were assigned in parts per million. All MALDI-TOF MS experiments were performed using a Bruker Autoflex II MALDI-TOF mass spectrometer. LC ESI-TOF MS was performed using an X-Bridge Shield RP18 3.5  $\mu\text{m}$  (2.1  $\times$  50 mm) short column coupled to a Micromass ZQ-4000 single quadrupole mass spectrometer. High-resolution mass was taken on an Exactive Plus Orbitrap (Thermo Scientific) with an Agilent Poroshell 300SB-C8 column (5  $\mu\text{m}$ , 75  $\times$  1 mm). To monitor reaction progress of glycan-Q $\beta$  conjugates, a 1  $\mu\text{L}$  aliquot was taken from each reaction mixture and mixed with 0.2  $\mu\text{L}$  of 1 M dithiothreitol

(DTT) in separate 0.2mL PCR tubes. These samples were incubated at room temperature for 15 min to fully reduce the Q $\beta$  particle to its individual subunits and then mixed with 1  $\mu$ L Sannapic Acid (SA) matrix before being spotted on the MALDI target plate. After drying, an additional microliter of SA matrix was applied over each spot and the samples were analyzed under linear mode once dry. MALDI samples of BSA conjugates were prepared similarly but without DTT reducing agent. The concentration of each Q $\beta$  conjugate was measured by nanodrop at 280 nm ( $\epsilon = 26.3 \text{ L/g}\cdot\text{cm}$ ). The final concentration of the BSA conjugates were determined by Bradford assay (BioRad) using a BSA standard curve per the manufacturer's instructions.

### **Preparation of Asn-glycan Starting Materials**

N-glycan-Asn starting materials **2.1-2.5** were prepared following our previously reported method.<sup>129</sup>

#### **S2G2-GlcNAc<sub>2</sub>-Asn (2.1).**

72.8 mg, prepared from 200 mg of SGP (44.6% yield). ESI-MS: calcd for C<sub>88</sub>H<sub>144</sub>N<sub>8</sub>O<sub>64</sub>,  $M = 2336.8 \text{ Da}$ ; found,  $m/z$  1169.3 [M + 2H]<sup>2+</sup>, 780.2 [M + 3H]<sup>3+</sup>.

#### **S0G2-GlcNAc<sub>2</sub>-Asn (2.2).**

17.5 mg, prepared from 25 mg of compound **2.1** (93.2% yield). ESI-MS: calcd for C<sub>66</sub>H<sub>110</sub>N<sub>6</sub>O<sub>48</sub>,  $M = 1754.6 \text{ Da}$ ; found,  $m/z$  878.2 [M + 2H]<sup>2+</sup>, 585.9 [M + 3H]<sup>3+</sup>.

#### **S0G0-GlcNAc<sub>2</sub>-Asn (2.3).**

15.3 mg, prepared from 25 mg of compound **2.1** (98% yield). ESI-MS: calcd for C<sub>54</sub>H<sub>90</sub>N<sub>6</sub>O<sub>38</sub>,  $M = 1430.5 \text{ Da}$ , found,  $m/z$  1432.4 [M + 2H], 727.5 [M + Na + H]<sup>2+</sup>, 485.3 [M + Na + 2H]<sup>3+</sup>.

#### **Man9-GlcNAc<sub>2</sub>-Asn (2.4).**

19 mg, prepared from 2 g of crude soybean agglutinin (SBA). ESI-MS: calcd for  $C_{74}H_{124}N_4O_{58}$ ,  $M = 1996.7$  Da, found,  $m/z$  999.6  $[M + 2H]^{2+}$ .

#### **Man5-GlcNAc<sub>2</sub>-Asn (2.5).**

6 mg, prepared from 12 mg of compound **2.4** (74.4% yield). ESI-MS: calcd for  $C_{50}H_{84}N_4O_{38}$ ,  $M = 1348.5$  Da, found,  $m/z$  1349.7  $[M + H]$ , 686.5  $[M + Na + H]^{2+}$ .

#### **Synthesis of disuccinimidyl adipate linker (DSAP)**

Disuccinimidyl adipate was synthesized as previously reported by Narendra, et al <sup>130</sup> and recrystallized from hot isopropanol to afford the target compound as a fine white powder in 40% yield. <sup>130</sup> <sup>1</sup>H-NMR (400 MHz, DMSO-*d*<sub>6</sub>):  $\delta$ (ppm) 1.71–1.74 (m, 4H); 2.73–2.74 (m, 4H); 2.81 (s, 8H).

#### **General method for the synthesis of mono-adipoyl-NHS Functionalized glycans (2.1a-2.5a)**

Glycans **2.1-2.5** (1 mg) were first weighed as lyophilized powders and dissolved in 100  $\mu$ L anhydrous dimethylsulfoxide (DMSO), the solution was heated at 40 °C for five minutes for complete dissolution. The dissolved glycan was transferred to a 2 mL glass vial and while the solution was still stirring, 10 mol equivalents of DSAP linker was dissolved in 100  $\mu$ L DMSO and added slowly. Lastly, 10  $\mu$ L of triethylamine (TEA) was added and the reaction mixture was stirred for 2 h at room temperature. Reaction completion was confirmed by MALDI-TOF-MS at which point the crude product was quickly diluted in 50% aqueous acetonitrile and lyophilized. The white film was then washed thoroughly with 4 mL chloroform (3x) to remove excess DSAP linker. Before utilizing the mono-NHS activated glycan, residual chloroform was removed by lyophilization. Product yield of each pure NHS-functionalized glycan was estimated by LC-MS UV profile.

**S2G2-GlcNAc<sub>2</sub>-Asn mono-NHS (2.1a)**

0.98 mg (90% yield). HRMS (ESI-MS): calcd for C<sub>98</sub>H<sub>155</sub>N<sub>9</sub>O<sub>69</sub>,  $[M + 2H]^{2+} = 1282.4538$  Da;  
found,  $m/z$  1282.4470  $[M + 2H]^{2+}$ .

**S0G2-GlcNAc<sub>2</sub>-Asn mono-NHS (2.2a)**

0.85 mg (75% yield). HRMS (ESI-MS): calcd for C<sub>76</sub>H<sub>121</sub>N<sub>7</sub>O<sub>53</sub>,  $[M + 2H]^{2+} = 990.8567$  Da;  
found,  $m/z$  990.8556  $[M + 2H]^{2+}$ .

**S0G0-GlcNAc<sub>2</sub>-Asn mono-NHS (2.3a)**

1.04 mg (90% yield). HRMS (ESI-MS): calcd for C<sub>64</sub>H<sub>101</sub>N<sub>7</sub>O<sub>43</sub>,  $[M + 2H]^{2+} = 828.8039$  Da;  
found,  $m/z$  828.8028  $[M + 2H]^{2+}$ .

**Man9-GlcNAc<sub>2</sub>-Asn mono-NHS (2.4a)**

0.89 mg (80% yield). HRMS (ESI-MS): calcd for C<sub>84</sub>H<sub>135</sub>N<sub>5</sub>O<sub>63</sub>,  $[M + 2H]^{2+} = 1111.8830$  Da;  
found,  $m/z$  1111.8819  $[M + 2H]^{2+}$ .

**Man5-GlcNAc<sub>2</sub>-Asn mono-NHS (2.5a)**

1.1 mg (95% yield). HRMS (ESI-MS): calcd for C<sub>60</sub>H<sub>95</sub>N<sub>5</sub>O<sub>43</sub>,  $[M + H]^+ = 1574.5474$  Da;  
found,  $m/z$  1574.5469  $[M + H]^+$ .

**General Protocol for the Synthesis of Alkyne- Functionalized Glycans (2.1b-2.5b)**

The 4-pentynoic acid succinimidyl ester starting material was prepared following a previously reported procedure.<sup>131</sup> Glycans **2.1-2.5** (10 mg) were dissolved in 750  $\mu$ L saturated sodium bicarbonate in a 2 mL glass vial. Separately, three mole equivalents of 4-pentynoic acid succinimidyl ester was dissolved in 250  $\mu$ L acetonitrile and added to the glass vial. The reaction

was stirred for 1- 2 h and monitored by MALDI-TOF-MS until consumption of starting material was observed. After reaction completion, the products were purified by Sepharose G15 and finally reverse-phase preparative HPLC using a 5- 15% acetonitrile (0.1 % TFA) gradient over thirty minutes. Product purity was evaluated by LC ESI-TOF-MS, pure fractions were combined and lyophilized together to give the alkyne functionalized N-glycans. Proton chemical shifts were assigned according to reports by Kajihara, Pancera, and Shahzad-ul-Hussan.<sup>132-134</sup>

#### S2G2-GlcNAc<sub>2</sub>-Asn-Alkyne (**2.1b**)

Isolated in 61% yield (6.3 mg) after RP18-HPLC. <sup>1</sup>H-NMR (400 MHz, D<sub>2</sub>O): δ 5.11 (d, 1H, J = 5.9 Hz, Man-4 H-1), 5.03 (d, 1H, J = 6.4 Hz, GlcNAc-1 H-1), 4.92 (d, 1H, J = 6.9 Hz, Man-4' H-1), 4.60-4.55 (m, 3H, 2, GlcNAc-5 and GlcNAc-5' H-1), 4.46-4.43 (m, 2H, Gal-6 and Gal-6' H-1), 4.24 (s, 1H, Man-3 H-2), 4.18 (s, 1H, Man-4 H-2), 4.10 (s, 1H, Man-4' H-2), 4.04-3.47, 2.89-2.81 (m, 2H, Asn-CH<sub>2</sub>), 2.66-2.63 (m, 2H, NeuAc-7' and NeuAc-7 eq H-3), 2.48 (s, 4H, Alkyne-CH<sub>2</sub>), 2.35 (s, 1H, Alkyne C-H), 2.06-1.98 (m, 18H, NHAc), 1.78-1.75 (m, 2H, NeuAc-7' and NeuAc-7 ax H-3). <sup>13</sup>C-NMR (125 MHz, D<sub>2</sub>O): δ 174.9, 174.8, 174.7, 174.6, 174.4, 174.1, 173.9, 172.7, 102.9, 101.3, 100.4, 99.6, 99.5, 97.0, 95.5, 83.2, 80.4, 78.7, 78.5, 78.3, 76.4, 76.2, 75.3, 74.7, 74.4, 73.5, 72.9, 72.7, 72.5, 71.9, 71.4, 70.9, 70.4, 70.2, 70.2, 69.4, 68.5, 68.4, 68.3, 67.9, 67.3, 66.8, 63.2, 62.8, 61.6, 61.0, 59.9, 54.9, 54.9, 53.8, 52.1, 51.8 36.9, 34.1, 22.3. Analytical HPLC: t<sub>R</sub> = 13.4 min. HRMS (ESI-MS): calcd for C<sub>93</sub>H<sub>148</sub>N<sub>8</sub>O<sub>65</sub>, [M + 2H]<sup>2+</sup> = 1209.9351 Da; found, m/z 1209.9301 [M + 2H]<sup>2+</sup>.

#### S0G2-GlcNAc<sub>2</sub>-Asn-Alkyne (**2.2b**)

Isolated in 63% yield (6.6 mg) after RP18-HPLC. <sup>1</sup>H-NMR (400 MHz, D<sub>2</sub>O): δ 5.11 (s, 1H, Man-4 H-1), 5.04 (d, 1H, J = 6.5 Hz, GlcNAc-1 H-1), 4.92 (s, 1H, Man-4' H-1), 4.61-4.56 (m,

3H, GlcNAc-5 and GlcNAc-5' H-1), 4.47-4.45 (dd, 2H,  $J = 2.4, 5$  Hz, Gal-6 and Gal-6' H-1), 4.24 (s, 1H, Man-3 H-2), 4.18 (s, 1H, Man-4 H-2), 4.10 (s, 1H, Man-4' H-2), 3.98-3.46, 2.85-2.83 (m, 2H, Asn-CH<sub>2</sub>), 2.49 (s, 4H, Alkyne-CH<sub>2</sub>), 2.36 (s, 1H, Alkyne C-H), 2.07-1.99 (m, 12H, NHAc). <sup>13</sup>C-NMR (125 MHz, D<sub>2</sub>O):  $\delta$  174.8, 174.7, 174.6, 174.4, 172.7, 102.9, 102.9, 101.3, 100.4, 99.6, 99.5, 97.0, 83.3, 80.4, 79.5, 78.7, 78.5, 78.2, 76.4, 76.3, 76.2, 75.4, 74.7, 74.7, 74.4, 73.6, 72.9, 72.7, 72.5, 72.0, 71.9, 70.9, 70.2, 69.5, 69.4, 68.5, 67.4, 65.7, 61.6, 61.0, 59.9, 54.9, 54.9, 53.8, 37.0, 34.1, 22.3, 22.2, 22.1, 14.4. Analytical HPLC:  $t_R = 11.3$  min. HRMS (ESI-MS): calcd for C<sub>71</sub>H<sub>114</sub>N<sub>6</sub>O<sub>49</sub>,  $[M + 2H]^{2+} = 918.3382$  Da; found,  $m/z$  918.3328  $[M + 2H]^{2+}$ .

#### S0G0-GlcNAc<sub>2</sub>-Asn-Alkyne (**2.3b**)

Isolated in 58% yield (5 mg) after RP18-HPLC. <sup>1</sup>H-NMR (400 MHz, D<sub>2</sub>O):  $\delta$  5.10 (s, 1H, Man-4 H-1), 5.03 (d, 1H,  $J = 6.4$  Hz, GlcNAc-1 H-1), 4.90 (s, 1H, Man-4' H-1), 4.71 (t, 1H,  $J = 3.8$  Hz, Man-3 H-1), 4.60 (d, 1H,  $J = 5.3$  Hz, GlcNAc-2 H-1), 4.54 (d, 2H,  $J = 5.6$  Hz, GlcNAc-5 and GlcNAc-5' H-1), 4.24 (s, 1H, Man-3 H-2), 4.17 (s, 1H, Man-4 H-2), 4.09 (s, 1H, Man-4' H-2), 3.96-3.39 ppm, 2.83 (m, 2H, Asn-CH<sub>2</sub>), 2.48 (s, 4H, Alkyne-CH<sub>2</sub>), 2.35 (s, 1H, Alkyne C-H), 2.06-1.99 (m, 12H, NHAc). <sup>13</sup>C-NMR (125 MHz, D<sub>2</sub>O):  $\delta$  174.8, 174.8, 174.7, 174.5, 174.3, 172.8, 101.3, 100.4, 99.6, 97.0, 83.3, 80.5, 79.5, 78.6, 78.2, 76.4, 76.3, 76.2, 75.8, 74.4, 74.3, 73.6, 73.4, 73.3, 72.9, 72.7, 71.9, 70.3, 70.2, 69.9, 69.5, 69.4, 67.3, 67.3, 67.1, 65.9, 65.7, 63.2, 61.7, 61.6, 60.6, 59.9, 59.9, 55.3, 54.9, 53.8, 49.3, 37.1, 34.1, 22.3, 22.2, 22.1. Analytical HPLC:  $t_R = 10.6$  min. HRMS (ESI-MS): calcd for C<sub>59</sub>H<sub>94</sub>N<sub>6</sub>O<sub>39</sub>,  $[M + 2H]^{2+} = 756.2851$  Da; found,  $m/z$  756.2839  $[M + 2H]^{2+}$ .

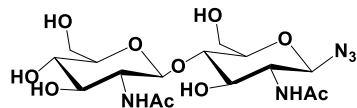
#### Man9-GlcNAc<sub>2</sub>-Asn-Alkyne (**2.4b**)

Isolated in 72% yield (7.5 mg) after RP18-HPLC. <sup>1</sup>H-NMR (400 MHz, D<sub>2</sub>O): δ 5.30 (s, 1H, ManA H-1), 5.23 (s, 1H, Man4 H-1), 5.21 (s, 1H, ManC H-1), 5.04 (s, 1H, ManB H-1), 4.96-4.94 (m, 3H, ManD1, ManD2, ManD3 H-1), 4.76 (s, 1H, Man4' H-1), 4.50 (d, 1H, J = 5.2 Hz, GlcNAc2 H-1), 4.13-4.12 (m, 1H, Man3 H-2), 4.05 (s, 1H, Man4' H-2), 4.01-3.48, 2.79-2.72 (m, 2H, Asn-CH<sub>2</sub>), 2.40 (m, 4H, Alkyne CH<sub>2</sub>), 2.26 (s, 1H, Alkyne CH), 1.96 (s, 3H, NHAc), 1.90 (s, 3H, NHAc). <sup>13</sup>C-NMR (125 MHz, D<sub>2</sub>O): 174.7, 174.5, 174.4, 174.4, 172.8, 102.2, 101.3, 100.8, 100.6, 100.2, 99.6, 98.0, 83.3, 81.1, 78.9, 78.6, 78.5, 78.2, 74.6, 74.2, 73.4, 73.3, 73.2, 73.2, 72.7, 71.9, 71.2, 70.3, 70.2, 70.1, 69.9, 69.4, 67.0, 66.9, 66.8, 66.8, 65.6, 65.4, 64.9, 61.0, 60.0, 59.9, 55.0, 53.8, 37.1, 34.1, 22.2, 22.0, 14.4. Analytical HPLC: t<sub>R</sub> = 9.4 min. HRMS (ESI-MS): calcd for C<sub>79</sub>H<sub>128</sub>N<sub>4</sub>O<sub>59</sub>, [M + 2H]<sup>2+</sup> = 1039.3642 Da; found, m/z 1039.3643 [M + 2H]<sup>2+</sup>.

#### Man5-GlcNAc<sub>2</sub>-Asn-Alkyne (**2.5b**)

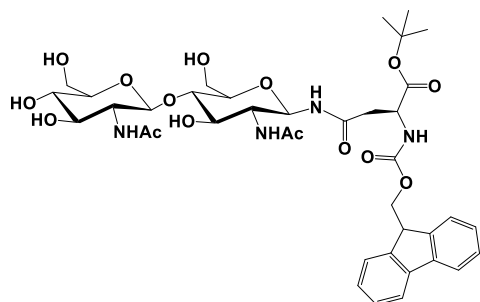
Isolated in 67% yield (7.1 mg) after RP18-HPLC. <sup>1</sup>H-NMR (400 MHz, D<sub>2</sub>O): δ 4.99-4.98 (m, 2H, ManE and ManF H-1), 4.94 (d, 1H, J = 6.4 Hz, ManG H-1), 4.80 (s, 1H, ManD H-1), 4.76 (s, 1H, ManC H-1), 4.50-4.49 (d, 1H, J = 5.2 Hz, GlcNAc-B H-1), 4.15 (m, 1H, ManC H-2), 4.04-4.03 (m, 1H, ManD H-2), 3.97-3.95 (m, 2H, ManE and ManF H-2), 3.89-3.44, 2.79-2.71 (m, 2H, Asn-CH<sub>2</sub>), 2.39 (s, 4H, Alkyne CH<sub>2</sub>), 2.26 (s, 1H, Alkyne CH), 1.95 (s, 3H, NHAc), 1.90 (s, 3H, NHAc). <sup>13</sup>C-NMR (125 MHz, D<sub>2</sub>O): δ 174.7, 174.5, 174.4, 174.3, 172.7, 102.5, 102.3, 101.4, 100.4, 99.9, 99.3, 83.2, 80.6, 79.5, 78.6, 74.5, 74.4, 73.3, 72.7, 71.9, 70.8, 70.6, 70.3, 70.2, 70.1, 69.9, 69.9, 69.4, 66.9, 66.7, 66.7, 65.9, 65.6, 65.5, 65.2, 61.0, 60.9, 59.9, 54.9, 53.8, 36.9, 34.1, 22.2, 22.0, 14.3. Analytical HPLC: t<sub>R</sub> = 10.7 min. HRMS (ESI-MS): calcd for C<sub>55</sub>H<sub>88</sub>N<sub>4</sub>O<sub>39</sub>, [M + H]<sup>+</sup> = 1429.5099 Da; found, m/z 1429.5125 [M + H]<sup>+</sup>.

#### Synthesis of Chitobiose-azide



Chitobiose azide was prepared from 50 mg chitobiose following the method of Tanaka, et al,<sup>135</sup> the final product was purified by preparative HPLC using a 100 % isocratic gradient of water containing 0.1 % formic acid. The final product (27 mg) was obtained as a fluffly white solid in 51 % yield.  $C_{16}H_{27}N_5O_{10}$ ,  $[M + H]^+ = 450.2$  Da; found,  $m/z$  450.3  $[M + H]^+$ .

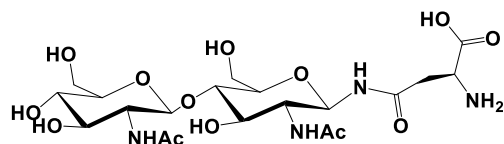
### Synthesis of Fmoc-Asn (Chitobiose)-OtBu



To a solution of chitobiose- $N_3$  (13.5 mg, 30  $\mu$ mol) in 2 mL DMF was added 10% w/v Pd/C (palladium on carbon) and this mixture was stirred vigorously under a hydrogen balloon for two hours. After reaction completion as judged by TLC, the chitobiose- $NH_2$  aminoglycoside was filtered through Celite and used directly in the next reaction step without further purification. Fmoc-Asn (Chitobiose)-OtBu was prepared according to method by Mallesham, et al with the exception that HBTU was replaced with HATU as coupling reagent.<sup>136</sup> The final compound, Fmoc-Asn (Chitobiose)-OtBu, was purified by reverse-phase preparative HPLC using a 20-70 % gradient of acetonitrile (0.1% formic acid) over 30 minutes and obtained in 35% yield.

$C_{39}H_{52}N_4O_{15}$ ,  $[M + H]^+ = 817.3$  Da; found,  $m/z$  817.3  $[M + H]^+$ .

### Synthesis of Chitobiose-Asn



Chitobiose-Asn was prepared by standard Fmoc deprotection using 20% piperidine in DMSO, the compound was lyophilized and the t-butyl protecting group was then removed by stirring in 50% DCM/ TFA solution for 6 hours as described by Mallesham, et al.<sup>136</sup> The target compound was purified by reverse-phase preparative HPLC using a 100% isocratic gradient of water (0.1% formic acid) over 30 minutes and obtained in 95% yield. <sup>1</sup>H-NMR (400 MHz, D<sub>2</sub>O): δ 5.04 (d, 1H, J = 9.6 Hz), 4.56 (d, 1H, J = 8.0 Hz), 4.16 (t, 1H, J = 5.2 Hz), 3.87-3.4 (m, 14H), 3.12 (t, 1H, J = 5.6 Hz), 2.95 (d, 2H, J = 5.6 Hz), 2.03 (s, 3H), 1.97 (s, 3H). <sup>13</sup>C-NMR (125 MHz, D<sub>2</sub>O): δ 174.8, 174.6, 171.8, 171.7, 101.3, 78.7, 78.1, 76.2, 75.9, 73.4, 72.7, 69.6, 60.5, 59.8, 55.5, 53.6, 49.8, 44.5, 38.7, 34.5, 22.2, 22.0, 21.9, 21.4. ESI-MS: calcd for C<sub>20</sub>H<sub>34</sub>N<sub>4</sub>O<sub>13</sub>, [M + H]<sup>+</sup> = 539.2 Da; found, m/z 539.3 [M + H]<sup>+</sup>.

### **General method for the synthesis of methoxy-squaric acid functionalized N-glycans (2.1c-2.5c) and Chitobiose.**

Glycans **2.1-2.5** or chitobiose (4 mg) were weighed out as lyophilized solids in separate 0.2 mL tubes and 150 μL 100 mM phosphate buffer pH 7.4 was then added. In a separate 0.2 mL tube, 2.6 mg 3,4-dimethoxy-3-cyclobutene-1,2-dione (20 mol equiv.) was weighed and dissolved in 50 μL 100 mM phosphate buffer pH 7.4 followed by 10 μL DMSO to completely dissolve the solid. The solutions were mixed and incubated at 37 °C, reaction progress was monitored by MALDI-TOF-MS. After 1 h, the mixture was purified by Sepharose G15 and lyophilized to obtain the methoxy-squarate functionalized N-glycans in high yield.

### **S2G2-GlcNAc<sub>2</sub>-Asn squaric acid monoamide (2.1c).**

3.4 mg (81% yield). HRMS (ESI-MS): calcd for C<sub>93</sub>H<sub>146</sub>N<sub>8</sub>O<sub>67</sub>,  $[M + 2H]^{2+} = 1224.9221$  Da; found,  $m/z$  1224.9170  $[M + 2H]^{2+}$ .

**S0G2-GlcNAc<sub>2</sub>-Asn squaric acid monoamide (2.2c).**

3.2 mg (76% yield). HRMS (ESI-MS): calcd for C<sub>71</sub>H<sub>112</sub>N<sub>6</sub>O<sub>51</sub>,  $[M + 2H]^{2+} = 933.3250$  Da; found,  $m/z$  933.3237  $[M + 2H]^{2+}$ .

**S0G0-GlcNAc<sub>2</sub>-Asn squaric acid monoamide (2.3c).**

3.6 mg (84% yield). HRMS (ESI-MS): calcd for C<sub>59</sub>H<sub>92</sub>N<sub>6</sub>O<sub>41</sub>,  $[M + 2H]^{2+} = 771.2722$  Da; found,  $m/z$  771.2728  $[M + 2H]^{2+}$ .

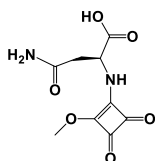
**Man9-GlcNAc<sub>2</sub>-Asn squaric acid monoamide (2.4c).**

2.8 mg (66% yield). HRMS (ESI-MS): calcd for C<sub>79</sub>H<sub>126</sub>N<sub>4</sub>O<sub>61</sub>,  $[M + 2H]^{2+} = 1054.3513$  Da; found,  $m/z$  1054.3530  $[M + 2H]^{2+}$ .

**Man5-GlcNAc<sub>2</sub>-Asn squaric acid monoamide (2.5c).**

3.6 mg (84% yield). HRMS (ESI-MS): calcd for C<sub>55</sub>H<sub>86</sub>N<sub>4</sub>O<sub>41</sub>,  $[M + H]^+ = 1459.4841$  Da; found,  $m/z$  1459.4880  $[M + H]^+$ .

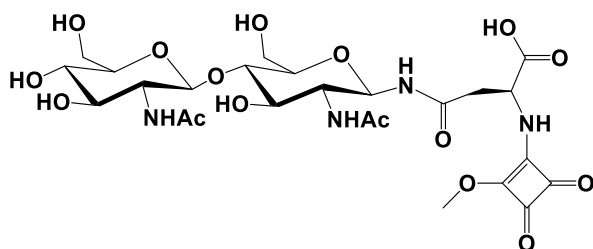
**Synthesis of mehoxy-squaric acid functionalized Asparagine (2.13)**



Squaric acid (16.1 mg, 0.1 mmol) was dissolved in 100  $\mu$ L DMSO and pH was neutralized by addition of 56  $\mu$ L 2 M NaOH. Asparagine (5 mg, 0.04 mmol) was dissolved in 100  $\mu$ L, mixed with the squaric acid solution, and incubated at 37  $^{\circ}$ C for one hour. The target compound was

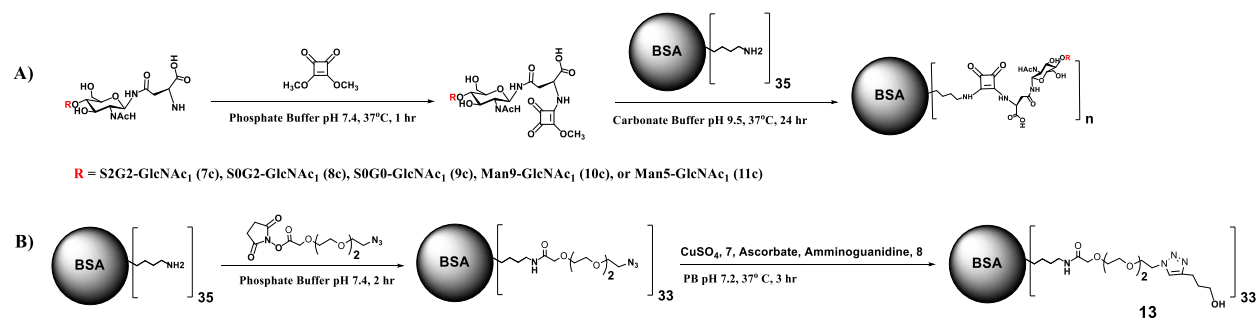
lyophilized and purified by reverse-phase HPLC using a 100 % isocratic gradient of water (0.1% formic acid) over 15 min. Methoxy-squaric acid Asparagine monoamide was isolated in 63.1 % yield. ESI-MS: calcd for  $C_9H_{10}N_2O_6$ ,  $[M + H]^+ = 243.1$  Da; found,  $m/z$  243.1  $[M + H]^+$ .

### Chitobiose-Asn squaric acid monoamide (2.14).



4.7 mg (98% yield) after size exclusion on a P2 column. ESI-MS: calcd for  $C_{25}H_{36}N_4O_{16}$ ,  $[M + H]^+ = 649.2$  Da; found,  $m/z$  649.1  $[M + H]^+$ .

### Synthesis of N-glycan-BSA (2.7c-2.11c) and triazole-BSA (2.21) coating antigens for ELISA



**Scheme S1.** A) Synthesis of N-glycan squaric acid monoamides and N-glycan-BSA conjugates **2.7c-2.11c**. B) Synthesis of triazole-BSA coating antigen **2.21**.

Commercial grade bovine serum albumin was weighed (1 mg, 15  $\mu$ mol) and dissolved in 150  $\mu$ L 200 mM carbonate buffer pH 9.5 in a 0.2 mL tube. Each methoxy-squarate functionalized glycan was weighed (0.9 mmol, 60 equiv.) as a lyophilized powder and dissolved in 50  $\mu$ L 200 mM carbonate buffer. The two solutions were mixed and incubated at 37 °C for approximately 18 hours. The reaction was monitored by MALDI-TOF-MS relative to the free BSA negative control (MW: 66,341 Da) to determine the number of glycans appended using the formula

below. The reaction was complete after 16-18 h, with 8-10 glycans appended on each glycan-BSA conjugate (**2.7c-2.11c**). Interestingly, an intermediate number of glycans (4-6) could be appended by incubating for 6 h at 37 °C. It should also be noted that the squaric acid linker is not stable at high pH, and extended incubation periods beyond 36 h are not recommended. The BSA-Triazole conjugate (**2.21**) was prepared by reacting 1 mg native BSA with 60 equivalents of the azido-(PEG)<sub>3</sub> NHS ester in 100 mM PB pH 7.4 for two hours at room temperature. The intermediate was purified by ultracentrifugation over a 10K MWCO spin filter, and then reacted with 50 equivalents 4-pentyn-1-ol using the same condition outlined above for the Qβ-triazole control immunogen. The final BSA-conjugates were purified by dialysis against water and then lyophilized. The fluffy solids were then redissolved in 1 mL Milli-Q H<sub>2</sub>O and diluted to a 5 ug/mL working concentration in PBS before used for coating the 96-well plates. Product yield was ≥ 90% for each conjugate.

$$n = \frac{(MW \text{ of glycan-BSA conjugate}) - (MW \text{ of free BSA})}{(Mass \text{ of N-glycan} + linker)}$$

### **Synthesis of BSA conjugates for epitope mapping studies**

Dimethoxy-squaric acid, Asn-squaric acid monoamide, or Chitobiose-Asn squaric acid monoamide (0.44 mmol, 30 equiv.) were dissolved in 200 mM carbonate pH 9.5 buffer with DMSO as cosolvent and reacted with BSA (1 mg, 15 μmol) as described for the N-glycan-BSA conjugates above. In each case, the reaction was complete after approximately six hours at 37° C as judged by MALDI-TOF MS. BSA reacted with dimethoxy-squaric acid was then capped with a 2% methylamine solution (w/v) in 200 mM carbonate buffer for 1 hour. All conjugates were purified over 10 kDa MWCO spin filter and recovered in ≥ 90% yield.

BSA conjugates bearing the reducing GlcNAc (i.e. GlcNAc-Asn-squarate-BSA) were prepared by digestion of 100  $\mu$ g conjugate Man5-BSA (**2.11c**) with wild-type Endo-CC endoglycosidase at a 1:100 enzyme: substrate ration (w/w) at 37 °C. After 48 hours, the reaction did not proceed even with further addition of enzyme, MALDI-TOF MS was used to confirm reaction completion. The final conjugate was used directly for ELISA without further purification.

### **Synthesis of Q $\beta$ -adipoyl-glycan conjugates (2.7a-2.11a).**

Bacteriophage Q $\beta$  was expressed in BL21 (*DE3*) *E. coli* cells according to a previously published procedure.<sup>137</sup> The mono-NHS activated glycans hydrolyze quickly in water and so reaction conditions had to be optimized to yield glycan-Asn-adipoyl-Q $\beta$  conjugates with moderate to high glycan loading. Glycan-Asn-adipoyl-NHS (2.8  $\mu$ mol, 40 equivalents) in a phosphate buffer (110  $\mu$ L, 100 mM, pH 7.4) was added to a solution of WT Q $\beta$  (7 mg/ mL, 7x10<sup>-8</sup> mol subunit, 160 uL) and the mixture was incubated at room temperature and reaction progress was monitored by MALDI-TOF-MS. After 2 h, the reactions had achieved suitable glycan loading and so were quenched by adding a Tris buffer (1 M, pH 7.4) to the reaction mixture. Lastly, purification of N-glycan-Q $\beta$  conjugates **2.7a-2.11a** was carried out by dialysis against PBS buffer (50 mM, pH 7.4) using a dialysis bag (MWCO 300 KDa, BIOTECH CE TRIAL<sup>®</sup>) and final glycan loading was determined by reducing SDS-PAGE. Product yield ranged from 70-95% after dialysis.

### **Synthesis of Q $\beta$ -(PEG)<sub>3</sub>-triazole-glycan conjugates (2.7b-2.11b), and triazole control (2.12).**

Azido-modified Q $\beta$  particles were prepared by acylation of free lysines with 16 equivalents of NHS-(PEG)<sub>3</sub>-N<sub>3</sub> in a phosphate buffer (100 mM, pH 7.2) supplemented with 10% DMSO to

provide Q $\beta$  particles functionalized with 270 azide groups.<sup>119</sup> The Q $\beta$ -(PEG)<sub>3</sub>-N<sub>3</sub> conjugate **2.6** was then purified by dialysis against water.

To perform the glycan-Q $\beta$  click reaction, **2.6** (900  $\mu$ L, 1.1 mg/mL in water,  $7 \times 10^{-8}$  mol subunit, 0.17  $\mu$ mol azide) was mixed with 1M phosphate buffer (pH 7.2, final 100 mM), 50% sucrose (final 10%), alkyne-tagged N-glycans **2.1b-2.5b** (4 equiv./ Q $\beta$  subunit), pre-mixed Cu-THPTA solution (CuSO<sub>4</sub>, 500 mM in water [4 equiv] + THPTA ligand, 1 M in water [20 equiv.]), aminoguanidinium chloride (1 M in water, 100 equiv. compared to **2.6**), and sodium ascorbate (1 M in water, 100 equiv. compared to **2.6**). After addition of sodium ascorbate, the reaction tubes were flushed with argon and sealed. The mixture was shaken at 37°C for one overnight (~24 h), and the reaction monitored by MALDI-TOF MS. The Q $\beta$  neoglycoconjugates had not reached a desirable loading and so were further elaborated by adding fresh click reagents as outlined above. Only 2-3 additional equivalents of glycan-Asn-alkyne were needed to push the reaction to a desirable glycan loading. The reaction was continued for another 16 hours at 37°C before the remaining unreacted azido groups on the Q $\beta$  virion were capped in a second CuAAC reaction with a large excess (50 equiv. compared to **2.6**) of 4-pentyn-1-ol over 2 hours.

Purification of N-glycan-Q $\beta$  conjugates was done by dialysis to afford target N-glycan-Q $\beta$  conjugates **2.7b-2.11b**. For the Q $\beta$ -Triazole control immunogen, **2.6** was reacted with 4-pentyn-1-ol (50 equiv. compared to Q $\beta$  subunit) in the presence of the other click reagents as described above. The final conjugate (**2.12**) was purified by dialysis in the same way as the N-glycan-Q $\beta$  conjugates. The final glycan loading was evaluated by denaturing SDS PAGE. Product yield for each conjugate ranged from 60-90% after dialysis.

### **Mouse Immunization.**

Pathogen-free C57BL/6 female mice age 5-6 weeks were received and monitored for a 72 hour quarantine period before study initiation at Washington Biotechnology, Inc in Baltimore, MD. All animal care procedures and experimental protocols have been approved by the Institutional Animal Care and Use Committee of University of Maryland. Groups of six C57BL/6 mice were injected subcutaneously under the scruff on day 0 with various Q $\beta$  conjugates as emulsions in complete Freund's adjuvant (0.1 mL, Fisher), final concentrations of each conjugate were adjusted so that 4  $\mu$ g glycan antigen was delivered with every injection. Boosters were given in incomplete Freund's adjuvant subcutaneously under the scruff on days 14 and 28 with the conjugates as emulsions in incomplete Freund's adjuvant (0.1 mL) adjuvant. Blood (200-500  $\mu$ L) was collected from all groups of mice on days 0, 7, and 35. Sera from each group of mice were isolated and kept frozen at -80  $^{\circ}$ C until further analysis.

#### **ELISA Evaluation of Antibody Titer.**

N-glycan-BSA conjugates **2.7c-2.11c** or triazole-BSA conjugate **2.13** were diluted to a final concentration of 5  $\mu$ g/mL in 1X PBS pH 7.4 and 100  $\mu$ L of this stock solution was added in duplicate to a high-binding polystyrene 96-well plate (Santa-Cruz Biotechnology Inc.). Microplates were incubated at 4  $^{\circ}$ C overnight and washed three times with 200  $\mu$ L PBST (PBS pH 7.4 with 0.05% Tween-20), also referred to as washing buffer. This washing step was repeated after every incubation step unless otherwise noted. Microplates were then blocked with 300  $\mu$ L of a 2% w/v BSA solution in 1X PBS and incubated at 37  $^{\circ}$ C for one hour. After washing, aliquots of pooled mouse sera from each group were diluted 1: 50 to a final volume of 400  $\mu$ L in 1X PBS and 100  $\mu$ L of this solution was added in duplicate to the plate. The remaining volume was diluted 1:2 by adding 200  $\mu$ L PBS, and after mixing, 100  $\mu$ L of the diluted antisera was added in duplicate to the 96-well plate. This was repeated for 12 serial

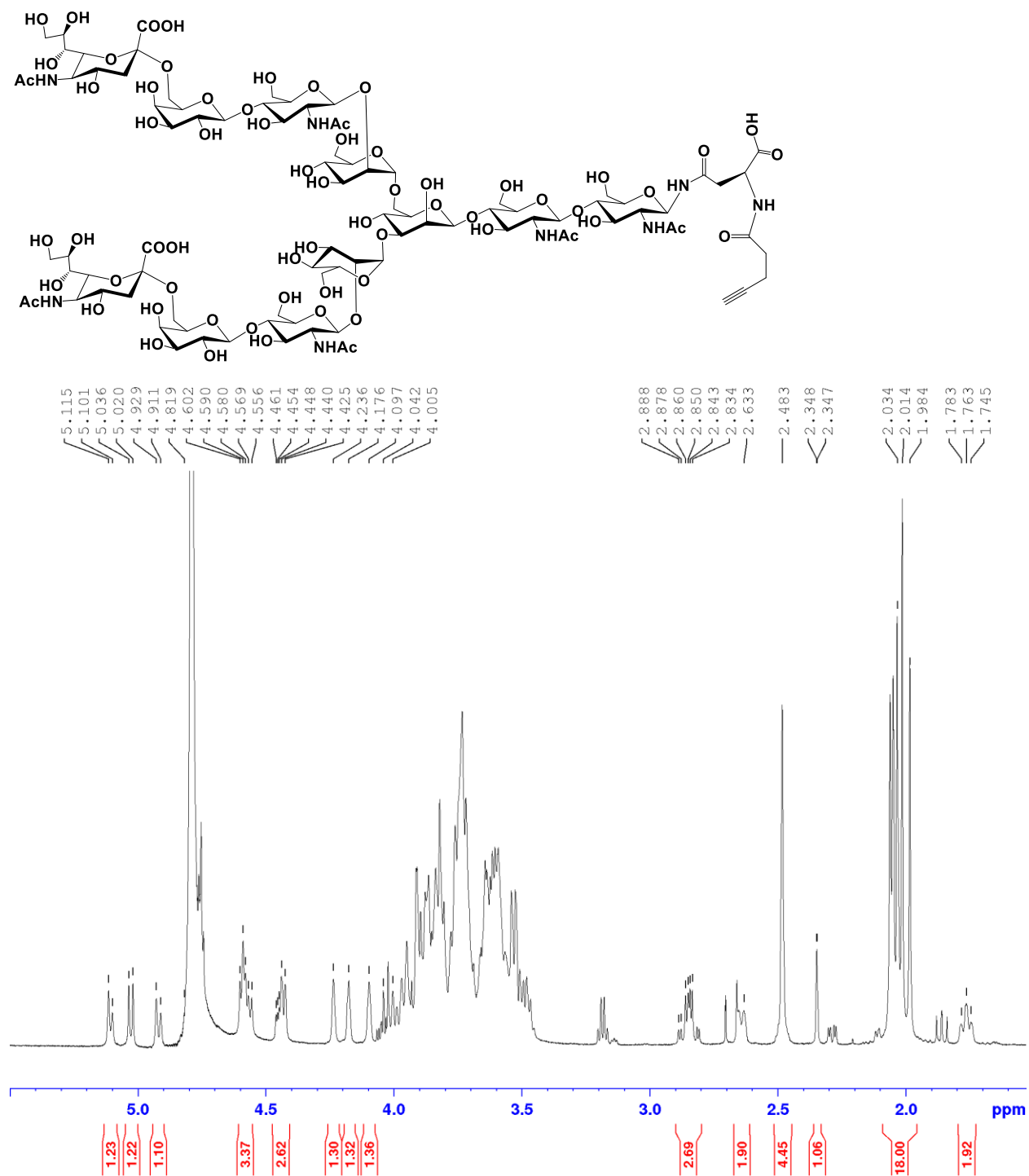
dilutions. The plate was incubated for 1 h at room temperature and then washed four times with washing buffer. Then a 1: 20,000 dilution of goat anti-mouse IgG-HRP secondary antibody (Invitrogen) was prepared in 1X PBS, and 100  $\mu$ L of this solution was added to each well. After washing five times with washing buffer, a 1:1 v/v mix of KPL Peroxidase substrate and KPL solution B (Seracare) was prepared, and 100  $\mu$ L of this mixture was added to each well. After a 30 minute incubation in the dark, 100  $\mu$ L of 1 M  $H_3PO_4$  stop solution was added to each well and the absorbance read at 450 nm with background correction at 550 nm in a Spectramax M5e microplate reader (Molecular Devices). IgM antibody titers were measured as outlined above but using a goat anti-mouse IgM secondary antibody with HRP label (Novus) at 1: 25,000 dilution in PBS.

### **Glycan Microarray**

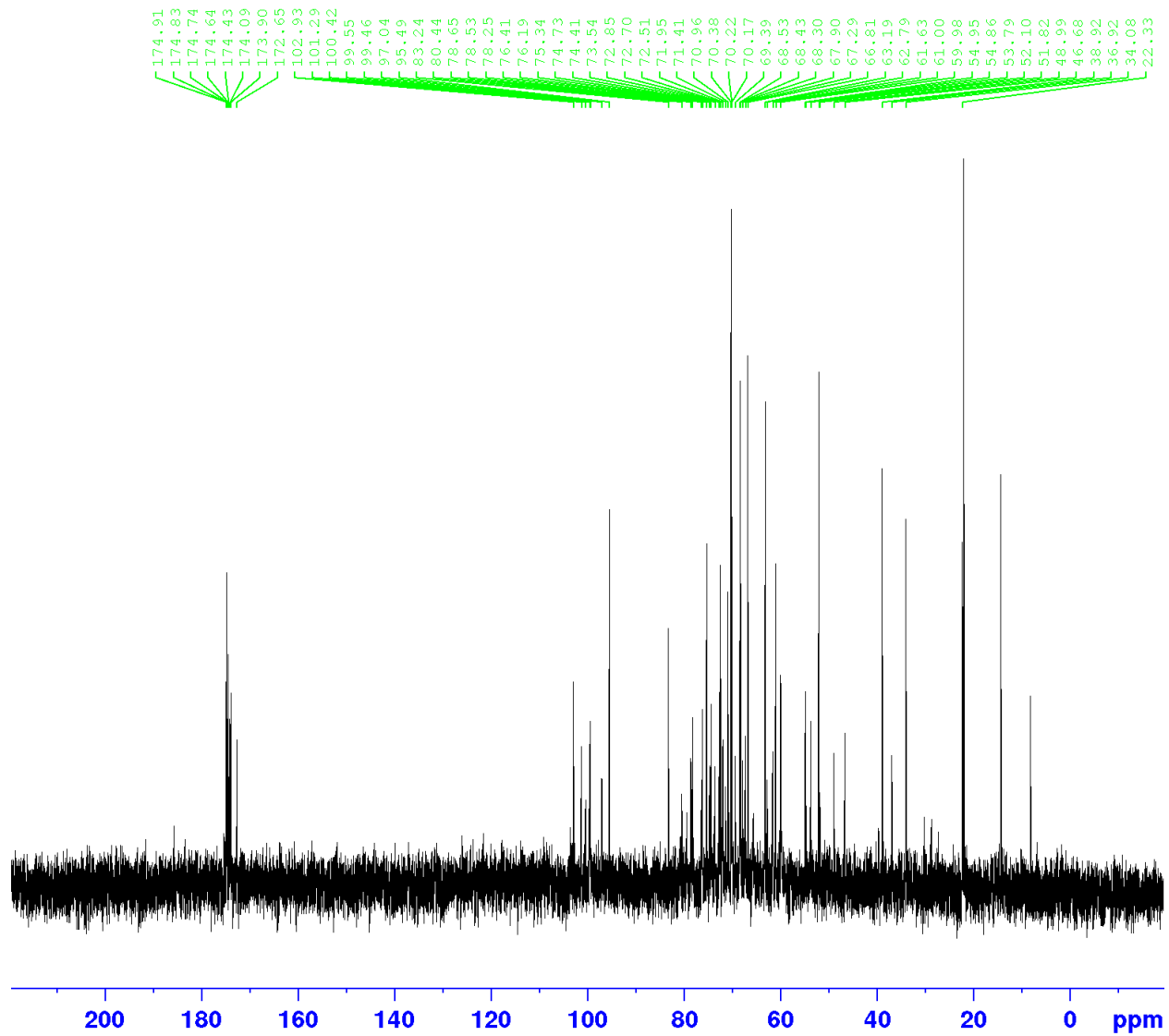
Glycan microarray slides were printed in house as previously described on Nexterion Slide E Epoxysilane coated slides (Nexterion #1066643).<sup>138, 139</sup> Briefly, the initial batch array was printed with 816 components in duplicate per array block and 8 array blocks were printed on each microarray slide. The second array batch was printed with 36 components in duplicate per array block, and 16 array blocks were printed on each microarray slide. Slides were covered with a ProPlate 8- or 16-well chamber (Grace Bio-labs, Bend, OR) and blocked overnight at 4 °C with 3% w/v BSA in PBST. The next day, the microarray wells were washed quickly twice with PBST and once with 1% w/v BSA in PBST. Mouse serum samples were diluted 1:100 in 1% w/v BSA in PBST and 60 $\mu$ l were added to each well, then slides were incubated for 3h at 37°C with gentle shaking. After incubation, wells were washed quickly three times then soaked for 2 minutes in PBST, followed by another quick wash with 1% w/v BSA in PBST. Cy3-labeled anti-mouse IgG (Jackson Immuno #115-165-071) and Alexa Fluor 647-labeled anti-mouse IgM

(Jackson Immuno #115-605-075) secondary antibodies were diluted 1:500 in 1% w/v BSA in PBST, then 60 $\mu$ l were added to each well, and slides were covered for 1h at 37°C with gentle shaking. After incubation, slides were washed quickly three times, soaked for 2 minutes, then completely submerged for 5 minutes in PBST. Slides were dried by centrifugation at 1000  $\times$  g for 4 minutes and were immediately scanned. Microarray slides were scanned on a an InnoScan 1100 AL fluorescence scanner (Innopsys; Chicago, IL). Analysis was performed using GenePix Pro 7 software (Molecular Devices Corporation; Sunnyvale, CA). Background fluorescence was subtracted from the median spot fluorescence and values were averaged for each duplicate component spot.

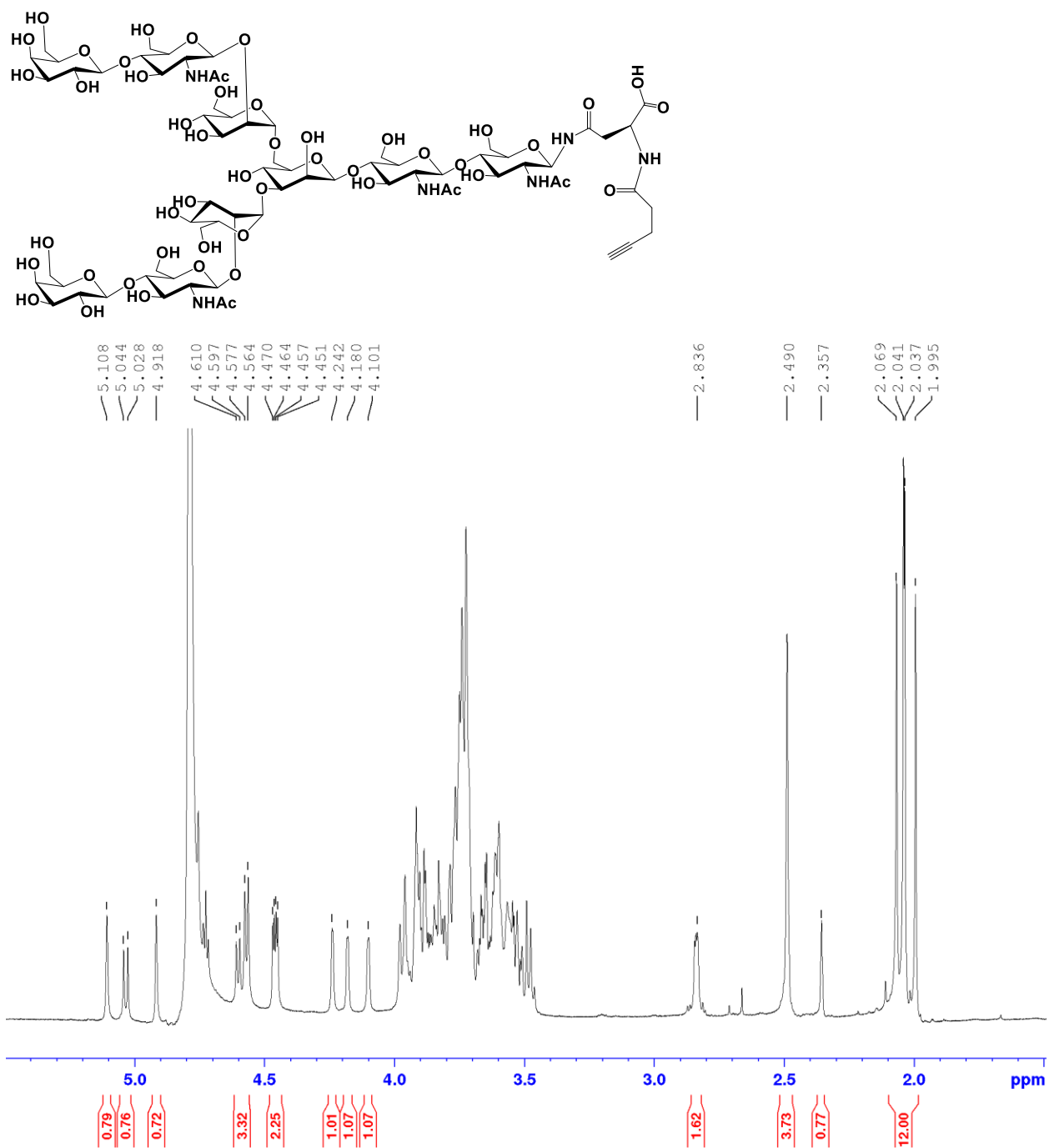
## 2.5 SUPPORTING INFORMATION



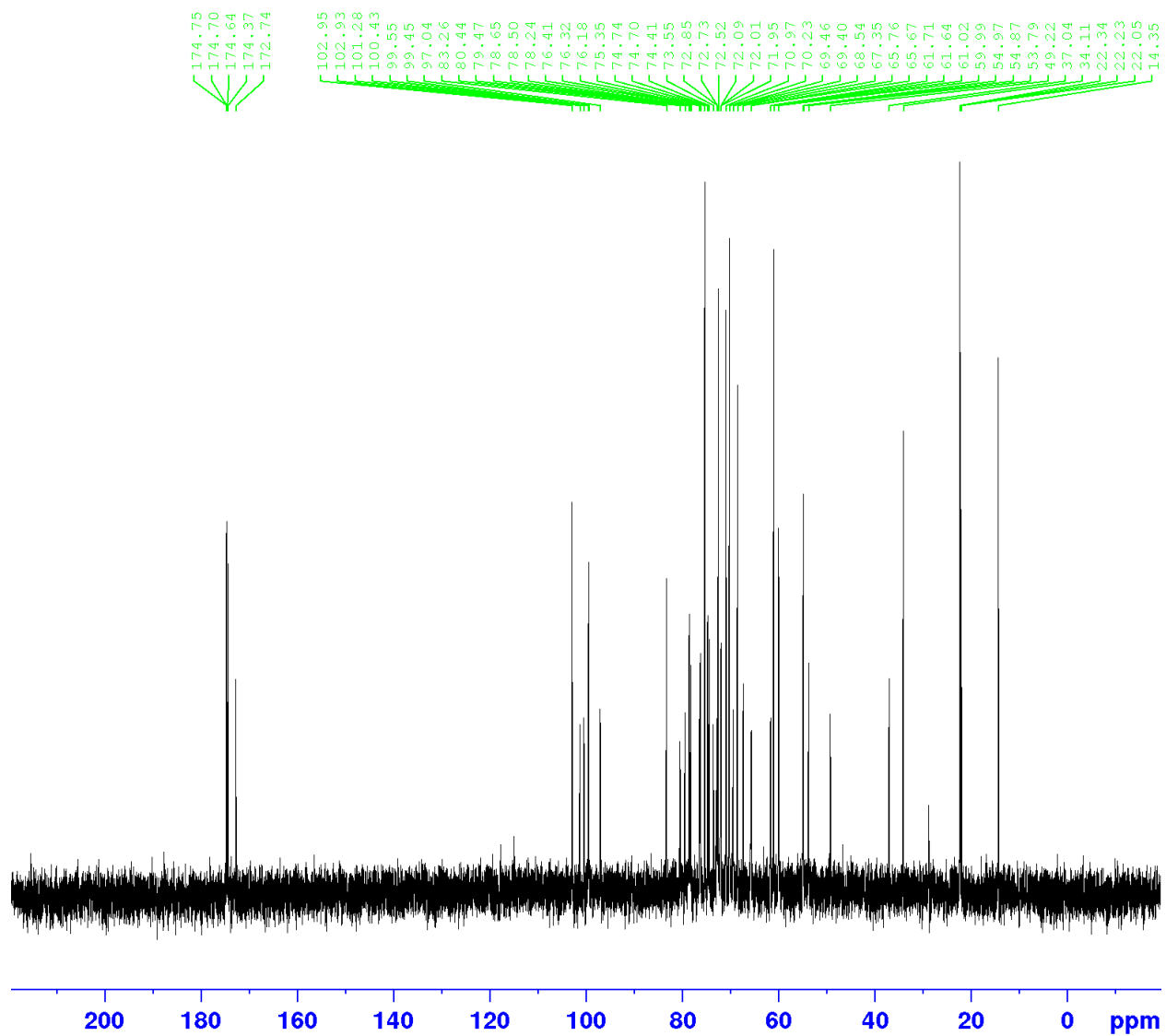
<sup>1</sup>H-NMR spectrum (400 MHz, D<sub>2</sub>O) of compound **2.1b**.



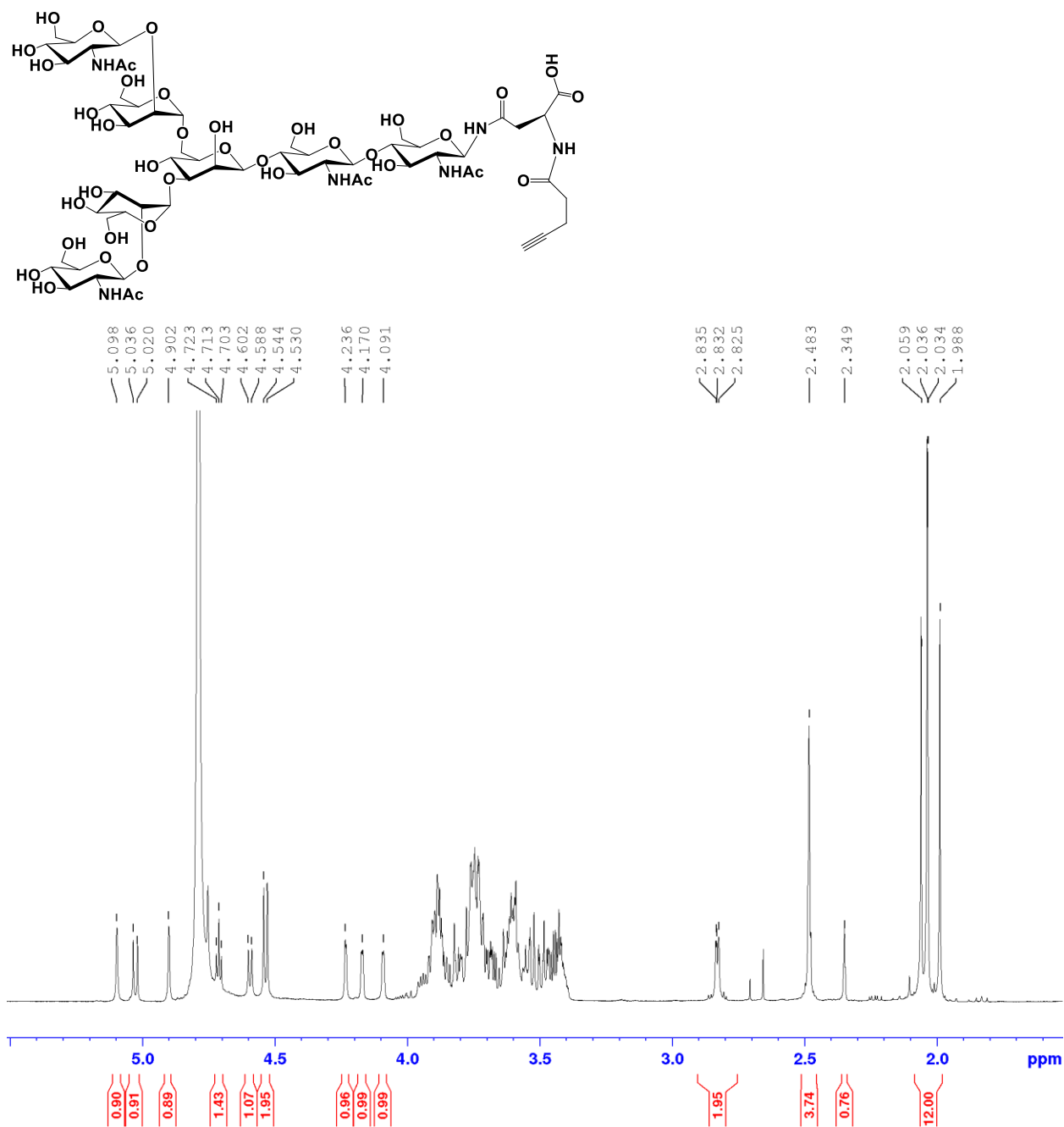
$^{13}\text{C}$ -NMR spectrum (125 MHz,  $\text{D}_2\text{O}$ ) of compound **2.1b**.



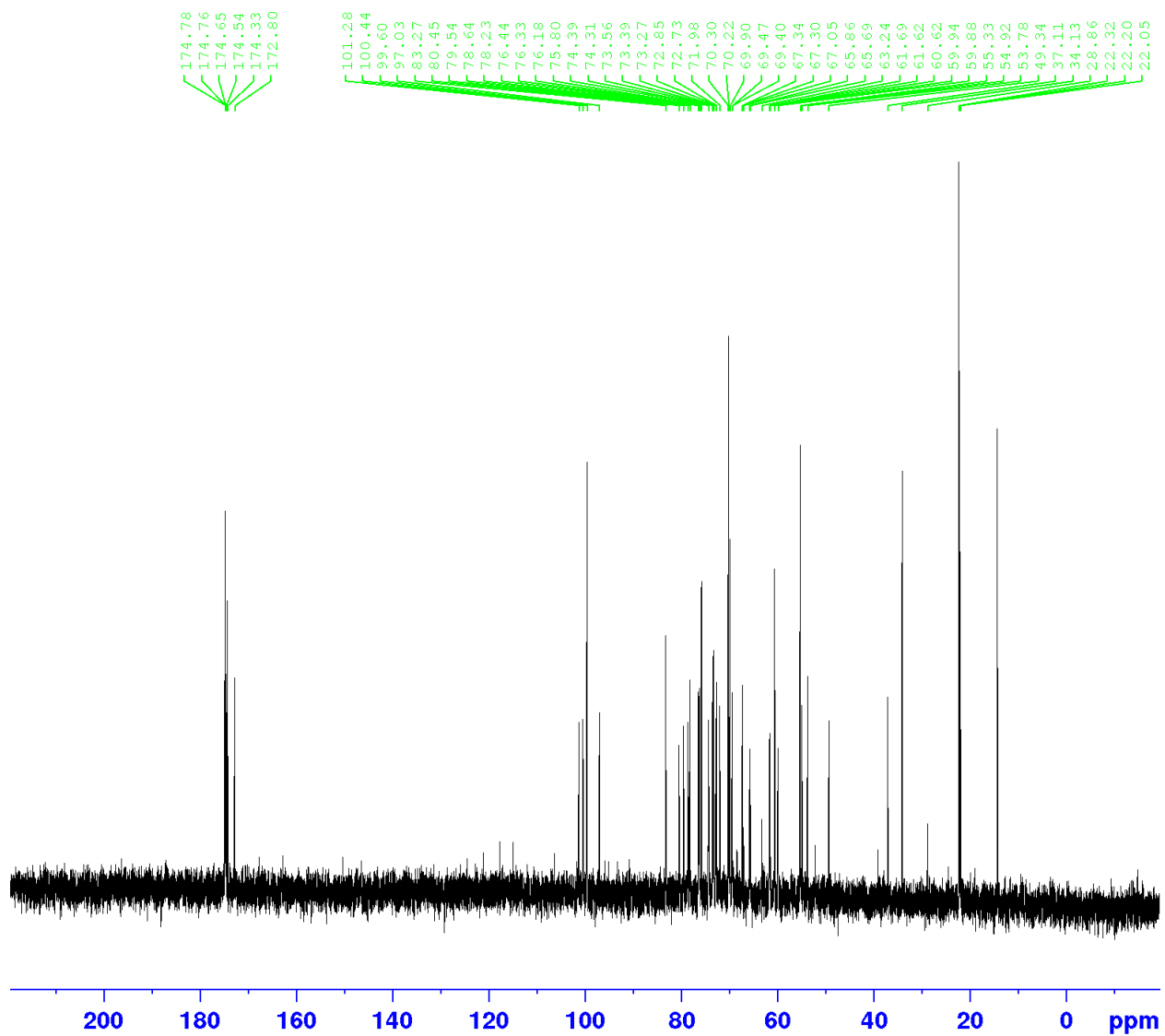
$^1\text{H-NMR}$  spectrum (400 MHz,  $\text{D}_2\text{O}$ ) of compound **2.2b**.



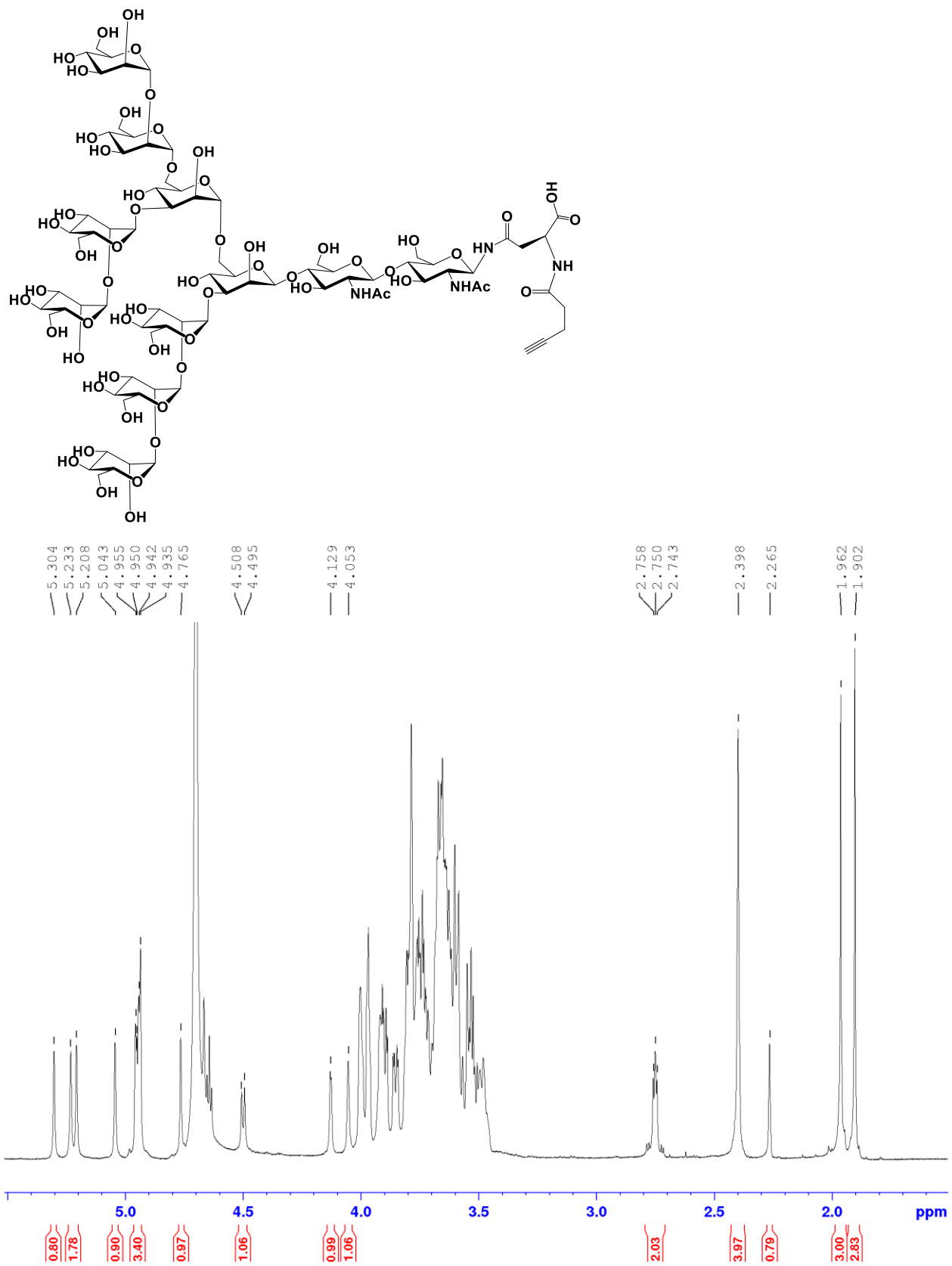
$^{13}\text{C}$ -NMR spectrum (125 MHz,  $\text{D}_2\text{O}$ ) of compound **2.2b**.



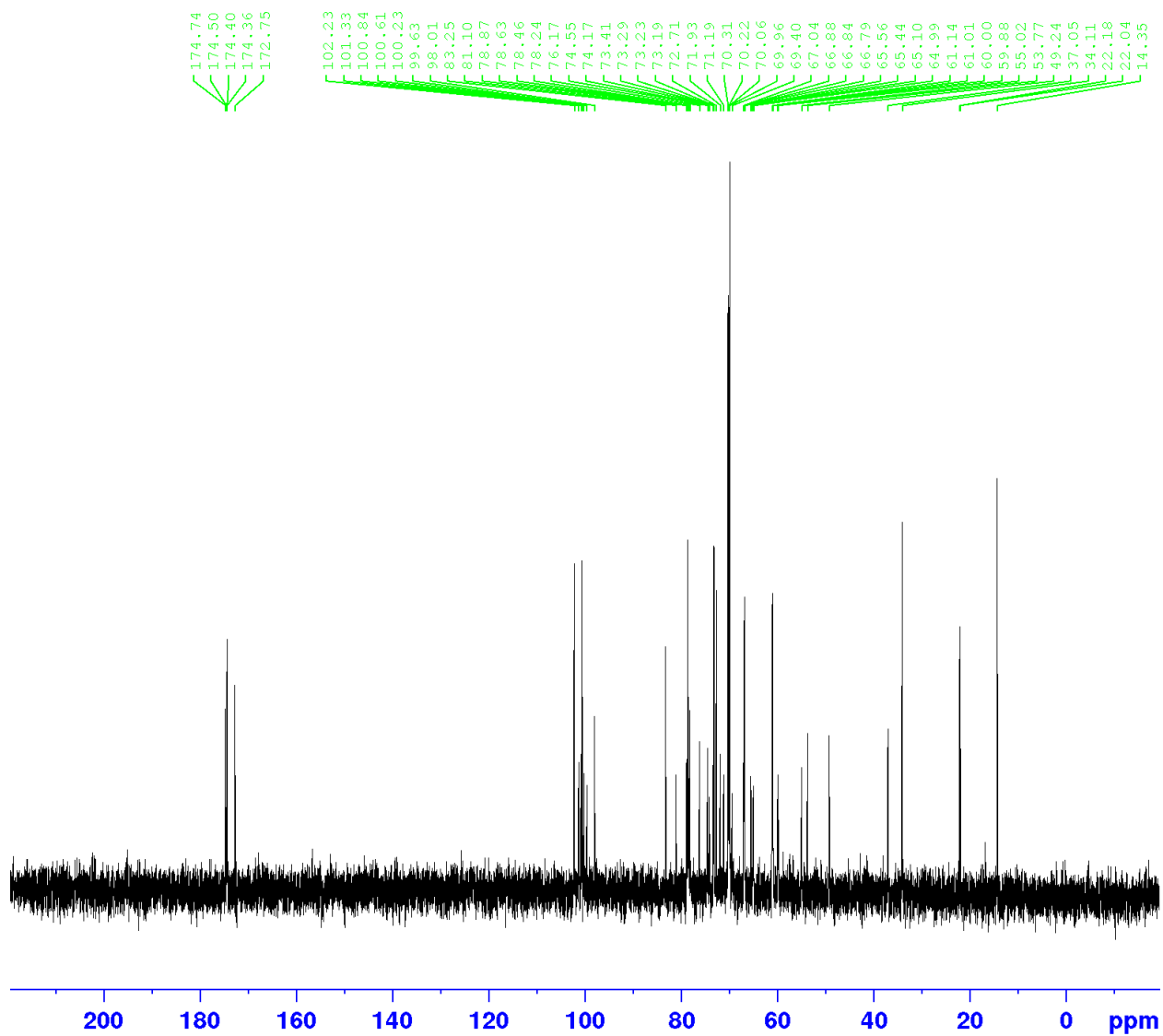
$^1\text{H-NMR}$  spectrum (400 MHz,  $\text{D}_2\text{O}$ ) of compound 2.3b.



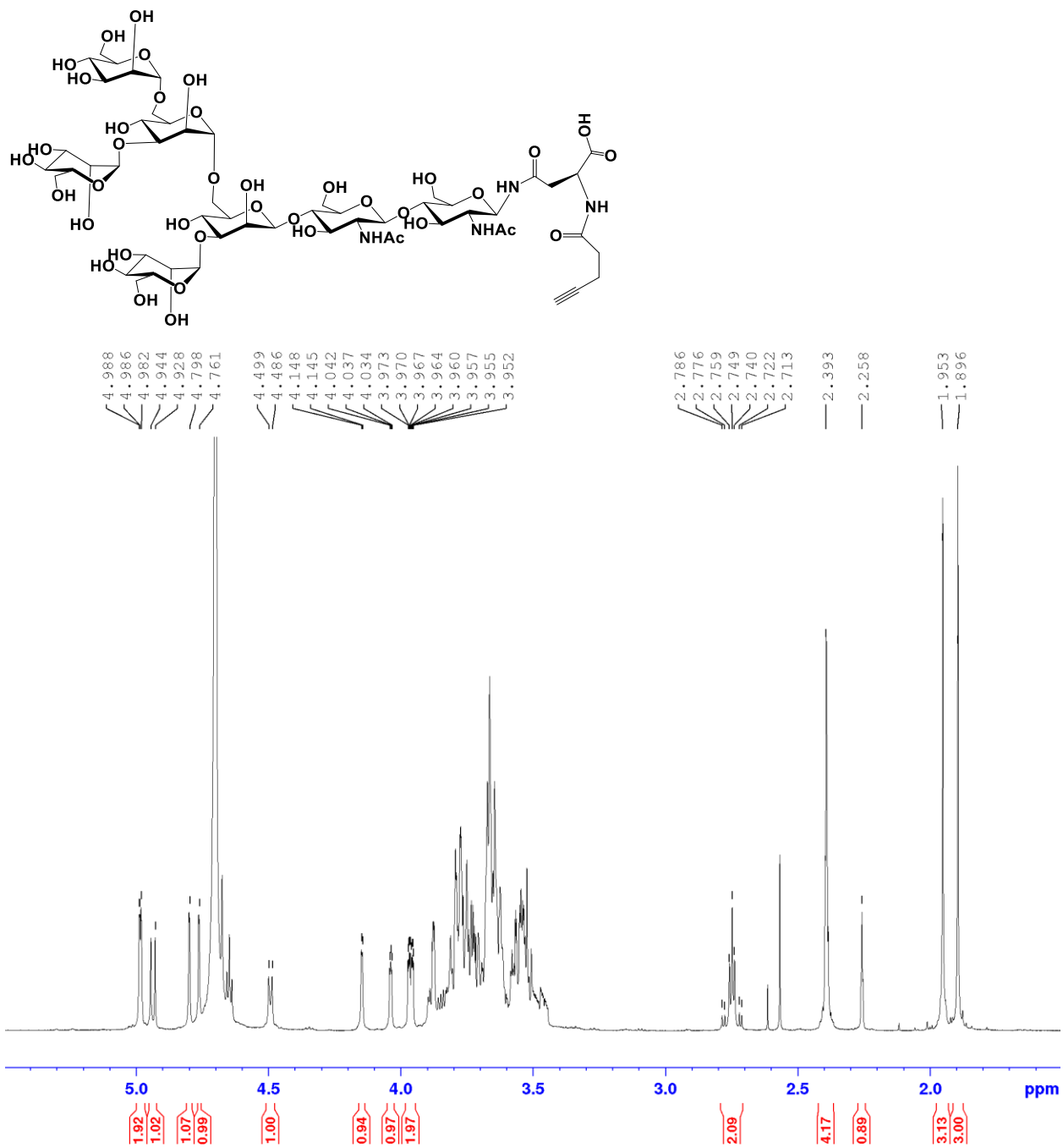
$^{13}\text{C}$ -NMR spectrum (125 MHz,  $\text{D}_2\text{O}$ ) of compound **2.3b**.



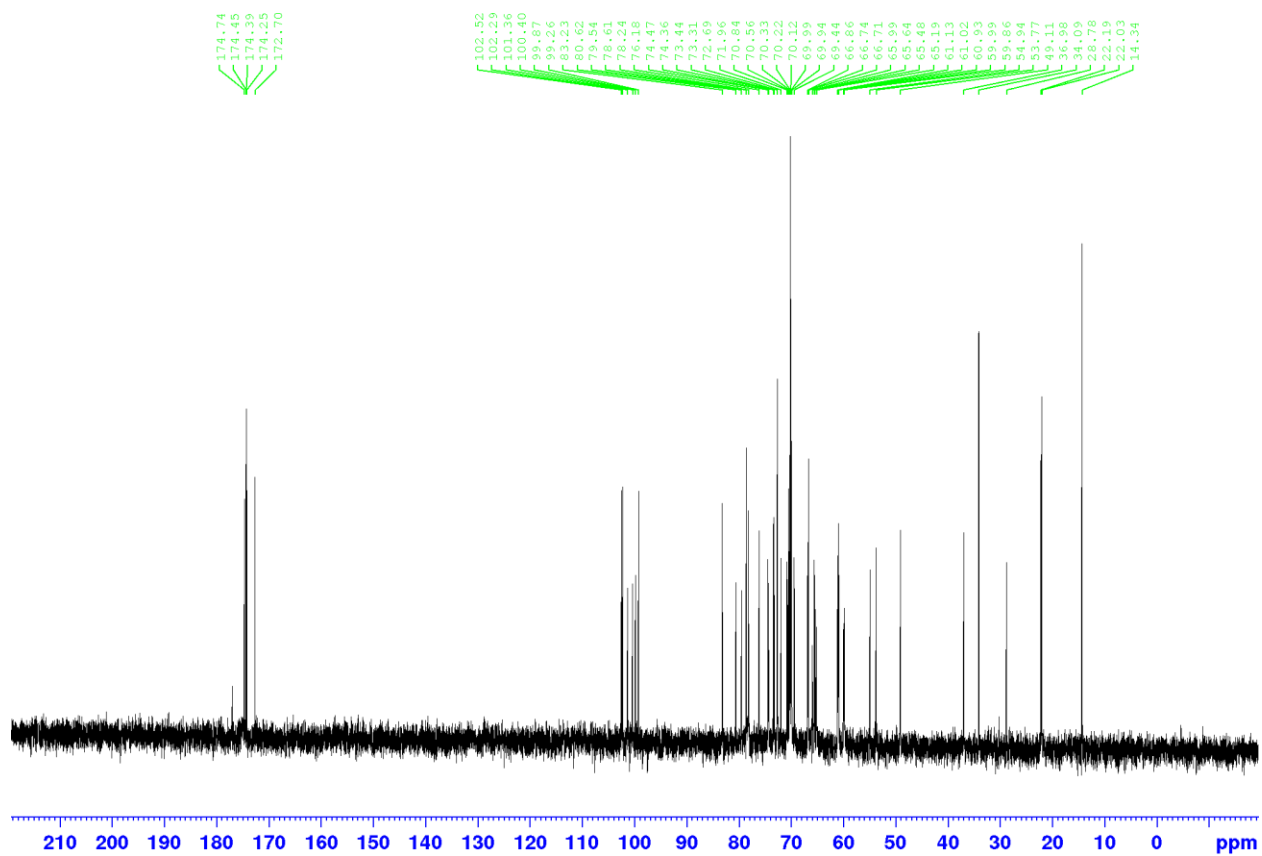
$^1\text{H-NMR}$  spectrum (400 MHz,  $\text{D}_2\text{O}$ ) of compound **2.4b**.



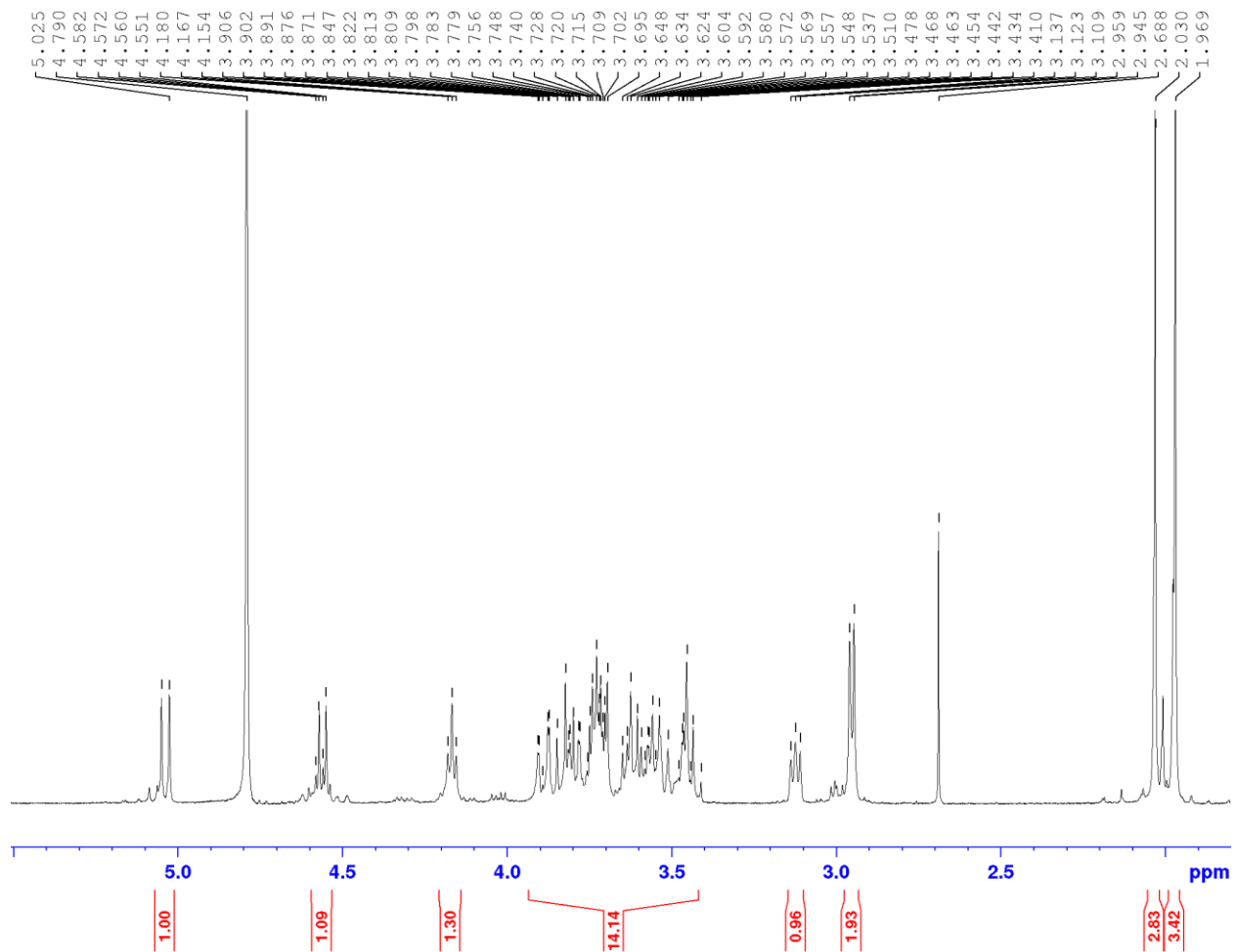
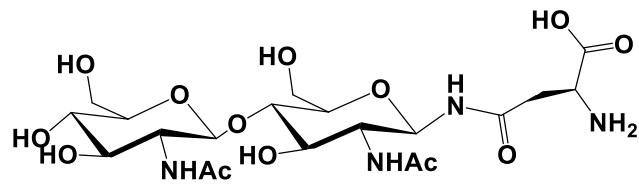
$^{13}\text{C}$ -NMR spectrum (125 MHz,  $\text{D}_2\text{O}$ ) of compound **2.4b**.



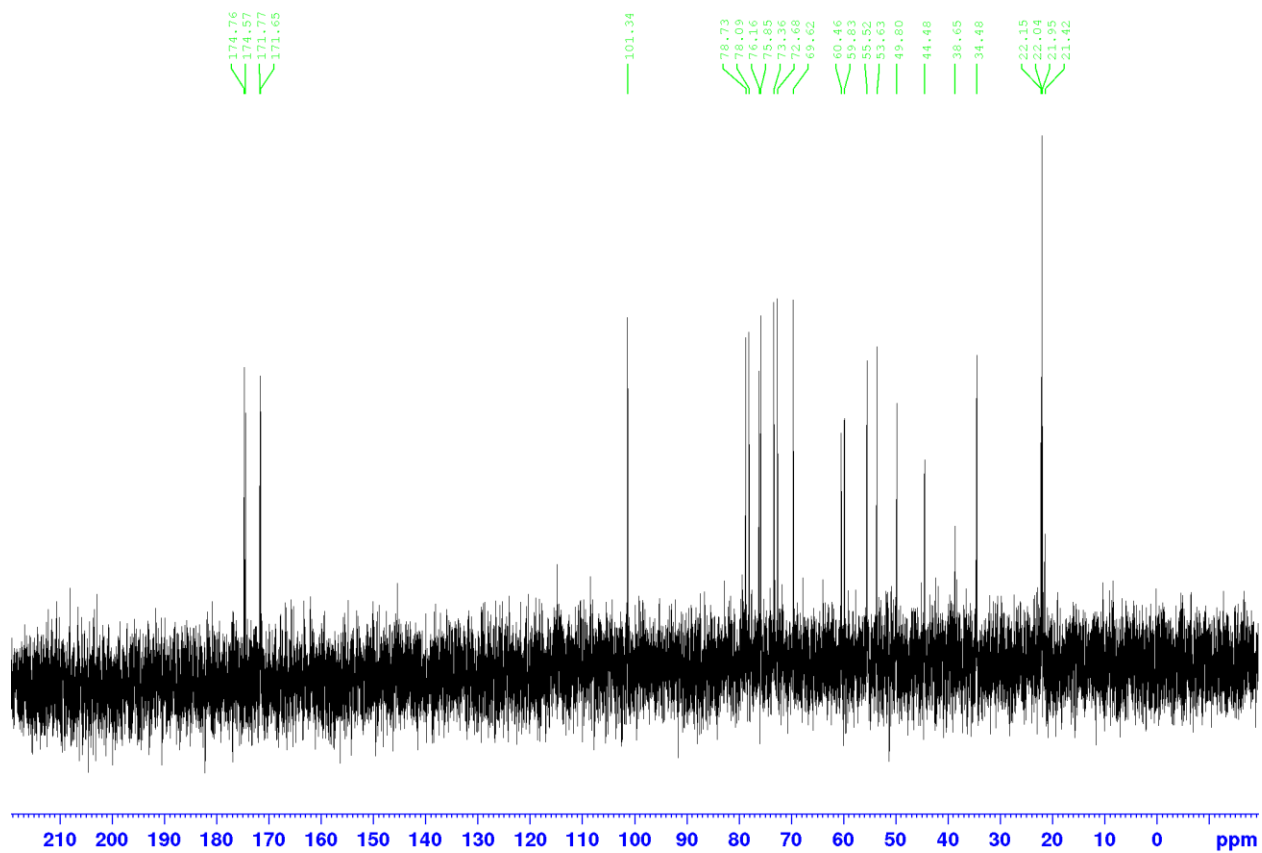
$^1\text{H-NMR}$  spectrum (400 MHz,  $\text{D}_2\text{O}$ ) of compound **2.5b**.



$^{13}\text{C}$ -NMR spectrum (125 MHz,  $\text{D}_2\text{O}$ ) of compound **2.5b**.



<sup>1</sup>H-NMR spectrum (400 MHz, D<sub>2</sub>O) of chitobiose-Asn.



$^{13}\text{C}$ -NMR spectrum (125 MHz,  $\text{D}_2\text{O}$ ) of chitobiose-Asn.

## Chapter 3: Catanionic Vesicles as a Facile Scaffold to Display Natural N-Glycan Ligands for Probing Multivalent Carbohydrate-Lectin Interactions

Part of this work was published in *Bioconjugate Chemistry*.<sup>140</sup>

Donahue, T. C.; Zong, G.; Ou, C.; DeShong, P.; Wang, L. X., Catanionic Vesicles as a Facile Scaffold to Display Natural N-Glycan Ligands for Probing Multivalent Carbohydrate-Lectin Interactions. *Bioconjug. Chem.*, **2023**, *34* (2), 392-404.

L.X.W. conceived the idea and supervised the research; T.C.D. and L.X.W. designed experiments; T.C.D performed the experiments; G. Z. assisted in experimental design and data analysis; C. O. assisted in data analysis. P. D. provided advice and helped design experiments. T.C.D. and L.X.W. analyzed the data and wrote the manuscript; all co-authors contributed to the revision of the manuscript.

### **3.1 INTRODUCTION**

Glycans are ubiquitous molecules of the cell that play active roles in biological recognition processes, including cell signaling, cell adhesion, and host immunity.<sup>12, 141</sup> The biological functions of glycans are usually mediated by carbohydrate-binding proteins (CBP or lectin) that recognize specific glycan structures attached to glycoproteins, glycolipids, or other glycoconjugates. While the affinity of a CBP for a single monosaccharide is usually weak ( $K_D = \sim 10^{-3}$  M), biological systems frequently adopt multivalent display of carbohydrate ligands to enhance the binding affinity and specificity of CBPs.<sup>142, 143</sup> Tremendous efforts have been devoted to the design, synthesis, and evaluation of various multivalent carbohydrate ligands for studying protein-carbohydrate interactions and for developing efficient inhibitors to block specific protein-carbohydrate interactions associated with viral and bacterial infections, inflammation, and cancer progression.<sup>30, 31</sup> Attempts have been made to use various scaffolds

such as liposomes, dendrimers, cyclodextrin, and metal nanoparticles for the multivalent display of small glycans.<sup>23, 63, 144-151</sup> However, multivalent display of the more biologically relevant natural O- and N-linked glycans remains to be an interesting area deserving further investigation.<sup>152-154</sup> For example, phospholipid-based liposomes have been used to display modified N-glycan ligands for targeted delivery of anti-cancer drugs and for immunomodulation.<sup>153, 154</sup> Nevertheless, major drawbacks of liposome-based vesicles include the tedious procedures of formulation, polydispersity, and the inherent instability under biological conditions. On the other hand, catanionic vesicles, prepared from cationic and anionic surfactants in water or buffer, offer an alternative multivalent display scaffold that is easy to use and retains a unilamellar equilibrium phase for extended periods in buffer.<sup>155, 156</sup> The advantage of these catanionic vesicles over conventional liposomes is that they are derived from cheap ionic surfactants, do not require solubilization by organic solvents or tedious extrusion procedures, provide vesicles with a narrow size distribution, and exhibit long term stability (months typically) in aqueous media.

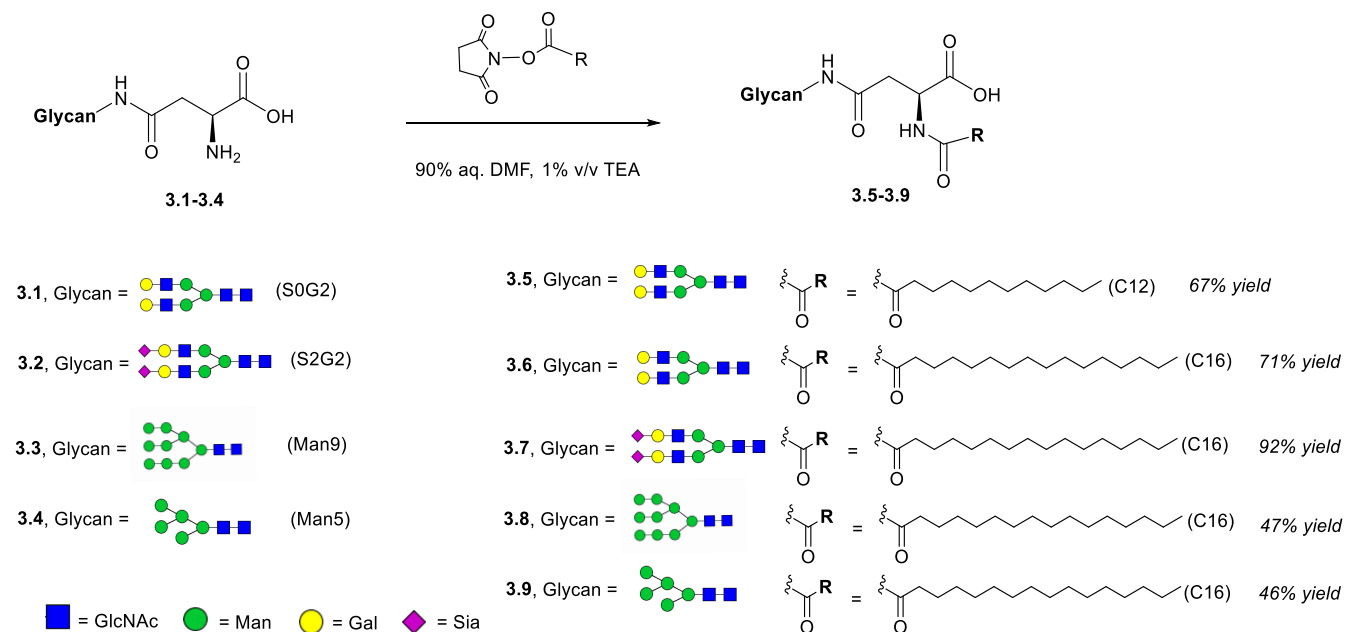
Catanionic vesicles were first employed for the multivalent display of sugars by Raghavan and co-workers in 2005, where C12 functionalized chitosan was shown to form a gel in the presence of catanionic vesicles.<sup>157</sup> In 2008, the versatility of catanionic vesicles to display structurally diverse carbohydrates was demonstrated by DeShong and coworkers, where mono- and tri-saccharides bearing a C8 lipid tail were incorporated into the vesicle bilayer and the resulting sugar coated vesicles were evaluated for lectin-mediated hemagglutination.<sup>158</sup> Particularly, DeShong and co-workers have demonstrated that the sugar density can be controlled in the vesicle bilayer. Since then, sugar-coated catanionic vesicles have been employed in carbohydrate microarrays and in the display of proteins, and bacterial

lipopolysaccharides for prophylactic vaccines against bacteria.<sup>156, 159-161</sup> The exceptional stability of cationic vesicles and their ability to display a diverse array of biomolecules on their surface makes them attractive scaffolds to characterize protein-carbohydrate interactions; however, this scaffold has not been employed for the multivalent display of the more biologically relevant natural O- and N-linked glycans. We report in this paper the synthesis and evaluation of cationic vesicle scaffolded natural N-glycans as multivalent glycan ligands for lectins. Our results indicate that cationic vesicles are a powerful scaffold that allows for the high-density multivalent display of high-mannose and complex-type N-glycans on the vesicle surface, which significantly enhances the affinity for the respective lectins with clear clustering glycoside effect. These novel glycan-coated vesicles offer a new and valuable platform for the investigation of carbohydrate-protein interactions and potentially for targeted drug delivery.

### **3.2 RESULTS AND DISCUSSION**

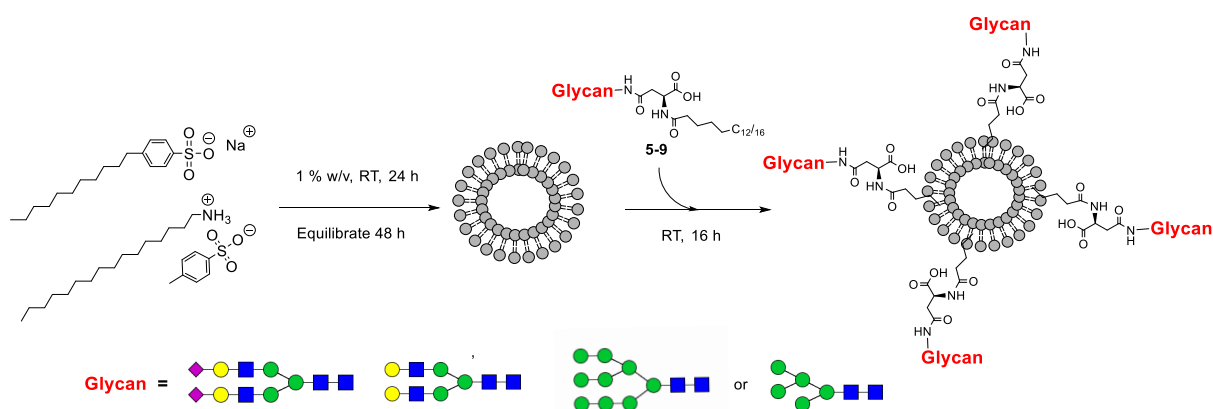
**Synthesis of N-glycan lipids.** Previous studies have shown that glycolipids containing simple sugars and a C8-C12 lipid tail can be efficiently incorporated into the outer leaflet of cationic vesicles.<sup>158, 159</sup> Thus, we sought to prepare N-glycan-based glycolipids and evaluate their efficiency of insertion into the cationic vesicle bilayer. For this purpose, we chose to use the asparagine-containing natural N-glycans as the starting materials and take advantage of the free amino group in the asparagine residue to introduce a lipid chain. We selected four typical N-glycans as model sugars, including the sialylated bi-antennary complex type glycan (S2G2-Asn), the asialylated bi-antennary Asn-glycan (S0G2), and the two high-mannose type N-glycans (Man9-Asn and Man5-Asn), which we have previously prepared by digestion of the chicken egg

yolk sialoglycopeptide (SGP) and soybean agglutinin with pronase, respectively, followed by size-exclusion chromatographic purification.<sup>66 129</sup> Glycolipids bearing lipids with different lengths were synthesized to investigate if a longer lipid chain is required to incorporate the large natural N-glycans in the vesicles. Thus, reaction of the asialo-complex type N-glycan (**3.1**) with the NHS activated ester of dodecanoic acid gave the corresponding N-glycolipid (**3.5**) containing a C12 lipid chain in excellent yield. Treatment of **3.1** with the N-hydroxysuccinimide ester of palmitic acid gave the N-glycolipid (**3.6**) containing a C16 lipid chain. Similarly, reaction of the sialylated N-glycan (S2G2-GlcNAc<sub>2</sub>-Asn, **3.2**), high-mannose type N-glycan (Man<sub>9</sub>-GlcNAc<sub>2</sub>-Asn, **3.3**) and the smaller high-mannose glycan (Man<sub>5</sub>GlcNAc<sub>2</sub>-Asn, **3.4**) with the N-hydroxysuccinimide ester of palmitic acid afforded the corresponding glycolipids (**3.7-3.9**) carrying a C16 lipid chain, respectively (Scheme 3.1). The glycolipids were purified by reverse phase HPLC, and their identity was confirmed by MS and NMR analysis.



**Scheme 3.1.** Synthesis of N-glycan lipids using free asparagine-linked N-glycans as the starting materials.

**Preparation and characterization of N-glycan-coated vesicles.** With the synthetic glycolipids (**3.5-3.9**) in hand, glycan-coated vesicles were prepared by mixing cationic vesicles with varying concentrations of N-glycolipids in water (Scheme 3.2). Three different concentrations were used for each of the glycolipids to prepare vesicles with low (L), medium (M), and high (H) glycolipid incorporation. Importantly, preformed vesicles were utilized to restrict N-glycan presentation to the outer membrane leaflet (Scheme 3.2).



**Scheme 3.2.** Assembly of N-glycan coated cationic vesicles. Cationic vesicles were formulated from SDBS and CTAT detergents in water and allowed to equilibrate. Preformed vesicles were mixed with N-glycolipids **3.5-3.9** at room temperature for 16 h to obtain N-glycan-coated vesicles.

N-Glycan-coated vesicles (N-gCVs) were then purified by size-exclusion chromatography (SEC) using a Sepharose G50 column, with characteristic vesicle elution between 13-19 mL as determined by Dynamic Light Scattering (DLS) intensity of the SEC fractions (Figure 3.1A). Vesicle N-glycolipid incorporation was determined for pure vesicle-

containing SEC fractions by the optimized phenol-sulfuric acid assay reported by Lee and coworkers.<sup>162</sup> This assay is robust and requires minimal work-up. Incorporation values were calculated relative to the recorded weight of dried vesicle and reported in mol/w %. In initial experiments, the uncharged S0G2-GlcNAc<sub>2</sub>-Asn N-glycan was used as a model, functionalized with C12 (**3.5**) and C16 (**3.6**) lipid tails, and tested for incorporation into the vesicle bilayer. Figure 3.1B showed the glycolipid incorporation values for the C12 and C16 functionalized N-glycans as a function of N-glycolipid concentration. It was found that the C16 functionalized N-glycan achieved up to 10-fold higher incorporation than the shorter C12 glycolipid at the same glycolipid concentration. This result suggests that for large glycans, a relatively long lipid chain is essential to have an efficient coating of the preformed cationic vesicles.

Having demonstrated that the C16 functionalized S0G2-GlcNAc<sub>2</sub>-Asn has superior glycolipid incorporation, presumably due to stronger interactions with lipids of the vesicle bilayer than the C12 glycolipid, C16 functionalized N-glycans were used in all subsequent experiments. N-Glycolipids containing S2G2, Man9, and Man5 headgroups were synthesized and tested for glycolipid incorporation at different concentrations (Scheme 3.2). Glycolipid incorporation was found to have a roughly linear relationship with final N-glycolipid concentration for all four glycolipids, indicating that the amount of N-glycan on the vesicle surface could be predictably tuned by adjusting the concentration of N-glycolipid in the vesicle formulation (Fig. 3.1 B-E). Up to  $9.9 \times 10^{-6}$ ,  $1 \times 10^{-5}$ ,  $1.7 \times 10^{-5}$ , and  $3.1 \times 10^{-5}$  mol/w % of S0G2-GlcNAc<sub>2</sub>-Asn-C16, S2G2-GlcNAc<sub>2</sub>-Asn-C16, Man9-GlcNAc<sub>2</sub>-Asn-C16, and Man5-GlcNAc<sub>2</sub>-Asn-C16 were incorporated into cationic vesicles, respectively.

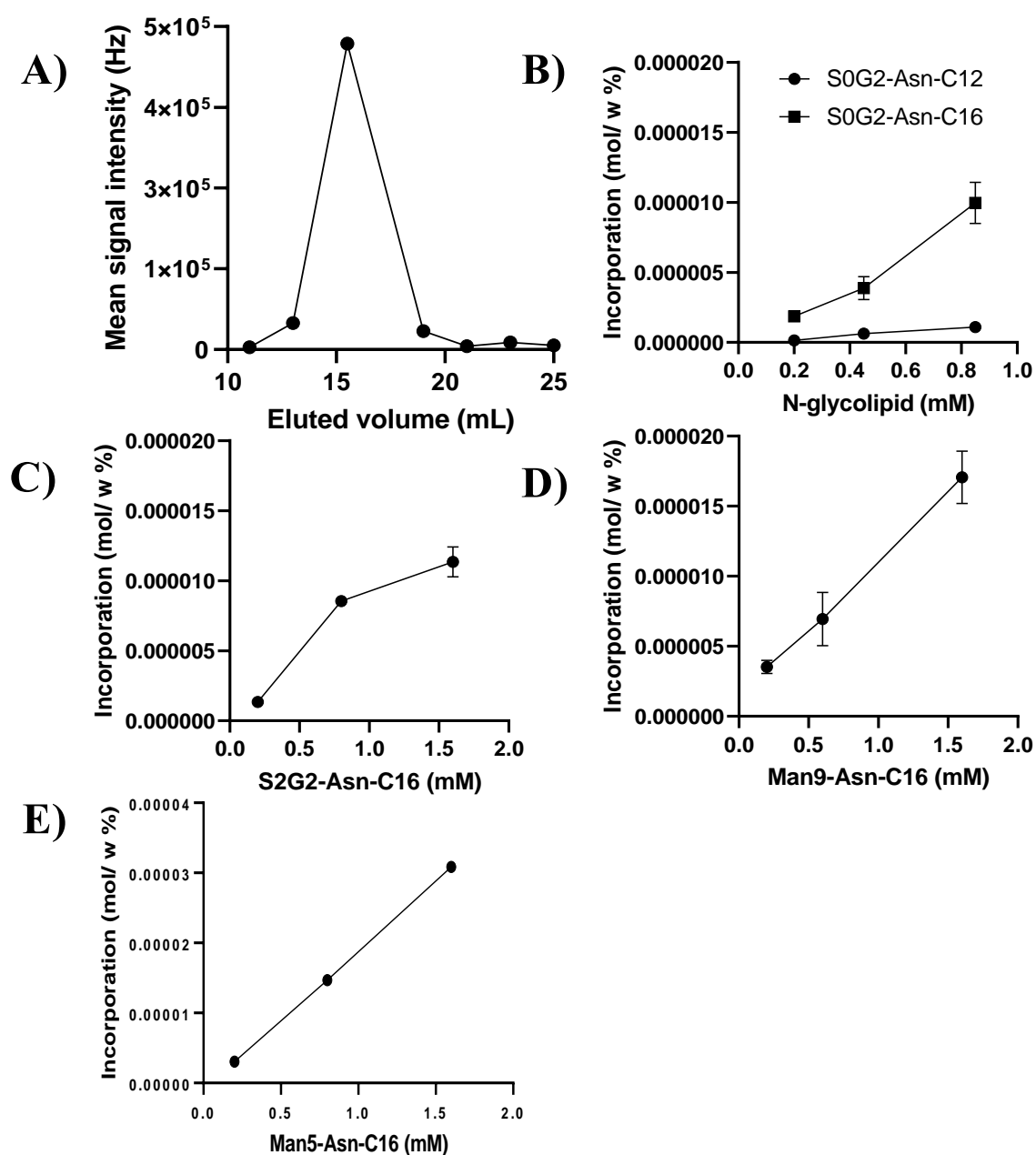


**Figure 3.1.** A) Vesicle elution profile from Sepharose G-50 column, peak observed between 13-19 mL elution volume by DLS at 633 nm. B) Glycolipid incorporation for C12 and C16 functionalized S0G2-GlcNAc<sub>2</sub>-Asn at varying concentrations of N-glycolipid (0.2, 0.45, and 0.85 mM). C) Glycolipid incorporation of S2G2-GlcNAc<sub>2</sub>-Asn-C16 at 0.2, 0.8, and 1.6 mM N-glycolipid. D) Glycolipid incorporation of Man9-GlcNAc<sub>2</sub>-Asn-C16 at 0.2, 0.6, and 1.6 mM N-glycolipid. E) Glycolipid incorporation of Man5-GlcNAc<sub>2</sub>-Asn-C16 at 0.2, 0.8, and 1.6 mM N-glycolipid. All measurements of glycolipid incorporation were done in triplicate.

**Table 3.1.** Hydrodynamic diameter and Polydispersity Index of N-glycan-coated and bare vesicles.

Vesicle sample	Hydrodynamic diameter (nm)	PDI*	Glycan type	Number of glycans per particle	Glycans/ nm <sup>2</sup>
Bare vesicle	228	0.05	-	-	-
S2G2-Asn-C16 gCV (L)	144	0.1	S2G2	906	0.007
S2G2-Asn-C16 gCV (M)	168	0.03	S2G2	4,460	0.03
S2G2-Asn-C16 gCV (H)	193	0.03	S2G2	11,725	0.05
S0G2-Asn-C16 gCV (L)	107	0.03	S0G2	1,082	0.02
S0G2-Asn-C16 gCV (M)	195	0.07	S0G2	7,492	0.03
S0G2-Asn-C16 gCV (H)	177	0.01	S0G2	10,098	0.05
Man9-Asn-C16 gCV (L)	144	0.05	Man9	3,715	0.03
Man9-Asn-C16 gCV (M)	227	0.08	Man9	14,907	0.05
Man9-Asn-C16 gCV (H)	124	0.07	Man9	9,706	0.1
S0G2-Asn-C12 gCV (L)	227	0.08	S0G2	313	0.001
S0G2-Asn-C12 gCV (M)	195	0.17	S0G2	869	0.004
S0G2-Asn-C12 gCV (H)	144	0.05	S0G2	912	0.007
Man5-Asn-C16 gCV (L)	190	0.08	Man5	4,316	0.02
Man5-Asn-C16 gCV (M)	257	0.07	Man5	34,123	0.08
Man5-Asn-C16 gCV (H)	299	0.12	Man5	108,511	0.2
S2G2/ Man5-Asn-C16 gCV (LL)	163	0.18	S2G2	509	0.003
			Man5	503	0.003
S2G2/ Man5-Asn-C16 gCV (MM)	117	0.01	S2G2	988	0.01
			Man5	1,045	0.01
S2G2/ Man5-Asn-C16 gCV (HH)	184	0.05	S2G2	4,401	0.02
			Man5	7,785	0.04
S2G2/ Man5-Asn-C16 gCV (ML)	139	0.37	S2G2	1,904	0.02
			Man5	389	0.003
S2G2/ Man5-Asn-C16 gCV (HL)	163	0.08	S2G2	3,347	0.02
			Man5	336	0.002

\*Polydispersity Index

N-Glycan-coated vesicles and bare vesicles (containing no sugar) were characterized for hydrodynamic size by dynamic light scattering (DLS). Bare vesicles were found to have a hydrodynamic diameter of  $228 \pm 51$  nm, which matched well with the previously reported values.<sup>158, 159</sup> N-Glycan-coated vesicles were found to be 107-299 nm in diameter, with vesicles containing higher N-glycolipid concentrations typically being larger (Table 3.1). Nevertheless, there was no clear correlation between vesicle size and the types of incorporated N-glycans. All

vesicles were fairly monodisperse with most vesicle samples having polydispersity indices below 0.1, suggesting homogeneity in the vesicle size distribution (Table 3.1). Glycan-coated vesicles were also found to be extraordinarily stable, retaining their particle size for up to 6 months as judged by DLS. To confirm that the N-glycolipids had been specifically incorporated into the cationic vesicles, SEC-purified N-gCVs were treated with endoglycosidase-CC (Endo-CC) from *Coprinopsis cinerea*, an endoglycosidase enzyme that cleaves between the two N-acetylglucosamines (GlcNAc) of the chitobiose core and with activity towards complex-type and high-mannose N-glycans.<sup>163</sup> After Endo-CC digestion of each sample for 36 h at 37 °C, the reaction mixture was analyzed by MALDI-TOF MS and the observed  $m/z$  values were found to match the expected mass values of the free N-glycans cleaved from the vesicle surface (Figure 3.2A-D), confirming that each of the synthesized N-glycolipids were incorporated into a cationic vesicle, respectively.

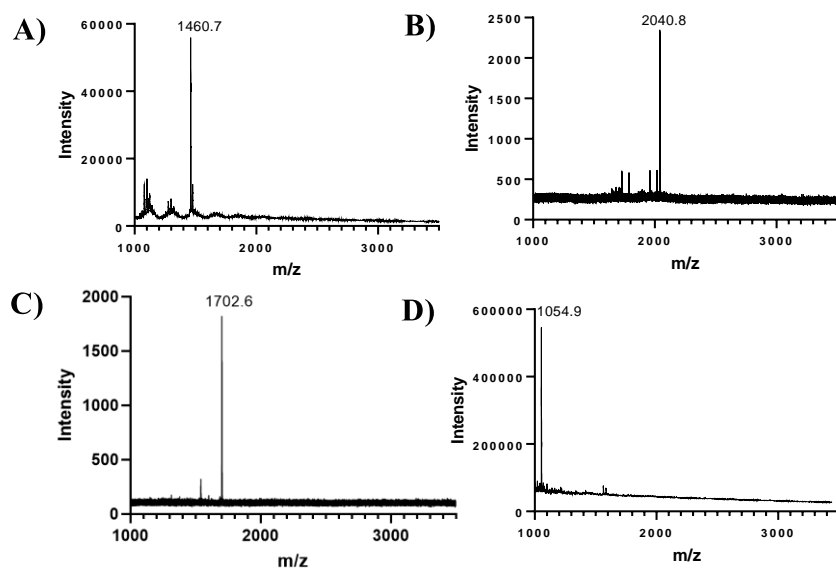


**Figure 3.2.** Endo-CC glycan release experiments on N-glycan-coated vesicles A) MALDI-TOF MS spectra for S0G2-GlcNAc<sub>1</sub>, calculated,  $M = 1437.5$  Da; found,  $m/z$  1460.7  $[M + Na]^+$ , B) S2G2-GlcNAc<sub>1</sub>, calculated,  $M = 2019.7$  Da; found,  $m/z$  2040.8  $[M + Na - 2H]^-$ , C) Man9-GlcNAc<sub>1</sub>, calculated,  $M = 1679.6$  Da; found,  $m/z$  1702.6  $[M + Na]^+$ . D) Man<sub>5</sub>-GlcNAc<sub>1</sub>, calculated,  $M = 1031.3$  Da; found,  $m/z$  1054.9  $[M + Na]^+$ .

**Binding affinity of the glycan-coated vesicles for respective lectins.** The binding affinity of the N-glycan-coated vesicles for several lectins was measured by a competitive inhibition assay. Specifically, N-glycan-coated vesicles were tested for their ability to inhibit binding of Concavalin A (ConA), *Sambucus Nigra* lectin (SNA), and human Galectin-3 (Gal-3) to synthetic N-glycan-BSA conjugates in a modified Enzyme-Linked Lectin Assay (ELLA; Figure 3.3A). Lectins ConA, SNA, and Gal-3 have specificity for terminal mannose, sialic acid, and galactose residues, respectively. N-Glycan-coated vesicles of varying N-glycan densities were used as inhibitors to reveal the influence of N-glycan presentation on lectin recognition.

The competitive inhibition curves (Figure 3.3B-E) demonstrate that ConA, SNA, and Gal-3 bind strongly to the clustered N-glycans on the vesicle surface. Figure 3.3B depicts the inhibition curve for ConA, where the monovalent Man9-Asn is the weakest inhibitor (IC<sub>50</sub> of 1.06  $\mu$ M) and a clear enhancement in lectin inhibition is observed for the Man9 glycan-coated vesicles (Man9-gCVs). The multivalent enhancement, or  $\beta$  value as coined by Whitesides and coworkers,<sup>30</sup> was calculated by comparing the IC<sub>50</sub> of each glycan-coated vesicle to its corresponding monovalent N-glycan ligand. In the case of ConA, the highest  $\beta$  value was observed for the Man9-gCV (M) sample with intermediate N-glycolipid incorporation ( $\beta = 7.6$ , IC<sub>50</sub> = 140 nM). Notably, inhibition of ConA binding was less effective with the densely coated Man9-gCV (H) vesicle, with a  $\beta$  value of 1.6 and the IC<sub>50</sub> value of 650 nM. These data suggest that ConA prefers multivalent N-glycan presentations of intermediate density and that higher-density N-glycan presentations sterically occlude lectin binding, possibly by limiting access to the core trimannoside which comprises the main epitope for ConA recognition.<sup>164</sup> Similar

observations have been reported by Kiessling and coworkers on mannose-containing glycopolymers as ConA inhibitors.<sup>165</sup> Importantly, the  $IC_{50}$  found for Man9-Asn in this assay matches the  $K_D$  previously reported for this lectin towards the Man9 oligosaccharide,<sup>166</sup> suggesting that the  $IC_{50}$  data obtained by this method are a good approximation of the affinities of the investigated lectins for their N-glycan ligands.

Similarly, the sialic acid-specific lectin SNA displayed a weak affinity for the monovalent S2G2-Asn N-glycan ( $IC_{50} = 20 \mu M$ ), but a significantly enhanced affinity for the S2G2-coated vesicles of intermediate glycan loading [ $\beta$  value = 38,  $IC_{50} = 520$  nM for S2G2-gCV (M)]. The multivalent binding enhancement was more pronounced than that observed for ConA, however, the enhancement was decreased for vesicle samples containing high levels of the S2G2-Asn-C16 glycolipid (i.e. S2G2-gCV (H)). The results suggest that dense N-glycan clustering may hinder accessibility to important glycan epitopes such as the internal LacNAc moiety of the  $\alpha(1,3)$ -mannose arm needed for SNA binding.<sup>167</sup>

Following these results, competitive inhibition experiments were performed with human galectin-3, a lectin overexpressed in several hepatic, pancreatic, and colorectal cancers.<sup>12</sup> Galectin-3 was found to have a weak affinity for the monomeric galactosylated bi-antennary N-glycan (S0G2-Asn,  $IC_{50} = 7.8 \mu M$ ), consistent with previous reports on this lectin.<sup>168</sup> Very modest affinities were observed for S0G2-coated vesicles of low and intermediate glycan density [S0G2-gCV (L) and gCV (M); Figure 3.3]. However, a pronounced enhancement in lectin binding was observed with the high-density vesicle, S0G2-gCV (H) ( $\beta$  value = 11,  $IC_{50} = 710$  nM; Figure 3.3D). Similar  $IC_{50}$  values have been reported for proteins bearing high-affinity synthetic ligands for Gal-3 and for LacdiNAc-bearing multivalent particles, making S0G2-coated vesicles potent multivalent inhibitors of human Gal-3.<sup>169-171</sup> In contrast to ConA and SNA, Gal-3

prefers high-density presentations of N-glycans bearing the cognate LacNAc ligand. The glycan density dependence in the multivalent binding with Gal-3 may be explained by the recognition mode as demonstrated with the crystal structure of human Gal-3, where the Gal-3 Carbohydrate Recognition Domain (CRD) interacts mainly with the terminal galactose residue of the LacNAc moiety which is more deeply buried in the binding pocket, and only makes contacts with the N-Acetyl and C3 hydroxyl groups of the internal GlcNAc residue.<sup>172</sup> Therefore, highly clustered S0G2 N-glycans could still be recognized by Gal-3 at the galactose terminus. Furthermore, Gal-3 is known to self-oligomerize into pentamers through the N-terminal domain, making a lattice of intermolecular glycan-lectin networks that would enhance binding affinity to highly clustered glyconanoparticles.<sup>173</sup>

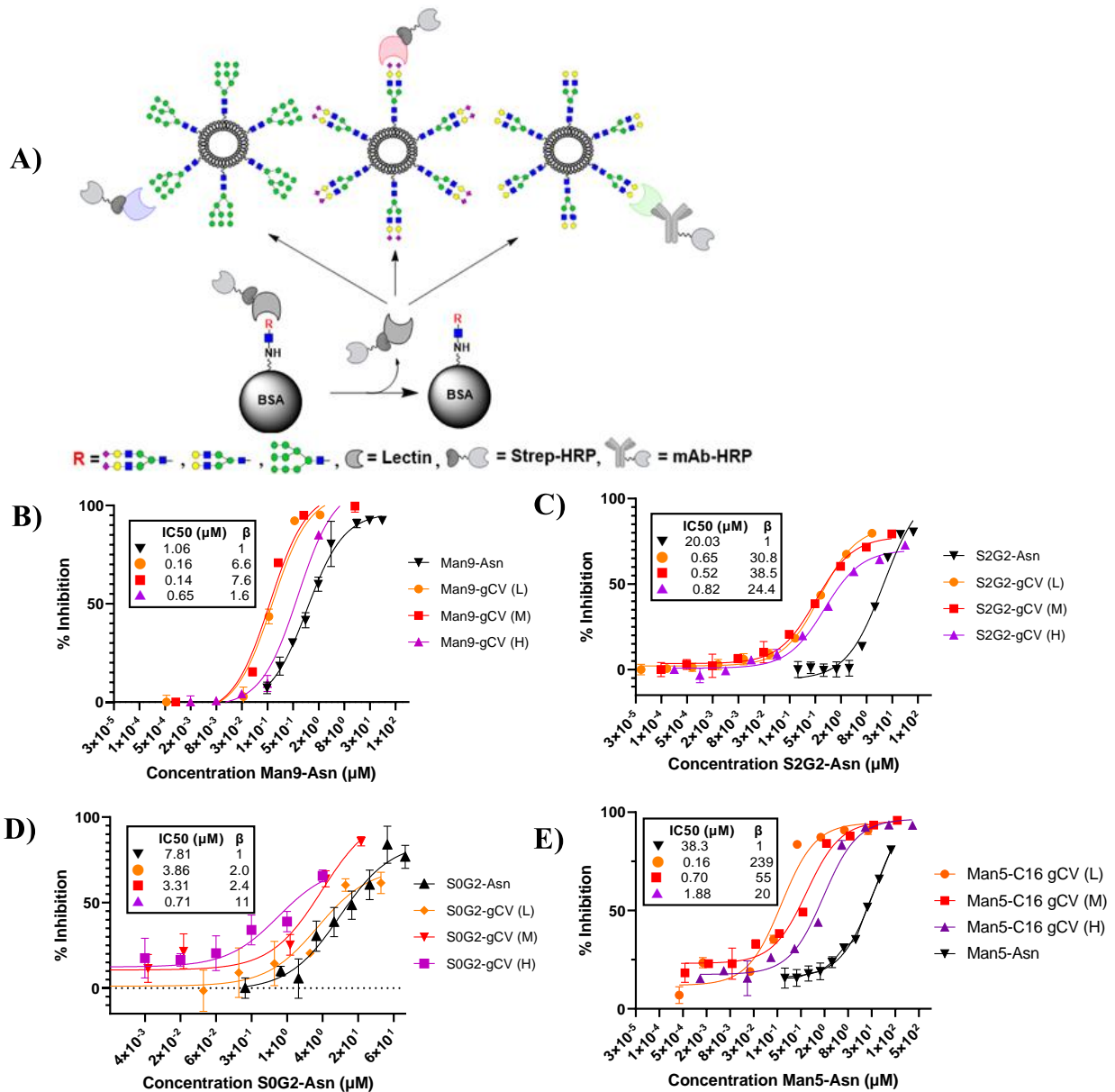


**Figure 3.3.** A) Design of microplate-based competitive inhibition assay, N-glycan-coated vesicles inhibit lectin binding to synthetic N-glycan-BSA conjugate coating antigens. Detection is done by Streptavidin-HRP (Strep-HRP), or a mAb-HRP conjugate in the case of Galectin-3. Colored shapes represent different lectins. B) Inhibition curve of ConA binding to Man9-BSA conjugates with Man9-gCVs as inhibitors. C) Inhibition of SNA binding to S2G2-BSA conjugates with S2G2-gCVs. D) Inhibition of Gal-3 binding to S0G2-BSA conjugates with S0G2-gCVs as the inhibitors. E) Inhibition curve of ConA binding to Man5-BSA conjugates with Man5-gCVs as inhibitors. Insets in each graph provide the IC<sub>50</sub> and multivalent enhancement (β) for the corresponding inhibitors shown on the right side. All data points were measured in triplicate.

Competitive inhibition experiments on ConA with Man5-containing vesicles revealed a remarkable enhancement of affinity for the cationic vesicle-based Man5 ligands. While the monovalent Man5-Asn glycan had a moderate affinity for ConA in the competitive assay ( $IC_{50} = 38.3 \mu\text{M}$ ), the Man5-containing vesicle with a relatively low ligand loading, Man5-gCV (L), showed over 200-fold enhanced affinity for ConA ( $IC_{50} = 0.16 \mu\text{M}$ ,  $\beta$  value = 239). Interestingly, vesicles displaying higher densities of the Man5 glycolipid showed less enhancement of the affinity for ConA (Figure 3.3E). This result may be explained by the higher incorporation efficiencies of the Man5 glycolipid as compared to the Man9 glycolipid (Figure 3.1), meaning that the Man5 headgroups are in closer proximity to one another and are not as accessible to protein recognition.

**Synthesis and Characterization of Mixed N-Glycan-coated Vesicles.** Glycan-coated vesicles displaying structurally diverse sugars are desirable as better mimics of heterogeneous mammalian glycosylation of the cell surface. As a proof of concept, we sought to prepare vesicles displaying different types of sugars such as the S2G2 and Man5 N-glycans, which also feature in variable regions 1 and 2 (V1/V2) of the HIV-1 gp120 trimer.<sup>174</sup> To enable quantification of multiple N-glycans on the vesicle surface, a new N-glycolipid incorporation assay based on endo-glycosidase catalyzed glycan release, 2-aminobenzoic acid (2AA) labeling, and HPLC analysis was developed.

Initial attempts to perform endo-glycosidase release directly from intact N-glycan coated vesicles were inefficient and required prolonged incubation periods (approximately three days). Furthermore, vesicle-associated detergents hampered reaction monitoring by MALDI-TOF MS. To maximize N-glycolipid purity and minimize sample loss, a small-scale purification method

was adapted from the biphasic water: phenol/ chloroform extraction protocol commonly used in DNA/RNA purification. Due to partial solubility of the N-glycolipids in chloroform, however, dichloromethane (DCM) was used as the organic solvent for the extraction. Importantly, both vesicle-associated detergents (CTAT and SDBS) are soluble in dichloromethane. Pooled N-glycan-coated vesicle samples were mixed with an equal volume of DCM and vortexed vigorously to extract vesicle-associated detergents, the suspension was centrifuged at high speed, and this process was repeated three times to afford pure N-glycolipid in the aqueous phase. The glycolipids were cleaved by wild-type Endo-CC, and the enzymatic hydrolysis was monitored by MALDI-TOF MS analysis. After reaction completion (24-30 h at 37 °C), reductive amination of the reducing oligosaccharides with 2-aminobenzoic acid in the presence of sodium cyanoborohydride afforded the 2AA-labeled N-glycans, which could be separated by analytical reverse-phase HPLC and quantified relative to standard curves of pure 2AA-labeled N-glycan standards by peak integration. The results were summarized in Figure 3.4B.

To validate the N-glycolipid incorporation assay, S2G2-Asn-C16 vesicles of different glycan densities were subjected to the above procedure and N-glycolipid incorporation was compared to values obtained by the phenol-sulfuric acid assay. As seen in Figure 3.4, no significant difference in N-glycolipid incorporation was found between the two methods, indicating that the HPLC-based assay is a reliable quantitation method giving comparable incorporation values to the well-established phenol-sulfuric acid assay.

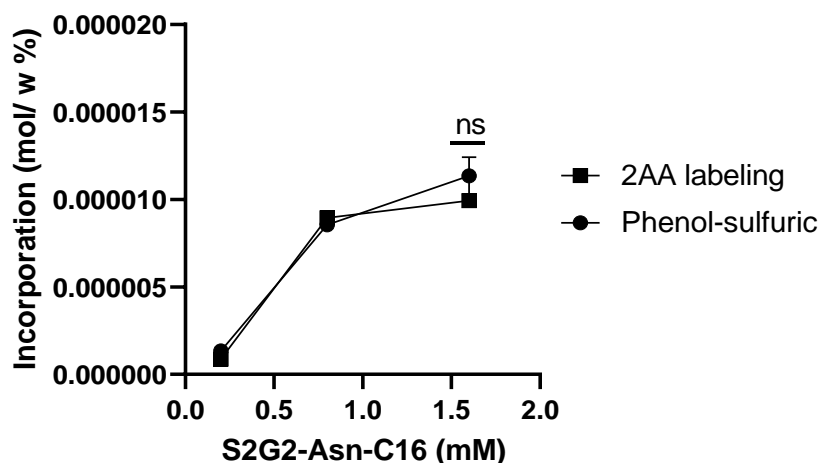
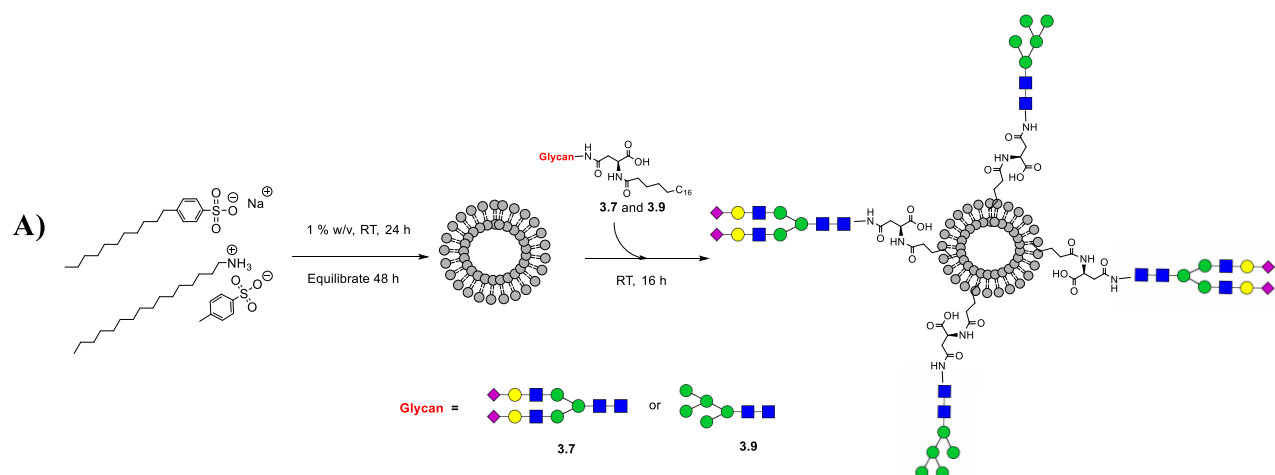


**Figure 3.4.** Vesicle N-glycolipid incorporation as determined by PSA and 2AA labeling assay for S2G2-Asn-C16 (H, M, and L) vesicle samples. “ns” = not significant. Measurements were done in duplicate.

Vesicles bearing both Man5 and S2G2 N-glycans were initially prepared by mixing bare vesicles with the respective N-glycolipids at equimolar concentrations of 0.2, 0.8, and 1.6 mM [S2G2/ Man5-gCV (LL), S2G2/ Man5-gCV (MM), and S2G2/ Man5-gCV (HH)]. The glycan content was then quantified by HPLC as described above. It was found that Man5-Asn-C16 incorporation values were very similar for vesicles Man5-gCV (M) and S2G2/ Man5-gCV (MM), with values of  $1.5 \times 10^{-6}$  mol/w % and  $1.4 \times 10^{-6}$  mol/w%, respectively. In addition, it was observed that an equimolar ratio of glycolipids S2G2-Asn-C16 and Man5-Asn-C16 were incorporated in samples S2G2/ Man5-gCV (LL) and S2G2/ Man5-gCV (MM), which were prepared by simply adding the two glycolipids at the same final concentration (Figure 3.5B). In the case of saturating glycolipid concentrations [i.e. S2G2/ Man5-gCV (HH)], approximately two times as much Man5-Asn-C16 was incorporated relative to S2G2-Asn-C16 when added at the same molar concentration, reflecting saturation of the vesicle surface with the bulky S2G2 headgroup and a corresponding increase in incorporation of the smaller Man5 N-glycolipid.

These results indicate that the smaller Man5 glycolipid incorporates into the vesicle bilayer at the expense of the bulky S2G2 glycolipid in vesicles bearing both glycans.

Heteromultivalent vesicles were also prepared which contain one glycolipid at a fixed concentration and the other glycolipid at variable concentrations. These samples serve to further clarify the influence of an unrelated glycan structure on recognition of the cognate glycan ligand. Thus, the Man5-GlcNAc<sub>2</sub>-Asn-C16 glycolipid was fixed at 0.2 mM concentration, while the S2G2-GlcNAc<sub>2</sub>-Asn-C16 concentration ranged from 0.2-1.6 mM, to prepare heteromultivalent vesicles of low Man5 and S2G2 incorporation [i.e. S2G2/ Man5-gCV (LL)], low Man5 and medium S2G2 incorporation [i.e. S2G2/ Man5-gCV (ML)], and low Man5 and high S2G2 incorporation [i.e. S2G2/ Man5-gCV (HL)]. Gratifyingly, these heteromultivalent vesicles contained comparable amounts of the Man5 glycolipid, and with a proportional increase in the S2G2 glycolipid as its concentration was increased (Figure 3.5B). We also measured the sizes of the nanoparticles by DLS analysis. It was found that heteromultivalent vesicles bearing both S2G2 and Man5 N-glycans were similar in size to the homomultivalent vesicles bearing the S2G2 or Man5 glycans only (Table 3.1).



**B)**

Vesicle sample	Glycan	Incorporation (mol/ w %)
S2G2/ Man5-gCV (LL)	Man5	$4.55 \times 10^{-7} \pm 0.01 \times 10^{-7}$
	S2G2	$4.6 \times 10^{-7} \pm 0.3 \times 10^{-7}$
S2G2/ Man5-gCV (MM)	Man5	$1.65 \times 10^{-6} \pm 0.07 \times 10^{-6}$
	S2G2	$1.56 \times 10^{-6} \pm 0.02 \times 10^{-6}$
S2G2/ Man5-gCV (HH)	Man5	$4.97 \times 10^{-6} \pm 0.05 \times 10^{-6}$
	S2G2	$2.81 \times 10^{-6} \pm 0.04 \times 10^{-6}$
S2G2/ Man5-gCV (ML)	Man5	$4.35 \times 10^{-7} \pm 0.05 \times 10^{-7}$
	S2G2	$2.13 \times 10^{-6} \pm 0.07 \times 10^{-6}$
S2G2/ Man5-gCV (HL)	Man5	$3.9 \times 10^{-7} \pm 0.1 \times 10^{-7}$
	S2G2	$3.89 \times 10^{-6} \pm 0.08 \times 10^{-6}$

**Figure 3.5.** A) Scheme for preparation of heteromultivalent vesicles from glycolipids **3.7** and **3.9**. B) N-glycolipid incorporation of hetero-multivalent S2G2/ Man5-gCV vesicles as quantified by HPLC-based assay.

**Lectin Recognition of Mixed Glycan-Containing Cationic Vesicles.** With the heteromultivalent N-gCVs in hand, we examined their interactions with mannose-specific lectin ConA and sialic acid specific lectin SNA. Previous work has demonstrated that an irrelevant glycan

could affect the affinity and specificity of protein-carbohydrate interactions such as the recognition of some lectins and antibodies for their cognate ligands and carbohydrate epitopes, which was coined as macromolecular crowding effect.<sup>36, 175-180</sup> Using a competitive binding assay, we first tested the lectin binding of the heteromultivalent vesicles containing equimolar amounts of S2G2 and Man5 glycans. It was found that at low loading of the Man5 ligand, the presence of the irrelevant sialylated complex N-glycan (S2G2) could significantly enhance the affinity (11 fold) of the Man5 ligand to lectin ConA in comparison with vesicle samples containing comparable levels of the Man5 ligand only (Figure 3.6A) [S2G2/ Man5-gCV (LL), IC<sub>50</sub> = 140 nM,  $\beta$  = 11]. Nevertheless, it was observed that in the case of medium and high loading of the Man5 glycolipid ligands [S2G2/ Man5 gCV (ML) and S2G2/ Man5 gCV (HL)], the presence of the sialylated N-glycan did not lead to further enhancement in ConA binding. The data suggest that the initial enhancement in ConA affinity is not due to specific recognition of the S2G2 glycan by ConA, but a result of a crowding effect, where recruitment of low-affinity glycan ligands promote entropically favorable and fast on-off binding events by carbohydrate-binding proteins, promoting a sliding mechanism by the lectin across the glycosylated surface and resulting in enhanced binding affinities.

We next tested the competitive inhibition of SNA with homo- and heteromultivalent vesicles containing similar amounts of the S2G2 N-glycolipid, namely, vesicles S2G2-gCV (L) and S2G2/ Man5-gCV (LL). Interestingly, the heteromultivalent vesicles were found to have slightly reduced affinity for the SNA lectin in comparison with the S2G2 glycolipid containing vesicles with similar ligand loading (Figure 3.6B). This result suggests that the presence of the irrelevant Man5 ligand is actually detrimental to the recognition of the S2G2 glycan by SNA, showing a negative crowding effect. By using synthetic sugar-bearing polymers to install a

mucin-like shield on red blood cell surface, Godula and co-workers have shown that glycocalyx crowding slows the rate of lectin SNA association with the sialylated glycan ligands on cell surface, but enhances the binding complex stability, resulting in an overall enhanced binding of soluble and virus-associated SNA to the host glycan receptors.<sup>181</sup> On the other hand, Kikkeri and coworkers have shown that several carbohydrate-binding proteins show decreased affinities for heteroglycoclusters when compared to homoglycoclusters bearing their cognate sugar ligands.<sup>36</sup> Taken together, these results suggest that molecular crowding can modulate the affinity of carbohydrate-binding proteins to their glycan ligands, and the effects (positive or negative) are dependent on the nature of the proteins/glycan ligands and the mode of the interactions. The glycan-bearing cationic vesicles described here provide a facile platform for further investigating specific lectin-glycan interactions.

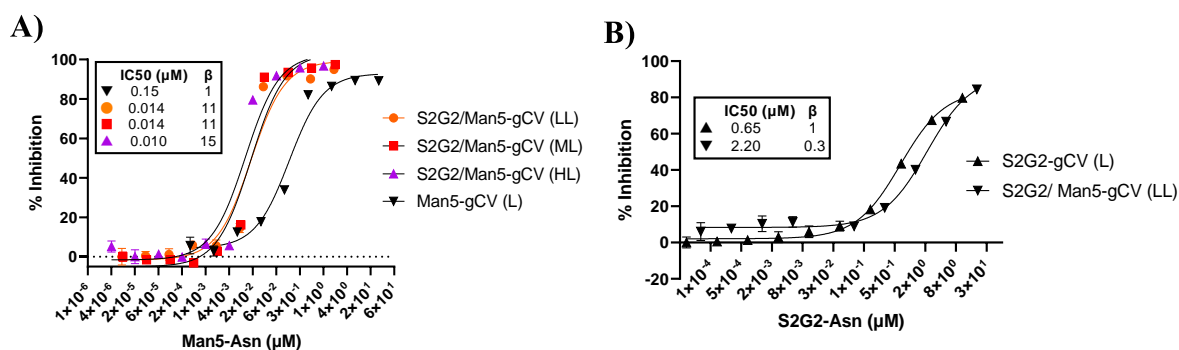


**Figure 3.6.** A) Competitive inhibition of ConA binding to Man5-BSA conjugates by S2G2/Man5-C16 heteromultivalent N-gCVs. B) Competitive inhibition of SNA binding to S2G2-BSA conjugates by S2G2/Man5-C16 heteromultivalent N-gCV and homomultivalent S2G2-C16 N-gCV.

### 3.3 CONCLUSION

A facile synthesis and characterization of cationic vesicle-based multivalent N-glycan ligands for lectins are described. The N-glycan-coated vesicles show significantly enhanced affinity for lectins *sambucus nigra* agglutinin (*SNA*), *concanavalin A* (*ConA*), and human galectin-3 over their specific monovalent N-glycan ligands (sialylated, high-mannose, and asialylated N-glycans), respectively, demonstrating a clear clustering glycoside effect. In addition, a positive crowding effect was observed on the binding of ConA to high-mannose N-glycan ligands when cationic vesicles bearing mixed high-mannose and complex type N-glycans were used. These N-glycan-coated cationic vesicles are stable and easy to formulate with variable density of ligands. The glycan bearing nanoparticles should be useful as a vehicle for drug delivery and as potent inhibitors for intervening specific carbohydrate-protein interactions in disease processes.

### **3.4 MATERIALS AND METHODS**

**Materials:** Lauric acid was purchased from Alfa Aesar. Sodium dodecylbenzenesulfonate (SDBS) and cetyltrimethylammonium tosylate (CTAT) were purchased from TCI America and Merck, respectively. N, N'-dicyclohexylcarbodiimide (DCC) coupling reagent was purchased from TCI America. High binding polystyrene 96-well ELISA plates were purchased from Santa Cruz Biotechnology, Inc. Biotin-ConA and biotin-SNA were purchased from Vector Laboratories. Galectin-3 with a His-tag at the N-terminus was purchased from Abcam. All other chemicals were purchased from Sigma Aldrich unless stated otherwise and used as received.

**Methods:** The biantennary complex-type containing sialoglycoprotein (SGP) was prepared from dried hen's egg yolk powder following the reported procedures.<sup>115, 116</sup> The crude soybean

agglutinin was prepared from soybean flour following a previously reported method.<sup>129</sup> Analytical reverse-phase HPLC was performed on a Waters Alliance® e2695 HPLC system equipped with a dual absorbance 2489 UV/Vis detector. Separations were performed using a C18 column (YMCTriart C18, 4.6 × 250 mm, 5 μm) at a flow rate of 1 mL/min using a linear gradient of 30-70% MeCN containing 0.1% TFA (trifluoroacetic acid) over 30 min and at 50 °C. Preparative HPLC was performed on a Waters 600 HPLC instrument with preparative reverse-phase C18 column (Waters Symmetry 300, 19x300 mm) and at a flow rate of 10 mL/min for all purifications. NMR spectra were measured with a Bruker AV III 600 MHz NMR spectrometer and the chemical shifts were assigned in parts per million. MALDI-TOF MS analysis was performed using a Bruker UltrafleXtreme (UTX) mass spectrometer with TOF/TOF detection and a dihydroxybenzoic acid/ dimethylaniline (DHB/DMA) matrix, samples were analyzed under reflectron ion mode. LC ESI-TOF MS was performed using an X-Bridge Shield RP18 3.5 μm (2.1 x 50 mm) short column coupled to a Micromass ZQ-4000 single quadrupole mass spectrometer. High-resolution mass was taken on an Exactive Plus Orbitrap (Thermo Scientific) with an Agilent Poroshell 300SB-C8 column (5 μm, 75 x 1 mm).

### **Synthesis of lauric acid and palmitic acid NHS esters**

N-hydroxysuccinimide (NHS) activated lipids NHS-C12 and NHS-C16 were prepared using N,N'-dicyclohexylcarbodiimide (DCC) as coupling reagent. Briefly, 1 g of lauric acid (C12) or palmitic acid (C16) was dissolved in 5 mL of dichloromethane (DCM) and 5 mL of tetrahydrofuran (THF) in a 50 mL round-bottom flask. The solution was then placed in an ice bath, capped with a rubber septum, and degassed under positive Argon pressure using a Schlenk-line. With Argon still passing through the solution, 1.1 mole equivalents of N-

hydroxysuccinimide (NHS) were added followed by 1.1 mole equivalents of DCC. Lastly, 0.05 mole equivalents of dimethyl-aminopyridine (DMAP) were added and the solution was stirred for 2 h when TLC indicated the completion of the reaction. The dicyclohexylurea (DCU) byproduct was precipitated by adding 5 mL of hexanes and 5 mL of diethyl ether, followed by vacuum filtration through a Celite pad. The filtrate was then concentrated under vacuum, and the residue was purified by flash chromatography using a Biotage SNAP Ultra 25 g cartridge: Mobile phase A: hexanes, mobile phase B: ethyl acetate; a 5-30% gradient of ethyl acetate over 25 column volumes. Fractions containing the product were pooled and concentrated *in vacuo* to obtain the target NHS-activated lipids.

*N-Hydroxysuccinimidyl lauric acid.* <sup>182</sup> 1.29 g NHS-C12 (87% yield) as a white solid. NHS-C12 <sup>1</sup>H-NMR (400 MHz, CDCl<sub>3</sub>): δ(ppm) 2.84 (s, 4H, CH<sub>2</sub> from NHS), 2.60 (t, 2H, J = 5.0 Hz, carbon C2), 1.74 (p, 2H, J = 5.0 Hz, carbon C3), 1.42 (m, 2H, CH<sub>2</sub>, carbon C4), 1.28 (m, 14H, CH<sub>2</sub>, carbons C5-11), 0.89 (t, 3H, J = 4.6 Hz, CH<sub>3</sub>).

*N-Hydroxysuccinimidyl palmitic acid.* <sup>182</sup> 1.31 g NHS-C16 (95% yield) as a white solid. <sup>1</sup>H-NMR (400 MHz, CDCl<sub>3</sub>): δ(ppm) 2.83 (s, 4H, CH<sub>2</sub> from NHS), 2.60 (t, 2H, J = 7.5 Hz, carbon C2), 1.73 (p, 2H, J = 7.5 Hz, carbon C3), 1.41 (m, 2H, carbon C4), 1.26 (m, 22H, CH<sub>2</sub> carbons C5-15), 0.89 (t, 3H, J = 7.0 Hz, CH<sub>3</sub>).

### General Method for Synthesis of the N-Glycolipids

Each glycan-Asn (10 mg) were first dissolved in 200  $\mu$ L of water, to which 800  $\mu$ L of N,N'-dimethylformamide (DMF) was added. Separately, 1.1 mole equivalents of the NHS activated lauric or palmitic acid was dissolved in 1 mL of DMF and the solution was added to the glycan-Asn solution in a 5 mL amber vial. To this reaction mixture was added 20  $\mu$ L of triethylamine (TEA). The resulting solution was stirred at room temperature for 3 h when LC-MS indicated the completion of the reaction. The mixture was diluted in 50% aqueous acetonitrile and lyophilized. The residue was then redissolved in 2 mL of water and purified by preparative RP-HPLC using a 30-70% MeCN (0.1% TFA) gradient over 30 min (mobile phase A: H<sub>2</sub>O containing 0.1% TFA, mobile phase B: acetonitrile containing 0.1% TFA). The fractions containing the glycolipid were pooled and lyophilized to obtain the respective glycolipids as a white solid. Proton chemical shifts for the N-glycan portions were assigned according to the previous NMR assignments of N-glycans reported by Kajihara, Pancera, and Shahzad-ul-Hussan.<sup>134, 183, 184</sup>

***S0G2-GlcNAc<sub>2</sub>-Asn-C12 (3.5)***: 7.4 mg (67% yield after HPLC purification). <sup>1</sup>H-NMR (400 MHz, D<sub>2</sub>O):  $\delta$  5.11 (s, 1H, Man-4 H-1), 5.04-5.03 (d, 1H, J = 9.2 Hz, GlcNAc-1 H-1), 4.94-4.90 (s, 1H, Man-4' H-1), 4.72-4.68 (m, 1H, Man-3 H-1) 4.64-4.54 (m, 3H, GlcNAc-2, GlcNAc-5 and GlcNAc-5' H-1), 4.49- 4.43 (m, 2H, Gal-6 and Gal-6' H-1), 4.24 (s, 1H, Man-3 H-2), 4.18 (s, 1H, Man-4 H-2), 4.10 (s, 1H, Man-4' H-2), 3.98-3.47, 2.85-2.74 (m, 2H, Asn-CH<sub>2</sub>), 2.29-2.22 (m, 2H, C2 of lipid) , 2.07-1.99 (m, 12H, NHAc), 1.60-1.53 (m, 2H, C3 of lipid), 1.31-1.20 (m, 16H, C4-C11 of lipid), 0.84 (t, 3H, J = 3.5 Hz, CH<sub>3</sub> of lipid). <sup>13</sup>C-NMR (125 MHz, D<sub>2</sub>O):  $\delta$  175.7, 174.2, 174.1, 174.0, 173.6, 172.1, 102.5, 100.9, 99.9, 98.9, 96.6, 79.8, 79.1, 78.2, 78.0, 77.8, 75.9, 75.9, 75.7, 74.9, 74.2, 73.9, 73.1, 72.4, 72.2, 72.0, 71.6, 71.5, 70.5, 69.7, 68.9, 68.1,

66.8, 65.2, 61.2, 60.5, 59.5, 54.4, 53.4, 48.6, 38.2, 36.6, 35.1, 31.0, 28.7, 28.5, 28.4, 28.3, 28.1, 24.8, 21.9, 21.8, 21.7, 13.2. Analytical HPLC:  $t_R = 10.55$  min. HRMS (ESI-MS): calcd for  $C_{78}H_{132}N_6O_{49}$ ,  $[M + 2H]^{2+} = 1938.8167$  Da; found,  $m/z$  1938.8165  $[M + 2H]^{2+}$ .

**S0G2-GlcNAc<sub>2</sub>-Asn-C16 (3.6):** 8 mg (71% yield after HPLC purification). <sup>1</sup>H-NMR (400 MHz, D<sub>2</sub>O):  $\delta$  5.10 (s, 1H, Man-4 H-1), 5.06-4.99 (m, 1H, GlcNAc-1 H-1), 4.9 (s, 1H, Man-4' H-1), 4.58- 4.51 (m, 2H, GlcNAc-5 and GlcNAc-5' H-1), 4.47-4.40 (m, 2H, Gal-6 and Gal-6' H-1), 4.21 (s, 1H, Man-3 H-2), 4.16 (s, 1H, Man-4 H-2), 4.08 (s, 1H, Man-4' H-2), 3.95-3.47, 2.85-2.65 (m, 2H, Asn-CH<sub>2</sub>), 2.25-2.15 (m, 2H, C2 of lipid), 2.09-1.95 (m, 12H, NHAc), 1.59-1.45 (m, 2H, C3 of lipid), 1.27-1.16 (m, 24H, C4-C11 of lipid), 0.84-0.78 (m, 3H, CH<sub>3</sub> of lipid). <sup>13</sup>C-NMR (125 MHz, D<sub>2</sub>O):  $\delta$  174.7, 174.2, 173.9, 173.3, 102.5, 100.9, 100.1, 99.1, 96.6, 79.7, 79.2, 78.1, 75.9, 74.9, 74.3, 74.0, 73.1, 72.1, 71.6, 71.5, 70.5, 69.8, 69.0, 68.1, 66.9, 65.3, 61.3, 60.6, 59.6, 54.4, 53.5, 48.5, 38.3, 35.3, 31.4, 29.3, 29.3, 29.2, 28.9, 28.7, 25.0, 22.1, 22.0, 21.8, 13.4. Analytical HPLC:  $t_R = 18.85$  min. HRMS (ESI-MS): calcd for  $C_{82}H_{140}N_6O_{49}$ ,  $[M + 2H]^{2+} = 1994.8793$  Da; found,  $m/z$  1984.8799  $[M + 2H]^{2+}$ .

**S2G2-GlcNAc<sub>2</sub>-Asn-C16 (3.7):** 10.1 mg (92% yield after HPLC purification). <sup>1</sup>H-NMR (400 MHz, D<sub>2</sub>O):  $\delta$  5.16 (s, 1H, Man-4 H-1), 5.09-5.02 (m, 1H, GlcNAc-1 H-1), 4.95 (s, 1H, Man-4' H-1), 4.66-4.56 (m, 3H, 2, GlcNAc-5 and GlcNAc-5' H-1), 4.45 (s, 2H, Gal-6 and Gal-6' H-1), 4.25 (s, 1H, Man-3 H-2), 4.20 (s, 1H, Man-4 H-2), 4.11 (s, 1H, Man-4' H-2), 4.06-3.48, 2.87-2.74 (m, 2H, Asn-CH<sub>2</sub>), 2.70-2.61 (m, 2H, NeuAc-7 and NeuAc-7' H-3<sub>eq</sub>), 2.33-2.19 (m, 2H, C2 of lipid), 2.12- 1.98 (m, 18H, NHAc), 1.86-1.76 (m, 2H, C3 of lipid), 1.62-1.51 (m, 2H,

NeuAc-7 and NeuAc-7' H-3<sub>ax</sub>), 1.32-1.20 (m, 24H, C4-C15 of lipid), 0.86 (t, 3H, J = 6.9 Hz, CH<sub>3</sub> of lipid). <sup>13</sup>C-NMR (125 MHz, D<sub>2</sub>O): δ 174.4, 174.2, 103.1, 100.0, 98.8, 95.1, 80.1, 79.4, 77.9, 75.9, 73.9, 73.1, 72.3, 72.0, 71.6, 70.7, 70.2, 69.8, 69.7, 68.9, 67.8, 67.2, 66.9, 66.4, 65.5, 62.7, 62.4, 61.2, 60.6, 59.7, 54.2, 53.5, 51.6, 51.3, 38.8, 38.5, 31.4, 29.2, 28.9, 24.9, 22.1, 22.00, 21.7, 21.6, 13.4. Analytical HPLC: t<sub>R</sub> = 17.82 min. HRMS (ESI-MS): calcd for C<sub>104</sub>H<sub>174</sub>N<sub>8</sub>O<sub>65</sub>, [M + 2H]<sup>2+</sup> = 1289.0368 Da; found, m/z 1289.0327 [M + 2H]<sup>2+</sup>.

**Man9-GlcNAc<sub>2</sub>-Asn-C16 (3.8):** 5.3 mg (47% yield after HPLC purification). <sup>1</sup>H-NMR (400 MHz, D<sub>2</sub>O): δ 5.39 (s, 1H, ManA H-1), 5.35-5.25 (m, 2H, Man4, ManC H-1), 5.12 (s, 1H, ManB H-1), 5.08-4.99 (m, 3H, Man D1-D3), 4.85 (s, 1H, Man4' H-1), 4.20 (s, 1H, Man3 H-2), 4.14-3.50, 2.87-2.65 (m, 2H, Asn-CH<sub>2</sub>), 2.28-2.14 (m, 2H, C2 of lipid), 2.05 (s, 3H, NHAc), 1.97 (s, 3H, NHAc), 1.60-1.47 (m, 2H, C3 of lipid), 1.30-1.16 (m, 24H, C4-C15 of lipid), 0.86-0.79 (m, 3H, CH<sub>3</sub> of lipid). <sup>13</sup>C-NMR (125 MHz, D<sub>2</sub>O): δ 174.7, 174.1, 173.3, 101.7, 100.2, 99.0, 97.5, 78.2, 77.9, 72.7, 72.3, 70.7, 69.9, 69.5, 69.0, 66.4, 65.2, 60.7, 60.6, 38.3, 36.7, 35.2, 31.4, 29.3, 29.2, 28.9, 28.7, 25.00, 22.1, 21.8, 13.4. Analytical HPLC: t<sub>R</sub> = 18.55 min. HRMS (ESI-MS): calcd for C<sub>90</sub>H<sub>154</sub>N<sub>4</sub>O<sub>59</sub>, [M + 2H]<sup>2+</sup> = 2236.9319 Da; found, m/z 2236.9345 [M + 2H]<sup>2+</sup>.

**Man5-GlcNAc<sub>2</sub>-Asn-C16 (3.9):** 6.5 mg (46% yield after HPLC purification). <sup>1</sup>H-NMR (400 MHz, D<sub>2</sub>O): δ 5.09-5.00 (m, 2H, ManE, ManF H-1, and ManG H-1), 4.87-4.81 (m, 2H, ManD H-1 and ManC H-1), 4.61-4.52 (m, 1H, GlcNAc-B H-1), 4.25-4.17 (m, 1H, ManC H-2), 4.12-4.07 (m, 1H, ManD H-2), 4.05-4.00 (m, 2H, ManE and ManF H-2), 3.89-3.44, 2.83-2.67 (m, 2H, Asn-CH<sub>2</sub>), 2.26-2.11 (m, 2H, C2 of lipid), 2.02 (s, 3H, NHAc), 1.94 (s, 3H, NHAc),

1.57-1.44 (m, 2H, C3 of lipid), 1.26-1.12 (m, 24H, C4-C15 of lipid), 0.81-0.75 (m, 3H, CH<sub>3</sub> of lipid). <sup>13</sup>C-NMR (125 MHz, D<sub>2</sub>O): δ 174.6, 173.9, 173.4, 172.0, 105.3, 102.1, 101.8, 101.4, 101.2, 100.1, 99.3, 98.9, 94.9, 93.3, 89.9, 81.0, 80.4, 79.2, 78.6, 78.1, 75.8, 73.9, 72.9, 72.3, 71.6, 70.5, 70.2, 70.0, 69.8, 69.6, 69.0, 66.5, 66.4, 65.3, 64.8, 60.7, 60.6, 59.4, 54.6, 53.6, 50.3, 48.7, 46.4, 44.1, 35.3, 31.5, 29.5, 29.3, 29.0, 28.8, 25.1, 22.2, 22.0, 21.9, 13.4. Analytical HPLC: t<sub>R</sub> = 19.92 min. HRMS (ESI-MS): calcd for C<sub>66</sub>H<sub>114</sub>N<sub>4</sub>O<sub>39</sub>, [M + H]<sup>+</sup> = 1587.7133 Da; found, m/z 1587.7001 [M + H]<sup>+</sup>.

### **General method for the synthesis of methoxy-squaric acid functionalized glycans.**

N-glycans S2G2-GlcNAc<sub>2</sub>-Asn, S0G2-GlcNAc<sub>2</sub>-Asn, Man9-GlcNAc<sub>2</sub>-Asn, and Man5-GlcNAc<sub>2</sub>-Asn were functionalized at the asparagine (Asn) N-terminus with 3,4-dimethoxy-3-cyclobutene-1,2-dione as previously described to yield the corresponding N-glycan-Asn-squaric acid monoamides.<sup>66</sup>

### **Formulation of bare and glycan-coated vesicles**

Catanionic vesicles were prepared according to a previously published procedure.<sup>158</sup> Briefly, 35.3 mg SDBS (0.1 mmol) was dissolved in 5 mL of water and 15.4 mg of CTAT (3.4 x 10<sup>-2</sup> mmol) was directly added to achieve a 1% w/v final surfactant concentration. The suspension was stirred for one hour to ensure complete dissolution and then allowed to equilibrate in the dark for 48 hours. Vesicles were purified from free detergent by Sepharose G-50 and elution was confirmed by Dynamic Light Scattering (DLS) scattering intensity.

Glycan-coated vesicles were prepared from 1 mL aliquots of crude vesicle solution taken prior to purification by Sepharose G-50 (performed vesicle). Then, varying amounts of each N-linked glycolipid were added from a 10 mg/ mL stock solution to reach final concentrations

ranging from 0.2 mM to 1.6 mM in water. The mixture was then stirred at room temperature for 24 hours and the vesicles purified by Sepharose G-50.

### **DLS measurements of hydrodynamic size**

Intact vesicles were characterized for mean hydrodynamic radius using a Photocor-FC dynamic light scattering instrument. Measurements were done using a 5 mW laser polarized at 633nm and the scattering angle was 90° for all measurements. All measurements were conducted at room temperature in 1 mL glass vials.

### **General Method for Endo-CC Catalyzed Glycan Release**

Aliquots of each glycan-coated vesicle (0.5 mL) were incubated with ethanol at a 20% final concentration (v/v) for 1 h and then lyophilized. The lyophilized film was dissolved in 1 mL of water containing 0.1% TFA and loaded onto a preconditioned 100MG Hypersep C18 column (per manufacturer instructions). The column was then washed with 1 mL of water and a gradient 5%-90%) of aqueous acetonitrile containing 0.1% TFA. The fractions were analyzed by MALDI-TOF MS with DHB as matrix under reflectron-positive or negative mode. Efficient separation of the glycolipids from the surfactants was achieved, with the 30 % and 40 % acetonitrile fractions containing the glycolipids and the 90 % acetonitrile fraction containing the vesicle-associated detergents. Fractions containing the glycolipid were combined and lyophilized, and then resuspended in 200  $\mu$ L of 100 mM PB buffer (pH 7.4) prior to hydrolysis by 1  $\mu$ L of Endo-CC (1 mg/ mL) at 37 °C for 36 h.

***Endo-CC cleavage of S0G2-GlcNAc<sub>2</sub>-Asn-C16***: MALDI-TOF-MS of the released glycan, calcd for S0G2-GlcNAc<sub>1</sub> (C<sub>54</sub>H<sub>91</sub>N<sub>3</sub>O<sub>41</sub>),  $M = 1437.5$  Da; found,  $m/z$  1460.7 [M + Na]<sup>+</sup>

***Endo-CC cleavage of S2G2-GlcNAc<sub>2</sub>-Asn-C16:*** MALDI-TOF-MS of the released glycan, calcd for S2G2-GlcNAc<sub>1</sub> (C<sub>76</sub>H<sub>125</sub>N<sub>5</sub>O<sub>57</sub>),  $M = 2019.7$  Da; found,  $m/z$  2040.8 [M + Na – 2H]<sup>+</sup>

***Endo-CC cleavage of Man9-GlcNAc<sub>2</sub>-Asn-C16:*** MALDI-TOF-MS of the released glycan, calcd for Man9-GlcNAc<sub>1</sub> (C<sub>62</sub>H<sub>105</sub>NO<sub>51</sub>),  $M = 1679.6$  Da; found,  $m/z$  1702.6 [M + Na]<sup>+</sup>

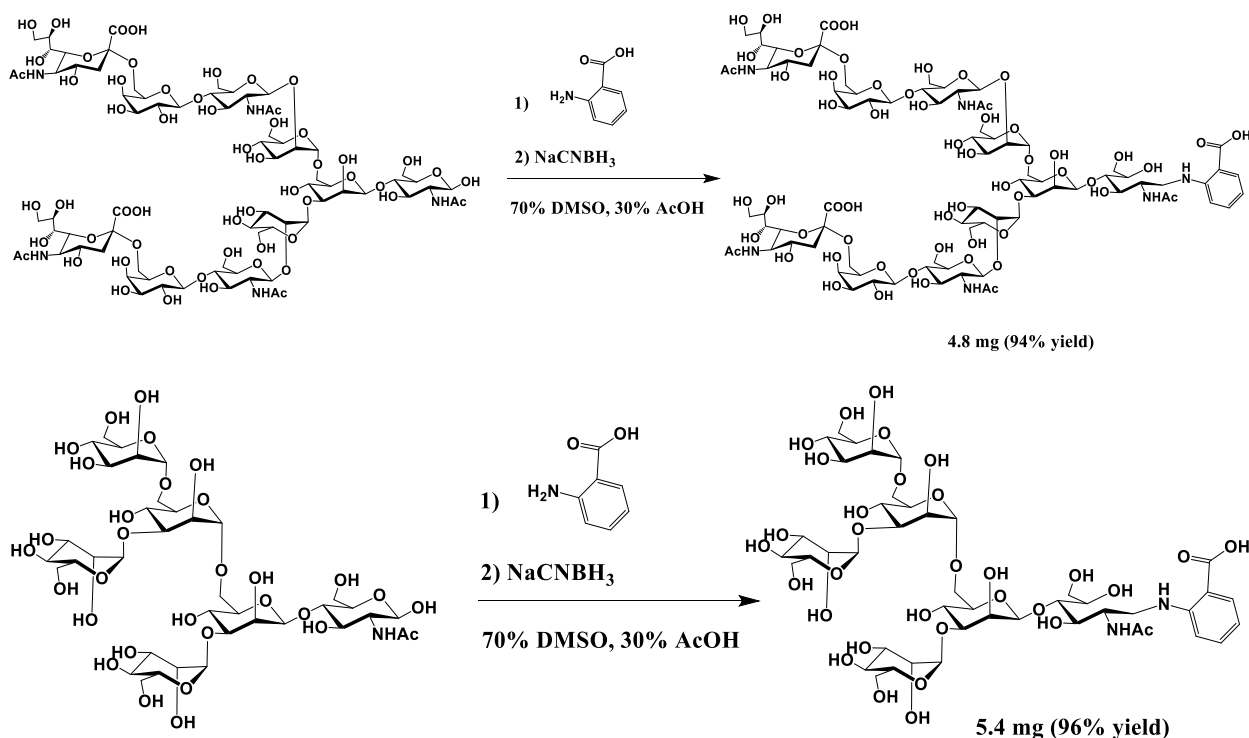
***Endo-CC cleavage of Man5-GlcNAc<sub>2</sub>-Asn-C16:*** MALDI-TOF-MS of the released glycan, calcd for Man5-GlcNAc<sub>1</sub> (C<sub>38</sub>H<sub>65</sub>NO<sub>31</sub>),  $M = 1031.3$  Da; found,  $m/z$  1054.9 [M + Na]<sup>+</sup>

### **Quantification of glycan incorporation by Phenol-Sulfuric acid assay (PSA)**

Glycan incorporation was measured using a variation of the phenol-sulfuric acid assay method employed by Lee and coworkers.<sup>162</sup> First, stock solutions of the relevant glycan-Asn (S0G2-GlcNAc<sub>2</sub>-Asn, Man9-GlcNAc<sub>2</sub>-Asn, and S2G2-GlcNAc<sub>2</sub>-Asn) were prepared at 2 mg/ mL in water for use as standards. These stock solutions were serially diluted in 1.5 mL microcentrifuge tubes to obtain 0.8 μg/ μL, 0.6 μg/ μL, 0.4 μg/ μL, 0.2 μg/ μL and 0 μg/ μL final concentrations in 50 μL volumes. G-50 fractions of glycan-coated vesicles were combined into a 1 mL aliquot in a pre-weighed microcentrifuge tube before being lyophilized. The final weight of the vesicle was recorded and the solid was resuspended in 250 μL of water. Fifty microliters of each vesicle solution were taken for analysis by PSA assay. For samples with high final concentrations of the glycolipid (≥ 0.4 mM), the resuspended solution was diluted 1: 2 in water.

To each 50  $\mu\text{L}$  of the solution in a microcentrifuge tube, was added 150  $\mu\text{L}$  of concentrated sulfuric acid quickly followed by 30  $\mu\text{L}$  of 5% aqueous phenol. The mixtures were vortexed and then incubated in a 90° C heat block for 5 min, followed by a room temperature water bath for 5 min. When the tubes had reached room temperature, 60  $\mu\text{L}$  of 95% ethanol were added to each tube to a final concentration of 20% v/v. The solution in the microcentrifuge tubes was then transferred to a 96-well microplate and allowed to incubate for 1 h before reading the absorbance at 490 nm. A bare vesicle sample was used as a negative control, all samples were plated in triplicate. Glycan incorporation was quantified using the line of best fit for the plot of N-glycan-Asn concentration vs. absorbance at 490 nm as a standard curve. Incorporation percent (mol/w %) was then calculated by dividing the amount of vesicle-incorporated glycolipid by the recorded weight of dry vesicle.

## Synthesis of S2G2-2AA and Man5-2AA HPLC standards

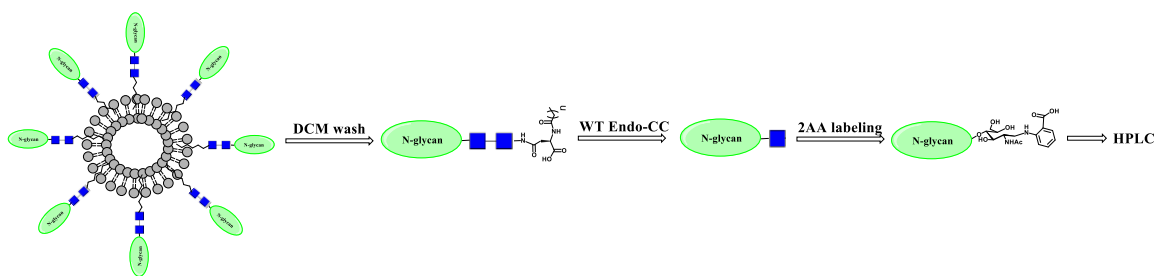


Each N-glycan (~6 mg) was weighed out into separate 2 mL centrifuge tubes and dissolved in 500  $\mu$ L of PBS (pH 7.4), to which wild-type Endo-CC enzyme was added to a 1:1,000 enzyme: substrate ratio (w/w). The tubes were placed in a 37  $^{\circ}$ C incubator and the reaction was continued overnight. Reaction progress was checked by MALDI-TOF MS and LC-MS, both reactions were complete after 30 h. The cleaved N-glycans were each purified by Sepharose G-10 and lyophilized. The lyophilized solids were then weighed and reacted with 50 mol equiv. of 2-aminobenzoic acid (2AA) and sodium cyanoborohydride (NaCNBH<sub>3</sub>) in 500  $\mu$ L of 70% DMSO/30% acetic acid (AcOH) at 65  $^{\circ}$ C over 3 h when LC-MS indicated the completion of the reaction. The 2AA-labeled glycans were diluted in 50% aqueous acetonitrile (MeCN) and lyophilized. The residues were purified by Sepharose G-15 to afford the 2AA-labeled glycans.

**S2G2-2AA:** 4.8 mg (94% yield) from 5.6 mg S2G2-GlcNAc<sub>2</sub>-Asn. ESI-MS: calcd for C<sub>83</sub>H<sub>132</sub>N<sub>6</sub>O<sub>58</sub>,  $[M + 2H]^{2+} = 1071.4$  Da; found,  $m/z$  1071.7  $[M + 2H]^{2+}$ .

**Man5-2AA:** 5.4 mg (96% yield) from 6.6 mg Man5-GlcNAc<sub>2</sub>-Asn. ESI-MS: calcd for C<sub>45</sub>H<sub>72</sub>N<sub>2</sub>O<sub>32</sub>,  $[M + H]^+ = 1153.4$  Da; found,  $m/z$  1153.7  $[M + H]^+$ .

### I. Method for novel HPLC-based glycolipid incorporation assay



A 0.5-1 mL pooled sample of Sepharose G-50 purified N-glycan coated cationic vesicle was lyophilized in a pre-weighed 2 mL Eppendorf tube. Final weight after lyophilization was recorded and the sample was resuspended in 500  $\mu$ L of water and the same volume of dichloromethane (DCM). The biphasic mixture was vortexed at high speed for 1 min to extract vesicle-associated detergents. The sample was then centrifuged at 14,000 rpm for 5 min or until clarification of the emulsion. The upper aqueous layer was carefully pipetted into a new 2 mL Eppendorf tube, making sure to avoid the white emulsion (detergent) at the water-DCM interface. Fresh DCM (0.5 mL) was added, and the process was repeated twice, each time pipetting the top aqueous layer into a new Eppendorf tube. Each of the DCM layers were then back-extracted with 250  $\mu$ L aliquot of water, and this volume was combined with the previous aqueous extract, bringing the final volume to 750  $\mu$ L. Care was taken to avoid pipetting DCM into the pooled aqueous layers.

To the aqueous vesicle extract was added 1 M PBS (pH 7.4) to a final concentration of 100 mM, followed by 5  $\mu$ L of WT Endo-CC (0.88 mg/ mL) for the hydrolysis of the N-glycans. This mixture was incubated at 37 °C for 24 h when MALDI-TOF MS indicated the complete hydrolysis of glycolipids by Endo-CC. The enzyme was denatured by incubation at 95 °C for 5 min followed by high-speed centrifugation. The supernatant was transferred to a new tube and lyophilized.

Following cleavage of the glycolipids, the free N-glycans were tagged with 2-aminobenzoic acid (2AA) by reductive amination at the free reducing end. A stock 2AA labeling solution was first prepared by dissolving 6.3 mg of 2AA and 6 mg of sodium cyanoborohydride (NaCNBH<sub>3</sub>) in 100  $\mu$ L of 70% DMSO/ 30% acetic acid. Next, the lyophilized glycan was mixed with 30  $\mu$ L of the stock labeling solution and the resulting solution was incubated at 65 °C for 3 h in a heat block. After reaction completion, the sample was briefly centrifuged and then dissolved in 1 mL of 5% acetonitrile containing 0.1% TFA. To purify the 2AA labeled N-glycans from buffer salts and excess labeling reagent, a 50MG PGC cartridge (Thermo Scientific) was used. The PGC cartridge was washed and preconditioned per the manufacturer's instructions, the sample in 5% MeCN containing 0.1% TFA was loaded onto the cartridge and then washed once with 1 mL of 5% MeCN, twice with 1 mL of 30% MeCN, and twice with 1 mL of 90% MeCN, all containing 0.1% TFA. The fraction containing the 2AA-labeled glycans as indicated by MALDI-TOF MS analysis were pooled and lyophilized.

Samples were then resuspended in 30  $\mu$ L of water and analyzed with a Waters Alliance® e2695 HPLC system. Separations were performed using a C18 column (YMCTriart C18, 4.6  $\times$  250 mm, 5  $\mu$ m) at a flow rate of 1 mL/min using a linear gradient of 5-15% MeCN containing 0.1% TFA over 30 min and with dual UV detection at 214 nm and 266 nm. All samples were

injected in duplicate. Relevant peaks were collected and analyzed by MALDI-TOF MS to confirm product elution, LC peaks were integrated using Chromeleon™ data processing software at 266 nm wavelength. Glycan incorporation was determined relative to the standard curve of the corresponding 2AA labeled N-glycan and expressed relative to the recorded vesicle weight.

### **Synthesis of N-glycan-BSA coating antigens for ELLA.**

Commercial grade bovine serum albumin was allowed to react with each N-glycan-Asn-squaric acid monoamide in 200 mM carbonate buffer pH 9.5 as previously described.<sup>66</sup> The BSA-conjugates were purified by dialysis against water and then lyophilized. The fluffy solids were redissolved in water and diluted to a 5 µg/mL working concentration in PBS before coating the 96-well plates.

### **Competitive Enzyme-linked Lectin Assay (ELLA)**

BSA conjugates (100 µL of a 5 µg/mL solution in PBS, pH 7.4) were added to a 96 well plate (Santa Cruz Biotechnology, Inc. High-binding polystyrene) and incubated at 4 °C overnight. Liquid was removed and the wells were washed three times with 200 µL of PBST (PBS + 0.05% Tween-20). The wells were then blocked with 300 µL of the blocking buffer (3% BSA w/v in PBS) at 37 °C for 1 h. After washing, 100 µL serial dilutions of each lectin [ $10^{-2}$ - $10^{-8}$  mg/ mL lectin, in PBS for biotin-SNA and His-Galectin-3, in 10 mM HEPES (+ 0.15 M NaCl, 0.01 mM  $Mn^{2+}$  and 0.1 mM  $Ca^{2+}$ ) for biotin-ConA] were added to the wells and incubated at room temperature for 1 hour. The wells were washed with PBST four times. For the biotinylated lectins (i.e. ConA and SNA), 100 µL of a 1: 15,000 dilution Streptavidin-HRP (abcam) in PBS were added and incubated for 1 hour at room temperature. For Galectin-3, 100 µL of a 1: 1,000 dilution of anti-His tag mouse mAb (R&D Systems) in PBS were added to each well and incubated for 1 hour at room temperature. Wells were washed five times with PBST before mixing equal volumes of

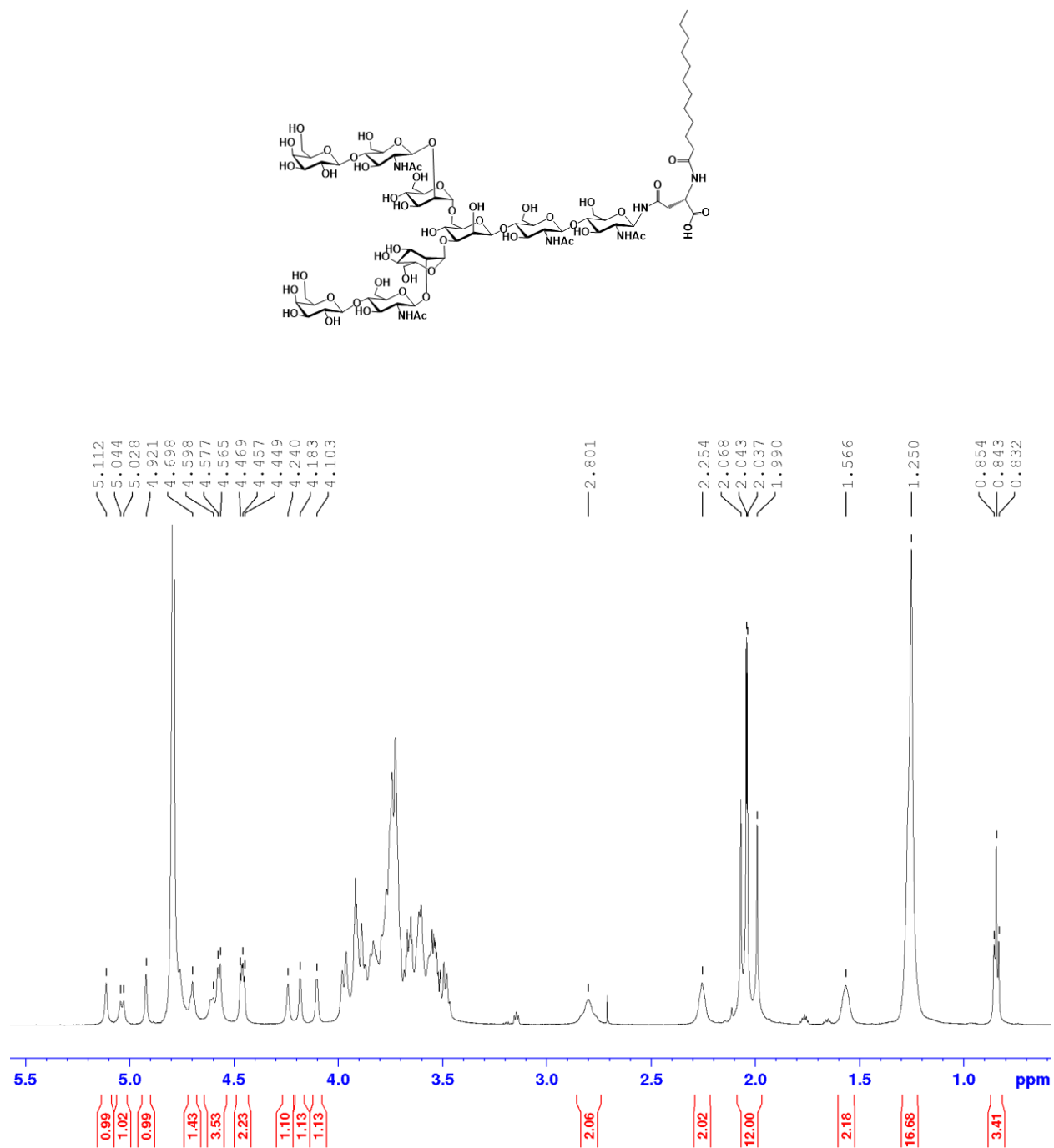
KPL TMB Peroxidase Substrate and KPL TMB Peroxidase Substrate Solution B and adding 100  $\mu\text{L}$  to each well. The plate was incubated for 30 min at room temperature in the dark, and the reaction was stopped by addition of 100  $\mu\text{L}$  of 1 M phosphoric acid. Absorbance was measured at 450 nm with a Spectramax M5e microplate reader with background correction at 550 nm. The optimal concentration of each lectin was taken as that resulting in an absorbance reading of 0.8 – 1 AU and were as follows:  $5 \times 10^{-6}$  mg/ mL biotin-ConA,  $1 \times 10^{-5}$  mg/ mL biotin-SNA,  $2 \times 10^{-3}$  mg/ mL His-Galectin-3.

For inhibition experiments, 2-fold serial dilutions of each monovalent glycan-Asn (1 mM stock solution) and 4-fold serial dilutions of each N-glycan-coated vesicle were prepared. 100 ml of each inhibitor solution was premixed with the corresponding biotinylated lectin (at the optimal concentration noted above) and incubated for 30 min at r.t. in a separate U-bottom 96 well plate. The lectin/ inhibitor mixture was then added to the blocked, N-glycan-BSA coated plate and incubated for 1 h at r.t. The rest of the procedure was followed as outlined above. Percent inhibition was determined using the equation below, where ‘A’ represents absorbance:

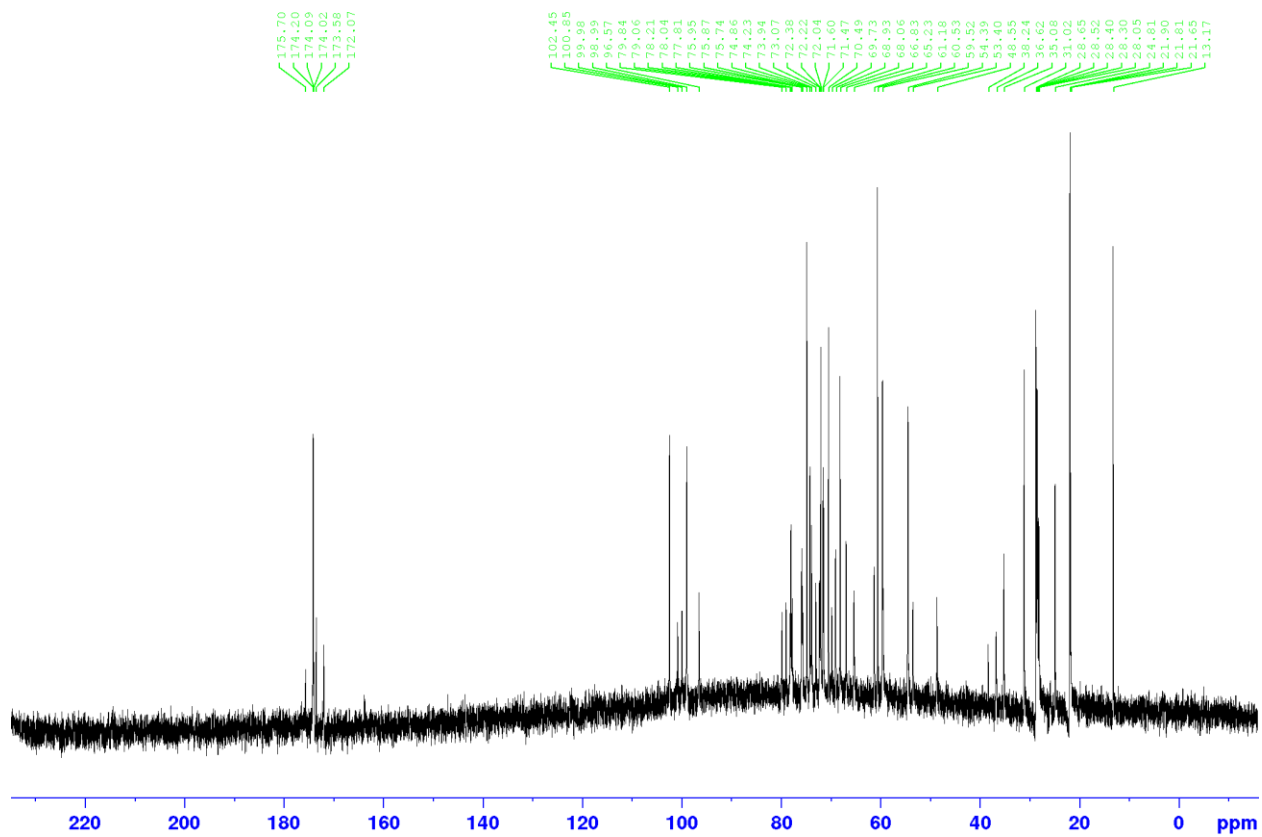
$$\% \text{ Inhibition} = (A_{(\text{no inhibitor})} - A_{(\text{with inhibitor})}) / A_{(\text{no inhibitor})} \times 100$$

Each sample was plated in triplicate for competitive ELLA and in direct binding assays.  $\text{IC}_{50}$  values were determined by nonlinear regression using Graphpad Prism software.

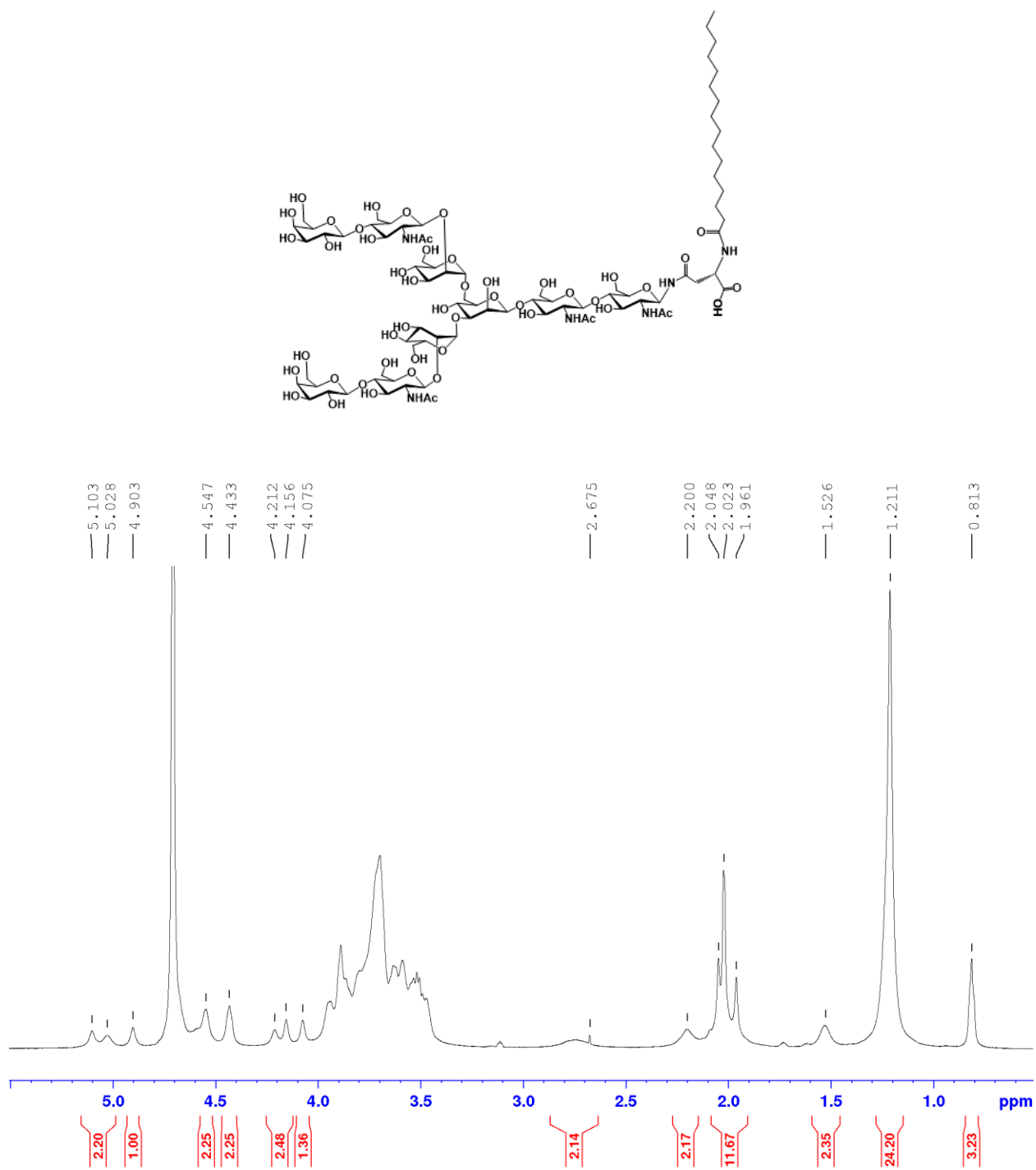
### 3.5 SUPPORTING INFORMATION



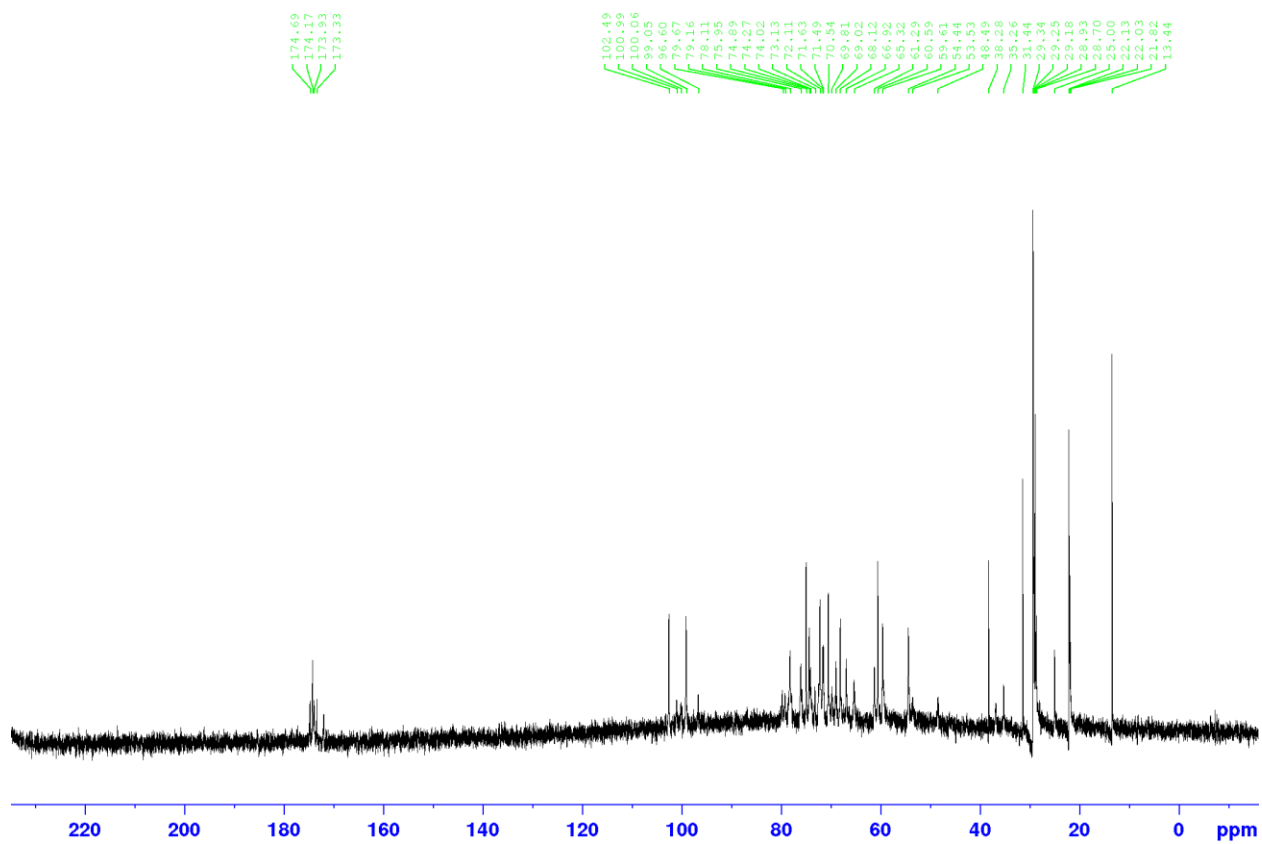
<sup>1</sup>H-NMR spectrum (600 MHz, D<sub>2</sub>O) of compound 3.5.



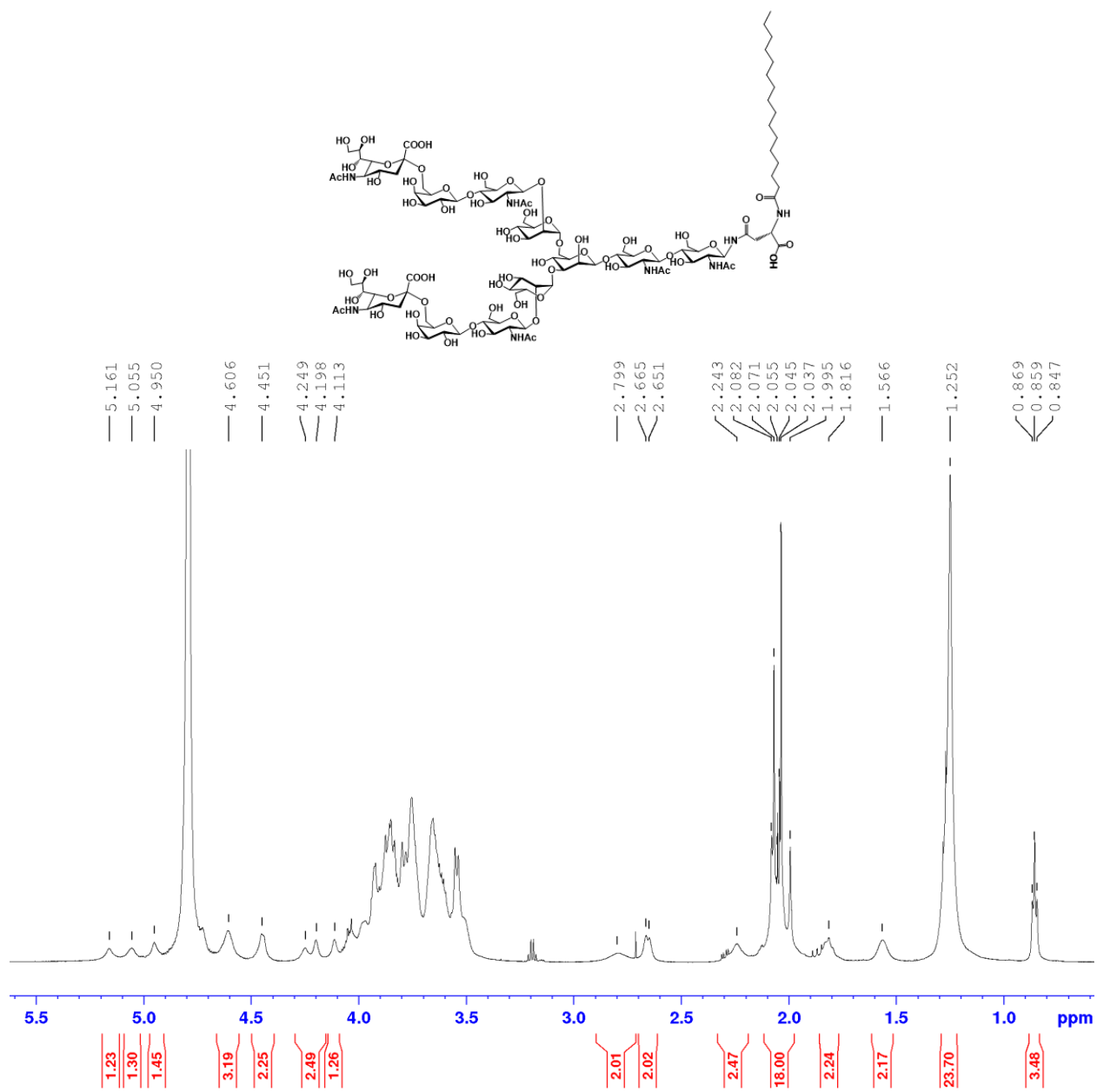
$^{13}\text{C}$ -NMR spectrum (125 MHz,  $\text{D}_2\text{O}$ ) of compound **3.5**.



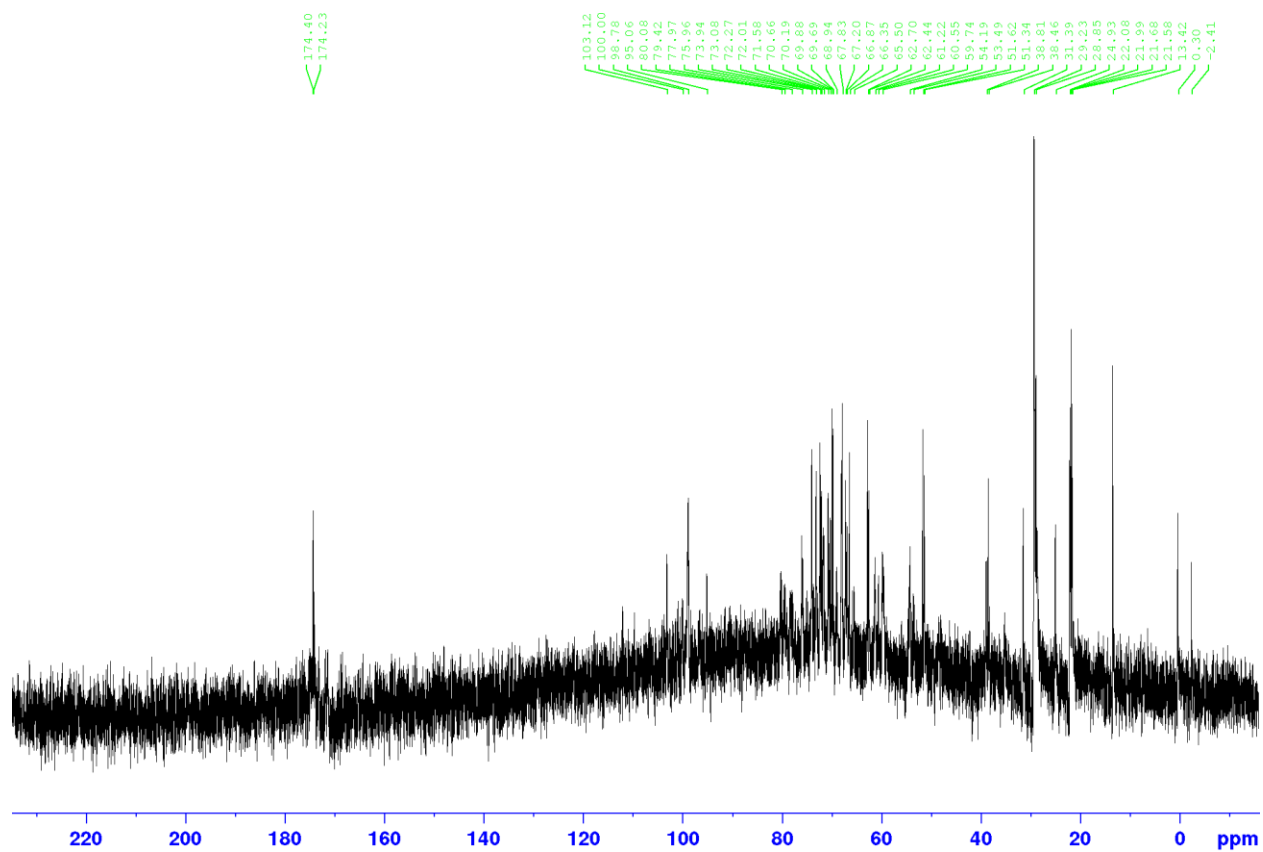
<sup>1</sup>H-NMR spectrum (600 MHz, D<sub>2</sub>O) of compound 3.6.



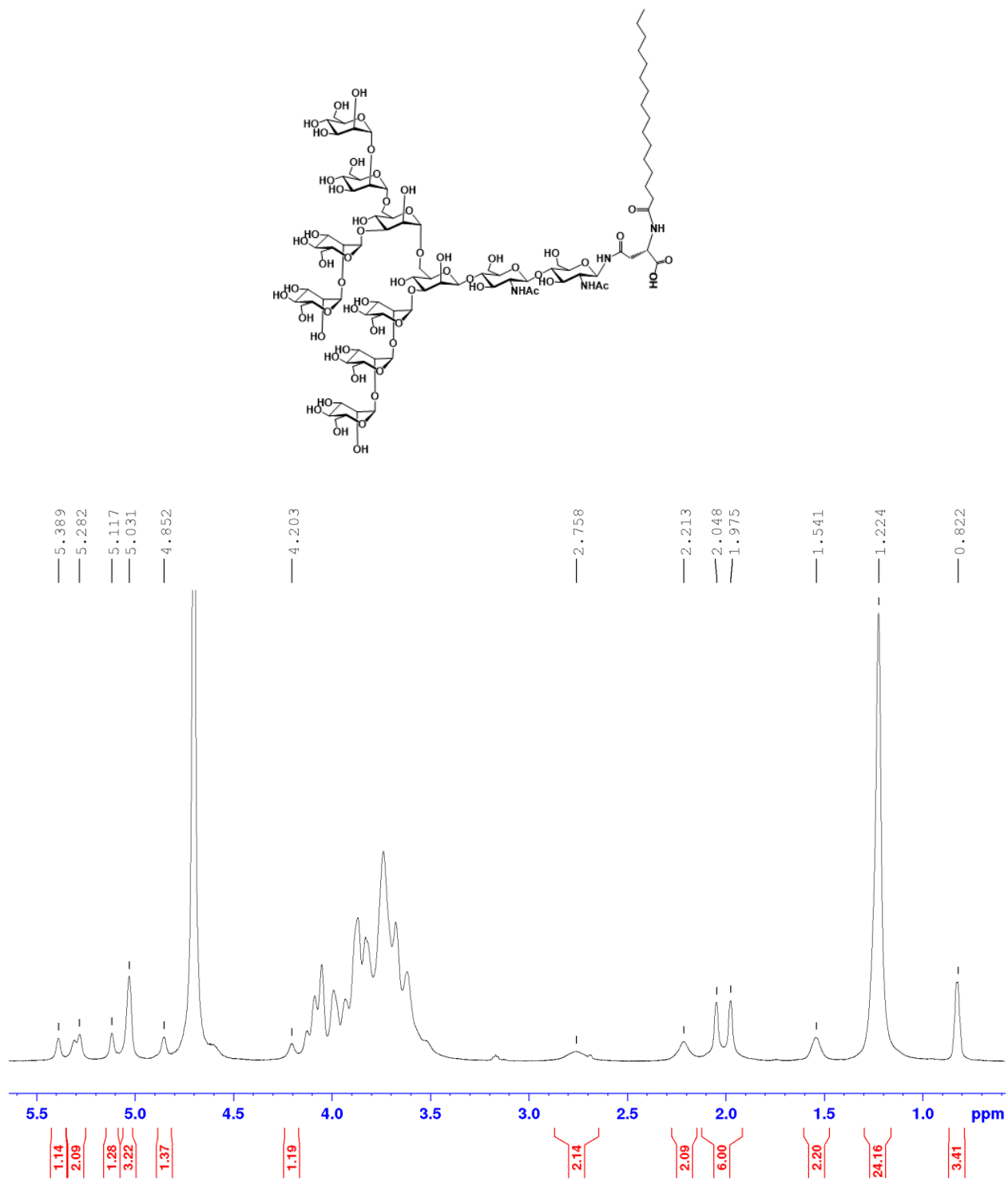
$^{13}\text{C}$ -NMR spectrum (125 MHz,  $\text{D}_2\text{O}$ ) of compound **3.6**.



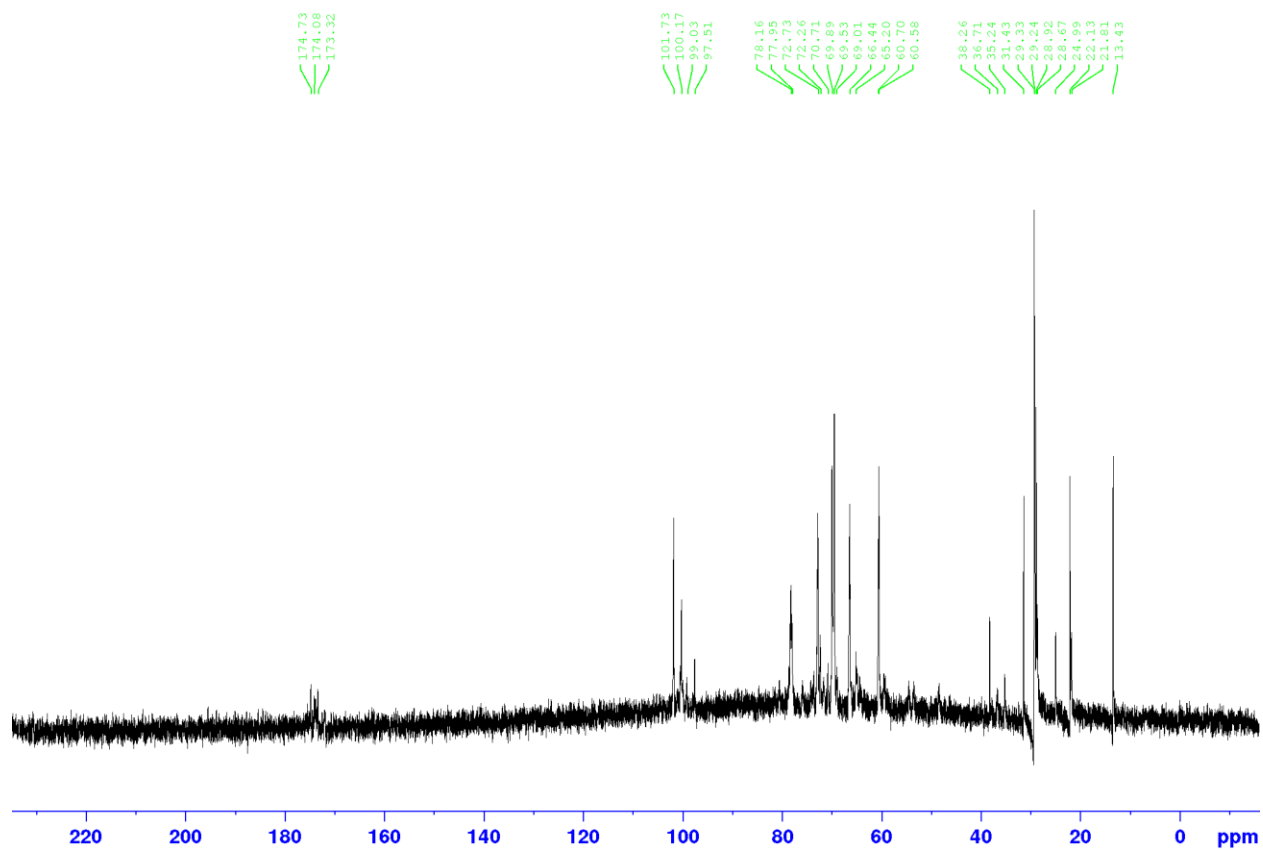
<sup>1</sup>H-NMR spectrum (600 MHz, D<sub>2</sub>O) of compound 3.7.



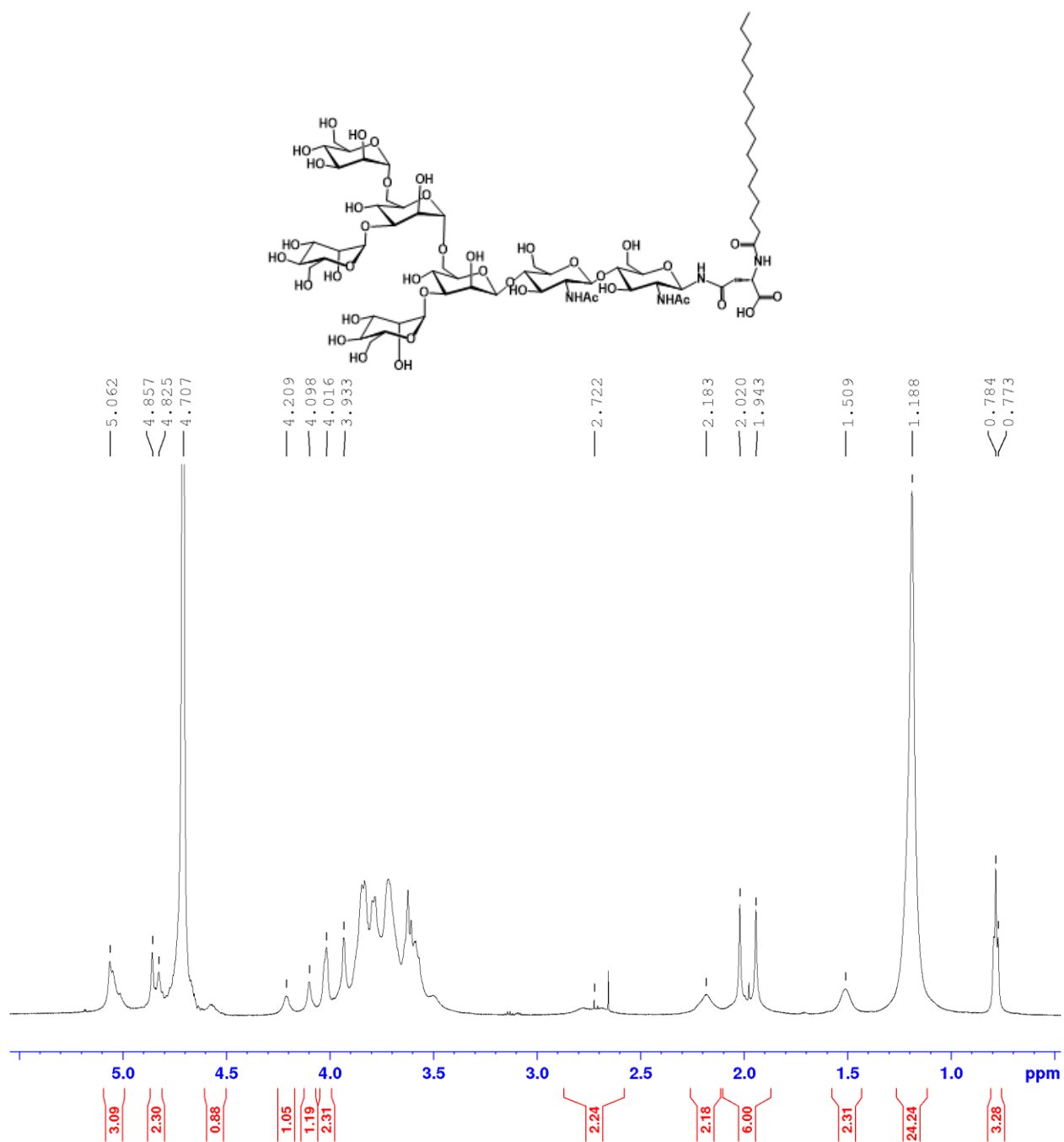
$^{13}\text{C}$ -NMR spectrum (125 MHz,  $\text{D}_2\text{O}$ ) of compound **3.7**.



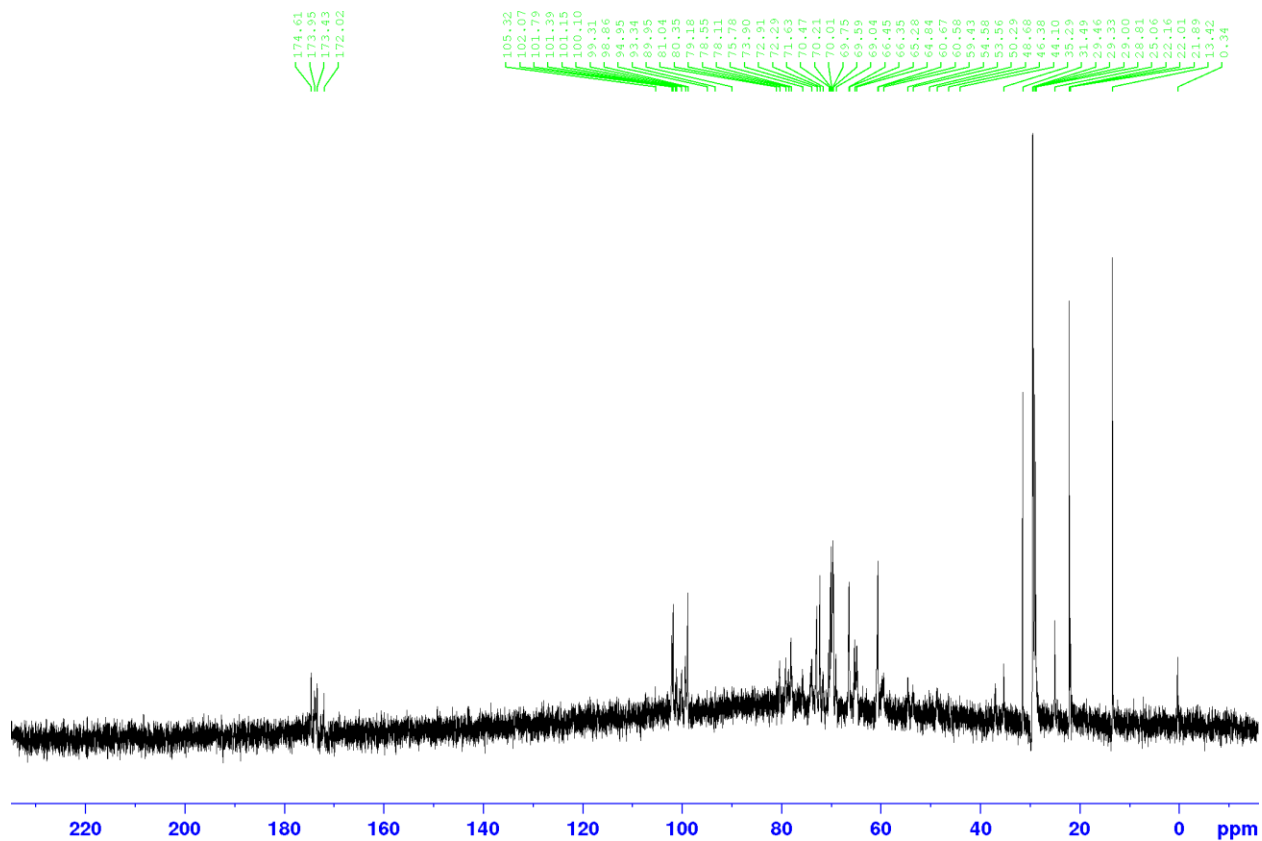
$^1\text{H-NMR}$  spectrum (600 MHz,  $\text{D}_2\text{O}$ ) of compound **3.8**.



<sup>13</sup>C-NMR spectrum (125 MHz, D<sub>2</sub>O) of compound **3.8**.



$^1\text{H-NMR}$  spectrum (600 MHz,  $\text{D}_2\text{O}$ ) of compound 3.9.



$^{13}\text{C}$ -NMR spectrum (125 MHz,  $\text{D}_2\text{O}$ ) of compound **3.9**.

## Chapter 4: Synthetic Site-Specific Antibody-Ligand Conjugates Promote Degradation of Extracellular Human PCSK9 Mediated by the Liver Asialoglycoprotein Receptor

This work was published in *ACS Chemical Biology*.<sup>185</sup>

Donahue, T. C.; Ou, C.; Yang, Q.; Flinko, R.; Zhang, X.; Zong, G.; Lewis, G.; Wang, L. X., Site-Specific Antibody Conjugates Promote the Degradation of Human PCSK9 Mediated by the Liver Asialoglycoprotein Receptor. *ACS Chem. Biol.*, **2023**. Published online: <https://doi.org/10.1021/acscchembio.3c00229>

T.C.D. and L.X.W. conceived the idea; T.C.D., Q.Y. and L.X.W. designed experiments; T.C.D performed the experiments; C.O. performed part of the cell-based experiments; R.F. and G.L. performed flow cytometry experiments and analyzed data; X.Z. and G.Z. assisted in chemical synthesis; T.C.D. and L.X.W. wrote the manuscript; all the co-authors contributed to the revision of the manuscript.

### **4.1 INTRODUCTION**

Protein degradation is an important mechanism in biological systems to maintain protein homeostasis and protein quality control.<sup>186, 187</sup> In eukaryotes, there are several degradation compartments including the proteasome, lysosome, and autophagosome.<sup>188</sup> The degradative mechanisms of these compartments have been leveraged to perform targeted-protein degradation and deplete pathogenic proteins or other proteins of interest (POI) with great success.<sup>189-191</sup> For example, Deshaies and co-workers have reported the first proteolysis targeting chimeras (PROTACs), consisting of a small molecule ligand for an E3 ubiquitin ligase and a ligand specific for the POI, as bifunctional molecules that can recruit ubiquitin ligase enzymes to target proteins resulting in their polyubiquitination and proteasomal degradation.<sup>189</sup> PROTACs were shown to be effective degraders of intracellular target proteins, which encouraged the development of several other targeted-protein degradation (TPD) strategies employing similar

mechanisms of action such as specific and non-genetic inhibitor of apoptosis protein (IAP)-dependent protein erasers (SNIPERs), molecular glues, autophagy-targeting chimeras (AUTACs), and even bacteria PROTACs (BacPROTACs) for degradation of bacterial proteins.<sup>191-194</sup> The early development of sweeping antibodies, Abdegs and Seldegs, which make use of the FcRn receptor for degradation of extracellular proteins by protein-engineered pH responsive antibodies or Fc-antigen fusions, has spurred the development of other TPD platforms for the degradation of extracellular proteins.<sup>195-197</sup> For example, Bertozzi and co-workers have developed lysosome targeting antibody chimeras (LYTACs) as a strategy for targeted degradation of extracellular proteins.<sup>190</sup> This strategy has been expanded by other groups using different antibodies, novel heterobifunctional small molecules, and/or different receptors for targeted degradation of extracellular as well as membrane-associated proteins.<sup>190, 197-199</sup>

The LYTAC approach makes use of extracellular lysosome targeting receptors (LTRs) such as the asialoglycoprotein receptor (ASGPR) with specificity for galactose or N-acetylgalactosamine (GalNAc)-containing glycoproteins. Synthetic ligands for the LTRs are conjugated to monoclonal antibodies specific for the POI. In this way, the LYTAC can bridge the POI and the LTR to enable endocytosis and delivery of the POI to the lysosome for degradation. To date, several LTRs, including CI-M6PR (Cation-Independent Mannose-6-Phosphate Receptor), ASGPR, integrin, and membrane bound E3 ligase RNF43 have been successfully utilized for targeted protein degradation.<sup>190, 198, 200-202</sup> Despite the recent progress in ASGPR-dependent degradation strategies, much remains to be known about the substrate scope of this receptor and what constitutes an effective glycan ligand for successful lysosomal delivery of the protein target. In fact, since the optimization of the high-affinity synthetic tri-GalNAc ligand for ASGPR, it has been used almost exclusively for the delivery of therapeutics or probes

to the liver.<sup>11</sup> Also, in most reports leveraging lectin-based LTRs for targeted-degradation, synthetic glycan ligands are attached by random conjugation chemistries resulting in highly heterogenous antibody conjugates that are difficult to characterize and optimize.<sup>190, 200, 201</sup> On the other hand, previous work from our lab showed that chemoenzymatic antibody glycan remodeling could be used to install a minimal M6P-containing structure site-specifically on Asn297 of the antibody Fc and result in significant CI-M6PR mediated degradation of membrane-bound protein targets, demonstrating that this can be a viable approach to obtain structurally well-defined and homogeneous LYTACs.<sup>203</sup>

LYTAC strategies have been attempted for the degradation of several clinically relevant extracellular proteins, such as PDL-1 and HER-2.<sup>190, 198, 200, 202, 203</sup> In the present study, we chose the proprotein convertase subtilisin/ kexin type 9 (PCSK9) as a target to demonstrate the clinical potential of LYTACs for the treatment of diseases like hypercholesterolemia. PCSK9 is a liver secreted protease, the presence of which is known to reduce low-density lipoprotein receptor (LDLR) levels, resulting in higher levels of the low-density lipoprotein (LDL-C) and thus higher risk of cardiovascular disease.<sup>204</sup> Extracellular PCSK9 binds LDLR receptor inducing receptor-mediated endocytosis, where PCSK9 prevents the recycling of LDLR to the cell surface and redirects the receptor to the lysosome for degradation (Figure 4.1).<sup>205, 206</sup> Several compelling genetic studies have established a clear association between PCSK9 activity and levels of circulating low-density lipoprotein (LDL-C), the main vehicle for cholesterol transport in the blood and a major risk factor for heart disease and stroke.<sup>207-210</sup> Specifically, patients with loss-of-function mutations in the PCSK9 gene were reported to have remarkably low LDL-C levels,<sup>209, 210</sup> and PCSK9 gain-of-function mutants such as PCSK9 D374Y with 10-fold higher affinity for LDLR result in high LDL-C levels and hypercholesterolemia.<sup>208</sup> Several therapies have

been developed to block PCSK9 function including PCSK9 small molecule inhibitors, siRNAs, and monoclonal antibodies, with monoclonal antibodies and siRNAs being the most advanced in the clinical pipeline.<sup>211, 212</sup> However, paradoxically, dosing with anti-PCSK9 monoclonal antibodies results in elevated total serum PCSK9 levels in animal models and humans, which could be problematic after antibody clearance.<sup>213-216</sup> Here we sought to explore the LYTAC strategy for targeted degradation of extracellular PCSK9, which may enhance the efficacy of anti-PCSK9 antibody for the treatment of hypercholesteremia (Figure 4.1). To test this hypothesis, we synthesized an array of site-specific antibody-ligand conjugates carrying natural bi- and tri-antennary *N*-glycans as well as the tri-GalNAc ligands using an Fc glycan remodeling method. A flow cytometry analysis demonstrated an interesting profile of binding of different antibody-glycan ligand conjugates to the cell-surface ASGPR. In addition, our cell-based assay indicated that the synthetic antibody-glycan ligand conjugates could significantly degrade the extracellular PCSK9. Interestingly, the antibody-conjugates carrying the tri-antennary *N*-glycans or the tri-GalNAc cluster moiety showed difference in receptor binding and degradation of PCSK9, and a clear hook effect was observed for the antibody-tri-GalNAc conjugate in these processes, but not for the antibody-natural *N*-glycan conjugate. During the preparation of this manuscript, Bagdanoff and co-workers have reported that heterobifunctional molecules capable of binding to PCSK9 and the asialoglycoprotein receptor (ASGPR) could accelerate PCSK9 clearance in an animal model.<sup>217</sup> Taken together, these studies demonstrate the potential of the LYTAC strategy for the accelerated clearance and degradation of pathogenic proteins in circulation such as PCSK9.

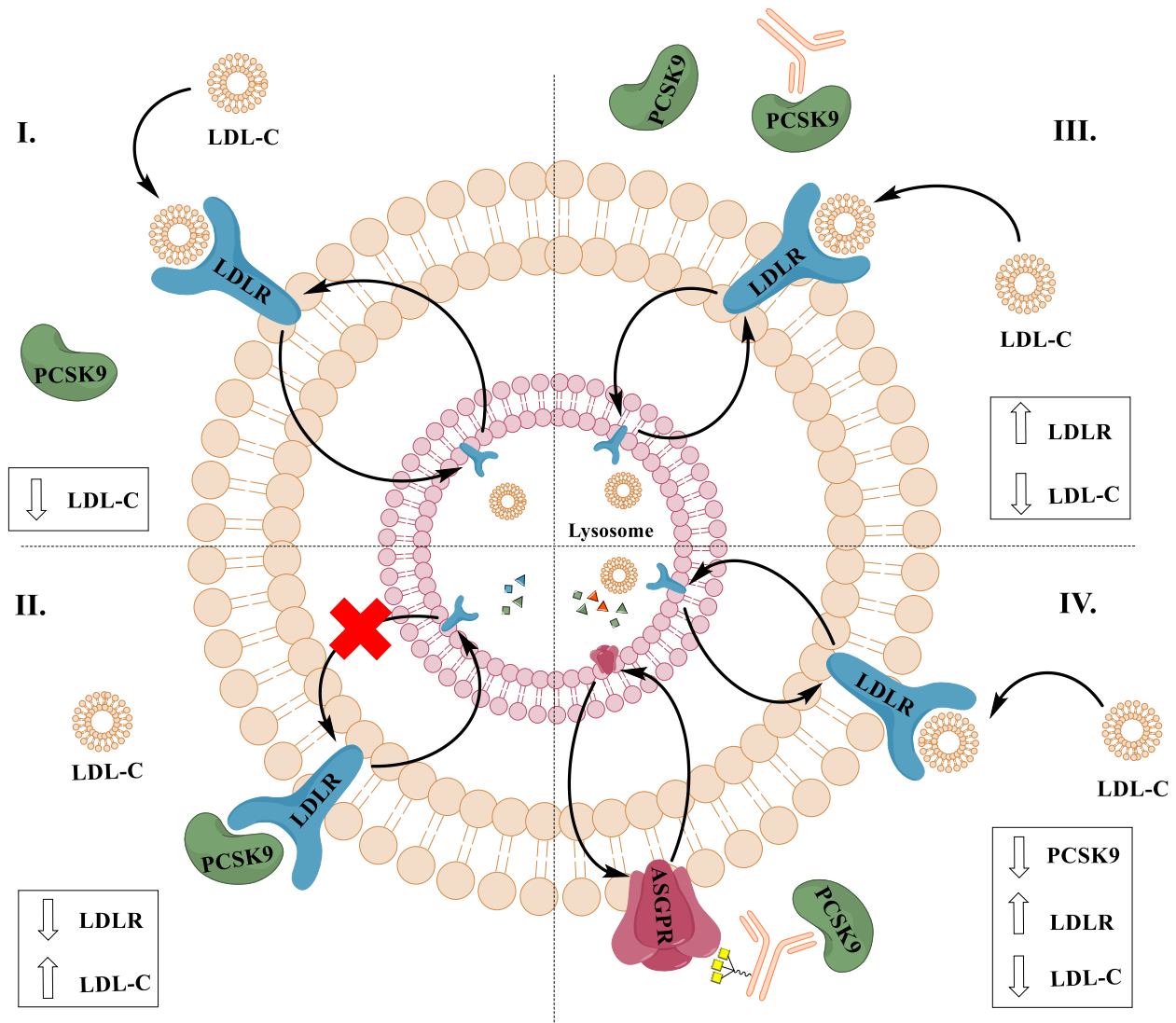


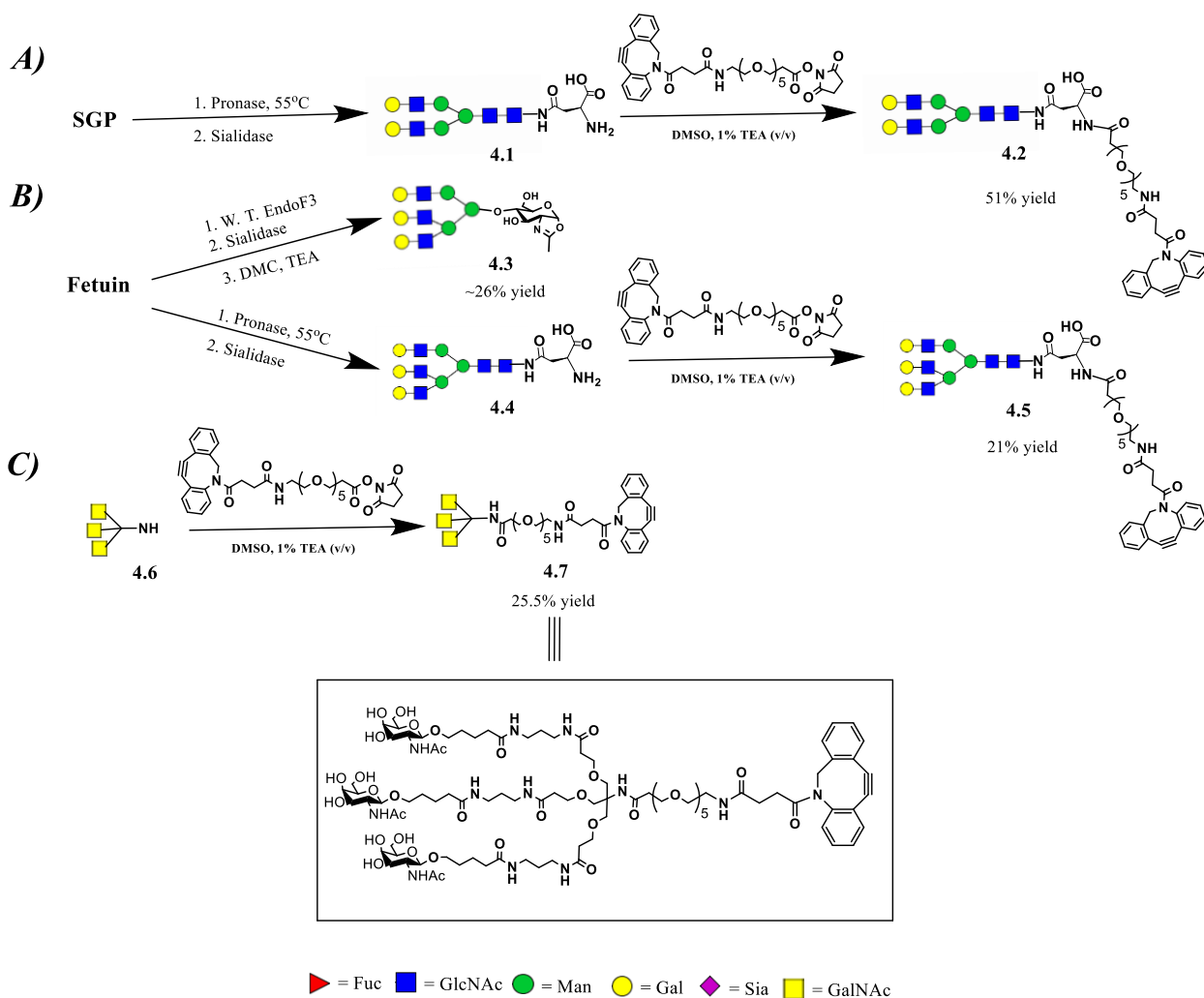
**Figure 4.1.** Cholesterol regulation by the low-density lipoprotein receptor (LDLR) in human hepatocytes. *I)* LDLR promotes the endocytic uptake of LDL-C to the endosome. *II)* PCSK9 binds LDLR, promoting its endocytosis and redirects LDLR to the lysosome for degradation resulting in reduced LDLR levels and higher LDL-C levels. *III)* PCSK9-specific monoclonal antibodies act as competitive inhibitors to disrupt PCSK9-LDLR interactions and rescue LDLR from PCSK9-mediated degradation. *IV)* PCSK9-specific LYTACs leverage liver cell ASGPR to promote PCSK9 degradation, removing it from circulation. LDLR is rescued from degradation and can bind and clear LDL-C from the blood.

## 4.2 RESULTS AND DISCUSSION

**Synthesis of high-affinity glycan ligands for ASGPR.** We have previously described the use of the chemoenzymatic Fc glycan remodeling approach to install drugs and mannose-6-phosphate glycan ligands site-specifically on monoclonal antibodies.<sup>218-220</sup> For example, we have reported that M6P-modified LYTACs prepared through this chemoenzymatic method can degrade transmembrane proteins effectively through the CI-M6PR receptor.<sup>203</sup> We sought to use the chemoenzymatic Fc glycan remodeling method to site-specifically install natural and synthetic glycan ligands of ASGPR to the Fc domain of an anti-PCSK9 antibody, which has not been explored before. Site-specific antibody conjugation is highly desirable since the method allows for tight control over location and valency of the attached cargoes.

Previous work from Lee and co-workers on rat hepatocytes has demonstrated that bi-, tri-, and tetra-antennary asialo-complex type *N*-glycans with terminal  $\beta$ -galactose moieties are recognized by the rat asialoglycoprotein receptor.<sup>9, 221</sup> The affinity of the bi-antennary complex type *N*-glycan for rat ASGPR is relatively weak (*ca.* 50  $\mu$ M), while the affinity of the tri- and tetra-antennary *N*-glycans is in the nanomolar range.<sup>9, 221</sup> Such  $\beta$ -galactosides are also known ligands for the human asialoglycoprotein receptor (hASGPR), however, the optimal glycan ligands for hASGPR binding and subsequent internalization remain to be further evaluated.<sup>10, 222</sup> This consideration is particularly relevant to the design of liver-specific LYTACs leveraging the ASGPR receptor, and warrants further investigation. To enable the chemoenzymatic synthesis of ASGPR-specific LYTACs and explore the substrate scope of the ASGPR receptor, several natural *N*-glycan structures were first prepared from the sialoglycopeptide (SGP) isolated from chicken egg yolks. Thus, the asialo-biantennary complex type *N*-glycan-Asn (G2-Asn, **4.1**) was prepared by protease digestion of SGP followed by sialidase digestion to remove terminal  $\alpha$ (2,6)-sialic acid as described from our previous reports.<sup>129, 223</sup> The asialylated *N*-glycan (G2-Asn) was

then reacted with 1.5 mol eq. NHS-PEG<sub>5</sub>-DBCO to prepare G2-Asn-DBCO (**4.2**) and install a chemical handle at the Asn N-terminus for click conjugation (Scheme 4.1). The final product was purified by reversed-phase preparative HPLC to give **4.2**. The tri-antennary *N*-glycan oxazoline (**4.3**), which serves as a substrate for antibody Fc glycan remodeling, was prepared from bovine fetuin following our previously reported procedure.<sup>224</sup> The DBCO-tagged tri-antennary *N*-glycan (**4.5**) was synthesized in several steps. First, protease digestion of bovine fetuin, followed by anion exchange and enzymatic desialylation, gave the Asn-linked tri-antennary *N*-glycan (**4.4**). Then treatment of **4.4** with 1.5 mol equiv. of NHS-PEG<sub>5</sub>-DBCO, followed by reversed-phase HPLC purification, afforded the G3-Asn-DBCO (**4.5**). After the synthesis of natural *N*-glycan ligands, the high-affinity tri-GalNAc ligand used by Bertozzi, Tang, and co-workers<sup>200, 201</sup> was synthesized to enable comparison of synthetic and natural ASGPR ligands. Chemical synthesis of **4.6** was accomplished following the reported procedures.<sup>225</sup> Compound **4.6** was then reacted with 3 mol equiv. NHS-PEG<sub>5</sub>-DBCO in DMSO and purified by reversed-phase HPLC to obtain pure tri-GalNAc-DBCO (**4.7**) (Scheme 4.1). The identity of compounds **4.2**, **4.5**, and **4.7** were confirmed by <sup>1</sup>H-NMR and LC-ESI-MS analysis.



**Scheme 4.1.** Synthesis of ASGPR ligands used in the LYTAC approach. *A)* Biantennary complex-type *N*-glycan-Asn is prepared by Pronase digestion of SGP followed by sialidase treatment to remove terminal sialic acid. Compound **4.1** is reacted with NHS-PEG<sub>5</sub>-DBCO to prepare G2-Asn-DBCO (Compound **4.2**). *B)* Tri-antennary complex-type *N*-glycans are prepared from fetuin by Endo-F3 digestion followed by sialidase treatment to obtain compound **4.3**. Alternatively, Pronase digestion of fetuin followed by sialidase treatment gives the asialo-complex type G3-Asn (**4.4**). Reaction with NHS-PEG<sub>5</sub>-DBCO gives G3-Asn-DBCO (Compound **4.5**). *C)* The tri-GalNAc-NH<sub>2</sub> (compound **4.6**) starting material is synthesized according to Prakash et al and reacted with NHS-PEG<sub>5</sub>-DBCO to give compound **4.7**.

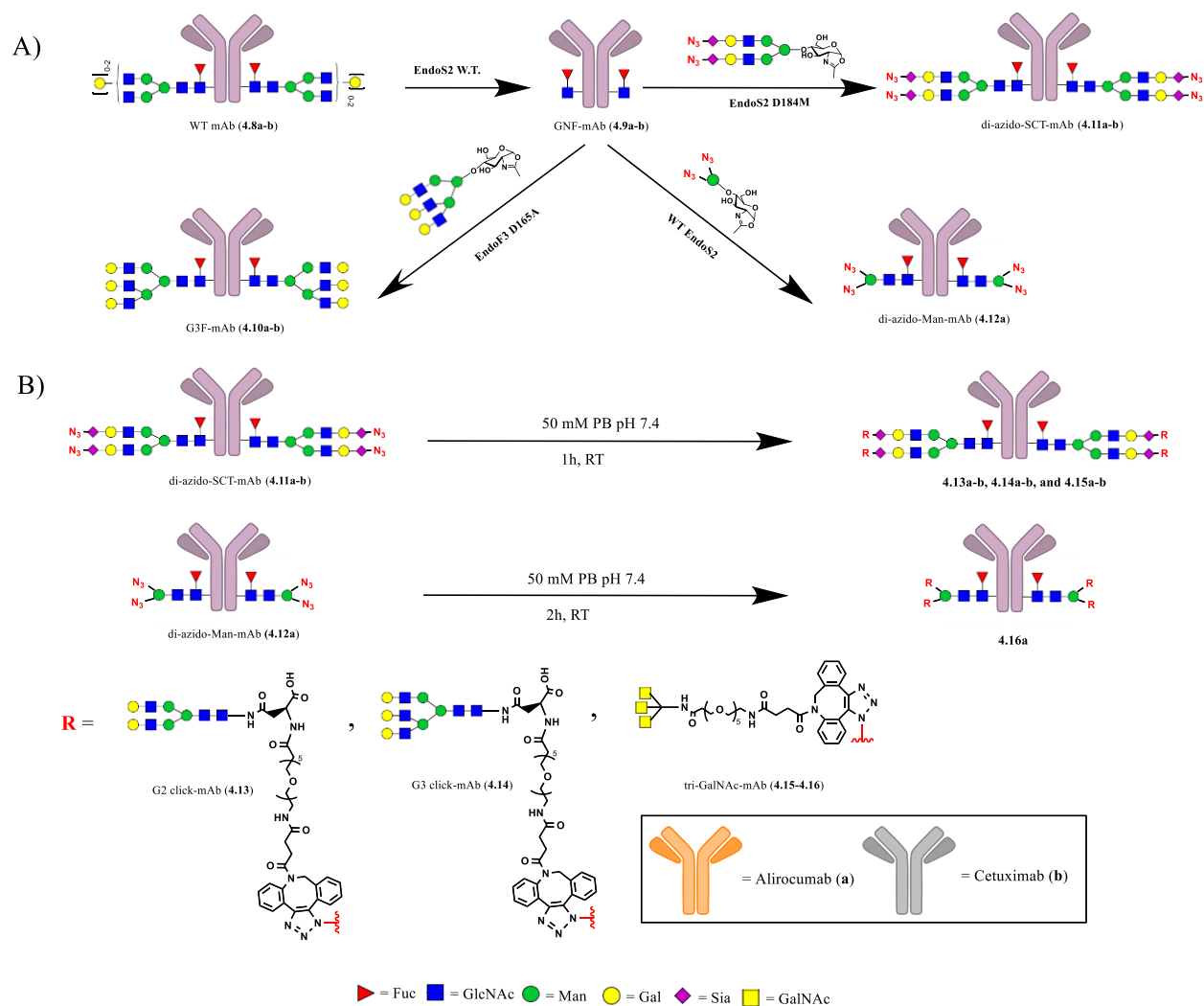
**Chemoenzymatic synthesis of the antibody-ligand conjugates carrying natural and synthetic ASGPR glycan ligands.** With compounds **4.2**, **4.3**, **4.5**, and **4.7** in hand, we next

examined their site-specific conjugation with Alirocumab (**4.8a**), an FDA-approved monoclonal

antibody specific for PCSK9 using the enzymatic Fc glycan remodeling method. Thus, Alirocumab (antibody **4.8a**) was deglycosylated with immobilized wild-type Endo-S2 from *Streptococcus pyogenes* to give the Fuc $\alpha$ 1,6GlcNAc-Alirocumab intermediate (**4.9a**), which serves as an acceptor for the subsequent transglycosylation (Scheme 4.2). A natural tri-antennary *N*-glycan structure was then site-specifically introduced by incubation of **4.9a** with Endo-F3 D165A mutant in the presence of G3-oxazoline (compound **4.3**) following previously reported procedures to give G3F-Alirocumab (antibody **4.10a**), with tri-antennary *N*-glycan on the Fc domain.<sup>224</sup> Alternatively, antibody **4.9a** could be incubated with azido-modified sugar oxazoline donors to install a click handle on the monoclonal antibody. This was done by two different methods to enable comparison of the effects of ligand-antibody distance on hASGPR binding/activity. Firstly, antibody **4.9a** was incubated with EndoS2 D184M in the presence of di-N<sub>3</sub>-S2G2-ox to install the azido-modified sialo-complex type *N*-glycan on the Fc, giving antibody **4.11a** as previously reported by our lab.<sup>226</sup> Separately, antibody **4.8a** was transformed in one-pot to antibody **4.12a** by incubation with the di-N<sub>3</sub>-Man-GN-ox disaccharide in the presence of WT Endo-S2, giving an antibody intermediate with azide groups attached to the shorter disaccharide (Scheme 4.2).<sup>62</sup> With intermediates **4.11a** and **4.12a** in hand, SPAAC (strain-promoted azide alkyne cycloaddition) click chemistry was performed to install high-affinity ASGPR ligands **4.2**, **4.5**, and **4.7** on the nonreducing ends of the Fc glycans. Three mole equivalents (per azide) of the DBCO-modified natural *N*-glycan ligands **4.2** and **4.5** were reacted with intermediate **4.11a** in phosphate buffer to afford novel antibody glycoclusters **4.13a** and **4.14a** in just one hour as determined by LC-ESI-MS. Alternatively, three mole equivalents of the synthetic tri-GalNAc-DBCO ligand were reacted with antibody intermediates **4.11a** and **4.12a** in phosphate buffer

containing 10% DMSO. The reactions were monitored by LC-ESI-MS and complete in 6-8 h to afford antibody conjugates **4.15a** and **4.16a**.

To demonstrate the feasibility of the conjugation method, we used Cetuximab as another model antibody to show the Fc site-specific conjugation even when additional *N*-glycans are present in the Fab domains. Cetuximab is an epidermal growth factor receptor (EGFR)-targeting monoclonal antibody used for the treatment of colorectal and head and neck cancers.<sup>227</sup> The cetuximab-ligand conjugates would provide an opportunity to test the targeted degradation of membrane-associated protein (EGFR) by the antibody conjugates. Commercially available Cetuximab (antibody **4.8b**) was deglycosylated using immobilized WT Endo-S2 as described above to prepare the GNF-Cetuximab acceptor (antibody **4.9b**, Scheme 4.2). Chemoenzymatic glycan remodeling was then done as described for the Alirocumab glycoforms to prepare antibodies **4.10b-4.11b**, the di-azido-dissaccharide-modified antibody was not prepared. Lastly, DBCO-modified ligands **4.2**, **4.5**, and **4.7** were conjugated to antibody intermediate **4.11b** by click chemistry to give conjugates **4.13b-4.15b** (Scheme 4.2).



**Scheme 4.2.** Chemoenzymatic synthesis of Alirocumab and Cetuximab site-specific LYTACs. *A)* Native antibodies are deglycosylated with immobilized WT EndoS2 to give the GNF-antibody acceptor which can be transformed to antibody variants **4.10-4.12** by transglycosylation with various mutant endoglycosidase enzymes and sugar-oxazolines. *B)* Click conjugation of ASGPR high-affinity ligands by reaction of DBCO-tagged glycans with azido-modified antibody intermediates.

**Binding of LYTAC glycan ligands to ASGPR on the liver cell surface.** The LYTACs carrying natural *N*-glycans and the synthetic tri-GalNAc cluster moiety were then evaluated for their ability to bind hASGPR on the liver cell surface by flow cytometry. To eliminate the contribution of antibody-antigen interactions associated with the anti-EGFR antibody

(Cetuximab), Alirocumab-based LYTACs were used in the binding studies and in a culturing condition where HepG2 cells secrete significantly reduced levels of PCSK9 (Figure 4.2).

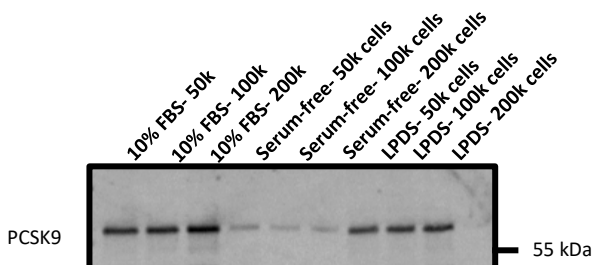


**Figure 4.2.** Western blot of PCSK9 protein secretion in HepG2 cell media under different culturing conditions. First three lanes represent PCSK9 secreted by HepG2 cells cultured in media containing 10% Fetal Bovine Serum (FBS) and at different cell densities. The middle three lanes represent the same for cells cultured in serum-free media and at different cell densities. The last three lanes represent PCSK9 secretion for cells cultured in media containing lipoprotein-deficient serum (LPDS) and at different cell densities.

Initially, an anti-human phycoerythrin (PE)-conjugated secondary antibody was used for detection of each LYTAC on the cell surface, however, the secondary antibody was unable to bind the antibody sugar conjugates **4.10a**, and **4.13a-4.16a**. Alternatively, the glycoengineered antibody conjugates were biotinylated chemically using an NHS-biotin activated ester and binding detected using a streptavidin-PE conjugate. Asialofetuin, a known binder of the asialoglycoprotein receptor, was also biotinylated and used as a positive control. Importantly, the number of biotin units conjugated to each glycoprotein is comparable so that cell-associated fluorescence intensity reflects the relative binding level of each conjugate. HepG2 cells were seeded in 96-well plates and incubated overnight in serum-free media. The next day, cells were incubated with serial dilutions of each biotinylated LYTAC and binding detected by flow cytometry. As expected, little to no binding was observed for the native Alirocumab antibody

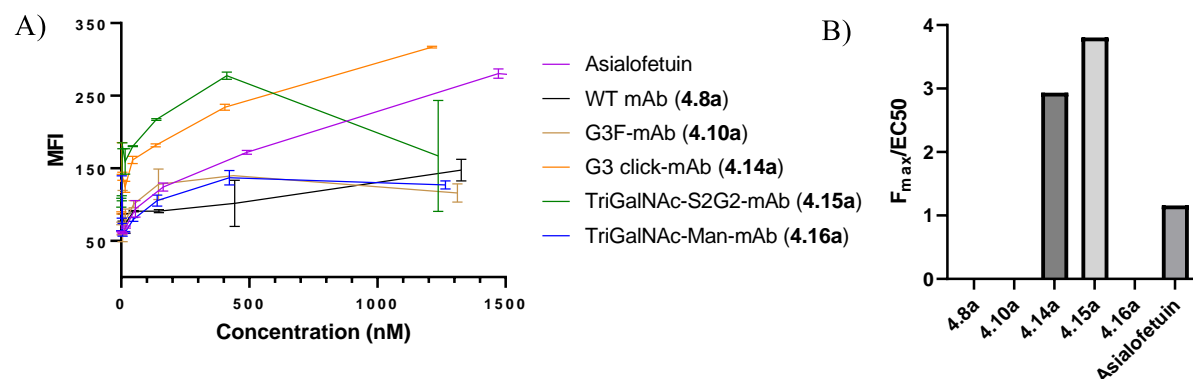


**Figure 4.3.** Recognition of glycan ligands of biotinylated-LYTACs by ASGPR on HepG2 cell surface. *A)* Mean fluorescence intensity (MFI) measurements of HepG2 cells incubated with serial dilutions of each LYTAC. *B)* Ratio of maximum fluorescence to EC<sub>50</sub> for each LYTAC, EC<sub>50</sub>'s were obtained by nonlinear regression of each hyperbolic segment of each binding curve. All measurements were done in duplicate.

containing mainly the agalacto-complex type *N*-glycan and robust binding was observed towards asialofetuin bearing asialo- bi- and tri-antennary complex type *N*-glycans (Figure 4.3A). This result confirms that cell-surface binding is dependent on the presence of terminal galactose.

Interestingly, LYTAC **4.10a** with the tri-antennary *N*-glycan directly attached to Asn297 of the antibody Fc, demonstrated only marginally better binding than the native antibody **4.8a**, suggesting that the *N*-glycans on this position might not be accessible to ASGPR recognition. Similarly, weak binding was observed by LYTAC **4.16a** containing the high-affinity tri-GalNAc ligand conjugated to the short disaccharide core at the Fc glycosylation site. On the other hand, LYTAC **4.15a** containing the same tri-GalNAc ligand attached by click chemistry to the more extended sialo-complex type *N*-glycan on the Fc domain was the strongest binder to cell-surface ASGPR, indicating that proper spacing from the bulky Fc domain is critical for effective recognition of glycan ligands attached to the antibodies. However, a decrease in the binding signal was observed at concentrations higher than 400 nM, suggesting that excess soluble **4.15a**

acts as a competitive inhibitor of the **4.15a**/ ASGPR complex, a phenomenon known as the prozone or hook effect.<sup>228</sup> The hook effect is an immunologic phenomenon whereby the effectiveness of antibodies to form immune complexes can be impaired when concentrations of an antibody or an antigen are very high. Lastly, LYTAC **4.14a** containing natural tri-antennary G3 N-glycans attached by click chemistry showed ASGPR binding comparable to the antibody-tri-GalNAc conjugate (**4.15a**) and was the strongest binding ligand above 400 nM concentration. In contrast to the antibody-tri-GalNAc conjugate (**4.15a**), the antibody-conjugate carrying the natural tri-antennary N-glycans (**4.14a**) did not exhibit the hook effect in binding to cell-surface ASGPR and demonstrated steadily increasing cell-associated fluorescence even to the highest concentration of 1.2  $\mu$ M. Some cell-surface binding was observed by the antibody conjugate (**4.13a**) carrying bi-antennary N-glycans. However, the binding profile was erratic and was not included for simplicity. As described in previous work, the affinity of the bi-antennary complex type N-glycan for rat ASGPR is relatively weak, in the range of *ca.* 50  $\mu$ M, while the affinity of the tri-antennary N-glycans for rat ASGPR is estimated in the range of nM concentrations.<sup>9, 221</sup> Our binding affinity data with the human ASGPR appear to be consistent with the previously reported results. However, it remains to be further investigated why the antibody conjugates carrying the natural N-glycans do not show the hook effect but the antibody conjugates carrying the synthetic tri-GalNAc cluster moiety demonstrate a clear hook effect in the receptor binding.

To assess the relative binding affinity of each glycoprotein more quantitatively, the EC50 was determined for each glycoprotein displaying significant binding above background levels (i.e. LYTACs **4.14a** and **4.15a**, and asialofetuin). This was done by nonlinear regression of the hyperbolic segments of the binding curves before decrease in fluorescence intensity due to the hook effect. These values were then normalized to the maximum fluorescence intensity achieved

by saturated binding of each biotinylated glycoprotein and plotted side-by-side for comparison (Figure 4.3B). Indeed, LYTAC **4.15a** is the best binder to cell-surface ASGPR with the highest  $F_{\max}/EC_{50}$  ratio (3.8). LYTAC **4.14a** was the next best binder ( $F_{\max}/EC_{50} = 2.9$ ) with comparable binding to the cell-surface ASGPR receptor. Lastly, the biotinylated asialofetuin bound only weakly with an  $F_{\max}/EC_{50}$  ratio of 1.2, indicating that the hASGPR can recognize tri-antennary *N*-glycans attached by long flexible linkers better than tri-antennary *N*-glycans in the context of highly glycosylated glycoproteins. These results provide important insights into glycan preference and selectivity of the human asialoglycoprotein receptor.

**Targeted-protein degradation of PCSK9 and effects on low-density lipoprotein receptor (LDLR).** Having confirmed that interactions of LYTACs **4.10a** and **4.13a-4.16a** with ASGPR on the liver cell surface depend on the presence of terminal galactose or N-acetylgalactosamine, Alirocumab-based LYTACs were then investigated for their ability to degrade extracellular PCSK9. Degradation of PCSK9 was assessed by western blot of the cell culture media. Figure 4.4 demonstrates the western blot data for HepG2 cells treated with varying concentrations of each antibody or antibody conjugate in the presence of PCSK9 D374Y, the PCSK9 D374Y mutant alone, or serum-deficient media (control) over 48 hours. No significant degradation was observed by commercial antibody **4.8a**, consistent with previous reports on this antibody (Figure 4.4A).<sup>229</sup> Surprisingly, treatment with LYTACs **4.13a** and **4.10a** also failed to degrade extracellular PCSK9 despite cell surface ASGPR-binding detected by flow cytometry. This indicates that clustered biantennary *N*-glycans, and tri-antennary *N*-glycans attached directly to the bulky Fc domain are ineffective ligands for lysosomal targeting of extracellular soluble proteins (Figure 4.4B). Interestingly, however, LYTAC **4.14a** demonstrated ~30% degradation of extracellular PCSK9 at 200 nM concentration, indicating that the tri-antennary G3 *N*-glycan

can be an effective ligand for targeted-degradation when connected by a long linker to the *N*-glycan on Asn297.

Gratifyingly, more pronounced degradation was observed by LYTAC **4.15a** with a synthetic tri-GalNAc ligand attached to each arm of the biantennary sialoglycan (S2G2). Approximately 60% of extracellular PCSK9 D374Y mutant was degraded at a 50 nM concentration of **4.15a**, corresponding to an equimolar concentration of the LYTAC relative to PCSK9. The hook effect was also observed for this LYTAC, with reduced PCSK9 degradation observed at higher concentrations (i.e. 33% degradation at 100 nM **4.15a**, and 0% degradation at 200 nM **4.15a**) most likely due to competitive binding of adjacent tri-GalNAc clusters and resulting in fewer productive endocytosis events by the ASGPR-LYTAC-PCSK9 ternary complex. Notably, this effect was not observed for LYTAC **4.14a** bearing natural tri-antennary G3 *N*-glycans (Figure 4.4C) and is reflective of the same patterns observed in the cell-surface binding experiments. LYTAC **4.16a**, containing the same tri-GalNAc ligand attached to a short disaccharide, was less effective than LYTAC **4.15a** and degraded only 34% of extracellular PCSK9. The lower degradation induced by LYTAC **4.16a** as opposed to LYTAC **4.15a** containing the same tri-GalNAc ligand, is likely due to the lower accessibility of tri-GalNAc ligands attached to the bulky IgG Fc domain by a shorter glycan 'linker'. Interestingly, the hook effect is also visible for LYTAC **4.16a**, which induces reduced PCSK9 degradation at higher concentrations. As demonstrated by the western blot data in Figure 4.4, this effect is unique to LYTACs containing the synthetic tri-GalNAc ligand. Furthermore, preliminary time-course experiments revealed that incubation of HepG2 cells with LYTAC **4.15a** for 48 hours resulted in maximal degradation of ~ 65% extracellular PCSK9 (Figure 4.5) demonstrating similar degradation kinetics as other antibody-based degraders reported by Bertozzi and coworkers.<sup>200</sup>

201 Thus, significant lysosomal degradation of the clinically relevant PCSK9 protein was achieved by LYTACs **4.14a-4.16a**, and demonstrated that natural tri-antennary *N*-glycan ligands can be leveraged for targeted-protein degradation for the first time.

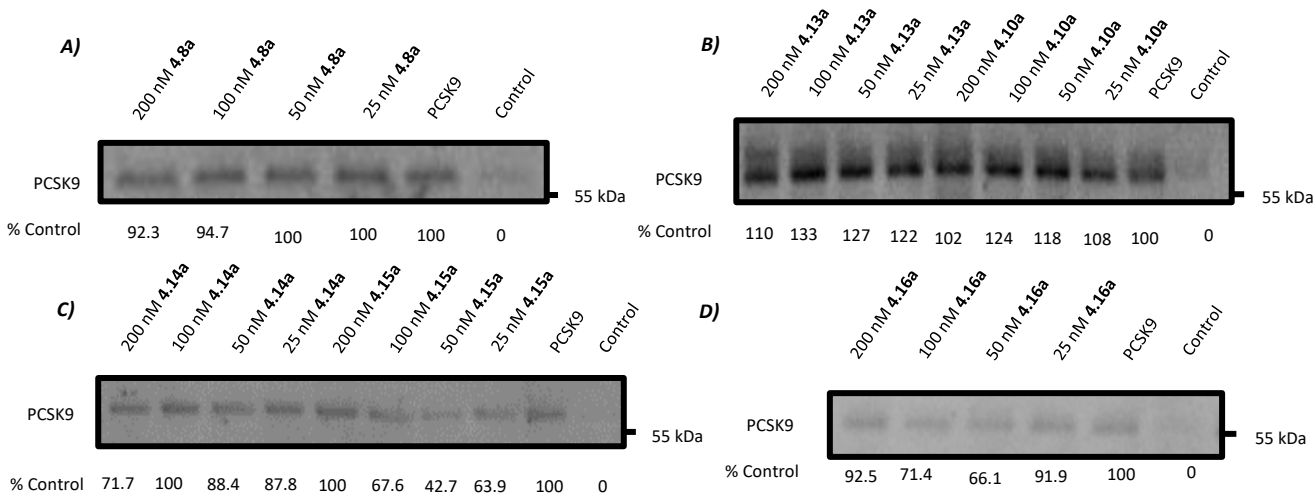


**Figure 4.4.** PCSK9 degradation assessed by western blot of HepG2 media after treatment with each LYTAC. HepG2 cells treated with PCSK9 D374Y and serial dilutions of A) native antibody **4.8a**, B) LYTAC **4.13a** or **4.10a**, C) LYTAC **4.14a** or **4.15a**, and D) LYTAC **4.16a** for 48 hours. Media of cells treated with PCSK9 D374Y only and OptiMEM media were included as positive and negative controls of each blot, respectively.

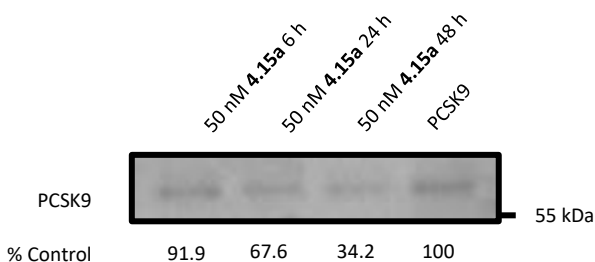


**Figure 4.5.** Western blot of HepG2 cell media to evaluate PCSK9 degradation after treatment with tri-GalNAc-S2G2-Alirocumab LYTAC (**4.15a**) for different time points. HepG2 cells were treated with 50 nM **4.15a** for 6, 24, or 48 h in serum-free media and PCSK9 degradation was assessed by western blot of the cell media at each time point.

To determine the effects of PCSK9 degradation on low-density lipoprotein levels (LDLR), western blots were done on the lysates of treated cells. Specifically, LDLR levels were compared in cells treated with commercial antibody **4.8a** and LYTACs **4.14a** and **4.15a** to determine whether targeted degradation of PCSK9 is a viable means of increasing cellular LDLR. As expected, treatment of cells with exogenous PCSK9 reduced levels of LDLR (approximately 20%) relative to the untreated control bands. Interestingly, a lower molecular weight double band was also observed for the PCSK9 treated cells and this was attributed to partial LDLR proteolysis as previously reported in some cases (Figure 4.6A-B).<sup>230, 231</sup> LDLR levels were rescued from PCSK9-induced degradation by treatment with commercial antibody **4.8a**, and an additional 17% increase in LDLR protein was detected at the highest antibody concentration tested (Figure 4.6A). By comparison, treatment with LYTAC **4.14a** did not result in any significant increase in LDLR relative to the control sample. However, treatment with tri-GalNAc-modified LYTAC **4.15a** resulted in a 40% increase in total LDLR at 50 nM concentration (Figure 4.6B). Importantly, significant levels of PCSK9 degradation were detected for LYTAC **4.15a** at this concentration suggesting that PCSK9 degradation is responsible. These results indicate that PCSK9 degradation may be a relevant therapeutic avenue for the upregulation of the LDLR responsible for the uptake and clearance of circulating LDL-C.

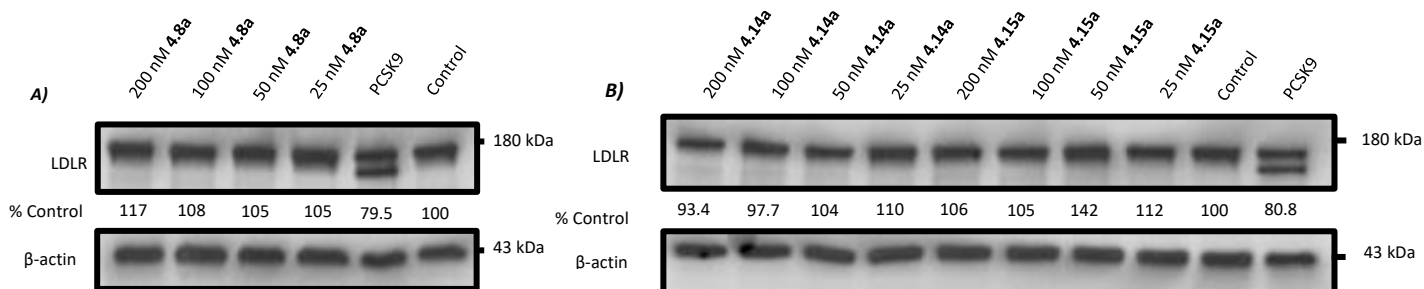


**Figure 4.6.** LDLR levels assessed by western blot of HepG2 cell lysates after treatment with each LYTAC. HepG2 cells treated with PCSK9 D374Y and serial dilutions of A) native antibody **4.8a**, and B) LYTAC **4.14a** or **4.15a** for 48 hours. Media of cells treated with PCSK9 D374Y only and OptiMEM media were included as positive and negative controls of each blot, respectively.

Further experiments are needed to determine if the upregulation in total LDLR observed after treatment with PCSK9-targeting LYTAC **4.15a** results in significantly increased LDL-C clearance *in vivo*. However, during the preparation of this manuscript, Bagdanoff and coworkers demonstrated the preparation of tri-GalNAc ligands attached to PCSK9-specific antibodies using ThioBridge technology to form a covalent linkage between the ligand and the reduced disulfide bonds of the antibody heavy chain.<sup>217</sup> The tri-GalNAc-modified PCSK9 antibody and other small heterobifunctional molecules were evaluated for PCSK9 degradation in mouse models and found to degrade approximately 60-70% PCSK9 in mouse serum, in accordance with the results reported herein. This report also provides the first *in vivo* example of the clinical relevance for PCSK9 targeted degradation. However, the study by Bagdanoff, et al utilizes wild-type PCSK9 as their model target protein and bioconjugation strategies such as ThioBridge that leverage reduction of inter-chain disulfides are known to affect antibody stability. Here, the targeted-protein degradation approach is demonstrated on PCSK9 gain-of-function mutant D374Y, a

more potent driver of hypercholesterolemia than WT PCSK9. Furthermore, the glycosite-specific chemoenzymatic engineering approach applied here has been shown to not alter antibody stability or recognition by Fc receptors.<sup>232</sup>

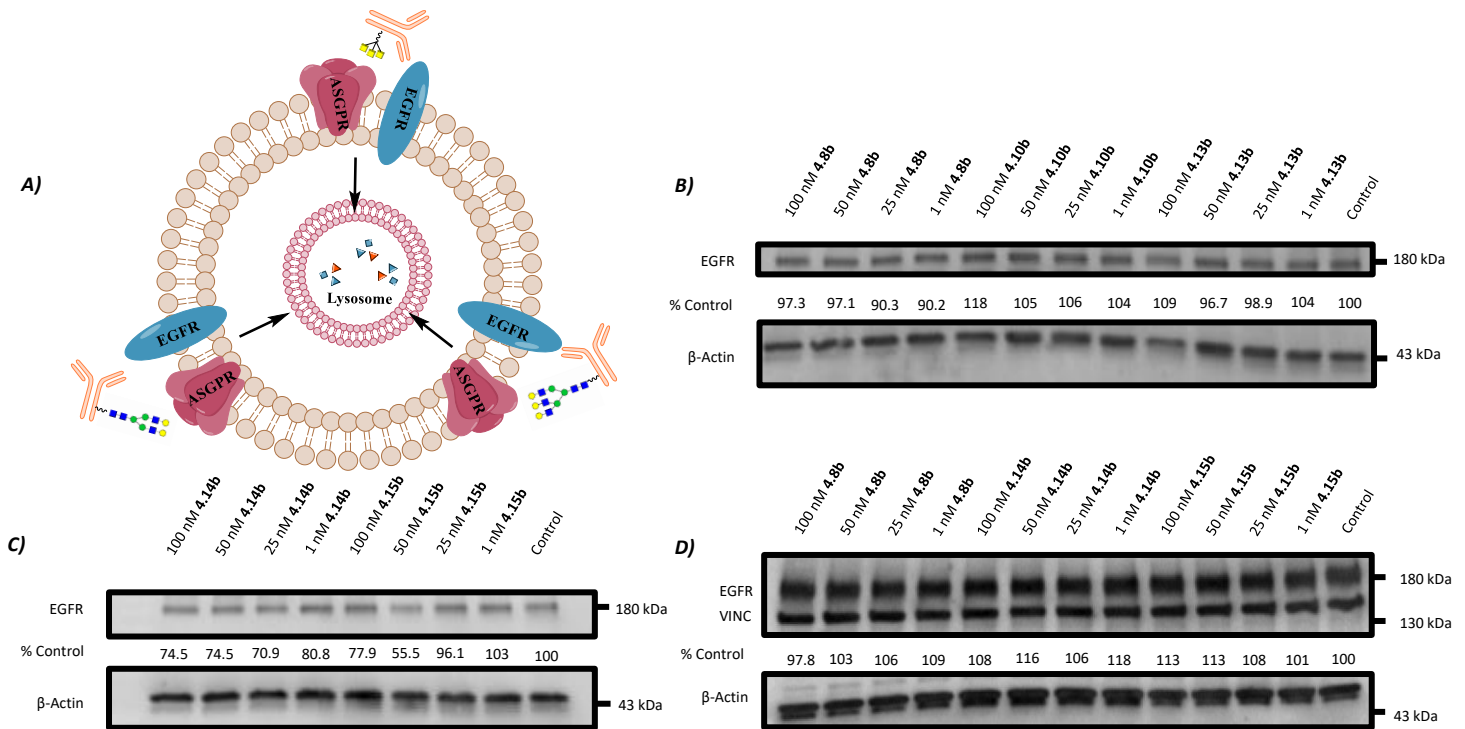


**Figure 4.7.** A) Scheme of EGFR degradation by Cetuximab-based LYTACs containing different ASGPR glycan ligands. EGFR levels assessed by western blot of HepG2 cell lysates after treatment with each LYTAC. HepG2 cells treated with serial dilutions of B) native antibody 4.8b, or LYTACs 4.10b, or 4.13b C) LYTACs 4.14b or 4.15b for 48 hours. C) EGFR<sup>+</sup>ASGPR<sup>-</sup> Hela cells treated with native antibody 4.8b or LYTACs 4.14b and 4.15b for 48 hours. Lysates of cells treated with complete growth media were included as negative controls for each blot.

**Targeted-protein degradation of epidermal growth factor receptor (EGFR).** To demonstrate the versatility of this platform in generating site-specific LYTACs targeting various proteins of interest, Cetuximab-based LYTACs were chemoenzymatically engineered for the targeted degradation of membrane-bound EGFR (Figure 4.7A). HepG2 cells were treated with various concentrations of commercially available Cetuximab 4.8b and LYTACs 4.10b and 4.13b-4.15b

for 48 hours in complete growth media. Total EGFR levels were then evaluated by western blot on the lysates of treated cells. As expected, little to no degradation was observed by commercial Cetuximab (**4.8b**). LYTACs bearing a tri-antennary *N*-glycan attached directly to the Fc domain (i.e. G3F-Cetuximab, LYTAC **4.10b**) or G2 glycans attached by click chemistry (LYTAC **4.13b**) failed to degrade cell-surface EGFR (Figure 4.7B). However, LYTAC **4.14b** bearing tri-antennary G3 *N*-glycans attached by click chemistry, induced significant degradation of EGFR (up to 30%) at concentrations as low as 25 nM **4.14b**. Tri-GalNAc-modified LYTAC **4.15b**, on the other hand, degraded as much as 45% EGFR at a concentration of 50 nM, with lower degradation values at higher LYTAC concentrations (Figure 4.7C). This result is comparable to degradation values of EGFR achieved with site-specifically modified M6P-based LYTACs, as well as by AbTAC bispecific antibodies leveraging E3 ligase RNF43.<sup>203, 233</sup> To demonstrate that the observed degradation is ASGPR-dependent, HeLa cells (EGFR<sup>+</sup> ASGPR<sup>-</sup>) were exposed to commercial Cetuximab **4.8b** and LYTACs **4.14b** and **4.15b**. Indeed, no EGFR-degradation was observed after any of the treatments, suggesting that EGFR degradation induced by LYTACs **4.14b** and **4.15b** was ASGPR dependent (Figure 4.7D). Time-course degradation experiments were also performed for EGFR LYTACs, and maximal degradation was found after 48 hours, in accordance with reports by Bertozzi and coworkers (Figure 4.8).<sup>200, 201</sup>

These results provide evidence that natural tri-antennary asialo-complex type *N*-glycans (G3) can be effective ligands for the lysosome-targeted degradation of membrane-bound and secreted extracellular proteins when attached with a sufficiently long synthetic linker to monoclonal antibodies. Albeit antibodies displaying the synthetic tri-GalNAc ligand were found to be more effective degraders of both secreted and membrane-bound target proteins. It is well known that ASGPR interactions with Gal/ GalNAc residues are weakened in the acidic pH

environment of the endosome, resulting in dissociation of the calcium ion required for glycan binding, leading to glycan-receptor dissociation, and receptor recycling. Several studies have identified three key residues in the carbohydrate recognition-domain of the ASGPR that are protonated at reduced pH, including His<sup>256</sup> which makes hydrophobic contacts with the methyl group of the GalNAc N-acetyl group and is responsible for the strong selectivity for GalNAc over galactose.<sup>234-236</sup> We propose that this extra hydrophobic contact may disfavor protonation of His<sup>256</sup> and make the ASGPR-GalNAc interaction more resistant to the acid-induced dissociation. This would allow for recycling of the ASGPR-tri-GalNAc-LYTAC complex to the cell surface to capture and deliver more target protein to the lysosome compared to the G3-based LYTACs.

Interestingly, the hook effect was observed in the targeted degradation of both PCSK9 and EGFR, however, this effect was unique to antibody conjugates containing the synthetic tri-GalNAc ligand and was not observed for LYTACs displaying the natural G3 *N*-glycan. Furthermore, in contrast to chemoenzymatically-engineered M6P-based LYTACs, natural tri-antennary *N*-glycan structures transferred enzymatically to the antibody Fc domain are not able to promote ASGPR-dependent degradation of target proteins.<sup>203</sup> This finding highlights the distinct structural requirements of CI-M6PR and ASGPR-dependent LYTACs for the degradation of target proteins. For example, the CI-M6PR receptor is composed of a long stalk of 15 receptor subunits, several of which contain mannose-6-phosphate binding domains that could accommodate binding to small M6P-containing glycans on antibodies while still allowing the antibody to form a ternary complex with the protein of interest.<sup>20</sup> The asialoglycoprotein receptor on the other hand, consists of two distinct subunits (ASGR1 and ASGR2) that each traverse the membrane and bind Gal and GalNAc containing oligosaccharides only when displayed in a specific geometry.<sup>221, 237, 238</sup> The antibody-conjugated ASGPR ligand, therefore,

must be in the proper orientation so that each Gal/ GalNAc arm can engage a respective ASGPR subunit, an accommodation that cannot be made by tri-antennary *N*-glycans attached directly to the Fc domain.

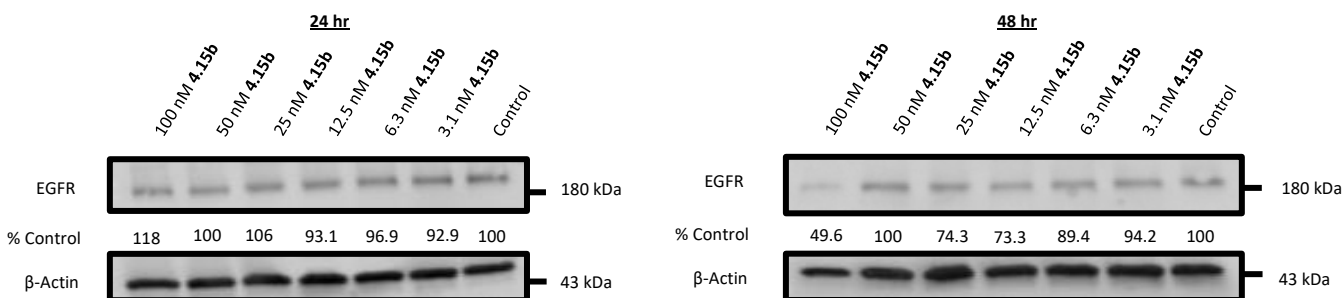


**Figure 4.8.** Western blot of HepG2 cell lysate after to evaluate EGFR degradation by different concentrations of tri-GalNAc-S2G2-Cetuximab LYTAC (**4.15b**) and for different time points. HepG2 cells were treated with LYTAC **4.15b** in EMEM media containing 10% FBS at the indicated time points and concentrations, western blotting was performed on the cell lysates and degradation was evaluated relative to the untreated control.

### 4.3 CONCLUSION

A facile synthesis of site-specific antibody-ligand conjugates carrying different ligands for asialoglycoprotein receptor (ASGPR), including natural *N*-glycans and the synthetic tri-GalNAc cluster, was achieved by a chemoenzymatic Fc glycan remodeling method. Alirocumab and Cetuximab, two therapeutic monoclonal antibodies that are against circulating PCSK9 and membrane-associated EGFR, respectively, were chosen for evaluating the ASGPR-mediated protein degradation. It was found that both the nature of the glycan ligands and the length of the spacer for the conjugation are critical for the receptor binding and the receptor-mediated

degradation of PCSK9 and EGFR. Interestingly, the antibody-tri-GalNAc cluster conjugates showed a clear hook effect for their binding to hASGPR and the degradation of PCSK9, i.e., a high-concentration of the antibody-tri-GalNAc conjugates results in decreased affinity for the receptor and reduced efficacy for PCSK9 degradation. However, the antibody conjugates carrying the natural tri-antennary complex type N-glycans showed significant affinity for the cell-surface receptor and dose-dependent degradation of PCSK9 without the adverse hook effect. This new finding provides important insight in the selection of appropriate glycan ligands for ASGPR-mediated targeted protein degradation. Future work should be directed to more detailed mechanistic analysis of an extended panel of natural and synthetic glycan ligands for cell-surface receptor binding and cell-based protein degradation to identify the best ligands for ASGPR-mediated protein degradation. In addition, *In vivo* experiments will be needed to evaluate the clinical potential of the site-specific antibody-glycan conjugates and the targeted-degradation of PCSK9, which offers a promising avenue for the treatment of high cholesterol.

#### **4.4 MATERIALS AND METHODS**

**Materials:** Chemicals, reagents, and solvents were purchased from Sigma-Aldrich or TCI America and used as received unless otherwise specified. Monoclonal antibodies Cetuximab and Alirocumab were purchased from RefDrug and buffer exchanged to PBS before use. Preparative HPLC was performed with Waters 1525 Binary HPLC pump coupled with 2489 UV/Vis Detector under UV 214 nm and 280 nm with a Waters Symmetry C18 column (7  $\mu$ m, 19  $\times$  300 mm) using water containing 0.1% trifluoroacetic acid as phase A, MeCN containing 0.1% trifluoroacetic acid as phase B and at a flow rate of 10 mL/min for all purifications. Semi-preparative HPLC was performed on the same instrument with an Agilent Eclipse XDB-C18 column (5  $\mu$ m, 9.4  $\times$  250 mm) using water containing 0.1% trifluoroacetic acid as phase A,

MeCN containing 0.1% trifluoroacetic acid as phase B and at a flow rate of 4 mL/min for all purifications.

### **LC-ESI-MS analysis of glycans**

LC-ESI-MS analysis of glycans was conducted on a Waters HPLC-SQD2 system. Glycans were separated using a Waters e2695 HPLC module equipped with a Waters XBridge C18 column (3.5  $\mu$ m, 2.1  $\times$  50 mm) and dual UV detection at 214 nm and 280 nm. Water containing 0.1 % formic acid was used as phase A, and MeCN containing 0.1% formic acid as phase B. Peaks were then identified by ESI-MS detection using a Waters SQD2 instrument.

### **LC-ESI-MS analysis of intact antibodies and derivatives**

LC-ESI-MS analysis of intact antibodies and LYTACs was performed with Exactive Plus Orbitrap Mass Spectrometer (Thermo Scientific) equipped with a Waters XBridge BEH300 C4 column (3.5  $\mu$ m, 2.1  $\times$  50 mm). Gradient elution was performed with water containing 0.1% formic acid as phase A, MeCN containing 0.1% formic acid as phase B. Mass spectra were deconvoluted using MagTran (ver 1.03 b2).

### **LC-ESI-MS analysis of antibody Fc fragments after IdeS digestion**

For the antibody Fc analysis, the antibody samples in PBS were incubated with 0.5 % w/w IdeS at 37 °C for 10-15 minutes. The samples were analyzed with Exactive Plus Orbitrap Mass Spectrometer (Thermo Scientific) equipped with an Agilent Poroshell 300SB C8 column (5  $\mu$ m, 1.0  $\times$  75 mm). Gradient elution was performed with water containing 0.1% formic acid as phase A, MeCN containing 0.1% formic acid as phase B. Mass spectra were deconvoluted using MagTran (ver 1.03 b2).

## **NMR analysis of glycans**

<sup>1</sup>H and <sup>13</sup>C- NMR spectra were measured with Bruker AV III HD NanoBay 400 MHz NMR spectrometer and the chemical shifts were assigned in parts per million. Solvent was D<sub>2</sub>O for glycan samples and chemical shifts were reported relative to the solvent peak.

## **Synthesis of G3-oxazoline (compound 4.3)**

Sialylated tri-antennary N-glycan as an oxazoline precursor was prepared from bovine fetuin following a previously reported procedure,<sup>239</sup> except that fetuin was purchased from a commercial source and not purified from fetal bovine serum. Endo-F3 released N-glycans were purified by anion exchange using a Cytiva 5 mL HiTrap QXL column on an AKTA Pure 25L FPLC system to separate bi- and tri-antennary N-glycans. A 0-50% linear gradient over 60 minutes was used for the separation, with Milli-Q water as phase A and 200 mM NaCl as phase B. The final product was desalted by Sepharose G-10 column chromatography. Terminal sialic acid was removed by treatment with  $\alpha$ -(2,6)-neuraminidase from *Micromonospora viridifaciens* (1: 1,000 enzyme: substrate w/w) in PBS to give G3-GlcNAc<sub>1</sub> as the oxazoline precursor. The final compound was purified by preparative reversed-phase HPLC using an isocratic gradient of 100% water with 0.1% TFA (trifluoroacetic acid) over 30 minutes. After lyophilization, synthesis and purification of the glycan oxazoline was done as reported previously.<sup>239</sup>

## **Synthesis of di-azido-S2G2-oxazoline**

The di-azido-S2G2-oxazoline was prepared from pure sialylated biantennary N-glycan (S2G2-GlcNAc<sub>1</sub>) following previously reported procedures from our lab.<sup>240</sup>

## **Synthesis of di-azido-Mannose- $\beta$ (1,4)-GlcNAc oxazoline**

The di-azido-Mannose- $\beta$ (1,4)-GlcNAc oxazoline was synthesized from mannose and 2-aminoglucose starting materials as previously described by our lab.<sup>62</sup>

#### **Preparation of G2-Asn (compound 4.1)**

Sialylated biantennary N-glycan-Asn was prepared from sialo-glycoprotein (SGP) that was isolated from egg yolk powder as previously described.<sup>223</sup> SGP hexapeptide was proteolytically trimmed with a protease cocktail from *Streptomyces griseus* (Pronase<sup>®</sup>, Millipore) and purified by anion exchange followed by size exclusion. S2G2-Asn was treated with neuraminidase to remove the terminal sialic acid and purified by Sepharose G-10 to obtain the biantennary complex-type N-glycan bearing terminal  $\beta$ (1,4)-galactose (G2-Asn).

#### **Preparation of G3-Asn (compound 4.4) from bovine fetuin**

Bovine fetuin (EMD Millipore, 1 gram) was dissolved in 15 mL digestion buffer (100 mM Tris pH 8 containing 50 mM CaCl<sub>2</sub> and 0.05% NaN<sub>3</sub>), followed by the addition of 20 mg Pronase. The reaction mixture was incubated in a 55 °C water bath and the reaction was monitored by MALDI-TOF MS and SDS-PAGE (the pH was monitored carefully through the course of the digestion to prevent acid-catalyzed desialylation). After three days, another 20 mg of Pronase was added. Four days later, the reaction did not progress further, and the major product was a ~ 3.5 kDa molecular weight glycopeptide as determined by MALDI-TOF MS. The reaction mixture was purified by Sepharose G-50 using water containing 10 mM acetic acid as eluent, glycan elution was determined by TLC using p-anisaldehyde stain and elution of glycopeptide was confirmed by MALDI-TOF MS. All glycopeptide containing fractions were pooled and lyophilized, the fluffy solid was resuspended in 5 mL digestion buffer and digested with 20 mg Pronase for another three days. Analysis by MALDI-TOF MS confirmed a major product of ~ 3

kDa molecular weight. The reaction mixture was purified by Sepharose G-25, lyophilized, and purified by anion exchange as described above for compound **4.3**. Glycan containing fractions were collected and lyophilized to obtain the pure sialylated tri-antennary N-glycan (S3G3-Asn, 9 mg). After a final desalting step on a Sepharose G-10 column, the S3G3-Asn glycan was dissolved in PBS, digested with neuraminidase, and purified by Sepharose G-15 to obtain the asialo- tri-antennary complex-type N-glycan-Asn (G3-Asn) as a fluffly white solid (5.2 mg).

### **General method for synthesis of DBCO functionalized N-glycan-Asn**

To each pure lyophilized N-glycan-Asn (10 mg) in a 0.2 mL microcentrifuge tube was added DBCO-(PEG)<sub>5</sub>-NHS (1.5 mol eq., Broadpharm) from a stock solution in DMSO (50 mg/mL), followed by triethylamine (1% v/v). The mixture was vortexed at room temperature, and after two hours, the reaction was complete as judged by LC-ESI-MS. The reaction mixture was diluted to 2.5 mL with water and purified by preparative reversed-phase HPLC using a linear 10-50% gradient of acetonitrile with 0.1% FA (formic acid) over 30 minutes. Water containing 0.1% FA was used as phase A, and acetonitrile containing 0.1% FA as phase B, compound elution was monitored by dual UV detection at 214 nm and 280 nm. Product elution was determined by TLC and p-anisaldehyde stain, and confirmed by LC-ESI-MS. All pure fractions were combined and lyophilized to yield the DBCO functionalized N-glycans as fluffly white solids. All NMR spectra were compared to those previously reported for the unfunctionalized G2-Asn and G3-Asn N-glycans for confirmation of sample identity.<sup>132, 133, 241-243</sup>

#### *G2-Asn-DBCO* (compound **4.2**)

Isolated in 51% yield (6.8 mg) after RP18-HPLC. <sup>1</sup>H-NMR (600 MHz, D<sub>2</sub>O): δ 7.55 (d, 1H, J = 7.6 Hz), 7.45 (d, 1H, J = 7.0), 7.40-7.34 (m, 4H), 7.28 (t, 1H, J = 7.6 Hz), 7.19 (d, 1H, J = 7.3

Hz), 5.07 (s, 1H), 4.99 (d, 1H, J = 9.6 Hz), 4.94 (d, 1H, J = 14 Hz), 4.88 (s, 1H), 4.71 (s, 1H), 4.66 (t, 1H, J = 5.8 Hz), 4.56-4.53 (m, 3H), 4.42-4.41 (m, 2H), 4.21 (s, 1H), 4.15 (s, 1H), 4.06 (s, 1H), 3.94-3.39 (m, 69H), 3.34-3.31 (m, 1H), 3.14-3.13 (m, 2H), 2.79-2.73 (m, 2H), 2.67 (s, 1H), 2.50-2.48 (m, 4H), 2.19-2.11 (m, 2H), 2.02-1.94 (m, 12H). HRMS (ESI-MS): calcd for  $C_{98}H_{148}N_8O_{56}$ ,  $[M + H]^+ = 2334.9086$  Da; found, m/z 2334.9014.

#### *G3-Asn-DBCO* (compound **4.5**)

Isolated in 21% yield (2.7 mg) after RP18-HPLC.  $^1H$ -NMR (600 MHz,  $D_2O$ ):  $\delta$  7.51 (d, 1H, J = 7.5 Hz), 7.41-7.40 (m, 2H), 7.30 (t, 2H, J = 7.4 Hz), 7.26 (t, 2H, J = 7.2 Hz), 7.21-7.20 (m, 1H), 4.98 (s, 1H), 4.94 (s, 1H), 4.90 (t, 2H, J = 14 Hz), 4.78 (s, 1H), 4.61-4.60 (m, 1H), 4.53 (t, 2H, J = 5.8 Hz), 4.47-4.39 (m, 4H), 4.34-4.32 (m, 3H), 4.08 (m, 2H), 3.97 (s, 1H), 3.91-3.90 (m, 1H), 3.88-3.31 (m, 77H), 3.26-3.24 (m, 2H), 3.07-3.04 (m, 4H), 2.67-2.65 (m, 2H), 2.58 (s, 1H), 2.43-2.40 (m, 4H), 2.10-2.08 (m, 2H), 1.94-1.86 (m, 15H). HRMS (ESI-MS): calcd for  $C_{112}H_{171}N_9O_{66}$ ,  $[M + 2H]^{2+} = 1350.5240$  Da; found, m/z 1350.5146.

#### **Synthesis of tri-GalNAc-DBCO (compound 4.7)**

Synthesis of tri-GalNAc-NH<sub>2</sub> with free primary amine (compound **4.6**) was done according to procedures reported by Prakash et al.<sup>225</sup> DBCO chemical handle was attached by reaction of compound **4.6** (10 mg, 7  $\mu$ mol) in DMSO with DBCO-PEG<sub>5</sub>-NHS (21  $\mu$ mol, 3 mol eq.; Broadpharm) in the presence of triethylamine (1 % v/v) at 37 °C. After 22 h, the reaction was complete as judged by LC-ESI-MS. The product was purified by reversed-phase preparative HPLC using a linear gradient of 20-40% MeCN over 40 min, with water (0.1% formic acid) as phase A and acetonitrile (0.1% formic acid) as phase B. Dual UV detection was done at 214 nm and 280 nm to monitor product elution, product-containing fractions were pooled and lyophilized

to obtain compound **4.7** as a white powder. NMR spectra of compound **4.7** was confirmed by comparison with previously reported data on similar tri-GalNAc structural analogues.<sup>244-246</sup>

#### *Tri-GalNAc-DBCO*

Isolated in 25.5% yield (3.6 mg) after RP18-HPLC. <sup>1</sup>H-NMR (600 MHz, DMSO-*d*<sub>6</sub>): δ 7.87 (m, 3H), 7.77 (m, 3H), 7.66-7.62 (m, 3H), 7.52-7.46 (m, 4H), 7.40-7.34 (m, 4H), 7.31-7.30 (m, 1H), 7.16 (s, 1H), 5.03 (d, 1H, J = 14 Hz), 4.62 (m, 4H), 4.53 (m, 3H), 4.22 (d, 3H, J = 8.4 Hz), 3.71-3.30 (m, 84H), 3.05-3.00 (m, 14H), 2.51 (m, 2H), 2.33 (m, 2H), 2.29-2.27 (m, 6H), 2.05 (t, 6H, J = 7.4 Hz), 1.80 (s, 9H), 1.52-1.49 (m, 12H), 1.43-1.41 (m, 6H). <sup>13</sup>C-NMR (150 MHz, DMSO-*d*<sub>6</sub>): δ 172.05, 171.11, 171.02, 170.10, 169.53, 151.96, 151.57, 132.39, 129.59, 128.90, 128.11, 127.97, 127.65, 126.76, 125.13, 122.51, 121.38, 114.20, 108.12, 101.34, 75.21, 71.47, 69.72, 69.64, 69.50, 69.44, 68.95, 68.19, 67.86, 67.48, 67.31, 66.82, 60.42, 59.59, 59.50, 54.86, 52.03, 51.96, 40.38, 39.75, 39.61, 39.47, 39.33, 39.19, 36.35, 36.24, 36.12, 35.99, 35.07, 29.68, 29.28, 28.60, 23.01, 21.93. HRMS (ESI-MS): calcd for C<sub>93</sub>H<sub>148</sub>N<sub>12</sub>O<sub>35</sub>, [*M* + *H*]<sup>+</sup> = 1995.0277 Da; found, *m/z* 1995.0282.

#### **General method for antibody deglycosylation using immobilized WT Endo-S2**

Wild-type Endo-S2 enzyme was immobilized following previously reported procedures, the final concentration of the immobilized enzyme was determined to be 1.2 mg/mL by BCA assay. To a solution of monoclonal antibody in PBS (10 mg/mL) was added immobilized WT Endo-S2 to a final concentration of 0.5% w/w (50 μg), and the mixture was mixed end over end at room temperature overnight. The next day, the mixture was centrifuged to pellet the enzyme and

deglycosylation was confirmed by LC-ESI-MS. Once complete, the supernatant was filtered through a 0.2  $\mu\text{m}$  cellulose syringe filter and buffer-exchanged to 100 mM Tris pH 7 buffer.

ESI-MS: calcd for GNF-Ali (**4.9a**),  $M = 146,675$  Da; found (m/z), deconvolution of the ESI-MS,  $M = 146,677$  Da. Calcd for GNF-Ali Fc fragment (**4.9a**),  $M = 24,102$  Da; found (m/z), deconvolution of the ESI-MS,  $M = 24,102$  Da.

ESI-MS: calcd for GNF-Cet (**4.9b**),  $M = 150,009$  Da; found (m/z), deconvolution of the ESI-MS,  $M = 150,006$  Da. Calcd for GNF-Cet Fc fragment (**4.9b**),  $M = 24,123$  Da; found (m/z), deconvolution of the ESI-MS,  $M = 24,134$  Da.

### **Protein A purification of monoclonal antibodies and their conjugates**

Antibody reaction mixtures were diluted to 5 mL in PBS buffer pH 7.4 and loaded on to a pre-equilibrated HiTrap Protein A HP 1 mL column (GE Healthcare) by syringe pump. The column was washed thoroughly with 20 mL PBS pH 7.4 at 1 mL/min flow rate using an AKTA Pure FPLC system (Cytiva) and then eluted with 30 mM sodium citrate pH 2.6 buffer in one step. Samples were collected as 1 mL fractions in tubes containing 100  $\mu\text{L}$  1 M Tris pH 7. Antibody-containing fractions were identified by absorbance at 280 nm and immediately buffer-exchanged to the appropriate buffer using Amicon Ultra 10 kDa MWCO centrifugal filters (Millipore). Antibody samples were collected, and final concentrations were determined by nanodrop.

### **General method for transglycosylation of deglycosylated antibodies with G3-oxazoline**

Transglycosylation reactions with EndoF3 D165A mutant were done following a previously reported procedure with some modifications.<sup>224</sup> To a solution of deglycosylated GNF-antibody in Tris buffer (15 mg/mL) was added 40 mol. eq. of G3-oxazoline as a 100 mg/mL stock solution in water. Then, EndoF3 D165A mutant was added to a final concentration of 0.2 mg/mL (14  $\mu$ g) in a volume of  $\sim$ 70  $\mu$ L and incubated at 37 °C for 20 min. After 20 minutes, the reaction was found to be complete for the transglycosylation of Alirocumab and the mixture was purified by protein A column as described above to give antibody **4.10a**.

For transglycosylation of Cetuximab, the reaction was only 70% complete after 20 min as judged by LC-ESI-MS. Another 30 mol eq. of G3-oxazoline was added, and after 40 min, the reaction was complete and purified by protein A column to obtain antibody **4.10b**. LC-ESI-MS data for antibodies **4.10a** and **4.10b** can be found in the supporting information.

#### **Transglycosylation of deglycosylated antibodies with di-N<sub>3</sub>-S2G2-oxazoline**

Transglycosylation of deglycosylated Alirocumab and Cetuximab with di-N<sub>3</sub>-S2G2-oxazoline was done following previously reported procedures to prepare antibodies **4.11a** and **4.11b**.<sup>226</sup>

ESI-MS: calcd for di-N<sub>3</sub>-S2G2-Ali (**4.11a**), M = 151,835 Da; found (m/z), deconvolution of the ESI-MS, M = 151,835 Da. Calcd for di-N<sub>3</sub>-S2G2-Ali Fc fragment (**4.11a**), M = 26,681 Da; found (m/z), deconvolution of the ESI-MS, M = 26,681 Da.

ESI-MS: calcd for di-N<sub>3</sub>-S2G2-Cet (**4.11b**), M = 155,162 Da; found (m/z), deconvolution of the ESI-MS, M = 155,161 Da. Calcd for di-N<sub>3</sub>-S2G2-Cet Fc fragment (**4.11b**), M = 26,712 Da; found (m/z), deconvolution of the ESI-MS, M = 26,714 Da.

#### **Transglycosylation of deglycosylated antibodies with di-N<sub>3</sub>-mannose- $\beta$ (1,4)-GlcNAc-oxazoline**

Transglycosylation of deglycosylated Alirocumab with di-N<sub>3</sub>-mannose- $\beta$  (1,4)-GlcNAc-oxazoline was done following previously reported procedures to prepare antibody **4.12a**.<sup>62</sup>

ESI-MS: calcd for di-N<sub>3</sub>-Man-GlcNAc-Ali (**4.12a**), M = 148,034 Da; found (m/z), deconvolution of the ESI-MS, M = 148,038 Da. Calcd for di-N<sub>3</sub>-Man-GlcNAc-Ali Fc fragment (**4.12a**), M = 24,781 Da; found (m/z), deconvolution of the ESI-MS, M = 24,782 Da.

### **General method for click conjugation of azido-modified antibodies with DBCO-tagged glycan ligands**

To a solution of azido-modified antibody in PBS (2 mg/mL) was added 12 mol eq. of DBCO-tagged glycan ligand (3 mol eq. per azide). The mixture was inverted end-over-end at room temperature, and the reaction progress was monitored by LC-ESI-MS. After one hour, click conjugation of *N*-glycan-Asn-DBCO ligands was found to be complete with four units of the *N*-glycan ligand (bi- or tri-antennary) attached to the antibody Fc. Antibody conjugates were purified by spin filtration over a 10 kDa MWCO spin filter (Millipore). For conjugation of the synthetic Tri-GalNAc-DBCO ligand, longer reaction times of approximately 6-8 hours were required for reaction completion under the same conditions. Tri-GalNAc-modified antibody LYTACs were also purified by spin filtration. LC-ESI-MS data can be found in the supporting information.

### **Enzymatic desialylation of fetuin to prepare asialofetuin**

Bovine fetuin (2 mg) was dissolved in 1 mL PBS pH 7.4, and pH was adjusted to 7 with saturated NaHCO<sub>3</sub> solution. Neuraminidase was then added (1:1,000 enzyme: substrate ratio w/w) and the mixture was incubated at 37 °C. The reaction was monitored by MALDI-TOF-MS and judged to be complete after no further change in molecular weight was observed even after

prolonged incubation or addition of more enzyme (~ 36 hours). The reaction mixture was then heated at 95 °C for 5 minutes to deactivate the enzyme, and asialofetuin was purified by buffer exchange over a 10 kDa MWCO spin filter and stored in PBS buffer. The final concentration (0.97 mg/mL) was determined by BCA assay using commercially available bovine fetuin as a standard.

### **General method for biotinylation of Alirocumab LYTACs and asialofetuin with NHS-LC-LC-biotin**

To a solution of each Alirocumab LYTAC in PBS (1 mg/mL, 100 µg), was added NHS-LC-LC-biotin (12 mol eq., Thermo) from a 10 mM stock solution in DMSO. The reaction was incubated at room temperature and monitored by MALDI-TOF-MS. After one hour, each of the conjugates had been decorated with an average of 5-7 units of biotin, and the reaction was then quenched by addition of 1 M Tris pH 7 buffer to a final concentration of 100 mM. Each of the conjugates were then purified by buffer exchange over a 10 kDa MWCO Amicon Ultra spin filter (Millipore) and stored as 1 mg/mL solutions in PBS. Final biotin loading was determined by MALDI-TOF-MS after purification and determined by comparison to the molecular weight of the unmodified Alirocumab LYTACs.

Biotinylation of asialofetuin was done the same way as described above, except that excess NHS-LC-LC-biotin (30 mol eq.) and a longer incubation time of 20 hours was used in order to achieve a suitable biotin loading (i.e. 5 biotin units) that is comparable to the antibody-biotin conjugates. Biotinylated-asialofetuin was also purified by spin filtration as described above.

### **Cell lines and reagents**

HepG2 and Hela cells were purchased from ATCC and cultured in T75 flasks at 37 °C and with 5% CO<sub>2</sub>. HepG2 and Hela cells were cultured in EMEM medium containing 10% FBS and 1% penicillin/ streptomycin antibiotics. For serum-depletion of HepG2 cells, OptiMEM serum-free medium (Gibco) was used with no other additives. Antibodies used in western blotting experiments are listed in Table 4.1.

### **Flow cytometry binding assay of biotinylated LYTACs to cell surface ASGPR**

HepG2 cells in a T75 flask were serum-starved in OptiMEM media for 12-16 hours and then detached and resuspended in wash/ stain buffer (DPBS, 2% FBS, 0.1% NaN<sub>3</sub>) before counting. HepG2 cells were then seeded to 3 x 10<sup>5</sup> cells per well of a 96-well V-bottom plate in 200 µL volumes and the plate was spun at 1,400 rpm for 5 minutes to pellet the cells. The wash/ stain buffer was removed and 100 µL Fc block solution (Human BD Fc Block, BD Cat. # 564220) was added to the wells. The plate was incubated in the dark for 10 minutes at room temperature and spun again at 1,400 rpm for 5 minutes. Test antibody and LYTAC dilutions were then prepared in wash/ stain buffer in a fresh 96-well V-bottom plate and then added in 100 µL volumes to the cells. Wash/ stain buffer only was used as a negative control and added to the designated control wells. The plate was incubated for 30-45 minutes in the dark at room temperature and 100 µL of wash buffer was then added to each well before pelleting the cells again. The supernatant was removed and a diluted solution of Streptavidin-PE conjugate (BD Cat. # 349023) was added in 100 µL volumes to the test and control wells. As a positive control PE conjugated mouse anti-ASGPR1 antibody (BD Cat. # 563655) was added at .25ug per/test to the control wells. The plate was incubated for 30 minutes in the dark before pelleting the cells. The supernatant was removed, and each well was washed with 200 µL wash/ stain buffer. The cells were pelleted and washed again before resuspending the cells in 50 µL 1%

paraformaldehyde to fix the cells. The samples were analyzed for fluorescence intensity using a Fortessa/LSR instrument under the high-throughput option for the plate reader. Fluorescence data was analyzed with Flowjo Ver.9.9.6 (Flowjo, Ashland, OR).

### **Epidermal growth factor receptor (EGFR) protein degradation assay**

HepG2 and Hep3B cells were seeded at 100,000 cells/ well in a 24-well plate one day prior to the degradation assay. The following day, the media was discarded, and adherent cells were treated with variable concentrations of each Cetuximab LYTAC as a solution in EMEM complete growth medium (0.5 mL). Cells were incubated with Cetuximab LYTACs for 48 hours, at which point the media was discarded and cells were washed with twice with 0.5 mL PBS. Finally, 100  $\mu$ L of Pierce RIPA lysis buffer containing cOmplete Mini protease inhibitor (Sigma) and phosphatase inhibitor cocktail (Cell Signaling Technologies) was added and cells were lysed for 30 min on ice. Cells were scraped, transferred to 1.5 mL centrifuge tubes and centrifuged at 13,500 rpm for 15 min to pellet cell debris. Supernatant was collected into new microcentrifuge tubes and assayed for total protein concentration by Pierce BCA assay (Thermo). Equal amounts of cell lysate were loaded and separated on an 8-16% SDS-PAGE gel and imaged using a Biorad Gel Doc EZ imager. Lysate protein was then transferred to a nitrocellulose blot and blocked with 5% non-fat dairy milk (ChemCruz) for 1 hour at room temperature. Nitrocellulose blots were washed with TBST (Tris buffered saline containing 0.1% Tween-20) as the washing buffer and then incubated with primary antibodies overnight at 4 °C (rabbit anti-EGFR 1:1,000 dilution, and rabbit anti- $\beta$ -actin 1:5,000 dilution). Blots were washed three times in TBST, and then incubated with secondary antibody (goat anti-rabbit IgG [H + L] HRP-conjugate 1:2,500 dilution) for 1 hour at room temperature before washing four more times with TBST buffer. Finally, ECL Plus chemifluorescent reagent (Thermo) was added to the blots and incubated for 5 min before

performing fluorescent imaging using a Molecular Devices Storm 860 imager with excitation wavelength at 450 nm.

### **PCSK9 protein degradation assay**

HepG2 cells were seeded at 100,000 cells/ well in a 24-well plate one day prior to the degradation assay. The following day, the media was discarded, and wells washed once with 0.5 mL PBS before 0.5 mL of serum deficient OptiMEM media was added to each well. HepG2 cells were then serum-deprived for 12-16 hours. Meanwhile, human PCSK9 D374Y gain-of-function mutant (ACROBiosystems) was prepared as a 10 µg/mL stock solution in OptiMEM and, separately, Alirocumab LYTACs were diluted to two-fold higher than the desired concentration for the assay in OptiMEM. Equal volumes (150 µL) of the PCSK9 D374Y stock solution and LYTAC solution were then mixed and incubated for 30 min at room temperature. Importantly, the PCSK9 solution was incubated with varying concentrations of each LYTAC to test for a dose-response. A positive control consisted of the PCSK9 D374Y stock solution mixed with OptiMEM containing no LYTAC, and OptiMEM alone was used as a negative control. All experimental and control samples were added to the cells in the 24-well plate as 250 µL aliquots, and cells were incubated for 48 hours at 37 °C. Then, the media in each well was collected into separate 1.5 mL microcentrifuge tubes and labeled, and cells were washed twice with 0.5 mL PBS. Finally, 100 µL of RIPA lysis buffer containing cOmplete Mini protease inhibitor cocktail (Sigma) and phosphatase inhibitor cocktail (Cell Signaling Technologies) was added and cells were lysed for 30 min on ice. Cell lysate samples were then collected as described above. PCSK9 levels in the media were tested by western blot using a polyclonal anti-PCSK9 primary antibody (rabbit anti-PCSK9 1:1,000), where the total protein content was normalized by adding the same volume of media to each well of an 8-16 % SDS-PAGE gel. Protein was then transferred to a

nitrocellulose blot and processed as described above for the EGFR degradation assay. Levels of Low-Density Lipoprotein Receptor (LDLR) were also tested by western blot using an anti-LDLR primary antibody (rabbit anti-LDLR 1:2,000 dilution) on the HepG2 cell lysate and normalized to  $\beta$ -actin as a loading control (rabbit anti- $\beta$ -actin 1:5,000 dilution), following the general procedure outlined above for the EGFR degradation assay.

**Table 4.1.** All antibodies used in this study, including vendor and dilutions.

<b>Antibody</b>	<b>Vendor</b>	<b>Usage</b>
Rabbit anti- $\beta$ -actin mAb	CST (D6A8)	WB (1: 5,000)
Rabbit anti-PCSK9 pAb	Proteintech (55206-1-AP)	WB (1: 1,000)
Rabbit anti-LDLR pAb	Novus (NBP1-06709)	WB (1: 2,000)
Rabbit anti-EGFR mAb	CST (D38B1)	WB (1: 1,000)
Rabbit anti-Vinculin mAb	CST (E1E9V)	WB (1: 2,000)
Goat anti-rabbit IgG (HRP)	Millipore (AP307P)	WB (1: 2,500)
Alirocumab	RefDrug	Cell assays (50-200 nM)
Cetuximab	RefDrug	Cell assays (1-100 nM)

## 4.5 SUPPORTING INFORMATION

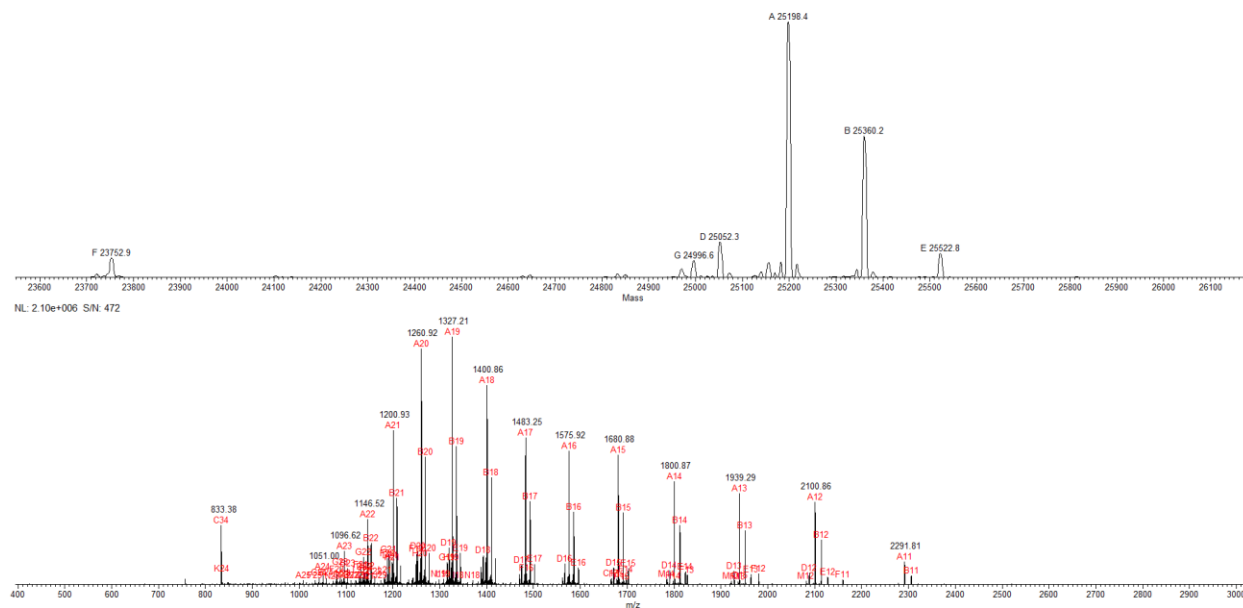


**Figure 4.9.** LC-MS analysis of IdeS treated native Alirocumab (**4.8a**). Peak at 25,522 Da represents the G2F glycoform, the peak at 25,360 Da represents the G1F glycoform, the peak at 25,198 Da represents the G0F glycoform, peak at 25,052 Da represents the G0 glycoform.

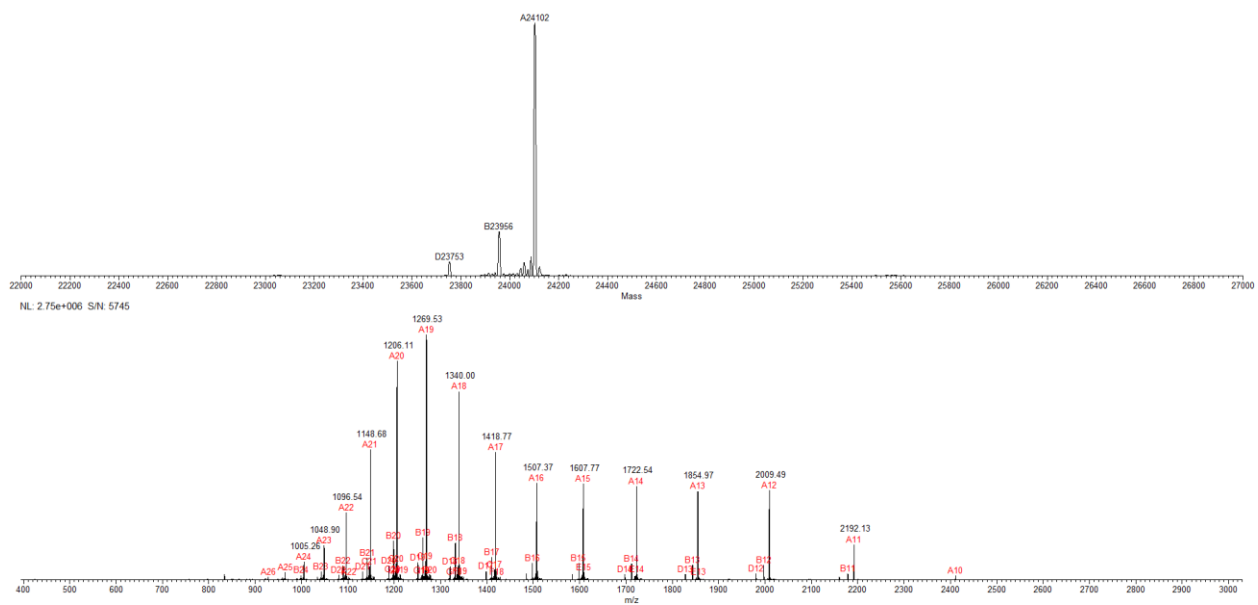


**Figure 4.10.** LC-MS analysis of IdeS treated GNF-Alirocumab (**4.9a**). ESI-MS: calcd for GNF-Ali (**4.9a**),  $M = 24,100$  Da; found (m/z), deconvolution of the ESI-MS,  $M = 24,102$  Da.

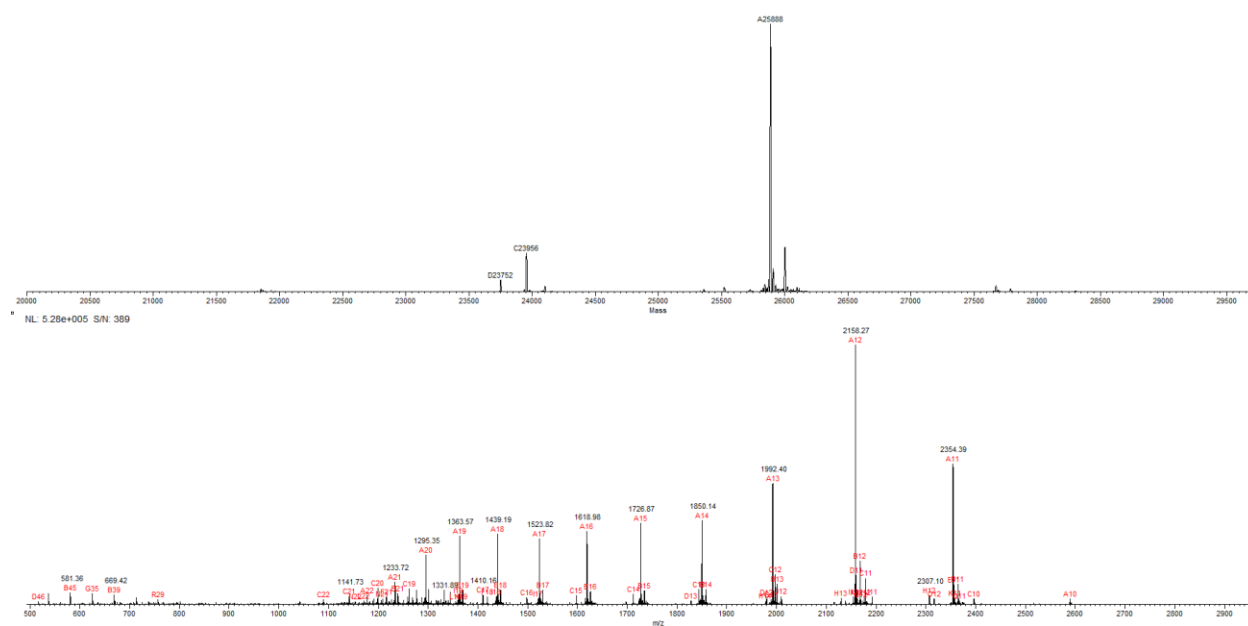


**Figure 4.11.** LC-MS analysis of IdeS treated G3F-Alirocumab (**4.10a**). ESI-MS: calcd for G3F-Ali (**4.10a**),  $M = 25,887$  Da; found (m/z), deconvolution of the ESI-MS,  $M = 25,888$  Da.

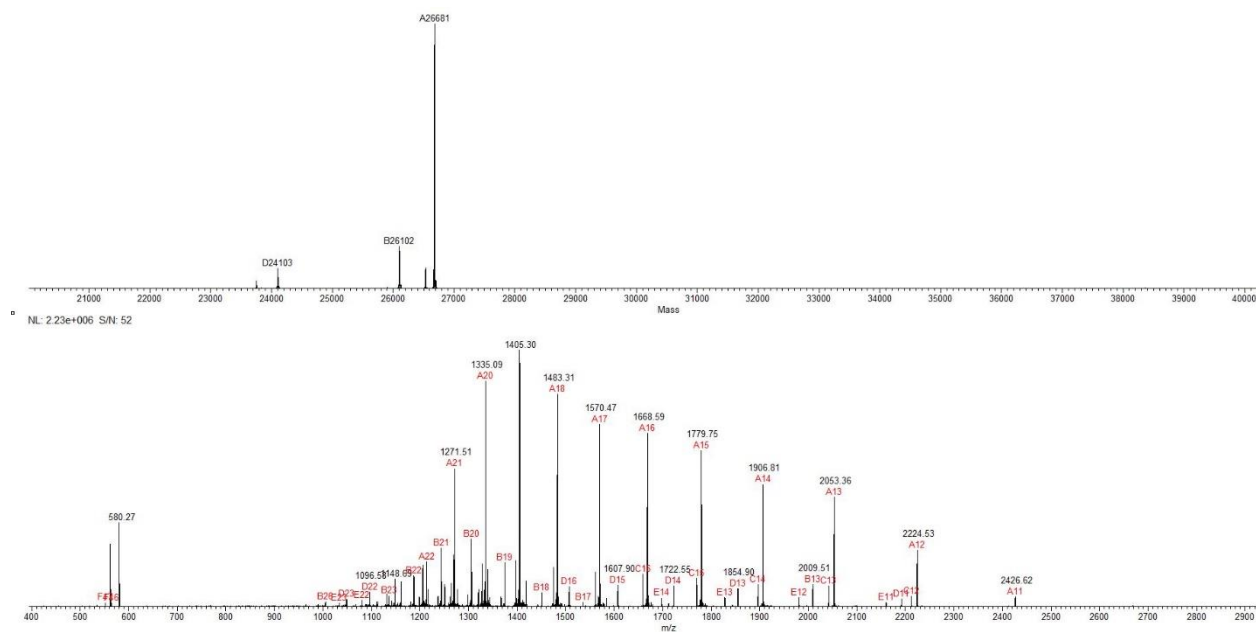


**Figure 4.12.** LC-MS analysis of IdeS treated di-N<sub>3</sub>-S<sub>2</sub>G<sub>2</sub>-Alirocumab (**4.11a**). ESI-MS: calcd for di-N<sub>3</sub>-S<sub>2</sub>G<sub>2</sub>-GlcNAc-Ali (**4.11a**), M = 26,681 Da; found (m/z), deconvolution of the ESI-MS, M = 26,681 Da.

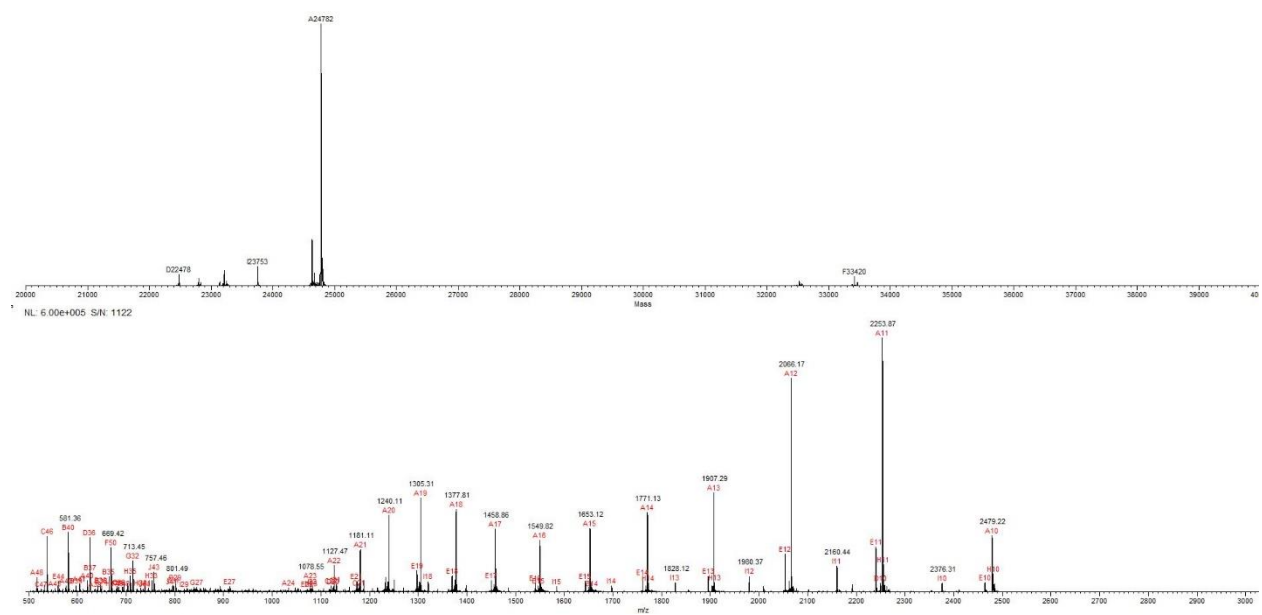


**Figure 4.13.** LC-MS analysis of IdeS treated di-N<sub>3</sub>-Man-Alirocumab (**4.12a**). ESI-MS: calcd for di-N<sub>3</sub>-Man-GlcNAc-Ali (**4.12a**), M = 24,781 Da; found (m/z), deconvolution of the ESI-MS, M = 24,782 Da.

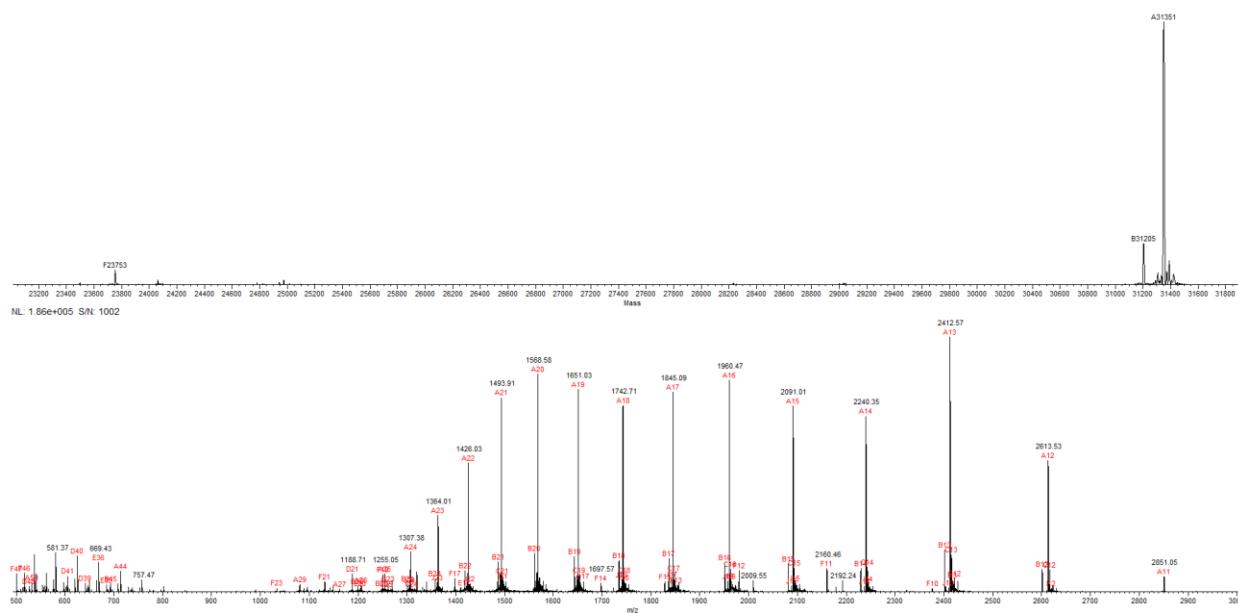


**Figure 4.14.** LC-MS analysis of IdeS treated G2 click-Alirocumab (**4.13a**). ESI-MS: calcd for G2 click-Ali (**4.13a**), M = 31,349 Da; found (m/z), deconvolution of the ESI-MS, M = 31,351 Da.

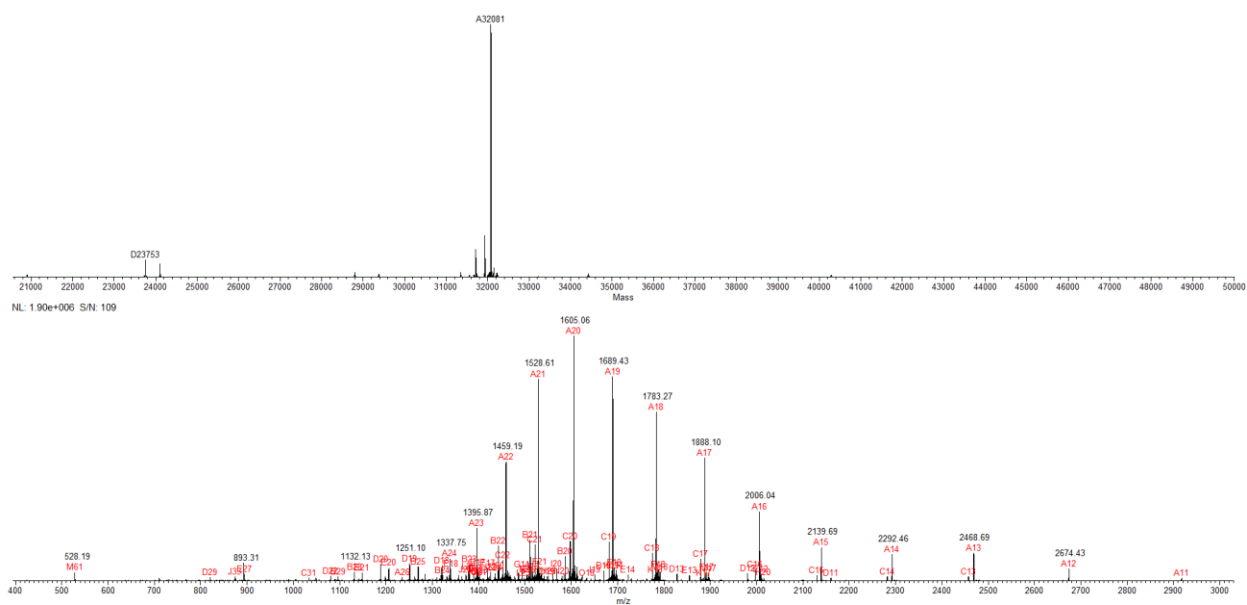


**Figure 4.15.** LC-MS analysis of IdeS treated G3 click-Alirocumab (**4.14a**). ESI-MS: calcd for G3 click-Ali (**4.14a**), M = 32,079 Da; found (m/z), deconvolution of the ESI-MS, M = 32,081 Da.

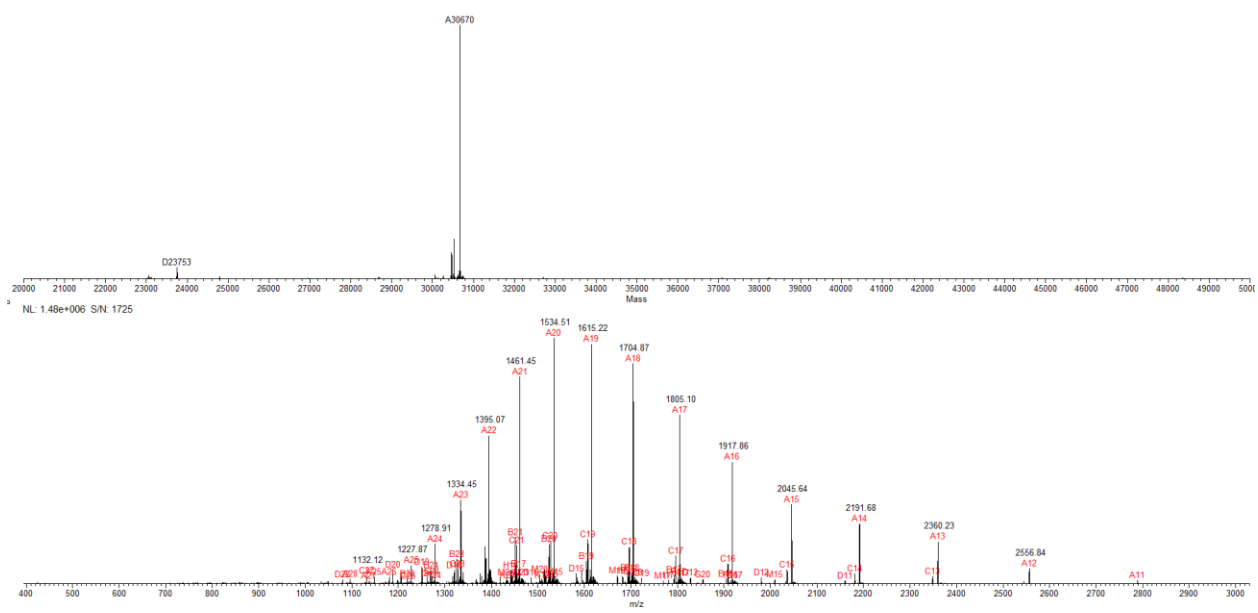


**Figure 4.16.** LC-MS analysis of IdeS treated tri-GalNAc-S2G2-Alirocumab (**4.15a**). ESI-MS: calcd for tri-GalNAc-S2G2-Ali (**4.15a**),  $M = 30,669$  Da; found ( $m/z$ ), deconvolution of the ESI-MS,  $M = 30,670$  Da.

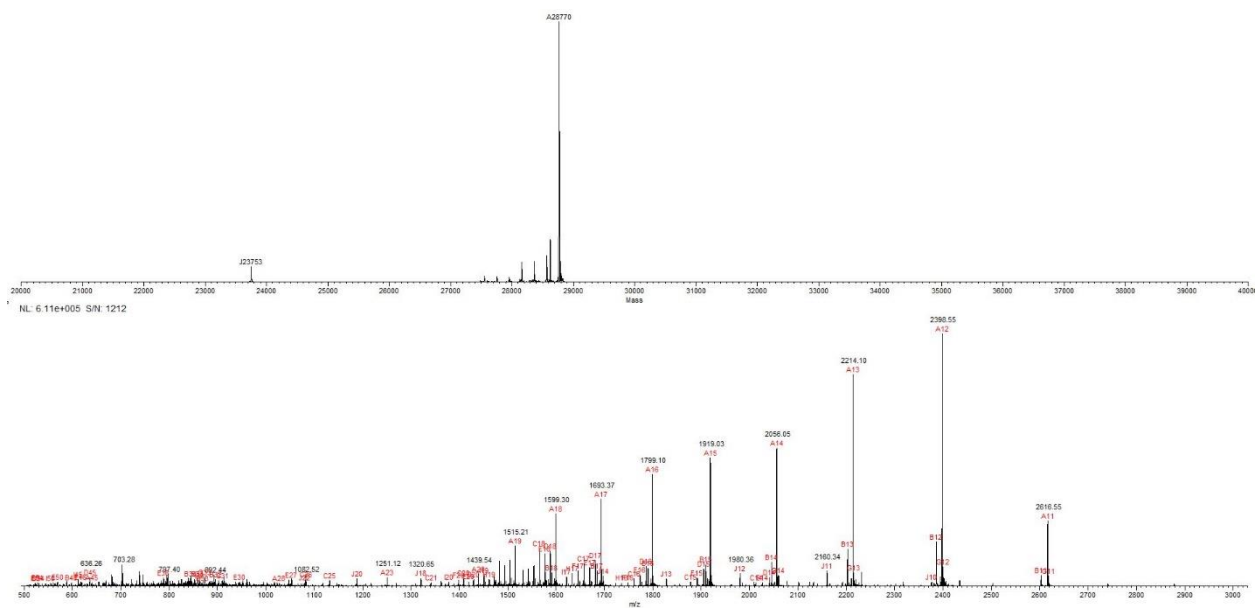


**Figure 4.17.** LC-MS analysis of IdeS treated tri-GalNac-Man-Alirocumab (**4.16a**). ESI-MS: calcd for tri-GalNac-Man-Ali (**4.16a**),  $M = 28,769$  Da; found ( $m/z$ ), deconvolution of the ESI-MS,  $M = 28,770$  Da.

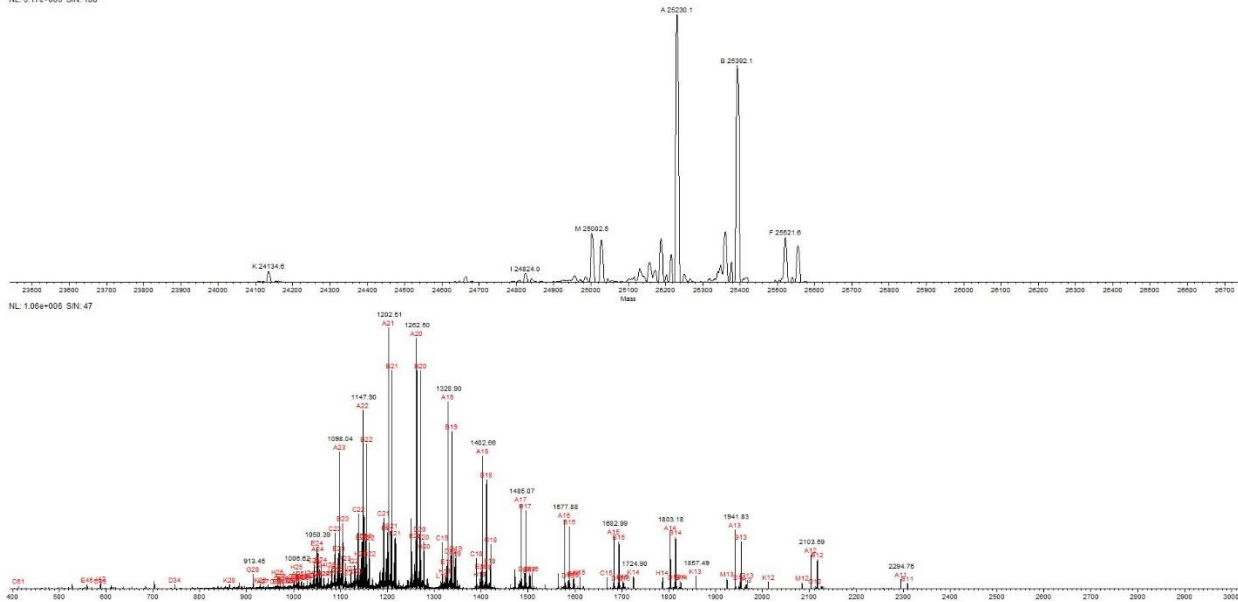


**Figure 4.18.** LC-MS analysis of IdeS treated native Cetuximab (**4.8b**). Peak at 25,521 Da represents G2F glycoform plus C-terminal lysine. Peak at 25,392 Da represents G2F glycoform. Peak at 25,230 Da represents G1F glycoform. Peak at 25,068 Da represents G0F glycoform.

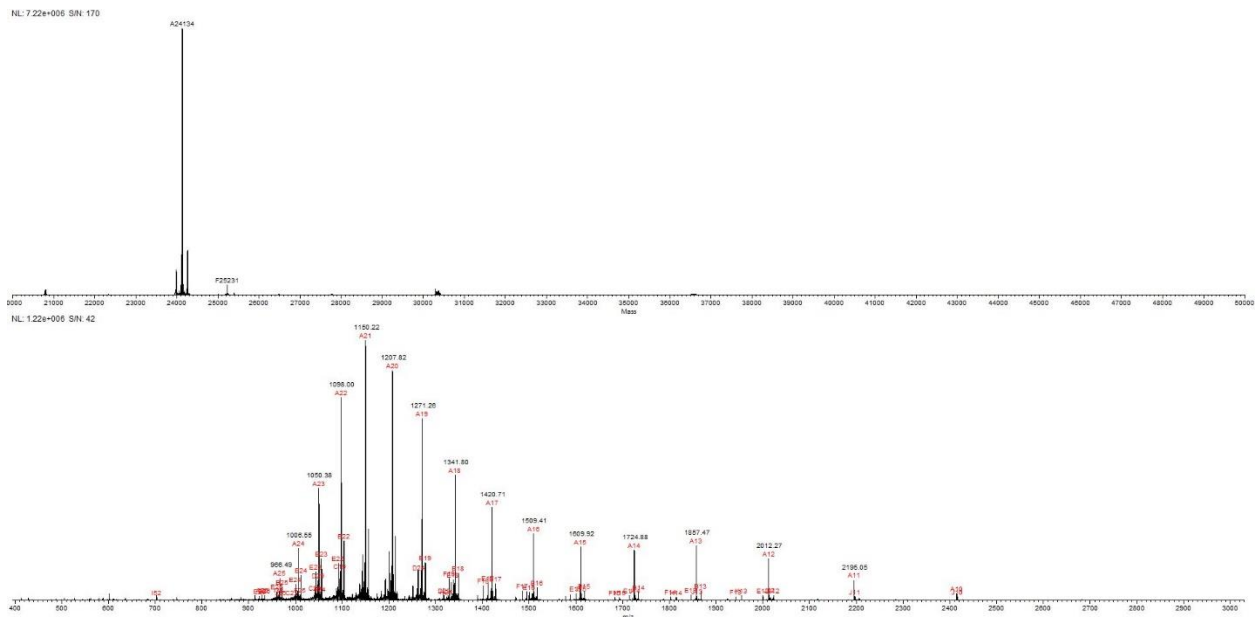


**Figure 4.19.** LC-MS analysis of IdeS treated GNF-Cetuximab (**4.9b**). ESI-MS: calcd for GNF-Cet (**4.9b**),  $M = 24,132$  Da; found ( $m/z$ ), deconvolution of the ESI-MS,  $M = 24,134$  Da.

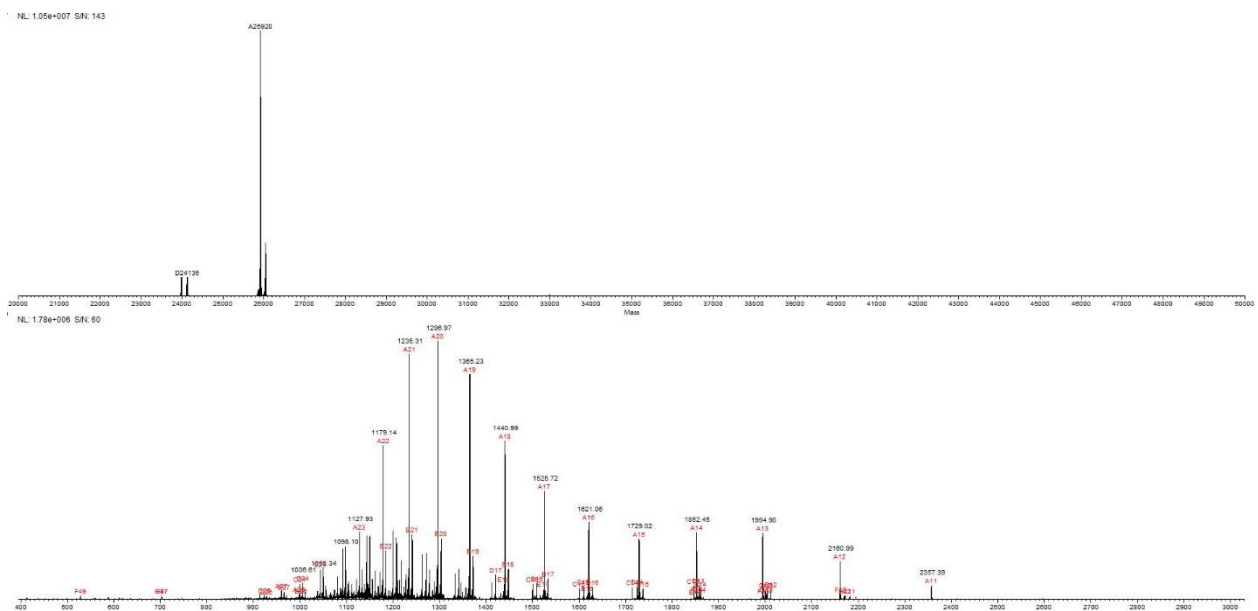


**Figure 4.20.** LC-MS analysis of IdeS treated G3F-Cetuximab (**4.10b**). ESI-MS: calcd for G3F-Cet (**4.10b**), M = 25,919 Da; found (m/z), deconvolution of the ESI-MS, M = 25,920 Da.

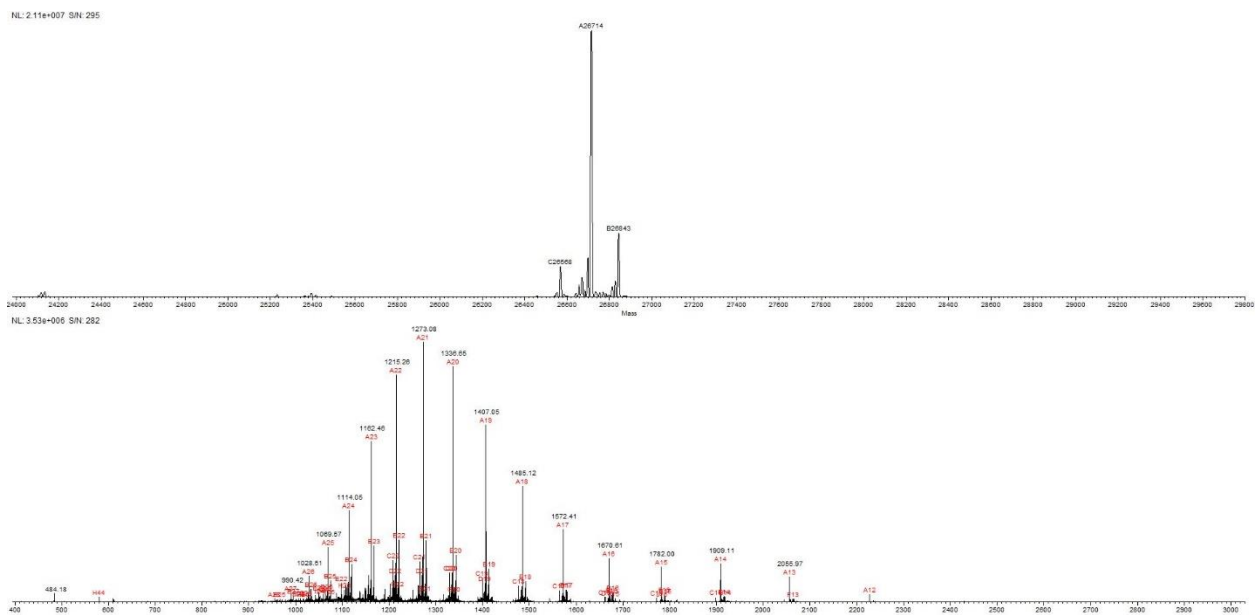


**Figure 4.21.** LC-MS analysis of IdeS treated di-N<sub>3</sub>-S2G2-Cetuximab (**4.11b**). ESI-MS: calcd for di-N<sub>3</sub>-S2G2-Cet (**4.11b**), M = 26,713 Da; found (m/z), deconvolution of the ESI-MS, M = 26,714 Da.

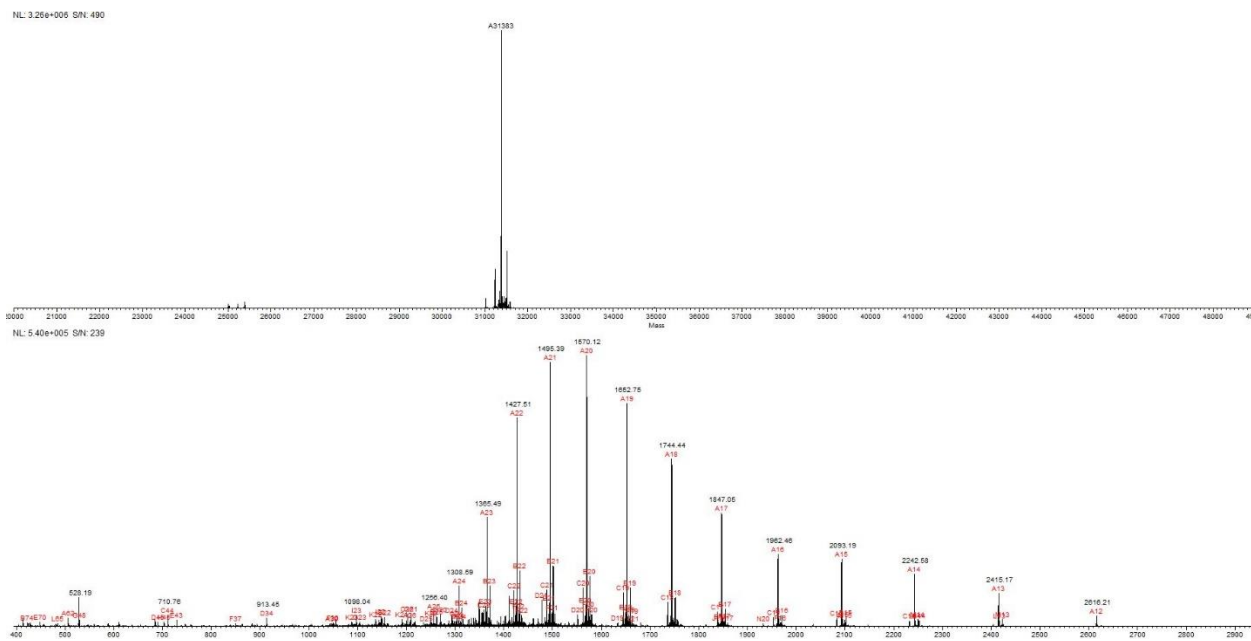


**Figure 4.22.** LC-MS analysis of IdeS treated G2 click-Cetuximab (**4.13b**). ESI-MS: calcd for G2 click-Cet (**4.13b**),  $M = 31,381$  Da; found ( $m/z$ ), deconvolution of the ESI-MS,  $M = 31,383$  Da.

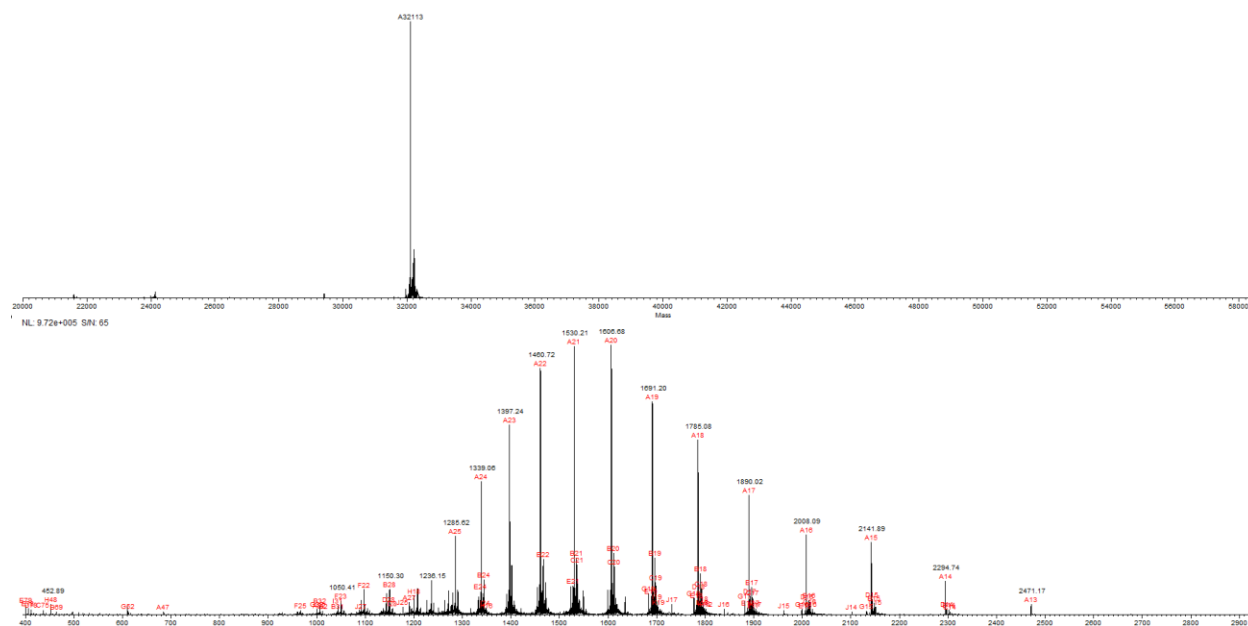


**Figure 4.23.** LC-MS analysis of IdeS treated G3 click-Cetuximab (**4.14b**). ESI-MS: calcd for G3 click-Cet (**4.14b**),  $M = 32,112$  Da; found ( $m/z$ ), deconvolution of the ESI-MS,  $M = 32,113$  Da.

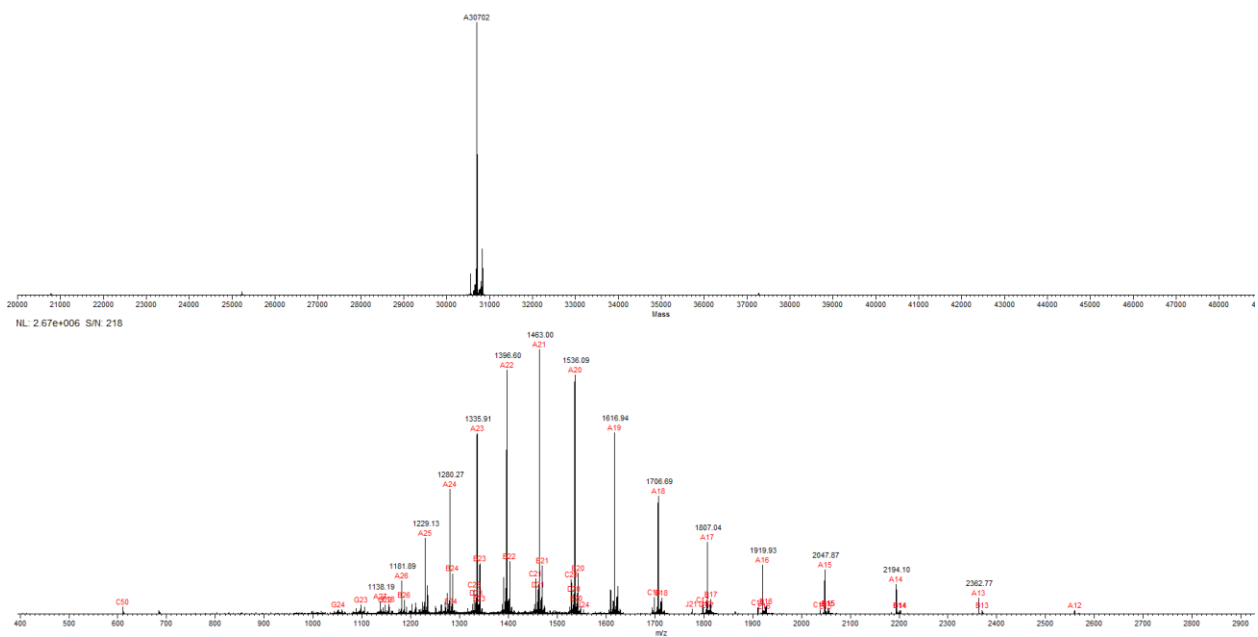


**Figure 4.24.** LC-MS analysis of IdeS treated tri-GalNAc-S2G2-Cetuximab (**4.15b**). ESI-MS: calcd for tri-GalNAc-S2G2-Cet (**4.15b**),  $M = 30,701$  Da; found ( $m/z$ ), deconvolution of the ESI-MS,  $M = 30,702$  Da.

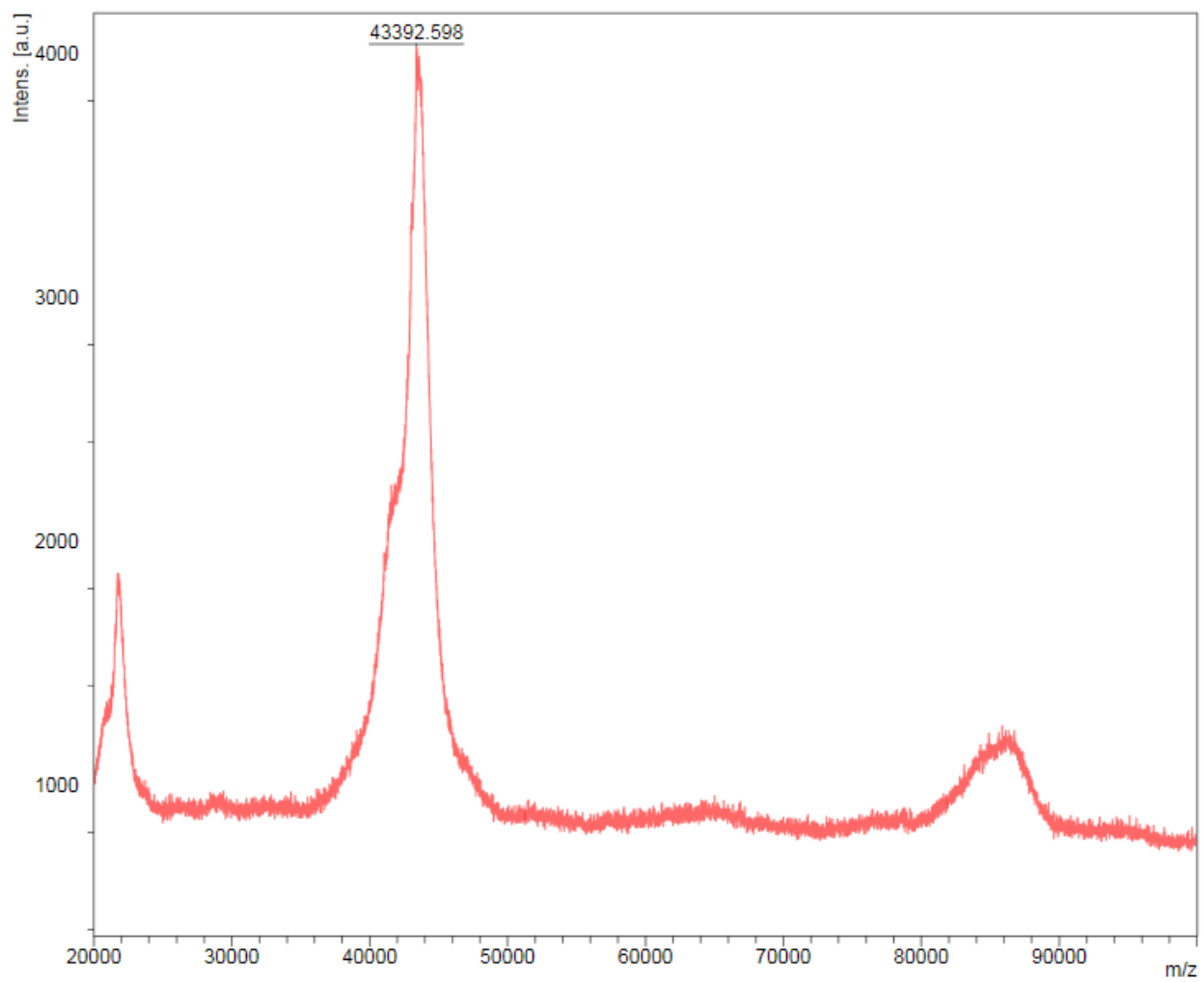


**Figure 4.25.** MALDI-TOF-MS of Asialofetuin in linear positive mode.

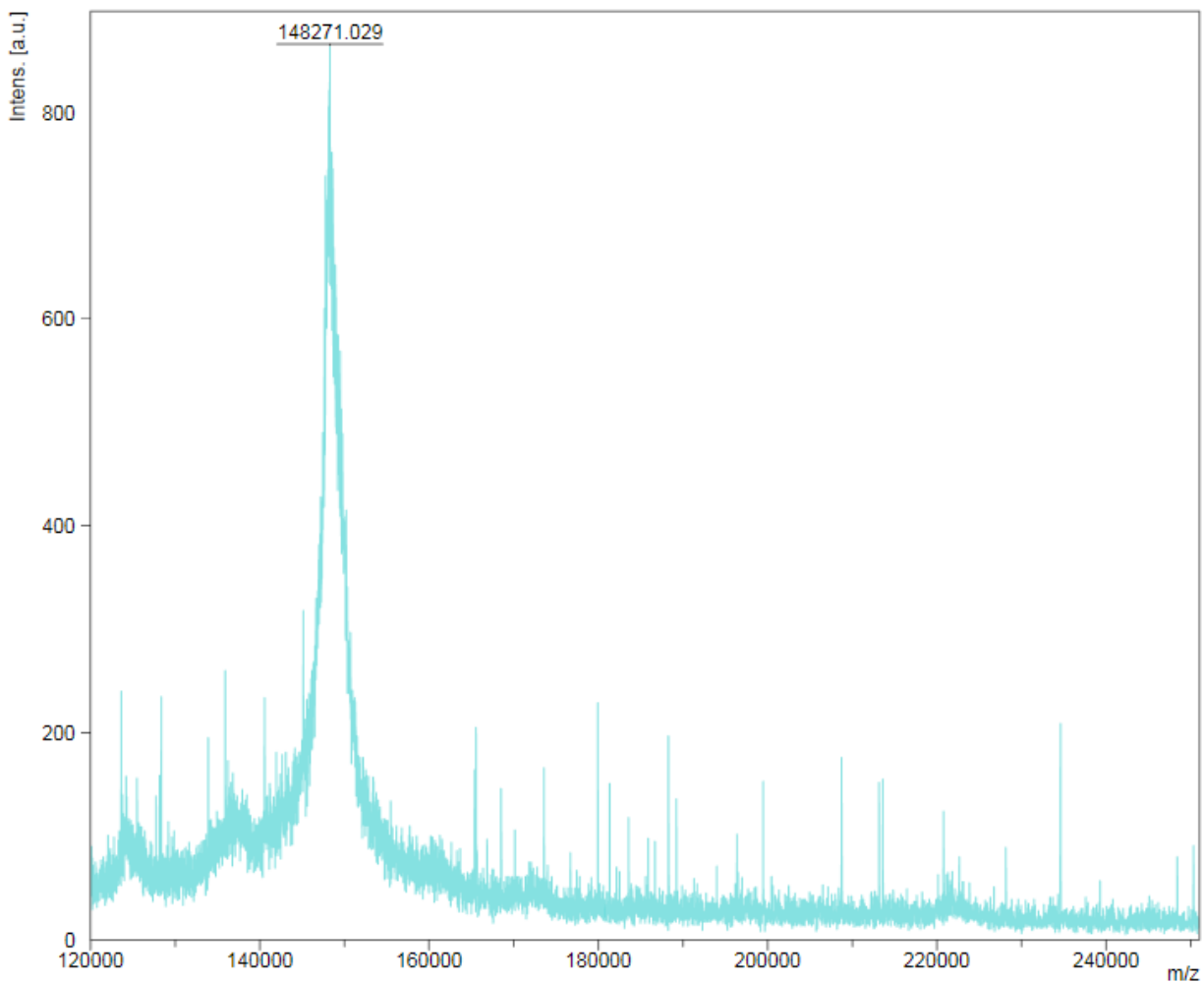


**Figure 4.26.** MALDI-TOF-MS of native Alirocumab (**4.8a**) in linear positive mode.

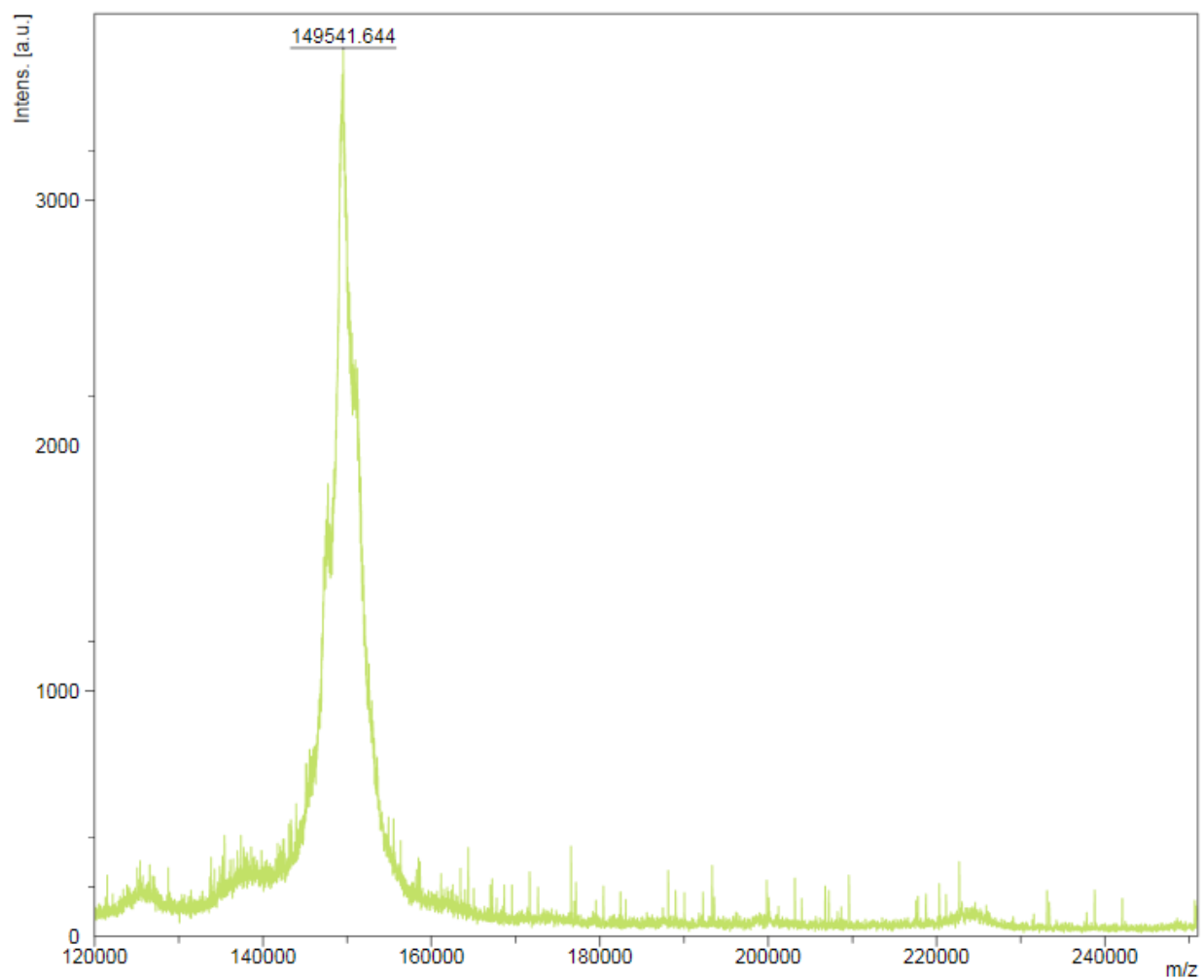


**Figure 4.27.** MALDI-TOF-MS of G3F-Alirocumab (**4.10a**) in linear positive mode.

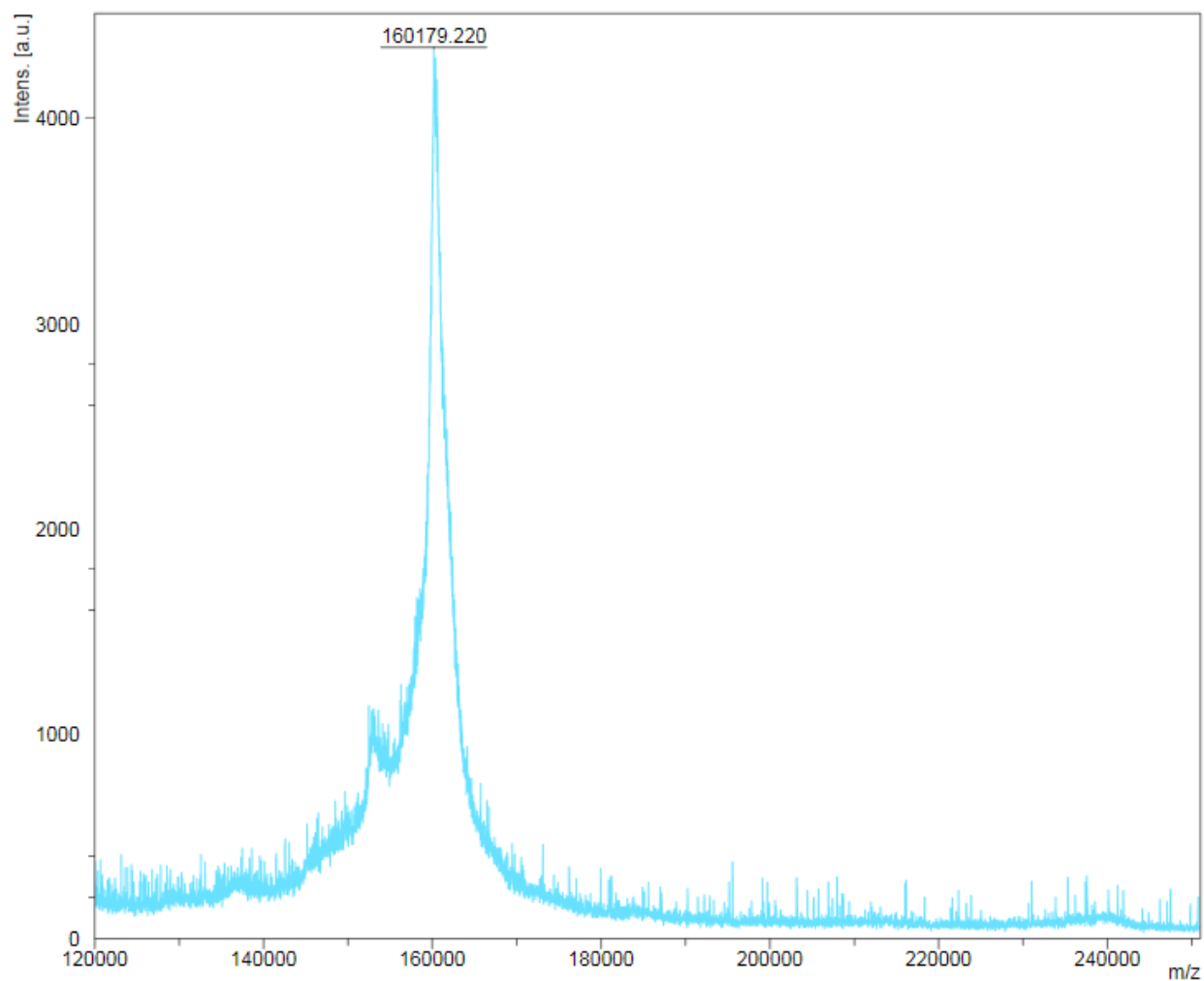


**Figure 4.28.** MALDI-TOF-MS of G2 click-Alirocumab (**4.13a**) in linear positive mode.

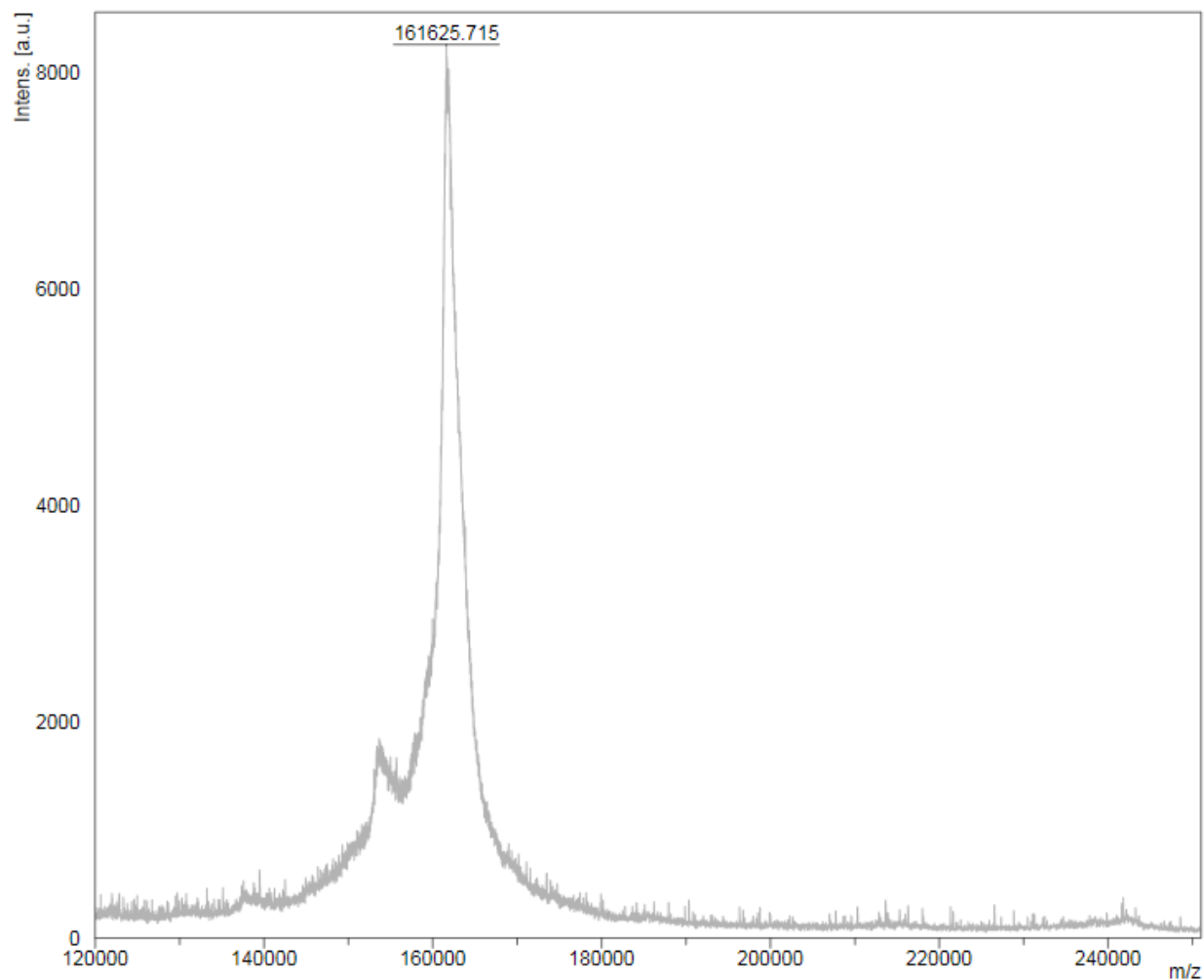


**Figure 4.29.** MALDI-TOF-MS of G3 click-Alirocumab (**4.14a**) in linear positive mode.

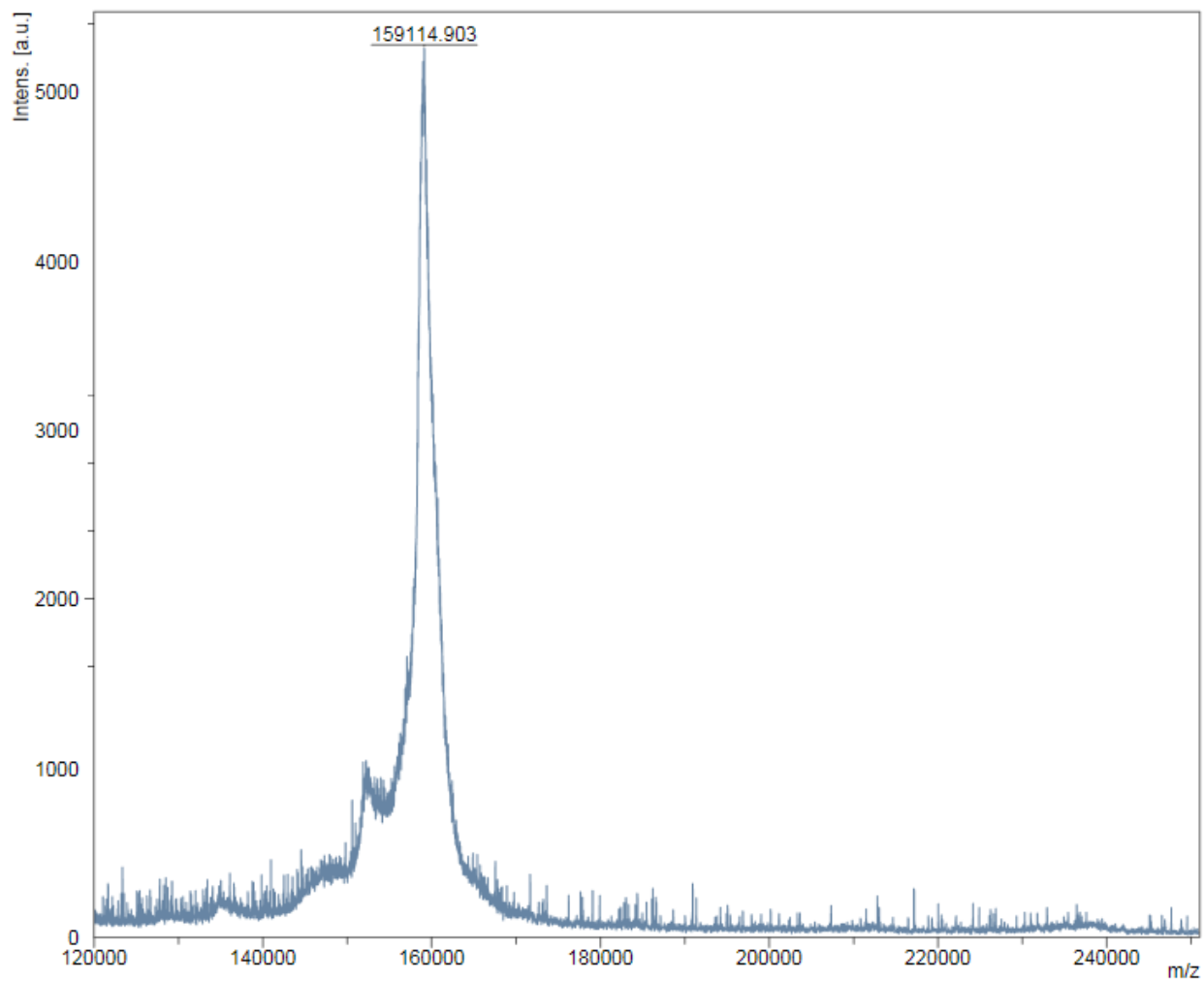


**Figure 4.30.** MALDI-TOF-MS of tri-GalNAc-S2G2-Alirocumab (**4.15a**) in linear positive mode.

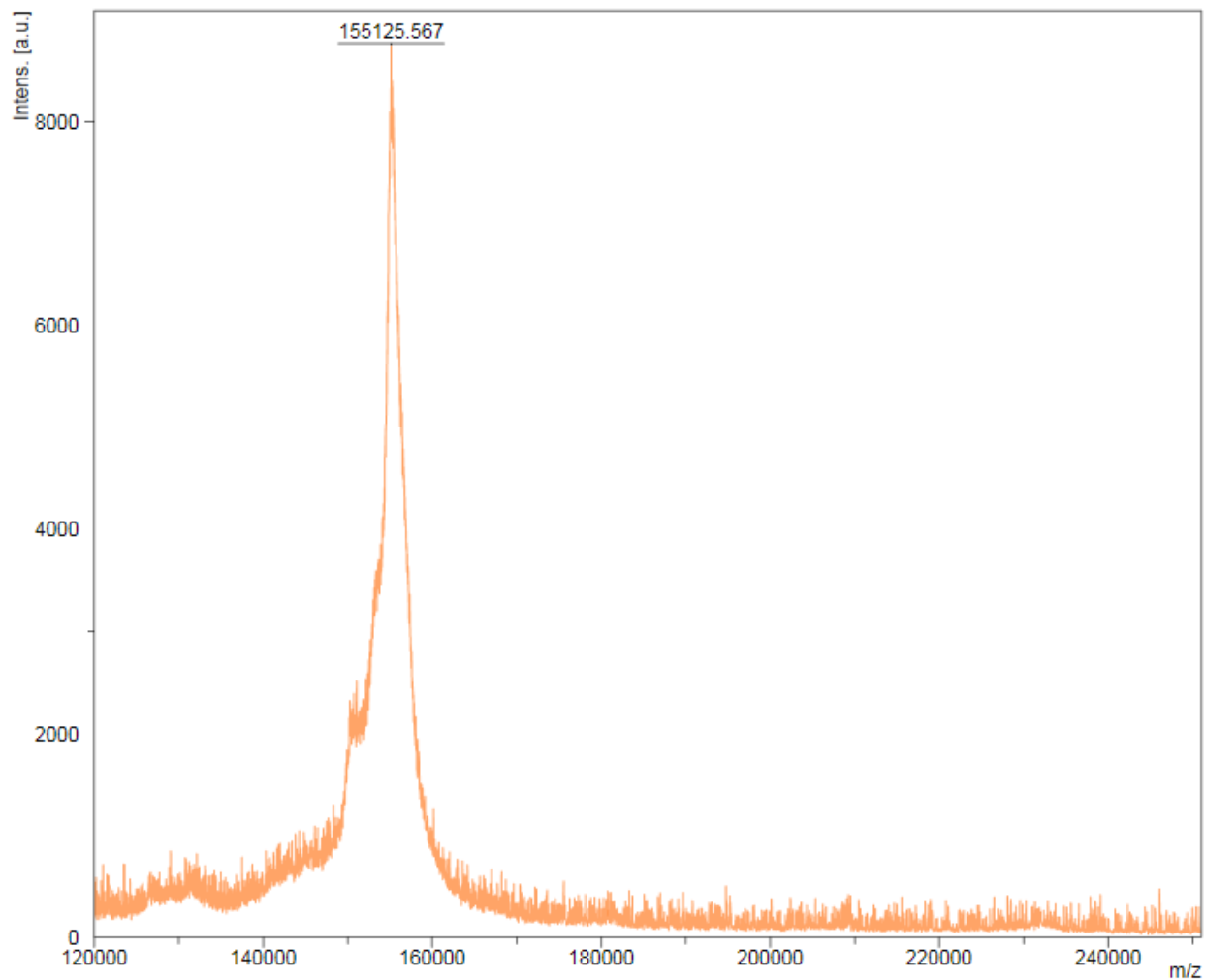


**Figure 4.31.** MALDI-TOF-MS of tri-GalNAc-Man-Alirocumab (**4.16a**) in linear positive mode.

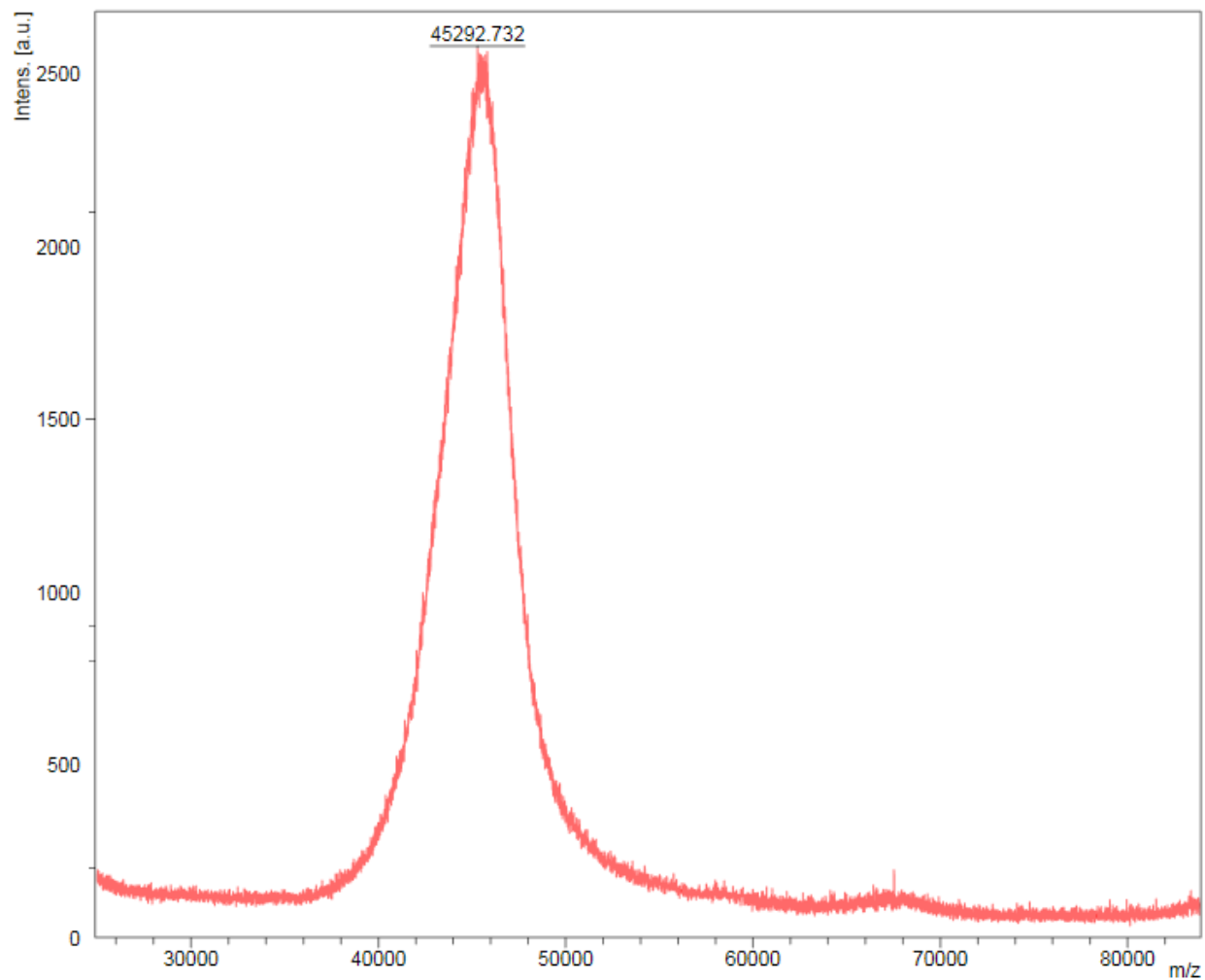


**Figure 4.32.** MALDI-TOF-MS of biotinylated asialofetuin for cell-based binding assay in linear positive mode. An average of four biotin units were attached.

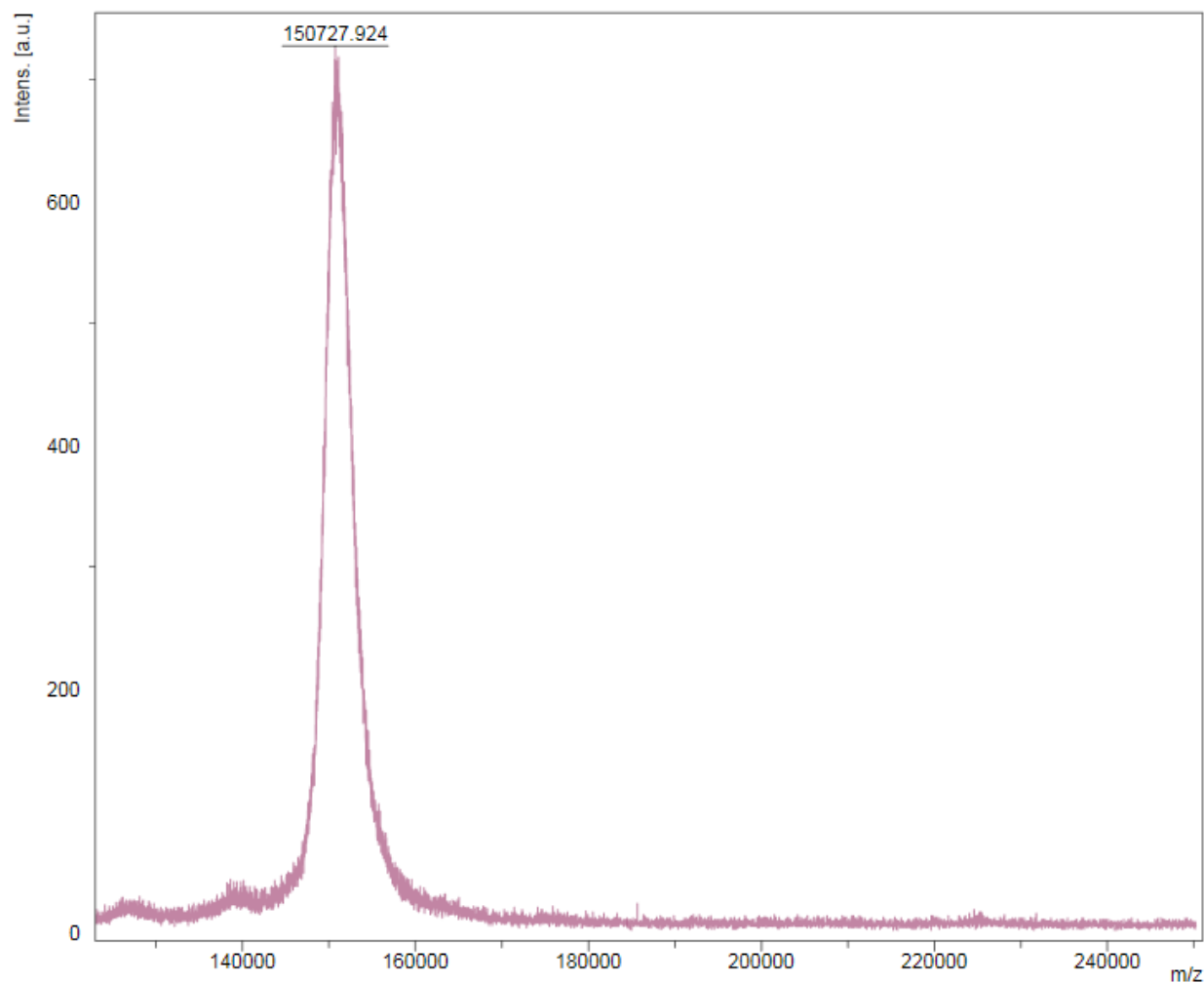


**Figure 4.33.** MALDI-TOF-MS of biotinylated native Alirocumab for cell-based binding assay in linear positive mode. An average of five biotin units were attached.

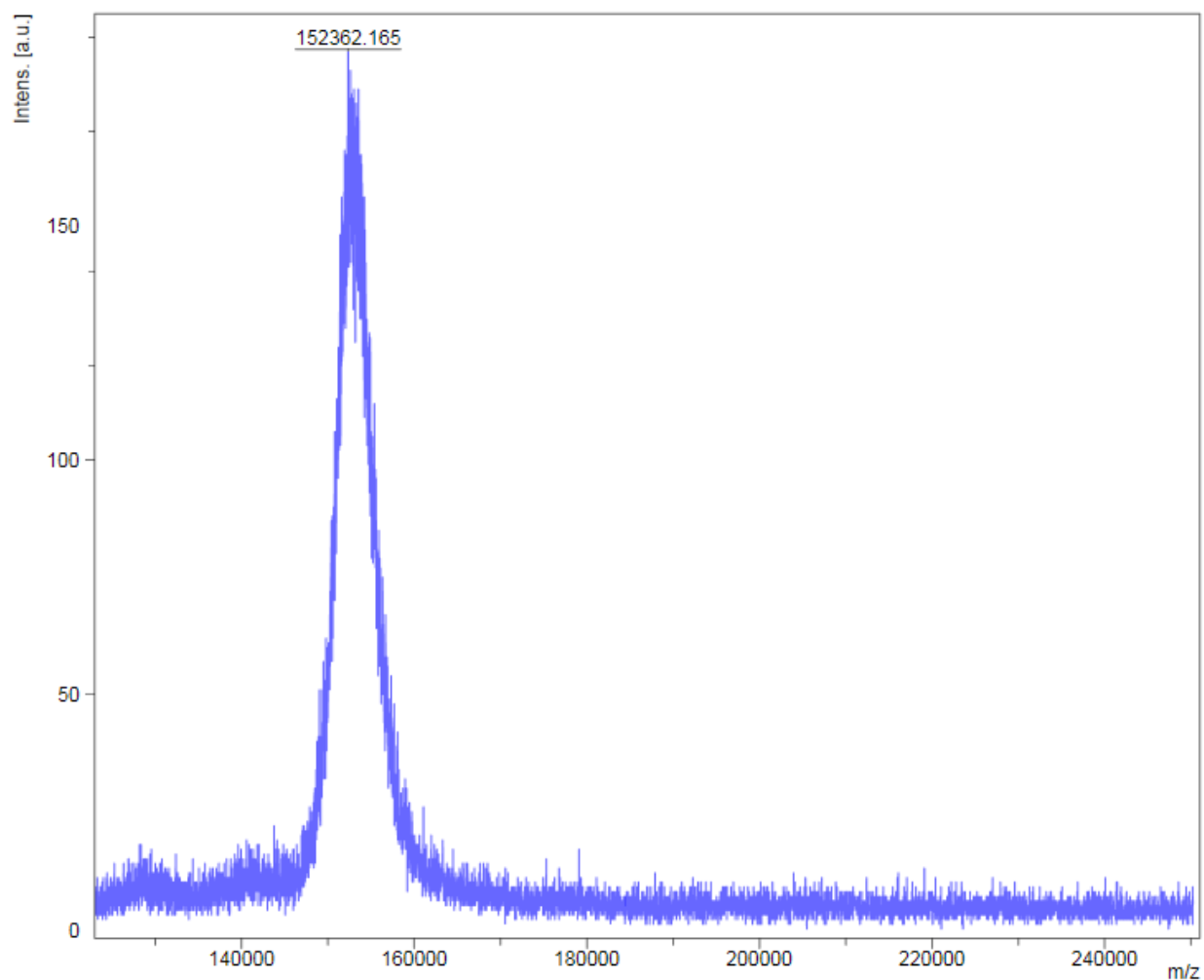


**Figure 4.34.** MALDI-TOF-MS of biotinylated G3F-Alirocumab for cell-based binding assay in linear positive mode. An average of six biotin units were attached.

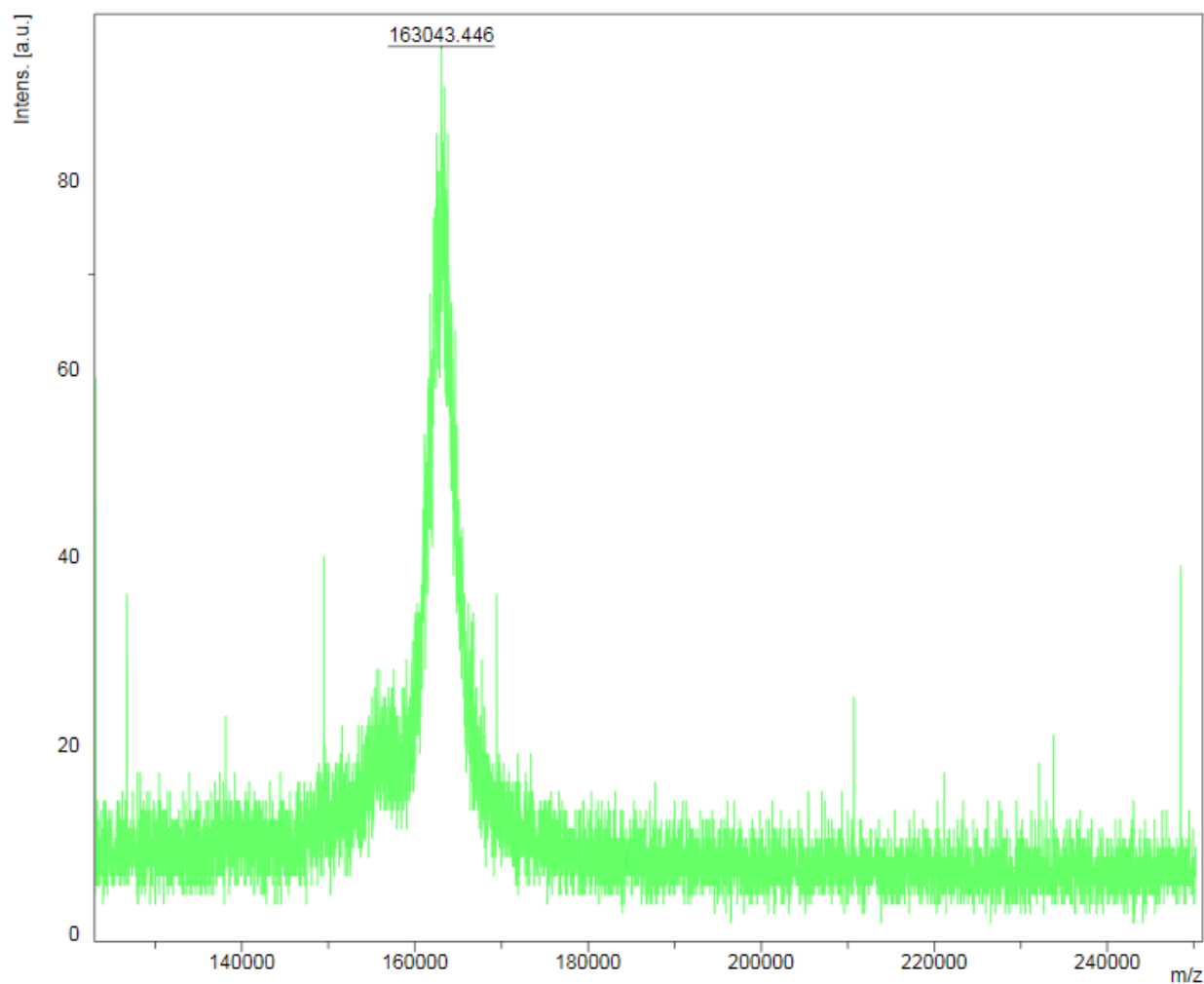


**Figure 4.35.** MALDI-TOF-MS of biotinylated G2 click-Alirocumab for cell-based binding assay in linear positive mode. An average of six biotin units were attached.

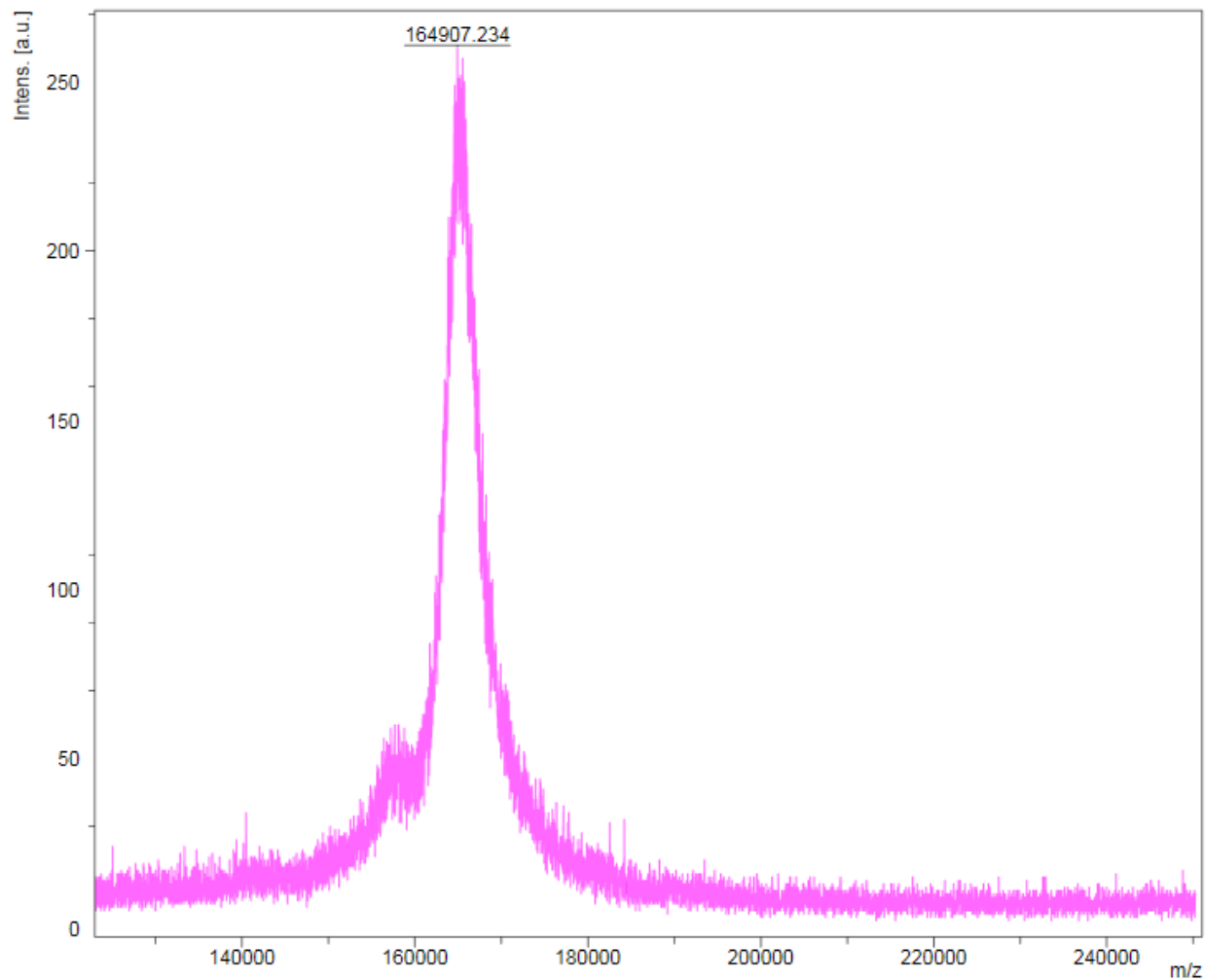


**Figure 4.36.** MALDI-TOF-MS of biotinylated G3 click-Alirocumab for cell-based assay in linear positive mode. An average of seven biotin units were attached.

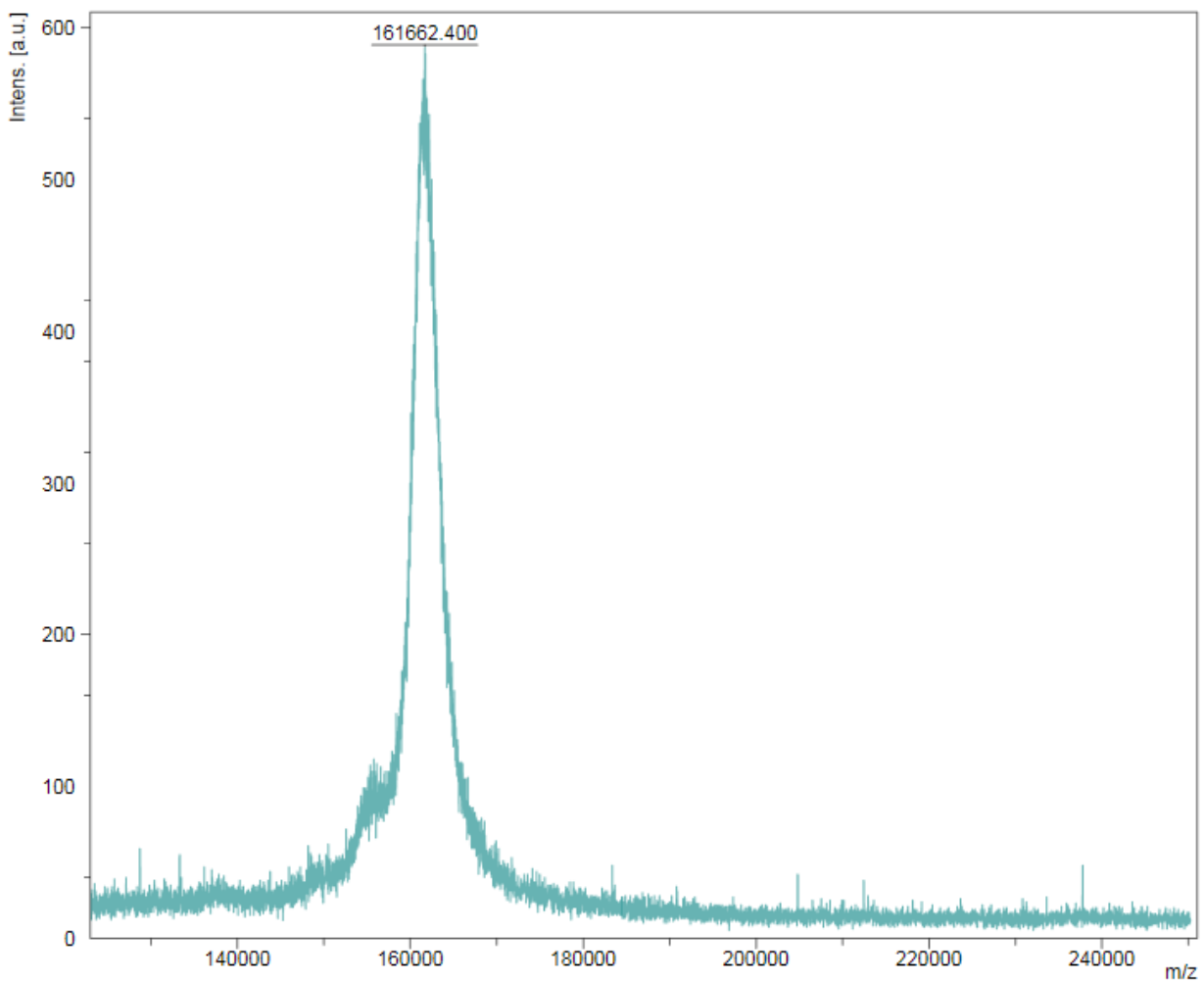


**Figure 4.37.** MALDI-TOF-MS of biotinylated tri-GalNAc-S2G2-Alirocumab for cell-based assay in linear positive mode. An average of six biotin units were attached.

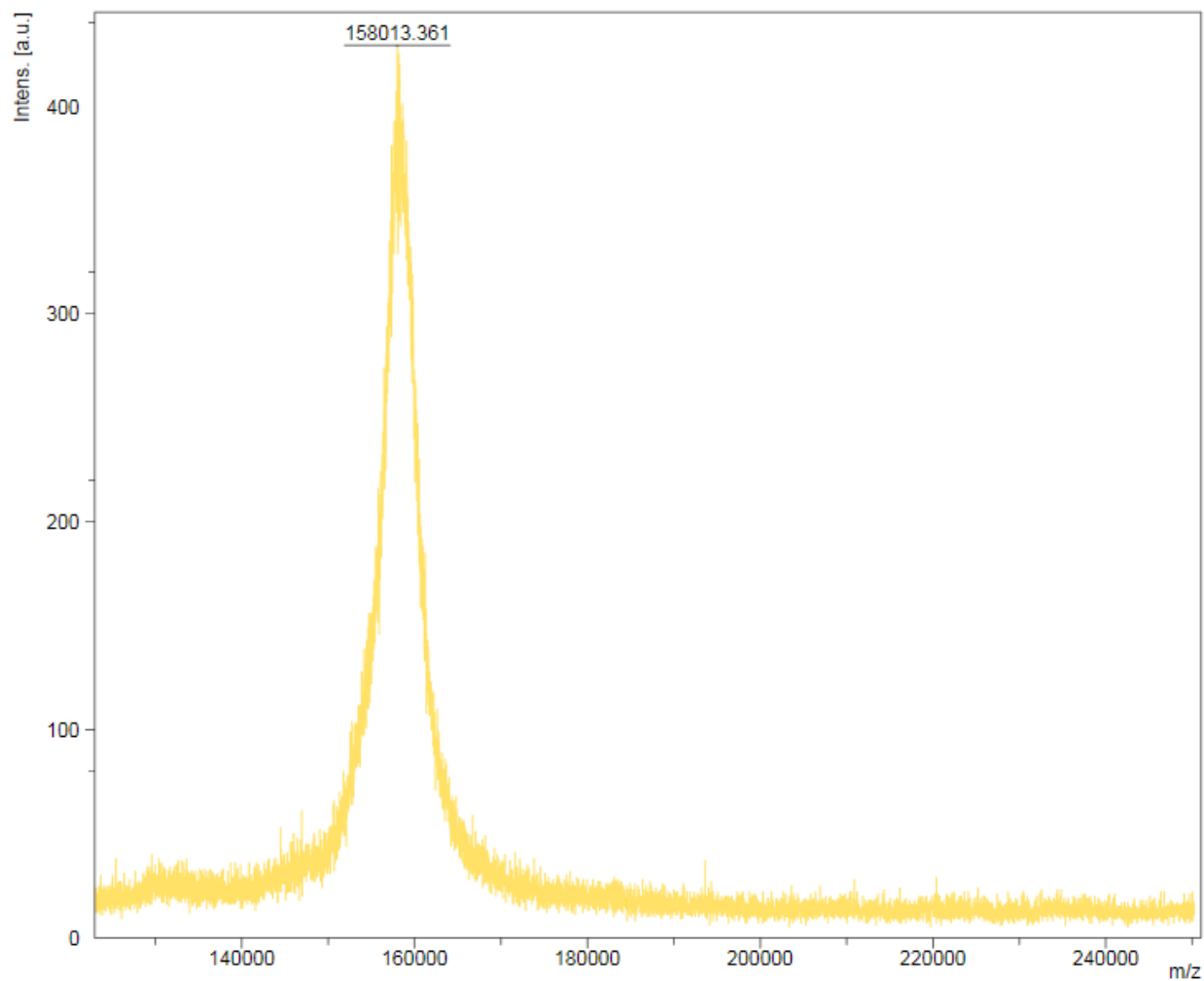
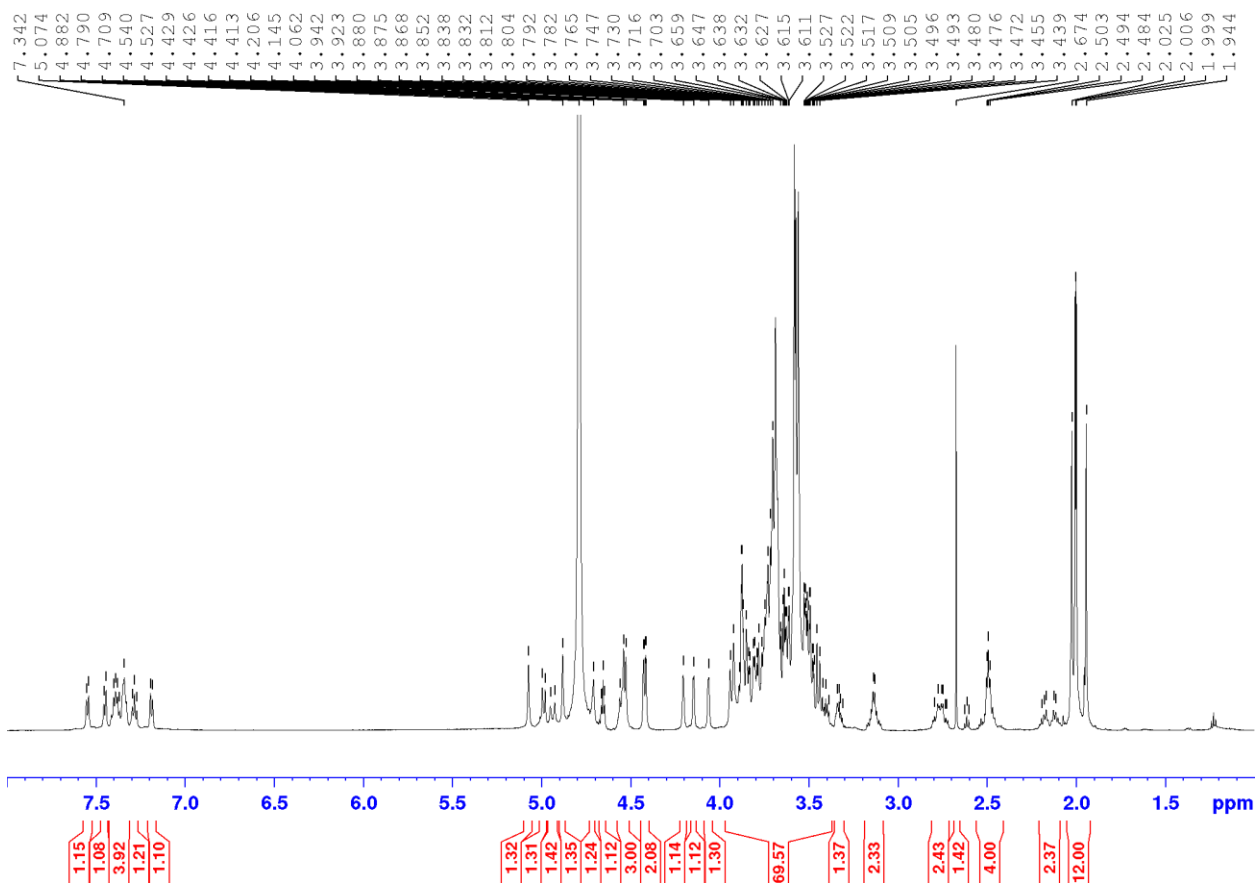
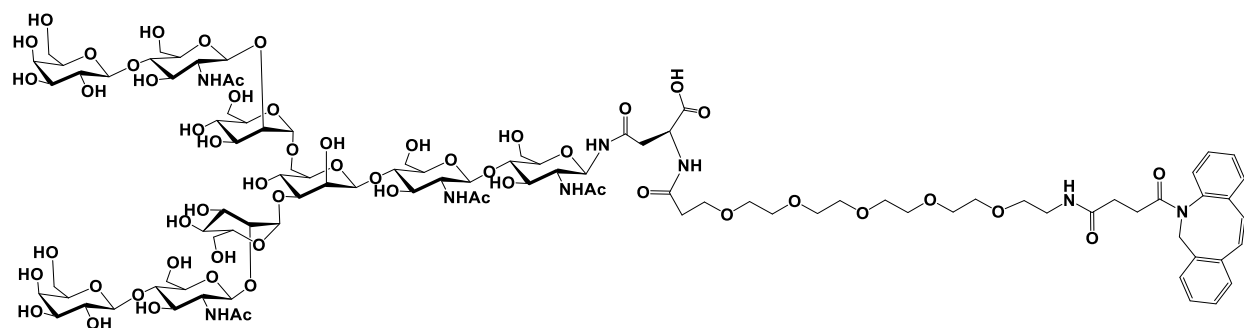
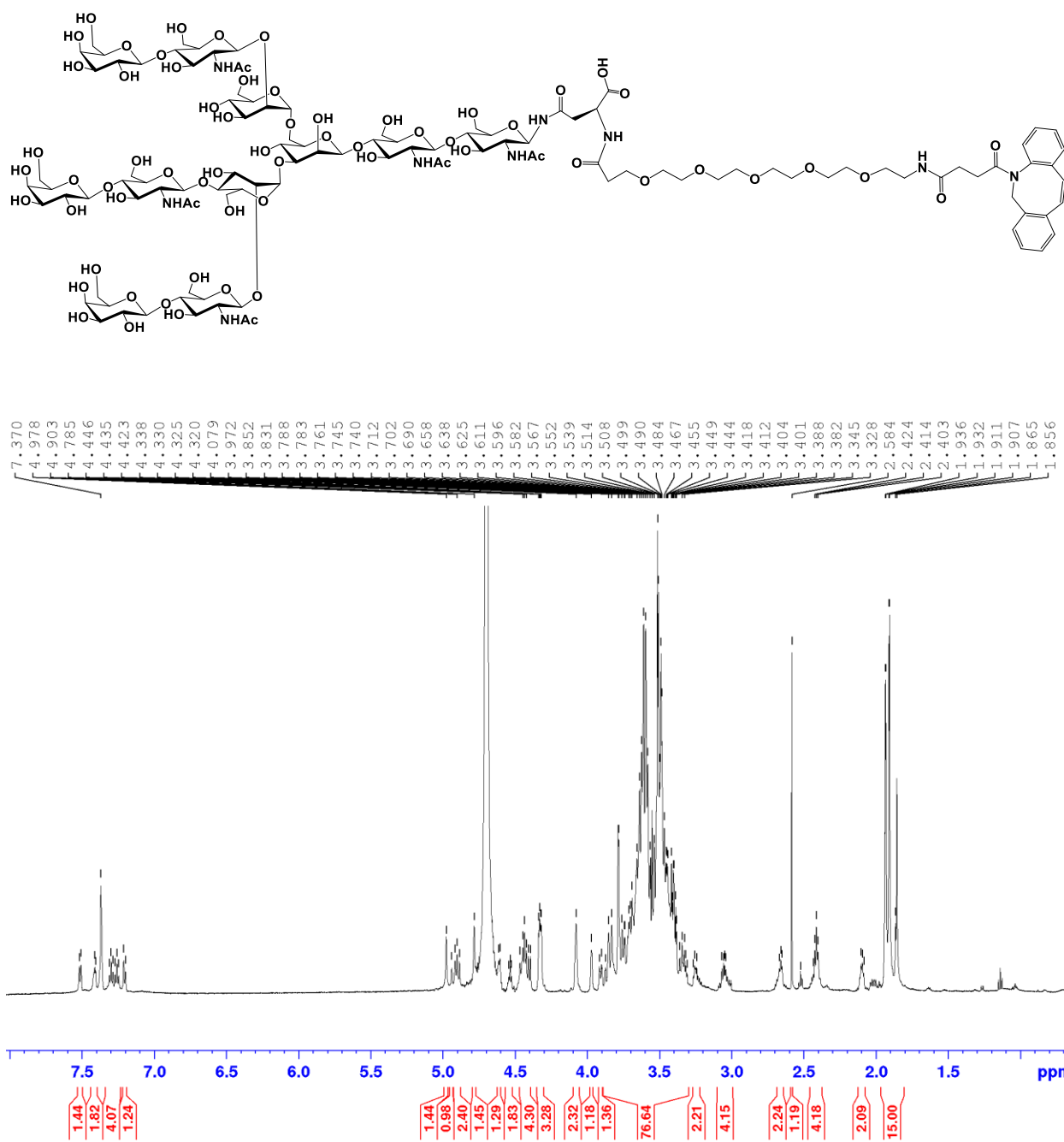


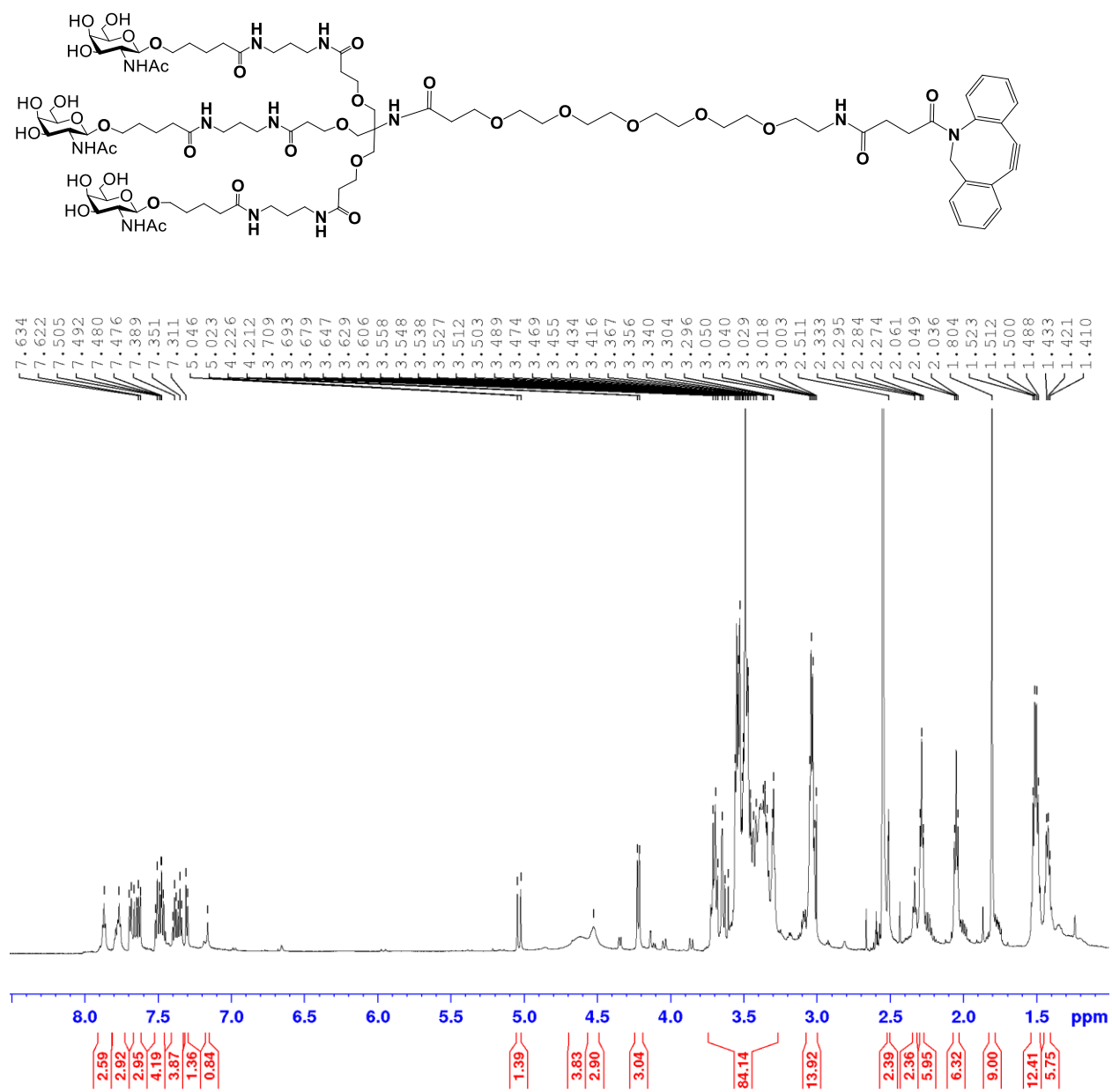
**Figure 4.38.** MALDI-TOF-MS of biotinylated tri-GalNAc-Man-Alirocumab for cell-based assay in linear positive mode. An average of six biotin units were attached.



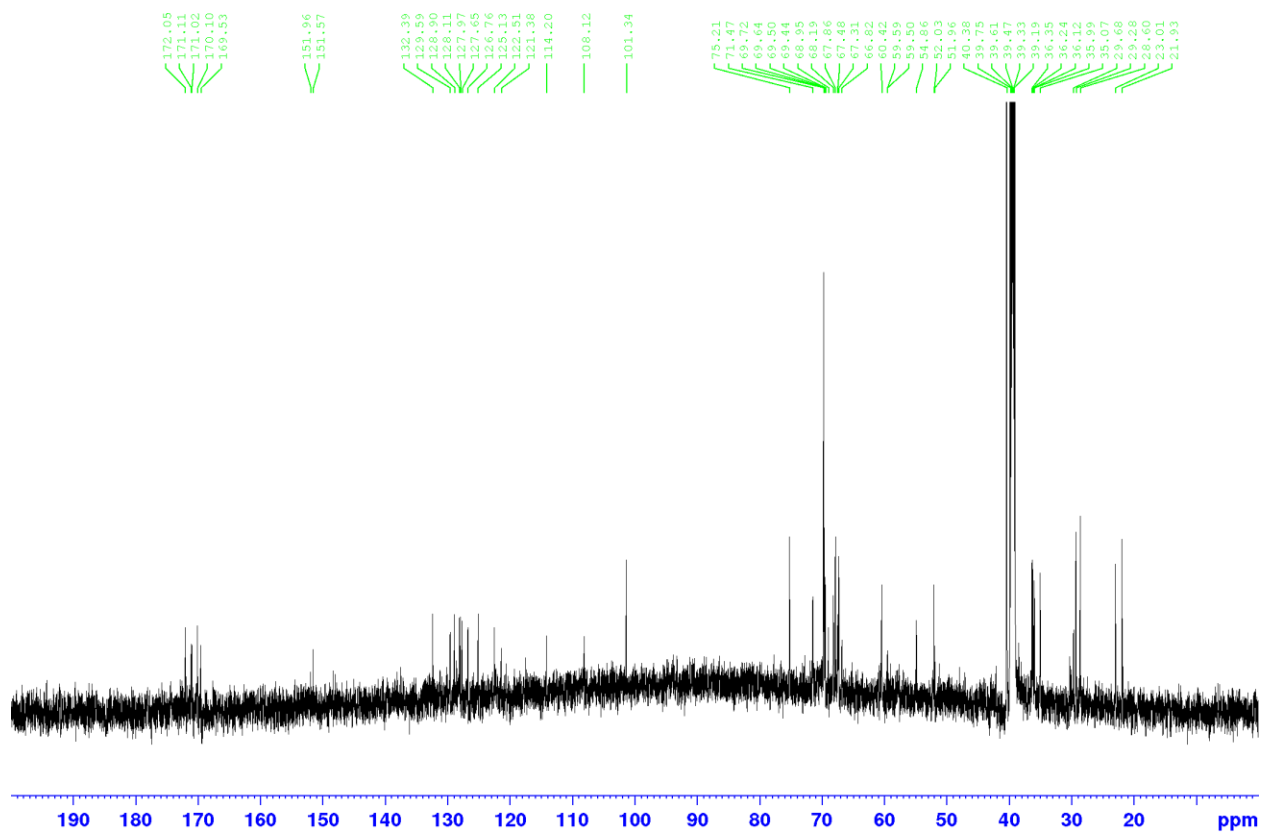
<sup>1</sup>H-NMR spectrum (600 MHz, D<sub>2</sub>O) of compound 4.2.



$^1\text{H-NMR}$  spectrum (600 MHz,  $\text{D}_2\text{O}$ ) of compound **4.5**.



$^1\text{H-NMR}$  spectrum (600 MHz,  $\text{DMSO-}d_6$ ) of compound 4.7.



$^{13}\text{C}$ -NMR spectrum (150 MHz,  $\text{DMSO-}d_6$ ) of compound **4.7**.

## Chapter 5: Conclusions and Future Directions

The focus of my thesis was to develop tools for elucidating glycan function and leverage human N-glycan structures for therapeutic indications. To accomplish this, various natural human N-glycan-Asn and synthetic glycan structures were functionalized with chemical tags to enable bioconjugation to carrier proteins, synthetic vesicle scaffolds, and antibodies. These glycoconjugates revealed unexpected immunological properties for several common N-glycan structures and put forward interesting new findings related to N-glycan multivalent recognition and therapeutic functions.

In Chapter 2, we reported the conjugation of five structurally diverse human N-glycans to a Q $\beta$  bacteriophage carrier protein by two different linker chemistries to prepare a series of N-glycan immunogens. Mice were immunized with the N-glycan-Q $\beta$  conjugates and the elicited antibodies were unexpectedly found to target the conserved chitobiose core regardless of the glycan immunogen used. Furthermore, linker chemistry was found to have significant impacts on antibody titer and the fine specificity of the generated antibodies. We also report for the first time that sialylated complex type N-glycans are weakly immunogenic and elicit low glycan-specific antibody titers. We expect these results will inform future glycan-based immunogen design for raising N-glycan-specific monoclonal antibodies as tools for probing glycan function, as well as the design of glycan-based vaccines against pathogens such as HIV and SARS-CoV2.

In Chapter 3, N-glycolipids bearing different N-glycan headgroups and acyl lipid chain lengths were synthesized, and glycolipid incorporation was optimized into catanionic vesicle bilayers. It was found that lipid chains of 16-carbons long (C16) had the highest efficiency of insertion into the vesicle bilayer, allowing various N-glycan headgroups to be displayed on the

vesicle surface. These N-glycan-coated vesicles (N-gCVs) were prepared at different N-glycan densities and used as multivalent probes for evaluating glycan recognition by carbohydrate-binding proteins. It was found that N-gCVs were potent inhibitors of glycan-binding proteins and lectins, they were also used to characterize lectin binding preferences, such as for human galectin-3 which prefers asialo-biantennary complex-type N-glycans displayed at high densities. Heteromultivalent glycan-coated vesicles were also prepared that displayed two structurally unrelated N-glycans and it was found that an unrelated glycan structure can significantly affect the affinity of a lectin for its cognate ligand. We expect that cationic vesicles will be useful tools for characterizing glycan-protein interactions, as potent inhibitors of disease-associated lectins, and as drug delivery vehicles.

In Chapter 4, the chemoenzymatic glycoengineering method developed by our group was used to prepare antibody-based protein-degraders that rely on activity of the liver asialoglycoprotein receptor. More specifically, the chemoenzymatic method was used to install bi- and tri-antennary complex type N-glycans site-specifically on the antibody Fc domain. Separately, azide-modified glycans were introduced to allow for click conjugation of various natural and synthetic glycan payloads containing terminal galactose or N-acetylgalactosamine. The antibody recognizes the protein target while the asialo-glycans are recognized by the asialoglycoprotein receptor to mediate lysosomal delivery and degradation of the antibody-target complex. The chemoenzymatic method enabled construction of a small library of sugar-antibody conjugates site-specifically to explore optimal glycan structures for targeted-protein degradation. Cell-surface binding assays were performed with these antibody conjugates, and unusual trends in ASGPR receptor binding were discovered that reveal glycan ligand preferences. Protein degradation assays demonstrated that these site-specific antibody conjugates can degrade

clinically relevant protein targets such as PCSK9, a well-validated target for people suffering from high cholesterol. We also reported for the first time that natural triantennary N-glycans are effective ASGPR ligands for promoting targeted-protein degradation. This may be a promising approach for treating high cholesterol in people at risk for heart disease. We expect that this approach may be applied more generally for the synthesis of other site-specific antibody conjugates able to degrade disease-associated proteins.

For future studies, as discussed briefly in Chapter 2, we will investigate methods for improving the immunogenicity of the terminal monosaccharides of N-glycans to obtain N-glycan specific antibodies with improved selectivity. This can be done by chemical fluorination, lactone protecting groups, or propionylation of the terminal monosaccharides which has previously been shown to elicit improved titers of glycan-specific antibodies crossreactive to the unmodified glycan.<sup>128, 247-249</sup> Alternatively, immunization with N-glycan-Q $\beta$  immunogens can be done in evolutionarily distant animal models such as lamprey, this has been done previously to obtain variable lymphocyte receptors (VLRs) able to recognize several abundant cell-surface glycans.<sup>93</sup>

It would also be interesting to investigate drug delivery applications for the cationic vesicles introduced in Chapter 3. Cationic vesicles can be formulated in solutions containing anticancer drugs or antibiotics, and then decorated on the surface with N-glycolipids to enable cell-specific targeting. Additionally, it would be desirable to develop methods for printing glycan arrays from glycan-coated vesicles. Cationic vesicles can easily be functionalized with several N-glycan structures simultaneously, allowing for quick access to a combinatorial library of mixed glycan populations more closely resembling those of the cell glycocalyx. Glycan arrays obtained from these samples would provide valuable insights into glycan-protein binding events in a more “cell-like” glycan landscape.

For Chapter 4, alternative monoclonal antibodies will be glycoengineered to target other disease-associated proteins for degradation, such as the large number of ‘undruggable’ G-protein coupled receptors (GPCRs) implicated in disease.<sup>250</sup> Current projects in the lab are using mutant galactotransferase enzymes to transfer GalNAc to the nonreducing ends of agalacto- complex type N-glycans. We will pursue optimization of this reaction for the transfer of GalNAc to the nonreducing ends of triantennary N-glycans lacking terminal galactose. Then, we will evaluate if natural GalNAc containing N-glycans can function as improved lysosome targeting ligands when compared to the synthetic tri-GalNAc ligand used by Bertozzi and coworkers. Lastly, we will explore other lysosome-targeting receptors, such as the sialic-acid specific Siglecs, to expand the scope of targeted-protein degradation by the LYTAC approach.

## Literature Cited

1. Schjoldager, K. T.; Narimatsu, Y.; Joshi, H. J.; Clausen, H., Global view of human protein glycosylation pathways and functions. *Nat. Rev. Mol. Cell Biol.* **2020**, *21* (12), 729-749.
2. Flynn, R. A.; Pedram, K.; Malaker, S. A.; Batista, P. J.; Smith, B. A. H.; Johnson, A. G.; George, B. M.; Majzoub, K.; Villalta, P. W.; Carette, J. E.; Bertozzi, C. R., Small RNAs are modified with N-glycans and displayed on the surface of living cells. *Cell* **2021**, *184* (12), 3109-3124 e22.
3. Gill, D. J.; Clausen, H.; Bard, F., Location, location, location: new insights into O-GalNAc protein glycosylation. *Trends Cell Biol.* **2011**, *21* (3), 149-58.
4. Moremen, K. W.; Tiemeyer, M.; Nairn, A. V., Vertebrate protein glycosylation: diversity, synthesis and function. *Nat. Rev. Mol. Cell Biol.* **2012**, *13* (7), 448-62.
5. Zhang, J.; Ten Dijke, P.; Wuhrer, M.; Zhang, T., Role of glycosylation in TGF- $\beta$  signaling and epithelial-to-mesenchymal transition in cancer. *Protein Cell* **2021**, *12* (2), 89-106.
6. Crocker, P. R.; Paulson, J. C.; Varki, A., Siglecs and their roles in the immune system. *Nat. Rev. Immunol.* **2007**, *7* (4), 255-66.
7. Büll, C.; Nason, R.; Sun, L.; Van Coillie, J.; Madriz Sørensen, D.; Moons, S. J.; Yang, Z.; Arbitman, S.; Fernandes, S. M.; Furukawa, S.; McBride, R.; Nycholat, C. M.; Adema, G. J.; Paulson, J. C.; Schnaar, R. L.; Boltje, T. J.; Clausen, H.; Narimatsu, Y., Probing the binding specificities of human Siglecs by cell-based glycan arrays. *Proc. Natl. Acad. Sci. U. S. A.* **2021**, *118* (17), e2026102118.
8. Nimrichter, L.; Burdick, M. M.; Aoki, K.; Laroy, W.; Fierro, M. A.; Hudson, S. A.; Von Seggern, C. E.; Cotter, R. J.; Bochner, B. S.; Tiemeyer, M.; Konstantopoulos, K.; Schnaar, R. L., E-selectin receptors on human leukocytes. *Blood* **2008**, *112* (9), 3744-52.
9. Lodish, H. F., Recognition of complex oligosaccharides by the multi-subunit asialoglycoprotein receptor. *Trends Biochem. Sci.* **1991**, *16* (10), 374-7.
10. Weigel, P. H.; Yik, J. H., Glycans as endocytosis signals: the cases of the asialoglycoprotein and hyaluronan/chondroitin sulfate receptors. *Biochim. Biophys. Acta* **2002**, *1572* (2-3), 341-63.
11. Huang, X.; Leroux, J. C.; Castagner, B., Well-Defined Multivalent Ligands for Hepatocytes Targeting via Asialoglycoprotein Receptor. *Bioconjugate Chem.* **2017**, *28* (2), 283-295.
12. Cerliani, J. P.; Blidner, A. G.; Toscano, M. A.; Croci, D. O.; Rabinovich, G. A., Translating the 'Sugar Code' into Immune and Vascular Signaling Programs. *Trends Biochem. Sci.* **2017**, *42* (4), 255-273.
13. Xiao, Q.; Ludwig, A. K.; Romanò, C.; Buzzacchera, I.; Sherman, S. E.; Vetro, M.; Vértesy, S.; Kaltner, H.; Reed, E. H.; Möller, M.; Wilson, C. J.; Hammer, D. A.; Oscarson, S.; Klein, M. L.; Gabius, H. J.; Percec, V., Exploring functional pairing between surface glycoconjugates and human galectins using programmable glycodendrimersomes. *Proc. Natl. Acad. Sci. U. S. A.* **2018**, *115* (11), E2509-E2518.
14. Farhadi, S. A.; Liu, R.; Becker, M. W.; Phelps, E. A.; Hudalla, G. A., Physical tuning of galectin-3 signaling. *Proc. Natl. Acad. Sci. U. S. A.* **2021**, *118* (19), e2024117118.
15. Peschke, B.; Keller, C. W.; Weber, P.; Quast, I.; Lünemann, J. D., Fc-Galactosylation of Human Immunoglobulin Gamma Isotypes Improves C1q Binding and Enhances Complement-Dependent Cytotoxicity. *Front. Immunol.* **2017**, *8*, 646-653.

16. Purcell, S. C.; Godula, K., Synthetic glycoscapes: addressing the structural and functional complexity of the glycocalyx. *Interface Focus* **2019**, *9* (2), 20180080.
17. Blixt, O.; Head, S.; Mondala, T.; Scanlan, C.; Huflejt, M. E.; Alvarez, R.; Bryan, M. C.; Fazio, F.; Calarese, D.; Stevens, J.; Razi, N.; Stevens, D. J.; Skehel, J. J.; van Die, I.; Burton, D. R.; Wilson, I. A.; Cummings, R.; Bovin, N.; Wong, C. H.; Paulson, J. C., Printed covalent glycan array for ligand profiling of diverse glycan binding proteins. *Proc. Natl. Acad. Sci. U. S. A.* **2004**, *101* (49), 17033-8.
18. Feinberg, H.; Mitchell, D. A.; Drickamer, K.; Weis, W. I., Structural basis for selective recognition of oligosaccharides by DC-SIGN and DC-SIGNR. *Science (Washington, DC, United States)* **2001**, *294* (5549), 2163-6.
19. van Kooyk, Y.; Rabinovich, G. A., Protein-glycan interactions in the control of innate and adaptive immune responses. *Nat. Immunol.* **2008**, *9* (6), 593-601.
20. Olson, L. J.; Misra, S. K.; Ishihara, M.; Battaile, K. P.; Grant, O. C.; Sood, A.; Woods, R. J.; Kim, J. P.; Tiemeyer, M.; Ren, G.; Sharp, J. S.; Dahms, N. M., Allosteric regulation of lysosomal enzyme recognition by the cation-independent mannose 6-phosphate receptor. *Commun. Biol.* **2020**, *3* (1), 498-512.
21. Vasconcelos-Dos-Santos, A.; Oliveira, I. A.; Lucena, M. C.; Mantuano, N. R.; Whelan, S. A.; Dias, W. B.; Todeschini, A. R., Biosynthetic Machinery Involved in Aberrant Glycosylation: Promising Targets for Developing of Drugs Against Cancer. *Front. Oncol.* **2015**, *5*, 138-160.
22. Thomas, D.; Rathinavel, A. K.; Radhakrishnan, P., Altered glycosylation in cancer: A promising target for biomarkers and therapeutics. *Biochim. Biophys. Acta Rev. Cancer* **2021**, *1875* (1), 188464.
23. Kiessling, L. L., Chemistry-driven glycoscience. *Bioorg. Med. Chem.* **2018**, *26* (19), 5229-5238.
24. Pasek, M.; Ramakrishnan, B.; Boeggeman, E.; Mercer, N.; Dulcey, A. E.; Griffiths, G. L.; Qasba, P. K., The N-acetyl-binding pocket of N-acetylglucosaminyltransferases also accommodates a sugar analog with a chemical handle at C2. *Glycobiology* **2012**, *22* (3), 379-88.
25. Ramírez, A. S.; de Capitani, M.; Pesciullesi, G.; Kowal, J.; Bloch, J. S.; Irobalieva, R. N.; Reymond, J. L.; Aebi, M.; Locher, K. P., Molecular basis for glycan recognition and reaction priming of eukaryotic oligosaccharyltransferase. *Nat. Commun.* **2022**, *13* (1), 7296.
26. Weis, W. I.; Drickamer, K., Structural basis of lectin-carbohydrate recognition. *Annu. Rev. Biochem.* **1996**, *65*, 441-73.
27. Boraston, A. B.; Bolam, D. N.; Gilbert, H. J.; Davies, G. J., Carbohydrate-binding modules: fine-tuning polysaccharide recognition. *Biochem. J.* **2004**, *382* (Pt 3), 769-81.
28. In *Essentials of Glycobiology*, Varki, A.; Cummings, R. D.; Esko, J. D.; Freeze, H. H.; Stanley, P.; Bertozzi, C. R.; Hart, G. W.; Etzler, M. E., Eds. © The Consortium of Glycobiology Editors, La Jolla, California.: Cold Spring Harbor NY, 2009.
29. Böhmer, V. I.; Szymanski, W.; Feringa, B. L.; Elsinga, P. H., Multivalent Probes in Molecular Imaging: Reality or Future? *Trends Mol. Med.* **2021**, *27* (4), 379-393.
30. Mammen, M.; Choi, S. K.; Whitesides, G. M., Polyvalent interactions in biological systems: Implications for design and use of multivalent ligands and inhibitors. *Angew. Chem. Int. Ed.* **1998**, *37*, 2754-2794.
31. Fasting, C.; Schalley, C. A.; Weber, M.; Seitz, O.; Hecht, S.; Koksche, B.; Dervedde, J.; Graf, C.; Knapp, E. W.; Haag, R., Multivalency as a chemical organization and action principle. *Angew. Chem. Int. Ed.* **2012**, *51* (42), 10472-98.

32. Kim, Y.; Hyun, J. Y.; Shin, I., Multivalent glycans for biological and biomedical applications. *Chem. Soc. Rev.* **2021**, *50* (18), 10567-93.
33. Sanders, W. J.; Gordon, E. J.; Dwir, O.; Beck, P. J.; Alon, R.; Kiessling, L. L., Inhibition of L-selectin-mediated leukocyte rolling by synthetic glycoprotein mimics. *J. Biol. Chem.* **1999**, *274* (9), 5271-8.
34. Wawrzinek, R.; Wamhoff, E. C.; Lefebvre, J.; Rentzsch, M.; Bachem, G.; Domeniconi, G.; Schulze, J.; Fuchsberger, F. F.; Zhang, H.; Modenutti, C.; Schnirch, L.; Marti, M. A.; Schwardt, O.; Bräutigam, M.; Guberman, M.; Hauck, D.; Seeberger, P. H.; Seitz, O.; Titz, A.; Ernst, B.; Rademacher, C., A Remote Secondary Binding Pocket Promotes Heteromultivalent Targeting of DC-SIGN. *J. Am. Chem. Soc.* **2021**, *143* (45), 18977-88.
35. Liu, M.; Huang, L. Z. X.; Smits, A. A.; Büll, C.; Narimatsu, Y.; van Kuppeveld, F. J. M.; Clausen, H.; de Haan, C. A. M.; de Vries, E., Human-type sialic acid receptors contribute to avian influenza A virus binding and entry by hetero-multivalent interactions. *Nat. Commun.* **2022**, *13* (1), 4054-4065.
36. Gade, M.; Alex, C.; Leviatan Ben-Arye, S.; Monteiro, J. T.; Yehuda, S.; Lepenies, B.; Padler-Karavani, V.; Kikkeri, R., Microarray Analysis of Oligosaccharide-Mediated Multivalent Carbohydrate-Protein Interactions and Their Heterogeneity. *ChemBioChem* **2018**, *19*, 1170-7.
37. Grabenstein, J. D.; Klugman, K. P., A century of pneumococcal vaccination research in humans. *Clin. Microbiol. Infect.* **2012**, *18 Suppl 5*, 15-24.
38. Yin, Z.; Huang, X., Recent Development in Carbohydrate Based Anticancer Vaccines. *J. Carbohydr. Chem.* **2012**, *31* (3), 143-186.
39. van der Put, R. M. F.; Smitsman, C.; de Haan, A.; Hamzink, M.; Timmermans, H.; Uittenbogaard, J.; Westdijk, J.; Stork, M.; Ophorst, O.; Thouron, F.; Guerreiro, C.; Sansonetti, P. J.; Phalipon, A.; Mulard, L. A., The First-in-Human Synthetic Glycan-Based Conjugate Vaccine Candidate against Shigella. *ACS Cent. Sci.* **2022**, *8* (4), 449-460.
40. Torosantucci, A.; Bromuro, C.; Chiani, P.; De Bernardis, F.; Berti, F.; Galli, C.; Norelli, F.; Bellucci, C.; Polonelli, L.; Costantino, P.; Rappuoli, R.; Cassone, A., A novel glyco-conjugate vaccine against fungal pathogens. *J. Exp. Med.* **2005**, *202* (5), 597-606.
41. Kappler, K.; Henet, T., Emergence and significance of carbohydrate-specific antibodies. *Genes Immun.* **2020**, *21* (4), 224-239.
42. Sterner, E.; Peach, M. L.; Nicklaus, M. C.; Gildersleeve, J. C., Therapeutic Antibodies to Ganglioside GD2 Evolved from Highly Selective Germline Antibodies. *Cell Rep.* **2017**, *20* (7), 1681-1691.
43. Hedberg, K. M.; Dellheden, B.; Wikstrand, C. J.; Fredman, P., Monoclonal anti-GD3 antibodies selectively inhibit the proliferation of human malignant glioma cells in vitro. *Glycoconj. J.* **2000**, *17* (10), 717-26.
44. Testa, L.; Mano, M.; Arai, R. J.; Bonadio, R. C.; Serrano, S. V.; Zorzetto, M. M. C.; Crocamo, S.; Smaletz, O.; Freitas-Junior, R.; Hoff, P. M., Phase II trial of humanized anti-Lewis Y monoclonal antibody for advanced hormone receptor-positive breast cancer that progressed following endocrine therapy. *Clinics (Sao Paulo)* **2021**, *76*, e3146.
45. Platt, F. M.; d'Azzo, A.; Davidson, B. L.; Neufeld, E. F.; Tiffit, C. J., Lysosomal storage diseases. *Nat. Rev. Dis. Primers* **2018**, *4* (1), 27-51.
46. Dordal, M. S.; Wang, F. F.; Goldwasser, E., The role of carbohydrate in erythropoietin action. *Endocrinology* **1985**, *116* (6), 2293-9.

47. Delorme, E.; Lorenzini, T.; Giffin, J.; Martin, F.; Jacobsen, F.; Boone, T.; Elliott, S., Role of glycosylation on the secretion and biological activity of erythropoietin. *Biochemistry* **1992**, *31* (41), 9871-6.
48. Guan, X.; Chaffey, P. K.; Wei, X.; Gulbranson, D. R.; Ruan, Y.; Wang, X.; Li, Y.; Ouyang, Y.; Chen, L.; Zeng, C.; Koelsch, T. N.; Tran, A. H.; Liang, W.; Shen, J.; Tan, Z., Chemically Precise Glycoengineering Improves Human Insulin. *ACS Chem. Biol.* **2018**, *13* (1), 73-81.
49. Niwa, R.; Shoji-Hosaka, E.; Sakurada, M.; Shinkawa, T.; Uchida, K.; Nakamura, K.; Matsushima, K.; Ueda, R.; Hanai, N.; Shitara, K., Defucosylated chimeric anti-CC chemokine receptor 4 IgG1 with enhanced antibody-dependent cellular cytotoxicity shows potent therapeutic activity to T-cell leukemia and lymphoma. *Cancer Res.* **2004**, *64* (6), 2127-33.
50. Li, T.; DiLillo, D. J.; Bournazos, S.; Giddens, J. P.; Ravetch, J. V.; Wang, L. X., Modulating IgG effector function by Fc glycan engineering. *Proc. Natl. Acad. Sci. U. S. A.* **2017**, *114* (13), 3485-3490.
51. Kaneko, Y.; Nimmerjahn, F.; Ravetch, J. V., Anti-inflammatory activity of immunoglobulin G resulting from Fc sialylation. *Science (Washington, DC, United States)* **2006**, *313* (5787), 670-3.
52. Anthony, R. M.; Wermeling, F.; Karlsson, M. C.; Ravetch, J. V., Identification of a receptor required for the anti-inflammatory activity of IVIG. *Proc. Natl. Acad. Sci. U. S. A.* **2008**, *105* (50), 19571-8.
53. Wang, L. X.; Tong, X.; Li, C.; Giddens, J. P.; Li, T., Glycoengineering of Antibodies for Modulating Functions. *Annu. Rev. Biochem.* **2019**, *88*, 433-459.
54. Li, C.; Wang, L. X., Chemoenzymatic Methods for the Synthesis of Glycoproteins. *Chem. Rev.* **2018**, *118* (17), 8359-8413.
55. Agatemor, C.; Buettner, M. J.; Ariss, R.; Muthiah, K.; Saeui, C. T.; Yarema, K. J., Exploiting metabolic glycoengineering to advance healthcare. *Nat. Rev. Chem.* **2019**, *3* (10), 605-620.
56. Narimatsu, Y.; Büll, C.; Chen, Y. H.; Wandall, H. H.; Yang, Z.; Clausen, H., Genetic glycoengineering in mammalian cells. *J. Biol. Chem.* **2021**, *296*, 100448.
57. Boltje, T. J.; Buskas, T.; Boons, G. J., Opportunities and challenges in synthetic oligosaccharide and glycoconjugate research. *Nat. Chem.* **2009**, *1* (8), 611-22.
58. Yang, Q.; Wang, L. X., Mammalian  $\alpha$ -1,6-Fucosyltransferase (FUT8) Is the Sole Enzyme Responsible for the N-Acetylglucosaminyltransferase I-independent Core Fucosylation of High-mannose N-Glycans. *J. Biol. Chem.* **2016**, *291* (21), 11064-71.
59. Malphettes, L.; Freyvert, Y.; Chang, J.; Liu, P. Q.; Chan, E.; Miller, J. C.; Zhou, Z.; Nguyen, T.; Tsai, C.; Snowden, A. W.; Collingwood, T. N.; Gregory, P. D.; Cost, G. J., Highly efficient deletion of FUT8 in CHO cell lines using zinc-finger nucleases yields cells that produce completely nonfucosylated antibodies. *Biotechnol. Bioeng.* **2010**, *106* (5), 774-83.
60. Okeley, N. M.; Alley, S. C.; Anderson, M. E.; Boursalian, T. E.; Burke, P. J.; Emmerton, K. M.; Jeffrey, S. C.; Klussman, K.; Law, C. L.; Sussman, D.; Toki, B. E.; Westendorf, L.; Zeng, W.; Zhang, X.; Benjamin, D. R.; Senter, P. D., Development of orally active inhibitors of protein and cellular fucosylation. *Proc. Natl. Acad. Sci. U. S. A.* **2013**, *110* (14), 5404-9.
61. Huang, W.; Giddens, J.; Fan, S. Q.; Toonstra, C.; Wang, L. X., Chemoenzymatic glycoengineering of intact IgG antibodies for gain of functions. *J. Am. Chem. Soc.* **2012**, *134* (29), 12308-18.

62. Zhang, X.; Ou, C.; Liu, H.; Prabhu, S. K.; Li, C.; Yang, Q.; Wang, L. X., General and Robust Chemoenzymatic Method for Glycan-Mediated Site-Specific Labeling and Conjugation of Antibodies: Facile Synthesis of Homogeneous Antibody-Drug Conjugates. *ACS Chem. Biol.* **2021**, *16* (11), 2502-2514.
63. Cecioni, S.; Imberty, A.; Vidal, S., Glycomimetics versus multivalent glycoconjugates for the design of high affinity lectin ligands. *Chem. Rev.* **2015**, *115* (1), 525-61.
64. Kalovidouris, S. A.; Gama, C. I.; Lee, L. W.; Hsieh-Wilson, L. C., A role for fucose alpha(1-2) galactose carbohydrates in neuronal growth. *J. Am. Chem. Soc.* **2005**, *127* (5), 1340-1.
65. Sauer, M. M.; Jakob, R. P.; Eras, J.; Baday, S.; Eriş, D.; Navarra, G.; Bernèche, S.; Ernst, B.; Maier, T.; Glockshuber, R., Catch-bond mechanism of the bacterial adhesin FimH. *Nat. Commun.* **2016**, *7*, 10738-50.
66. Donahue, T. C.; Zong, G.; O'Brien, N. A.; Ou, C.; Gildersleeve, J. C.; Wang, L. X., Synthesis and Immunological Study of N-Glycan-Bacteriophage Q $\beta$  Conjugates Reveal Dominant Antibody Responses to the Conserved Chitobiose Core. *Bioconjugate Chem.* **2022**, *33* (7), 1350-1362.
67. Helenius, A.; Aebi, M., Roles of N-linked glycans in the endoplasmic reticulum. *Annu. Rev. Biochem.* **2004**, *73*, 1019-49.
68. Sterner, E.; Flanagan, N.; Gildersleeve, J. C., Perspectives on Anti-Glycan Antibodies Gleaned from Development of a Community Resource Database. *ACS Chem. Biol.* **2016**, *11* (7), 1773-1783.
69. Kitamura, K.; Stockert, E.; Garin-Chesa, P.; Welt, S.; Lloyd, K. O.; Armour, K. L.; Wallace, T. P.; Harris, W. J.; Carr, F. J.; Old, L. J., Specificity analysis of blood group Lewis-y (Le(y)) antibodies generated against synthetic and natural Le(y) determinants. *Proc. Natl. Acad. Sci. U. S. A.* **1994**, *91* (26), 12957-61.
70. Loureiro, L. R.; Sousa, D. P.; Ferreira, D.; Chai, W.; Lima, L.; Pereira, C.; Lopes, C. B.; Correia, V. G.; Silva, L. M.; Li, C.; Santos, L. L.; Ferreira, J. A.; Barbas, A.; Palma, A. S.; Novo, C.; Videira, P. A., Novel monoclonal antibody L2A5 specifically targeting sialyl-Tn and short glycans terminated by alpha-2-6 sialic acids. *Sci. Rep.* **2018**, *8* (1), 12196-211.
71. Calarese, D. A.; Lee, H. K.; Huang, C. Y.; Best, M. D.; Astronomo, R. D.; Stanfield, R. L.; Katinger, H.; Burton, D. R.; Wong, C. H.; Wilson, I. A., Dissection of the carbohydrate specificity of the broadly neutralizing anti-HIV-1 antibody 2G12. *Proc. Natl. Acad. Sci. U. S. A.* **2005**, *102* (38), 13372-7.
72. Springer, G. F., T and Tn, general carcinoma autoantigens. *Science (Washington, DC, United States)* **1984**, *224* (4654), 1198-206.
73. Peixoto, A.; Relvas-Santos, M.; Azevedo, R.; Santos, L. L.; Ferreira, J. A., Protein Glycosylation and Tumor Microenvironment Alterations Driving Cancer Hallmarks. *Front. Oncol.* **2019**, *9*, 380-403.
74. Ahmed, A. A.; Giddens, J.; Pincetic, A.; Lomino, J. V.; Ravetch, J. V.; Wang, L. X.; Bjorkman, P. J., Structural characterization of anti-inflammatory immunoglobulin G Fc proteins. *J. Mol. Biol.* **2014**, *426* (18), 3166-79.
75. Pier, G. B.; Boyer, D.; Preston, M.; Coleman, F. T.; Llosa, N.; Mueschenborn-Koglin, S.; Theilacker, C.; Goldenberg, H.; Uchin, J.; Priebe, G. P.; Grout, M.; Posner, M.; Cavacini, L., Human monoclonal antibodies to *Pseudomonas aeruginosa* alginate that protect against infection by both mucoid and nonmucoid strains. *J. Immunol.* **2004**, *173* (9), 5671-8.
76. Berti, F.; Romano, M. R.; Micoli, F.; Adamo, R., Carbohydrate based meningococcal vaccines: past and present overview. *Glycoconj. J.* **2021**, *38* (4), 401-409.

77. Hutter, J.; Lepenies, B., Carbohydrate-Based Vaccines: An Overview. *Methods Mol. Biol.* **2015**, *1331*, 1-10.
78. Wei, M. M.; Wang, Y. S.; Ye, X. S., Carbohydrate-based vaccines for oncotherapy. *Med. Res. Rev.* **2018**, *38* (3), 1003-1026.
79. Pinho, S. S.; Reis, C. A., Glycosylation in cancer: mechanisms and clinical implications. *Nat. Rev. Cancer* **2015**, *15* (9), 540-55.
80. Reily, C.; Stewart, T. J.; Renfrow, M. B.; Novak, J., Glycosylation in health and disease. *Nat. Rev. Nephrol.* **2019**, *15* (6), 346-366.
81. Calarese, D. A.; Scanlan, C. N.; Zwick, M. B.; Deechongkit, S.; Mimura, Y.; Kunert, R.; Zhu, P.; Wormald, M. R.; Stanfield, R. L.; Roux, K. H.; Kelly, J. W.; Rudd, P. M.; Dwek, R. A.; Katinger, H.; Burton, D. R.; Wilson, I. A., Antibody domain exchange is an immunological solution to carbohydrate cluster recognition. *Science (Washington, DC, United States)* **2003**, *300* (5628), 2065-71.
82. Orwenyo, J.; Cai, H.; Giddens, J.; Amin, M. N.; Toonstra, C.; Wang, L. X., Systematic Synthesis and Binding Study of HIV V3 Glycopeptides Reveal the Fine Epitopes of Several Broadly Neutralizing Antibodies. *ACS Chem. Biol.* **2017**, *12* (6), 1566-1575.
83. Shivatare, V. S.; Shivatare, S. S.; Lee, C. D.; Liang, C. H.; Liao, K. S.; Cheng, Y. Y.; Saidachary, G.; Wu, C. Y.; Lin, N. H.; Kwong, P. D.; Burton, D. R.; Wu, C. Y.; Wong, C. H., Unprecedented Role of Hybrid N-Glycans as Ligands for HIV-1 Broadly Neutralizing Antibodies. *J. Am. Chem. Soc.* **2018**, *140* (15), 5202-5210.
84. Amin, M. N.; McLellan, J. S.; Huang, W.; Orwenyo, J.; Burton, D. R.; Koff, W. C.; Kwong, P. D.; Wang, L. X., Synthetic glycopeptides reveal the glycan specificity of HIV-neutralizing antibodies. *Nat. Chem. Biol.* **2013**, *9* (8), 521-6.
85. Pejchal, R.; Doores, K. J.; Walker, L. M.; Khayat, R.; Huang, P. S.; Wang, S. K.; Stanfield, R. L.; Julien, J. P.; Ramos, A.; Crispin, M.; Depetris, R.; Katpally, U.; Marozsan, A.; Cupo, A.; Malveste, S.; Liu, Y.; McBride, R.; Ito, Y.; Sanders, R. W.; Ogohara, C.; Paulson, J. C.; Feizi, T.; Scanlan, C. N.; Wong, C. H.; Moore, J. P.; Olson, W. C.; Ward, A. B.; Poignard, P.; Schief, W. R.; Burton, D. R.; Wilson, I. A., A potent and broad neutralizing antibody recognizes and penetrates the HIV glycan shield. *Science (Washington, DC, United States)* **2011**, *334* (6059), 1097-103.
86. Walker, L. M.; Huber, M.; Doores, K. J.; Falkowska, E.; Pejchal, R.; Julien, J. P.; Wang, S. K.; Ramos, A.; Chan-Hui, P. Y.; Moyle, M.; Mitcham, J. L.; Hammond, P. W.; Olsen, O. A.; Phung, P.; Fling, S.; Wong, C. H.; Phogat, S.; Wrin, T.; Simek, M. D.; Koff, W. C.; Wilson, I. A.; Burton, D. R.; Poignard, P., Broad neutralization coverage of HIV by multiple highly potent antibodies. *Nature* **2011**, *477* (7365), 466-70.
87. Doores, K. J.; Burton, D. R., Variable loop glycan dependency of the broad and potent HIV-1-neutralizing antibodies PG9 and PG16. *J. Virol.* **2010**, *84* (20), 10510-21.
88. Kong, L.; Lee, J. H.; Doores, K. J.; Murin, C. D.; Julien, J. P.; McBride, R.; Liu, Y.; Marozsan, A.; Cupo, A.; Klasse, P. J.; Hoffenberg, S.; Caulfield, M.; King, C. R.; Hua, Y.; Le, K. M.; Khayat, R.; Deller, M. C.; Clayton, T.; Tien, H.; Feizi, T.; Sanders, R. W.; Paulson, J. C.; Moore, J. P.; Stanfield, R. L.; Burton, D. R.; Ward, A. B.; Wilson, I. A., Supersite of immune vulnerability on the glycosylated face of HIV-1 envelope glycoprotein gp120. *Nat. Struct. Mol. Biol.* **2013**, *20* (7), 796-803.
89. McLellan, J. S.; Pancera, M.; Carrico, C.; Gorman, J.; Julien, J. P.; Khayat, R.; Louder, R.; Pejchal, R.; Sastry, M.; Dai, K.; O'Dell, S.; Patel, N.; Shahzad-ul-Hussan, S.; Yang, Y.; Zhang, B.; Zhou, T.; Zhu, J.; Boyington, J. C.; Chuang, G. Y.; Diwanji, D.;

- Georgiev, I.; Kwon, Y. D.; Lee, D.; Louder, M. K.; Moquin, S.; Schmidt, S. D.; Yang, Z. Y.; Bonsignori, M.; Crump, J. A.; Kapiga, S. H.; Sam, N. E.; Haynes, B. F.; Burton, D. R.; Koff, W. C.; Walker, L. M.; Phogat, S.; Wyatt, R.; Orwenyo, J.; Wang, L. X.; Arthos, J.; Bewley, C. A.; Mascola, J. R.; Nabel, G. J.; Schief, W. R.; Ward, A. B.; Wilson, I. A.; Kwong, P. D., Structure of HIV-1 gp120 V1/V2 domain with broadly neutralizing antibody PG9. *Nature* **2011**, *480* (7377), 336-43.
90. Fehr, T.; Skrastina, D.; Pumpens, P.; Zinkernagel, R. M., T cell-independent type I antibody response against B cell epitopes expressed repetitively on recombinant virus particles. *Proc. Natl. Acad. Sci. U. S. A.* **1998**, *95* (16), 9477-9481.
91. Hong, X.; Ma, M. Z.; Gildersleeve, J. C.; Chowdhury, S.; Barchi, J. J.; Mariuzza, R. A.; Murphy, M. B.; Mao, L.; Pancer, Z., Sugar-Binding Proteins from Fish: Selection of High Affinity "Lambodies" That Recognize Biomedically Relevant Glycans. *ACS Chem. Biol.* **2013**, *8* (1), 152-160.
92. McKittrick, T. R.; Eris, D.; Mondal, N.; Aryal, R. P.; McCurley, N.; Heimbürg-Molinaro, J.; Cummings, R. D., Antibodies from Lampreys as Smart Anti-Glycan Reagents (SAGRs): Perspectives on Their Specificity, Structure, and Glyco-genomics. *Biochemistry* **2020**, *59* (34), 3111-3122.
93. McKittrick, T. R.; Goth, C. K.; Rosenberg, C. S.; Nakahara, H.; Heimbürg-Molinaro, J.; McQuillan, A. M.; Falco, R.; Rivers, N. J.; Herrin, B. R.; Cooper, M. D.; Cummings, R. D., Development of smart anti-glycan reagents using immunized lampreys. *Commun. Biol.* **2020**, *3* (1), 91-102.
94. Bretscher, P.; Cohn, M., A theory of self-nonsel self discrimination. *Science (Washington, DC, United States)* **1970**, *169* (3950), 1042-9.
95. Speir, J. A.; Abdel-Motal, U. M.; Jondal, M.; Wilson, I. A., Crystal structure of an MHC class I presented glycopeptide that generates carbohydrate-specific CTL. *Immunity* **1999**, *10* (1), 51-61.
96. Akache, B.; Weeratna, R. D.; Deora, A.; Thorn, J. M.; Champion, B.; Merson, J. R.; Davis, H. L.; McCluskie, M. J., Anti-IgE Qb-VLP Conjugate Vaccine Self-Adjuvants through Activation of TLR7. *Vaccines (Basel)* **2016**, *4* (1), 3-10.
97. Bachmann, M. F.; Jennings, G. T., Vaccine delivery: a matter of size, geometry, kinetics and molecular patterns. *Nat. Rev. Immunol.* **2010**, *10* (11), 787-96.
98. Roldao, A.; Mellado, M. C.; Castilho, L. R.; Carrondo, M. J.; Alves, P. M., Virus-like particles in vaccine development. *Expert Rev. Vaccines* **2010**, *9* (10), 1149-76.
99. Yin, Z.; Comellas-Aragones, M.; Chowdhury, S.; Bentley, P.; Kaczanowska, K.; Benmohamed, L.; Gildersleeve, J. C.; Finn, M. G.; Huang, X., Boosting immunity to small tumor-associated carbohydrates with bacteriophage qbeta capsids. *ACS Chem. Biol.* **2013**, *8* (6), 1253-62.
100. Wang, P.; Huo, C. X.; Lang, S.; Caution, K.; Nick, S. T.; Dubey, P.; Deora, R.; Huang, X., Chemical Synthesis and Immunological Evaluation of a Pentasaccharide Bearing Multiple Rare Sugars as a Potential Anti-pertussis Vaccine. *Angew. Chem. Int. Ed.* **2020**, *59* (16), 6451-6458.
101. Huo, C.-X.; Dhara, D.; Baliban, S. M.; Tahmasebi Nick, S.; Tan, Z.; Simon, R.; Misra, A. K.; Huang, X., Synthetic and immunological studies of Salmonella enteritidis O-antigen tetrasaccharides as potential anti-Salmonella vaccines. *Chem. Commun. (Cambridge, U. K.)* **2019**, *55* (31), 4519-4522.

102. Wang, L. X., Synthetic carbohydrate antigens for HIV vaccine design. *Curr. Opin. Chem. Biol.* **2013**, *17* (6), 997–1005.
103. Ni, J.; Song, H.; Wang, Y.; Stamatou, N. M.; Wang, L. X., Toward a carbohydrate-based HIV-1 vaccine: synthesis and immunological studies of oligomannose-containing glycoconjugates. *Bioconjug. Chem.* **2006**, *17* (2), 493-500.
104. Joyce, J. G.; Krauss, I. J.; Song, H. C.; Opalka, D. W.; Grimm, K. M.; Nahas, D. D.; Esser, M. T.; Hrin, R.; Feng, M.; Dudkin, V. Y.; Chastain, M.; Shiver, J. W.; Danishefsky, S. J., An oligosaccharide-based HIV-1 2G12 mimotope vaccine induces carbohydrate-specific antibodies that fail to neutralize HIV-1 virions. *Proc. Natl. Acad. Sci. U. S. A.* **2008**, *105* (41), 15684-9.
105. Astronomo, R. D.; Lee, H.-K.; Scanlan, C. N.; Pantophlet, R.; Huang, C.-Y.; Wilson, I. A.; Blixt, O.; Dwek, R. A.; Wong, C.-H.; Burton, D. R., A glycoconjugate antigen based on the recognition motif of a broadly neutralizing human immunodeficiency virus antibody, 2G12, is immunogenic but elicits antibodies unable to bind to the self glycans of gp120. *J. Virol.* **2008**, *82* (13), 6359-6368.
106. Astronomo, R. D.; Kaltgrad, E.; Udit, A. K.; Wang, S. K.; Doores, K. J.; Huang, C. Y.; Pantophlet, R.; Paulson, J. C.; Wong, C. H.; Finn, M. G.; Burton, D. R., Defining criteria for oligomannose immunogens for HIV using icosahedral virus capsid scaffolds. *Chem. Biol.* **2010**, *17* (4), 357-70.
107. Nguyen, D. N.; Redman, R. L.; Horiya, S.; Bailey, J. K.; Xu, B.; Stanfield, R. L.; Temme, J. S.; La Branche, C. C.; Wang, S.; Rodal, A. A.; Montefiori, D. C.; Wilson, I. A.; Krauss, I. J., The Impact of Sustained Immunization Regimens on the Antibody Response to Oligomannose Glycans. *ACS Chem. Biol.* **2020**, *15* (3), 789-798.
108. Nguyen, D. N.; Xu, B.; Stanfield, R. L.; Bailey, J. K.; Horiya, S.; Temme, J. S.; Leon, D. R.; La Branche, C. C.; Montefiori, D. C.; Costello, C. E.; Wilson, I. A.; Krauss, I. J., Oligomannose Glycopeptide Conjugates Elicit Antibodies Targeting the Glycan Core Rather than Its Extremities. *ACS Cent. Sci.* **2019**, *5* (2), 237-249.
109. Cai, H.; Orwenyo, J.; Giddens, J. P.; Yang, Q.; Zhang, R.; LaBranche, C. C.; Montefiori, D. C.; Wang, L. X., Synthetic Three-Component HIV-1 V3 Glycopeptide Immunogens Induce Glycan-Dependent Antibody Responses. *Cell Chem. Biol.* **2017**, *24* (12), 1513-1522 e4.
110. Cai, H.; Orwenyo, J.; Guenaga, J.; Giddens, J.; Toonstra, C.; Wyatt, R. T.; Wang, L. X., Synthetic multivalent V3 glycopeptides display enhanced recognition by glycan-dependent HIV-1 broadly neutralizing antibodies. *Chem. Commun. (Camb)* **2017**, *53* (39), 5453-5456.
111. Cai, H.; Zhang, R.; Orwenyo, J.; Giddens, J.; Yang, Q.; LaBranche, C. C.; Montefiori, D. C.; Wang, L. X., Multivalent Antigen Presentation Enhances the Immunogenicity of a Synthetic Three-Component HIV-1 V3 Glycopeptide Vaccine. *ACS Cent. Sci.* **2018**, *4* (5), 582-589.
112. Cai, H.; Zhang, R. S.; Orwenyo, J.; Giddens, J.; Yang, Q.; LaBranche, C. C.; Montefiori, D. C.; Wang, L. X., Synthetic HIV V3 Glycopeptide Immunogen Carrying a N334 N-Glycan Induces Glycan-Dependent Antibodies with Promiscuous Site Recognition. *J. Med. Chem.* **2018**, *61* (22), 10116-10125.
113. Shivatare, S. S.; Cheng, T. R.; Cheng, Y. Y.; Shivatare, V. S.; Tsai, T. I.; Chuang, H. Y.; Wu, C. Y.; Wong, C. H., Immunogenicity Evaluation of N-Glycans Recognized by HIV Broadly Neutralizing Antibodies. *ACS Chem. Biol.* **2021**, *16* (10), 2016-2025.

114. Seko, A.; Koketsu, M.; Nishizono, M.; Enoki, Y.; Ibrahim, H. R.; Juneja, L. R.; Kim, M.; Yamamoto, T., Occurrence of a sialylglycopeptide and free sialylglycans in hen's egg yolk. *Biochim. Biophys. Acta* **1997**, *1335* (1-2), 23-32.
115. Sun, B.; Bao, W.; Tian, X.; Li, M.; Liu, H.; Dong, J.; Huang, W., A simplified procedure for gram-scale production of sialylglycopeptide (SGP) from egg yolks and subsequent semi-synthesis of Man3GlcNAc oxazoline. *Carbohydr. Res.* **2014**, *396*, 62-9.
116. Liu, L.; Prudden, A. R.; Bosman, G. P.; Boons, G. J., Improved isolation and characterization procedure of sialylglycopeptide from egg yolk powder. *Carbohydr. Res.* **2017**, *452*, 122-128.
117. Wang, L. X.; Ni, J.; Singh, S.; Li, H., Binding of high-mannose-type oligosaccharides and synthetic oligomannose clusters to human antibody 2G12: implications for HIV-1 vaccine design. *Chem. Biol.* **2004**, *11* (1), 127-34.
118. Toonstra, C.; Wu, L.; Li, C.; Wang, D.; Wang, L.-X., Top-Down Chemoenzymatic Approach to Synthesizing Diverse High-Mannose N-Glycans and Related Neoglycoproteins for Carbohydrate Microarray Analysis. *Bioconjugate Chem.* **2018**, *29* (6), 1911-1921.
119. Zong, G.; Toonstra, C.; Yang, Q.; Zhang, R.; Wang, L. X., Chemoenzymatic Synthesis and Antibody Binding of HIV-1 V1/V2 Glycopeptide-Bacteriophage Qbeta Conjugates as a Vaccine Candidate. *Int. J. Mol. Sci.* **2021**, *22* (22), 12538-50.
120. Hong, V.; Presolski, S. I.; Ma, C.; Finn, M. G., Analysis and optimization of copper-catalyzed azide-alkyne cycloaddition for bioconjugation. *Angew. Chem. Int. Ed.* **2009**, *48* (52), 9879-83.
121. Trattnig, N.; Mayrhofer, P.; Kunert, R.; Mach, L.; Pantophlet, R.; Kosma, P., Comparative Antigenicity of Thiourea and Adipic Amide Linked Neoglycoconjugates Containing Modified Oligomannose Epitopes for the Carbohydrate-Specific anti-HIV Antibody 2G12. *Bioconjugate Chem.* **2019**, *30* (1), 70-82.
122. Lubbers, J.; Rodriguez, E.; van Kooyk, Y., Modulation of Immune Tolerance via Siglec-Sialic Acid Interactions. *Front. Immunol.* **2018**, *9*, 2807-19.
123. Buskas, T.; Li, Y.; Boons, G.-J., The immunogenicity of the tumor-associated antigen Lewisy may be suppressed by a bifunctional cross-linker required for coupling to a carrier protein. *Chem. - Eur. J.* **2004**, *10* (14), 3517-3524.
124. Yin, Z.; Chowdhury, S.; McKay, C.; Baniel, C.; Wright, W. S.; Bentley, P.; Kaczanowska, K.; Gildersleeve, J. C.; Finn, M. G.; BenMohamed, L.; Huang, X., Significant impact of immunogen design on the diversity of antibodies generated by carbohydrate-based anticancer vaccine. *ACS Chem. Biol.* **2015**, *10* (10), 2364-2372.
125. Morelli, L.; Cancogni, D.; Tontini, M.; Nilo, A.; Filippini, S.; Costantino, P.; Romano, M. R.; Berti, F.; Adamo, R.; Lay, L., Synthesis and immunological evaluation of protein conjugates of *Neisseria meningitidis* X capsular polysaccharide fragments. *Beilstein J. Org. Chem.* **2014**, *10*, 2367-2376, 10 pp.
126. Palitzsch, B.; Gaidzik, N.; Hartmann, S.; Kunz, H.; Stergiou, N.; Gerlitzki, B.; Schmitt, E.; Stahn, S.; Teusch, N.; Flemming, P., A Synthetic Glycopeptide Vaccine for the Induction of a Monoclonal Antibody that Differentiates between Normal and Tumor Mammary Cells and Enables the Diagnosis of Human Pancreatic Cancer. *Angew. Chem. Int. Ed.* **2016**, *55* (8), 2894-8.
127. Higuchi, Y.; Eshima, Y.; Huang, Y.; Kinoshita, T.; Sumiyoshi, W.; Nakakita, S. I.; Takegawa, K., Highly efficient transglycosylation of sialo-complex-type oligosaccharide using

- Coprinopsis cinerea endoglycosidase and sugar oxazoline. *Biotechnol. Lett.* **2017**, *39* (1), 157-162.
128. Liu, C. C.; Huo, C. X.; Zhai, C.; Zheng, X. J.; Xiong, D. C.; Ye, X. S., Synthesis and Immunological Evaluation of Pentamannose-Based HIV-1 Vaccine Candidates. *Bioconjugate Chem.* **2022**, *33* (5), 807-20.
129. Toonstra, C.; Wu, L.; Li, C.; Wang, D.; Wang, L. X., Top-Down Chemoenzymatic Approach to Synthesizing Diverse High-Mannose N-Glycans and Related Neoglycoproteins for Carbohydrate Microarray Analysis. *Bioconjugate Chem.* **2018**, *29* (6), 1911-1921.
130. Mishra, N. K.; Krishna Deepak, R. N.; Sankararamkrishnan, R.; Verma, S., Controlling in Vitro Insulin Amyloidosis with Stable Peptide Conjugates: A Combined Experimental and Computational Study. *J. Phys. Chem. B* **2015**, *119* (50), 15395-406.
131. Horatscheck, A.; Wagner, S.; Ortwein, J.; Kim, B. G.; Lisurek, M.; Beligny, S.; Schutz, A.; Rademann, J., Benzoylphosphonate-based photoactive phosphopeptide mimetics for modulation of protein tyrosine phosphatases and highly specific labeling of SH2 domains. *Angew. Chem. Int. Ed. Engl.* **2012**, *51* (37), 9441-7.
132. Kajihara, Y.; Suzuki, Y.; Yamamoto, N.; Sasaki, K.; Sakakibara, T.; Juneja, L. R., Prompt chemoenzymatic synthesis of diverse complex-type oligosaccharides and its application to the solid-phase synthesis of a glycopeptide with Asn-linked sialyl-undeca- and asialo-nonasaccharides. *Chemistry* **2004**, *10* (4), 971-85.
133. Pancera, M.; Shahzad-UI-Hussan, S.; Doria-Rose, N. A.; McLellan, J. S.; Bailer, R. T.; Dai, K.; Loesgen, S.; Louder, M. K.; Staupe, R. P.; Yang, Y.; Zhang, B.; Parks, R.; Eudailey, J.; Lloyd, K. E.; Blinn, J.; Alam, S. M.; Haynes, B. F.; Amin, M. N.; Wang, L. X.; Burton, D. R.; Koff, W. C.; Nabel, G. J.; Mascola, J. R.; Bewley, C. A.; Kwong, P. D., Structural basis for diverse N-glycan recognition by HIV-1-neutralizing V1-V2-directed antibody PG16. *Nat. Struct. Mol. Biol.* **2013**, *20* (7), 804-13.
134. Shahzad-UI-Hussan, S.; Sastry, M.; Lemmin, T.; Soto, C.; Loesgen, S.; Scott, D. A.; Davison, J. R.; Lohith, K.; O'Connor, R.; Kwong, P. D.; Bewley, C. A., Insights from NMR Spectroscopy into the Conformational Properties of Man-9 and Its Recognition by Two HIV Binding Proteins. *Chembiochem* **2017**, *18* (8), 764-771.
135. Tanaka, T.; Nagai, H.; Noguchi, M.; Kobayashi, A.; Shoda, S., One-step conversion of unprotected sugars to beta-glycosyl azides using 2-chloroimidazolium salt in aqueous solution. *Chem. Commun. (Camb)* **2009**, (23), 3378-9.
136. Bejugam, M.; Flitsch, S. L., An efficient synthetic route to glycoamino acid building blocks for glycopeptide synthesis. *Org. Lett.* **2004**, *6* (22), 4001-4.
137. Fiedler, J. D.; Brown, S. D.; Lau, J. L.; Finn, M. G., RNA-directed packaging of enzymes within virus-like particles. *Angew. Chem. Int. Ed.* **2010**, *49* (50), 9648-51.
138. Xia, L.; Gildersleeve, J. C., The Glycan Array Platform as a Tool to Identify Carbohydrate Antigens. *Methods Mol. Biol.* **2015**, *1331*, 27-40.
139. Campbell, C. T.; Zhang, Y.; Gildersleeve, J. C., Construction and use of glycan microarrays. *Curr. Protoc. Chem. Biol.* **2010**, *2* (1), 37-53.
140. Donahue, T. C.; Zong, G.; Ou, C.; DeShong, P.; Wang, L. X., Catanionic Vesicles as a Facile Scaffold to Display Natural N-Glycan Ligands for Probing Multivalent Carbohydrate-Lectin Interactions. *Bioconjugate Chem.* **2023**, *34* (2), 392-404.
141. Varki, A., Biological roles of glycans. *Glycobiology* **2017**, *27* (1), 3-49.
142. Lee, Y. C.; Lee, R. T., Carbohydrate-protein interactions: Basis of glycobiology. *Acc. Chem. Res.* **1995**, *28*, 321-327.

143. Lundquist, J. J.; Toone, E. J., The cluster glycoside effect. *Chem. Rev.* **2002**, *102* (2), 555-78.
144. Lindhorst, T. K., Artificial multivalent sugar ligands to understand and manipulate carbohydrate-protein interactions. *Topics in Current Chemistry* **2002**, *218*, 200-235.
145. Chabre, Y. M.; Roy, R., Design and creativity in synthesis of multivalent neoglycoconjugates. *Adv. Carbohydr. Chem. Biochem.* **2010**, *63*, 165-393.
146. Adak, A. K.; Lin, H. J.; Lin, C. C., Multivalent glycosylated nanoparticles for studying carbohydrate-protein interactions. *Org. Biomol. Chem.* **2014**, *12* (30), 5563-73.
147. Wittmann, V.; Pieters, R. J., Bridging lectin binding sites by multivalent carbohydrates. *Chem. Soc. Rev.* **2013**, *42* (10), 4492-503.
148. Lindhorst, T. K.; Dubber, M., Octopus glycosides: multivalent molecular platforms for testing carbohydrate recognition and bacterial adhesion. *Carbohydr. Res.* **2015**, *403*, 90-7.
149. Ennist, J. H.; Termuehlen, H. R.; Bernhard, S. P.; Fricke, M. S.; Cloninger, M. J., Chemoenzymatic Synthesis of Galectin Binding Glycopolymers. *Bioconjugate Chem.* **2018**, *29* (12), 4030-4039.
150. Lu, W.; Pieters, R. J., Carbohydrate-protein interactions and multivalency: implications for the inhibition of influenza A virus infections. *Expert Opin. Drug Discov.* **2019**, *14* (4), 387-395.
151. Ramos-Soriano, J.; Ghirardello, M.; Galan, M. C., Carbon-based glyco-nanoplatforms: towards the next generation of glycan-based multivalent probes. *Chem. Soc. Rev.* **2022**, *51* (24), 9960-85.
152. Wang, H.; Huang, W.; Orwenyo, J.; Banerjee, A.; Vasta, G. R.; Wang, L. X., Design and synthesis of glycoprotein-based multivalent glyco-ligands for influenza hemagglutinin and human galectin-3. *Bioorg. Med. Chem.* **2013**, *21* (7), 2037-44.
153. Chen, W. C.; Completo, G. C.; Sigal, D. S.; Crocker, P. R.; Saven, A.; Paulson, J. C., In vivo targeting of B-cell lymphoma with glycan ligands of CD22. *Blood* **2010**, *115* (23), 4778-86.
154. Macauley, M. S.; Pfrengle, F.; Rademacher, C.; Nycholat, C. M.; Gale, A. J.; von Drygalski, A.; Paulson, J. C., Antigenic liposomes displaying CD22 ligands induce antigen-specific B cell apoptosis. *J. Clin. Invest.* **2013**, *123* (7), 3074-83.
155. Kaler, E. W.; Herrington, K. L.; Murthy, A. K.; Zasadzinski, J. A. N., Phase behavior and structures of mixtures of anionic and cationic surfactants. *J. Phys. Chem.* **1992**, *96* (16), 6698-707.
156. Chiruvolu, S.; Walker, S.; Israelachvili, J.; Schmitt, F. J.; Leckband, D.; Zasadzinski, J. A., Higher order self-assembly of vesicles by site-specific binding. *Science (Washington, DC, United States)* **1994**, *264* (5166), 1753-6.
157. Lee, J. H.; Gustin, J. P.; Chen, T.; Payne, G. F.; Raghavan, S. R., Vesicle--biopolymer gels: networks of surfactant vesicles connected by associating biopolymers. *Langmuir* **2005**, *21* (1), 26-33.
158. Park, J.; Rader, L. H.; Thomas, G. B.; Danoff, E. J.; English, D. S.; DeShong, P., Carbohydrate-functionalized catanionic surfactant vesicles: preparation and lectin-binding studies. *Soft Matter* **2008**, *4* (9), 1916-1921.
159. Thomas, G. B.; Rader, L. H.; Park, J.; Abezgauz, L.; Danino, D.; DeShong, P.; English, D. S., Carbohydrate modified catanionic vesicles: probing multivalent binding at the bilayer interface. *J. Am. Chem. Soc.* **2009**, *131* (15), 5471-7.

160. Richard, K.; Mann, B. J.; Stocker, L.; Barry, E. M.; Qin, A.; Cole, L. E.; Hurley, M. T.; Ernst, R. K.; Michalek, S. M.; Stein, D. C.; Deshong, P.; Vogel, S. N., Novel cationic surfactant vesicles protect against *Francisella tularensis* LVS and confer significant partial protection against *F. tularensis* Schu S4 strain. *Clin. Vaccine Immunol.* **2014**, *21* (2), 212-26.
161. Mahle, A.; Dashaputre, N.; DeShong, P.; Stein, D. C., Cationic Surfactant Vesicles as a New Platform for probing Glycan-Protein Interactions. *Adv. Funct. Mater.* **2018**, *28* (13), 1706215.
162. Masuko, T.; Minami, A.; Iwasaki, N.; Majima, T.; Nishimura, S.; Lee, Y. C., Carbohydrate analysis by a phenol-sulfuric acid method in microplate format. *Anal. Biochem.* **2005**, *339* (1), 69-72.
163. Eshima, Y.; Higuchi, Y.; Kinoshita, T.; Nakakita, S.; Takegawa, K., Transglycosylation Activity of Glycosynthase Mutants of Endo-beta-N-Acetylglucosaminidase from *Coprinopsis cinerea*. *PLoS one* **2015**, *10* (7), e0132859.
164. Gupta, D.; Oscarson, S.; Raju, T. S.; Stanley, P.; Toone, E. J.; Brewer, C. F., A comparison of the fine saccharide-binding specificity of *Dioclea grandiflora* lectin and concanavalin A. *Eur. J. Biochem.* **1996**, *242* (2), 320-6.
165. Gestwicki, J. E.; Cairo, C. W.; Strong, L. E.; Oetjen, K. A.; Kiessling, L. L., Influencing receptor-ligand binding mechanisms with multivalent ligand architecture. *J. Am. Chem. Soc.* **2002**, *124* (50), 14922-33.
166. Jang, H.; Lee, D. H.; Kang, H. G.; Lee, S. J., Concanavalin A targeting N-linked glycans in spike proteins influence viral interactions. *Dalton Trans.* **2020**, *49* (39), 13538-13543.
167. Smith, D. F.; Song, X.; Cummings, R. D., Use of glycan microarrays to explore specificity of glycan-binding proteins. *Methods Enzymol.* **2010**, *480*, 417-44.
168. Wang, M.; Zhu, J.; Lubman, D. M.; Gao, C., Aberrant glycosylation and cancer biomarker discovery: a promising and thorny journey. *Clin. Chem. Lab. Med.* **2019**, *57* (4), 407-416.
169. Zhang, H.; Laaf, D.; Elling, L.; Pieters, R. J., Thiodigalactoside-Bovine Serum Albumin Conjugates as High-Potency Inhibitors of Galectin-3: An Outstanding Example of Multivalent Presentation of Small Molecule Inhibitors. *Bioconjugate Chem.* **2018**, *29* (4), 1266-1275.
170. Bocker, S.; Laaf, D.; Elling, L., Galectin Binding to Neo-Glycoproteins: LacDiNAc Conjugated BSA as Ligand for Human Galectin-3. *Biomolecules* **2015**, *5* (3), 1671-96.
171. Filipova, M.; Bojarova, P.; Rodrigues Tavares, M.; Bumba, L.; Elling, L.; Chytil, P.; Gunar, K.; Kren, V.; Etrych, T.; Janouskova, O., Glycopolymers for Efficient Inhibition of Galectin-3: In Vitro Proof of Efficacy Using Suppression of T Lymphocyte Apoptosis and Tumor Cell Migration. *Biomacromolecules* **2020**, *21* (8), 3122-3133.
172. Seetharaman, J.; Kanigsberg, A.; Slaaby, R.; Leffler, H.; Barondes, S. H.; Rini, J. M., X-ray crystal structure of the human galectin-3 carbohydrate recognition domain at 2.1-Å resolution. *J. Biol. Chem.* **1998**, *273* (21), 13047-52.
173. Gordon-Alonso, M.; Hirsch, T.; Wildmann, C.; van der Bruggen, P., Galectin-3 captures interferon-gamma in the tumor matrix reducing chemokine gradient production and T-cell tumor infiltration. *Nat. Commun.* **2017**, *8* (1), 793-807.
174. Cao, L.; Diedrich, J. K.; Kulp, D. W.; Pauthner, M.; He, L.; Park, S. R.; Sok, D.; Su, C. Y.; Delahunty, C. M.; Menis, S.; Andrabi, R.; Guenaga, J.; Georgeson, E.; Kubitz, M.; Adachi, Y.; Burton, D. R.; Schief, W. R.; Yates III, J. R.; Paulson, J. C., Global site-specific N-glycosylation analysis of HIV envelope glycoprotein. *Nat. Commun.* **2017**, *8*, 14954-66.

175. Horan, N.; Yan, L.; Isobe, H.; Whitesides, G. M.; Kahne, D., Nonstatistical binding of a protein to clustered carbohydrates. *Proc. Natl. Acad. Sci. U. S. A.* **1999**, *96* (21), 11782-6.
176. Gomez-Garcia, M.; Benito, J. M.; Butera, A. P.; Ortiz Mellet, C.; Garcia Fernandez, J. M.; Jimenez Blanco, J. L., Probing carbohydrate-lectin recognition in heterogeneous environments with monodisperse cyclodextrin-based glycoclusters. *J. Org. Chem.* **2012**, *77* (3), 1273-88.
177. Liang, C. H.; Wang, S. K.; Lin, C. W.; Wang, C. C.; Wong, C. H.; Wu, C. Y., Effects of neighboring glycans on antibody-carbohydrate interaction. *Angew. Chem. Int. Ed.* **2011**, *50* (7), 1608-12.
178. Shahid, S.; Hasan, I.; Ahmad, F.; Hassan, M. I.; Islam, A., Carbohydrate-Based Macromolecular Crowding-Induced Stabilization of Proteins: Towards Understanding the Significance of the Size of the Crowder. *Biomolecules* **2019**, *9* (9), 477-99.
179. Wawrzinek, R.; Wamhoff, E. C.; Lefebvre, J.; Rentzsch, M.; Bachem, G.; Domeniconi, G.; Schulze, J.; Fuchsberger, F. F.; Zhang, H.; Modenutti, C.; Schnirch, L.; Marti, M. A.; Schwardt, O.; Brautigam, M.; Guberman, M.; Hauck, D.; Seeberger, P. H.; Seitz, O.; Titz, A.; Ernst, B.; Rademacher, C., A Remote Secondary Binding Pocket Promotes Heteromultivalent Targeting of DC-SIGN. *J. Am. Chem. Soc.* **2021**, *143* (45), 18977-88.
180. Shivatare, S. S.; Chang, S. H.; Tsai, T. I.; Tseng, S. Y.; Shivatare, V. S.; Lin, Y. S.; Cheng, Y. Y.; Ren, C. T.; Lee, C. C.; Pawar, S.; Tsai, C. S.; Shih, H. W.; Zeng, Y. F.; Liang, C. H.; Kwong, P. D.; Burton, D. R.; Wu, C. Y.; Wong, C. H., Modular synthesis of N-glycans and arrays for the hetero-ligand binding analysis of HIV antibodies. *Nat. Chem.* **2016**, *8* (4), 338-46.
181. Honigfort, D. J.; Altman, M. O.; Gagneux, P.; Godula, K., Glycocalyx crowding with mucin mimetics strengthens binding of soluble and virus-associated lectins to host cell glycan receptors. *Proc. Natl. Acad. Sci. U. S. A.* **2021**, *118* (40), e2107896118.
182. Cozzoli, L.; Gjonaj, L.; Stuart, M. C. A.; Poolman, B.; Roelfes, G., Responsive DNA G-quadruplex micelles. *Chem. Commun. (Camb)* **2018**, *54* (3), 260-263.
183. Kajihara, Y.; Suzuki, Y.; Yamamoto, N.; Sasaki, K.; Sakakibara, T.; Juneja, L. R., Prompt chemoenzymatic synthesis of diverse complex-type oligosaccharides and its application to the solid-phase synthesis of a glycopeptide with Asn-linked sialyl-undeca- and asialo-nonasaccharides. *Chem. Eur. J.* **2004**, *10* (4), 971-85.
184. Pancera, M.; Shahzad-ul-Hussan, S.; Doria-Rose, N. A.; McLellan, J. S.; Bailer, R. T.; Dai, K.; Loesgen, S.; Louder, M. K.; Staupe, R. P.; Yang, Y.; Zhang, B.; Parks, R.; Eudailey, J.; Lloyd, K. E.; Blinn, J.; Alam, S. M.; Haynes, B. F.; Amin, M. N.; Wang, L.-X.; Burton, D. R.; Koff, W. C.; Nabel, G. J.; Mascola, J. R.; Bewley, C. A.; Kwong, P. D., Structural basis for diverse N-glycan recognition by HIV-1-neutralizing V1-V2-directed antibody PG16. *Nat. Struct. Mol. Biol.* **2013**, *20* (7), 804-813.
185. Donahue, T. C.; Ou, C.; Yang, Q.; Flinko, R.; Zhang, X.; Zong, G.; Lewis, G. K.; Wang, L. X., Synthetic Site-Specific Antibody-Ligand Conjugates Promote Asialoglycoprotein Receptor-Mediated Degradation of Extracellular Human PCSK9. *ACS Chem. Biol.* **2023**.
186. Ciechanover, A., Proteolysis: from the lysosome to ubiquitin and the proteasome. *Nat. Rev. Mol. Cell Biol.* **2005**, *6* (1), 79-87.
187. Mahmoud, S. A.; Chien, P., Regulated Proteolysis in Bacteria. *Annu. Rev. Biochem.* **2018**, *87*, 677-696.
188. Rousseau, A.; Bertolotti, A., Regulation of proteasome assembly and activity in health and disease. *Nat. Rev. Mol. Cell Biol.* **2018**, *19* (11), 697-712.

189. Sakamoto, K. M.; Kim, K. B.; Kumagai, A.; Mercurio, F.; Crews, C. M.; Deshaies, R. J., Protacs: chimeric molecules that target proteins to the Skp1-Cullin-F box complex for ubiquitination and degradation. *Proc. Natl. Acad. Sci. U. S. A.* **2001**, *98* (15), 8554-9.
190. Banik, S. M.; Pedram, K.; Wisnovsky, S.; Ahn, G.; Riley, N. M.; Bertozzi, C. R., Lysosome-targeting chimaeras for degradation of extracellular proteins. *Nature* **2020**, *584* (7820), 291-297.
191. Takahashi, D.; Moriyama, J.; Nakamura, T.; Miki, E.; Takahashi, E.; Sato, A.; Akaike, T.; Itto-Nakama, K.; Arimoto, H., AUTACs: Cargo-Specific Degraders Using Selective Autophagy. *Mol. Cell* **2019**, *76* (5), 797-810 e10.
192. Naito, M.; Ohoka, N.; Shibata, N., SNIPERs-Hijacking IAP activity to induce protein degradation. *Drug Discov. Today Technol.* **2019**, *31*, 35-42.
193. Frere, G. A.; de Araujo, E. D.; Gunning, P. T., Emerging mechanisms of targeted protein degradation by molecular glues. *Methods Cell Biol.* **2022**, *169*, 1-26.
194. Morreale, F. E.; Kleine, S.; Leodolter, J.; Junker, S.; Hoi, D. M.; Ovchinnikov, S.; Okun, A.; Kley, J.; Kurzbauer, R.; Junk, L.; Guha, S.; Podlesainski, D.; Kazmaier, U.; Boehmelt, G.; Weinstabl, H.; Rumpel, K.; Schmiedel, V. M.; Hartl, M.; Haselbach, D.; Meinhart, A.; Kaiser, M.; Clausen, T., BacPROTACs mediate targeted protein degradation in bacteria. *Cell* **2022**, *185* (13), 2338-2353 e18.
195. Igawa, T.; Maeda, A.; Haraya, K.; Tachibana, T.; Iwayanagi, Y.; Mimoto, F.; Higuchi, Y.; Ishii, S.; Tamba, S.; Hironiwa, N.; Nagano, K.; Wakabayashi, T.; Tsunoda, H.; Hattori, K., Engineered monoclonal antibody with novel antigen-sweeping activity in vivo. *PLoS one* **2013**, *8* (5), e63236.
196. Vaccaro, C.; Zhou, J.; Ober, R. J.; Ward, E. S., Engineering the Fc region of immunoglobulin G to modulate in vivo antibody levels. *Nat. Biotechnol.* **2005**, *23* (10), 1283-8.
197. Ahn, G.; Banik, S. M.; Bertozzi, C. R., Degradation from the outside in: Targeting extracellular and membrane proteins for degradation through the endolysosomal pathway. *Cell Chem. Biol.* **2021**, *28* (7), 1072-1080.
198. Cotton, A. D.; Nguyen, D. P.; Gramespacher, J. A.; Seiple, I. B.; Wells, J. A., Development of Antibody-Based PROTACs for the Degradation of the Cell-Surface Immune Checkpoint Protein PD-L1. *J. Am. Chem. Soc.* **2021**, *143* (2), 593-598.
199. Caianiello, D. F.; Zhang, M.; Ray, J. D.; Howell, R. A.; Swartzel, J. C.; Branham, E. M. J.; Chirkin, E.; Sabbasani, V. R.; Gong, A. Z.; McDonald, D. M.; Muthusamy, V.; Spiegel, D. A., Bifunctional small molecules that mediate the degradation of extracellular proteins. *Nat. Chem. Biol.* **2021**, *17* (9), 947-953.
200. Ahn, G.; Banik, S. M.; Miller, C. L.; Riley, N. M.; Cochran, J. R.; Bertozzi, C. R., LYTACs that engage the asialoglycoprotein receptor for targeted protein degradation. *Nat. Chem. Biol.* **2021**, *17*, 937-946.
201. Zhou, Y.; Teng, P.; Montgomery, N. T.; Li, X.; Tang, W., Development of Triantennary N-Acetylgalactosamine Conjugates as Degraders for Extracellular Proteins. *ACS Cent. Sci.* **2021**, *7* (3), 499-506.
202. Zheng, J.; He, W.; Li, J.; Feng, X.; Li, Y.; Cheng, B.; Zhou, Y.; Li, M.; Liu, K.; Shao, X.; Zhang, J.; Li, H.; Chen, L.; Fang, L., Bifunctional Compounds as Molecular Degraders for Integrin-Facilitated Targeted Protein Degradation. *J. Am. Chem. Soc.* **2022**, *144* (48), 21831-21836.

203. Zhang, X.; Liu, H.; He, J.; Ou, C.; Donahue, T. C.; Muthana, M. M.; Su, L.; Wang, L. X., Site-Specific Chemoenzymatic Conjugation of High-Affinity M6P Glycan Ligands to Antibodies for Targeted Protein Degradation. *ACS Chem. Biol.* **2022**, *17* (11), 3013-23.
204. Lagace, T. A., PCSK9 and LDLR degradation: regulatory mechanisms in circulation and in cells. *Curr. Opin. Lipidol.* **2014**, *25* (5), 387-93.
205. Seidah, N. G.; Benjannet, S.; Wickham, L.; Marcinkiewicz, J.; Jasmin, S. B.; Stifani, S.; Basak, A.; Prat, A.; Chretien, M., The secretory proprotein convertase neural apoptosis-regulated convertase 1 (NARC-1): liver regeneration and neuronal differentiation. *Proc. Natl. Acad. Sci. U. S. A.* **2003**, *100* (3), 928-33.
206. Libby, P.; Tokgözoğlu, L., Chasing LDL cholesterol to the bottom — PCSK9 in perspective. *Nat. Cardiovas. Res.* **2022**, *1*, 554-61.
207. Abifadel, M.; Rabès, J. P.; Devillers, M.; Munnich, A.; Erlich, D.; Junien, C.; Varret, M.; Boileau, C., Mutations and polymorphisms in the proprotein convertase subtilisin kexin 9 (PCSK9) gene in cholesterol metabolism and disease. *Hum. Mutat.* **2009**, *30* (4), 520-9.
208. Abifadel, M.; Varret, M.; Rabès, J. P.; Allard, D.; Ouguerram, K.; Devillers, M.; Cruaud, C.; Benjannet, S.; Wickham, L.; Erlich, D.; Derré, A.; Villéger, L.; Farnier, M.; Beucler, I.; Bruckert, E.; Chambaz, J.; Chanu, B.; Lecerf, J. M.; Luc, G.; Moulin, P.; Weissenbach, J.; Prat, A.; Krempf, M.; Junien, C.; Seidah, N. G.; Boileau, C., Mutations in PCSK9 cause autosomal dominant hypercholesterolemia. *Nat. Genet.* **2003**, *34* (2), 154-6.
209. Cohen, J.; Pertsemlidis, A.; Kotowski, I. K.; Graham, R.; Garcia, C. K.; Hobbs, H. H., Low LDL cholesterol in individuals of African descent resulting from frequent nonsense mutations in PCSK9. *Nat. Genet.* **2005**, *37* (2), 161-5.
210. Cohen, J. C.; Boerwinkle, E.; Mosley, T. H., Jr.; Hobbs, H. H., Sequence variations in PCSK9, low LDL, and protection against coronary heart disease. *N. Engl. J. Med.* **2006**, *354* (12), 1264-72.
211. Rifai, M. A.; Ballantyne, C. M., PCSK9-targeted therapies: present and future approaches. *Nat. Rev. Cardiol.* **2021**, *18* (12), 805-806.
212. Chan, J. C.; Piper, D. E.; Cao, Q.; Liu, D.; King, C.; Wang, W.; Tang, J.; Liu, Q.; Higbee, J.; Xia, Z.; Di, Y.; Shetterly, S.; Arimura, Z.; Salomonis, H.; Romanow, W. G.; Thibault, S. T.; Zhang, R.; Cao, P.; Yang, X. P.; Yu, T.; Lu, M.; Retter, M. W.; Kwon, G.; Henne, K.; Pan, O.; Tsai, M. M.; Fuchslocher, B.; Yang, E.; Zhou, L.; Lee, K. J.; Daris, M.; Sheng, J.; Wang, Y.; Shen, W. D.; Yeh, W. C.; Emery, M.; Walker, N. P.; Shan, B.; Schwarz, M.; Jackson, S. M., A proprotein convertase subtilisin/kexin type 9 neutralizing antibody reduces serum cholesterol in mice and nonhuman primates. *Proc. Natl. Acad. Sci. U. S. A.* **2009**, *106* (24), 9820-5.
213. Robinson, J. G.; Farnier, M.; Kastelein, J. J. P.; Roth, E. M.; Taskinen, M. R.; Colhoun, H. M.; Brunet, A.; DiCioccio, A. T.; Lecorps, G.; Porady, R.; Baccara-Dinet, M. T.; Cannon, C. P., Relationship between alirocumab, PCSK9, and LDL-C levels in four phase 3 ODYSSEY trials using 75 and 150 mg doses. *J. Clin. Lipidol.* **2019**, *13* (6), 979-988 e10.
214. Zhang, L.; McCabe, T.; Condra, J. H.; Ni, Y. G.; Peterson, L. B.; Wang, W.; Strack, A. M.; Wang, F.; Pandit, S.; Hammond, H.; Wood, D.; Lewis, D.; Rosa, R.; Mendoza, V.; Cumiskey, A. M.; Johns, D. G.; Hansen, B. C.; Shen, X.; Geoghagen, N.; Jensen, K.; Zhu, L.; Wietecha, K.; Wisniewski, D.; Huang, L.; Zhao, J. Z.; Ernst, R.; Hampton, R.; Haytko, P.; Ansbros, F.; Chileski, S.; Chin, J.; Mitnau, L. J.; Pellacani, A.; Sparrow, C. P.; An, Z.; Strohl, W.; Hubbard, B.; Plump, A. S.; Blom, D.; Sitlani, A., An anti-PCSK9 antibody reduces

- LDL-cholesterol on top of a statin and suppresses hepatocyte SREBP-regulated genes. *Int. J. Biol. Sci.* **2012**, *8* (3), 310-27.
215. Kasichayanula, S.; Grover, A.; Emery, M. G.; Gibbs, M. A.; Somaratne, R.; Wasserman, S. M.; Gibbs, J. P., Clinical Pharmacokinetics and Pharmacodynamics of Evolocumab, a PCSK9 Inhibitor. *Clin. Pharmacokinet.* **2018**, *57* (7), 769-779.
216. Oleaga, C.; Shapiro, M. D.; Hay, J.; Mueller, P. A.; Miles, J.; Huang, C.; Friz, E.; Tavori, H.; Toth, P. P.; Wójcik, C.; Warden, B. A.; Purnell, J. Q.; Duell, P. B.; Pamir, N.; Fazio, S., Hepatic Sensing Loop Regulates PCSK9 Secretion in Response to Inhibitory Antibodies. *J. Am. Coll. Cardiol.* **2021**, *78* (14), 1437-1449.
217. Bagdanoff, J. T.; Smith, T. M.; Allan, M.; O'Donnell, P.; Nguyen, Z.; Moore, E. A.; Baird, J.; Wang, S.; Subramanian, V.; Tigani, B.; Nettleton, D. O.; Monovich, L. G.; Lewis, I.; Flyer, A. N.; Granda, B.; Blankenship, J. W.; Barnes-Seeman, D.; Clairmont, K. B., Clearance of plasma PCSK9 via the asialoglycoprotein receptor mediated by heterobifunctional ligands. *Cell Chem. Biol.* **2023**, *30* (1), 97-109 e9.
218. Ou, C.; Prabhu, S. K.; Zhang, X.; Zong, G.; Yang, Q.; Wang, L. X., Synthetic Antibody-Rhamnose Cluster Conjugates Show Potent Complement-Dependent Cell Killing by Recruiting Natural Antibodies. *Chemistry* **2022**, *28* (16), e202200146.
219. Zhang, X.; Ou, C.; Liu, H.; Wang, L. X., Synthesis and Evaluation of Three Azide-Modified Disaccharide Oxazolines as Enzyme Substrates for Single-Step Fc Glycan-Mediated Antibody-Drug Conjugation. *Bioconjugate Chem.* **2022**, *33* (6), 1179-1191.
220. Ochiai, H.; Huang, W.; Wang, L. X., Expeditious chemoenzymatic synthesis of homogeneous N-glycoproteins carrying defined oligosaccharide ligands. *J. Am. Chem. Soc.* **2008**, *130* (41), 13790-803.
221. Rice, K. G.; Weisz, O. A.; Barthel, T.; Lee, R. T.; Lee, Y. C., Defined geometry of binding between triantennary glycopeptide and the asialoglycoprotein receptor of rat hepatocytes. *J. Biol. Chem.* **1990**, *265* (30), 18429-34.
222. Park, E. I.; Mi, Y.; Unverzagt, C.; Gabius, H. J.; Baenziger, J. U., The asialoglycoprotein receptor clears glycoconjugates terminating with sialic acid alpha 2,6GalNAc. *Proc. Natl. Acad. Sci. U. S. A.* **2005**, *102* (47), 17125-9.
223. Donahue, T. C.; Zong, G.; O'Brien, N. A.; Ou, C.; Gildersleeve, J. C.; Wang, L. X., Synthesis and Immunological Study of N-Glycan-Bacteriophage Qbeta Conjugates Reveal Dominant Antibody Responses to the Conserved Chitobiose Core. *Bioconjugate Chem.* **2022**, *33* (7), 1350-1362.
224. Giddens, J. P.; Lomino, J. V.; Amin, M. N.; Wang, L.-X., Endo-F3 Glycosynthase Mutants Enable Chemoenzymatic Synthesis of Core-fucosylated Triantennary Complex Type Glycopeptides and Glycoproteins. *J. Biol. Chem.* **2016**, *291* (17), 9356-9370.
225. Prakash, T. P.; Graham, M. J.; Yu, J.; Carty, R.; Low, A.; Chappell, A.; Schmidt, K.; Zhao, C.; Aghajan, M.; Murray, H. F.; Riney, S.; Booten, S. L.; Murray, S. F.; Gaus, H.; Crosby, J.; Lima, W. F.; Guo, S.; Monia, B. P.; Swayze, E. E.; Seth, P. P., Targeted delivery of antisense oligonucleotides to hepatocytes using triantennary N-acetyl galactosamine improves potency 10-fold in mice. *Nucleic Acids Res.* **2014**, *42* (13), 8796-807.
226. Ou, C.; Li, C.; Zhang, R.; Yang, Q.; Zong, G.; Dai, Y.; Francis, R. L.; Bournazos, S.; Ravetch, J. V.; Wang, L. X., One-Pot Conversion of Free Sialoglycans to Functionalized Glycan Oxazolines and Efficient Synthesis of Homogeneous Antibody-Drug Conjugates through Site-Specific Chemoenzymatic Glycan Remodeling. *Bioconjug. Chem.* **2021**, *32* (8), 1888-1897.

227. Jonker, D. J.; O'Callaghan, C. J.; Karapetis, C. S.; Zalcborg, J. R.; Tu, D.; Au, H. J.; Berry, S. R.; Krahn, M.; Price, T.; Simes, R. J.; Tebbutt, N. C.; van Hazel, G.; Wierzbicki, R.; Langer, C.; Moore, M. J., Cetuximab for the treatment of colorectal cancer. *N. Engl. J. Med.* **2007**, *357* (20), 2040-8.
228. Miles, L. E.; Lipschitz, D. A.; Bieber, C. P.; Cook, J. D., Measurement of serum ferritin by a 2-site immunoradiometric assay. *Anal Biochem* **1974**, *61* (1), 209-24.
229. Ramanathan, A.; Gusarova, V.; Stahl, N.; Gurnett-Bander, A.; Kyrtasous, C. A., Alirocumab, a Therapeutic Human Antibody to PCSK9, Does Not Affect CD81 Levels or Hepatitis C Virus Entry and Replication into Hepatocytes. *PloS one* **2016**, *11* (4), e0154498.
230. Tveten, K.; Str, M. T.; Berge, K. E.; Leren, T. P., PCSK9-mediated degradation of the LDL receptor generates a 17 kDa C-terminal LDL receptor fragment. *J. Lipid Res.* **2013**, *54* (6), 1560-1566.
231. Poirier, S.; Mayer, G.; Benjannet, S.; Bergeron, E.; Marcinkiewicz, J.; Nassoury, N.; Mayer, H.; Nimpf, J.; Prat, A.; Seidah, N. G., The proprotein convertase PCSK9 induces the degradation of low density lipoprotein receptor (LDLR) and its closest family members VLDLR and ApoER2. *J. Biol. Chem.* **2008**, *283* (4), 2363-72.
232. Zhu, Z.; Ramakrishnan, B.; Li, J.; Wang, Y.; Feng, Y.; Prabakaran, P.; Colantonio, S.; Dyba, M. A.; Qasba, P. K.; Dimitrov, D. S., Site-specific antibody-drug conjugation through an engineered glycotransferase and a chemically reactive sugar. *MAbs* **2014**, *6* (5), 1190-200.
233. Gramespacher, J. A.; Cotton, A. D.; Burroughs, P. W. W.; Seiple, I. B.; Wells, J. A., Roadmap for Optimizing and Broadening Antibody-Based PROTACs for Degradation of Cell Surface Proteins. *ACS Chem. Biol.* **2022**, *17* (5), 1259-1268.
234. Feinberg, H.; Torgersen, D.; Drickamer, K.; Weis, W. I., Mechanism of pH-dependent N-acetylgalactosamine binding by a functional mimic of the hepatocyte asialoglycoprotein receptor. *J. Biol. Chem.* **2000**, *275* (45), 35176-84.
235. Kolatkar, A. R.; Leung, A. K.; Isecke, R.; Brossmer, R.; Drickamer, K.; Weis, W. I., Mechanism of N-acetylgalactosamine binding to a C-type animal lectin carbohydrate-recognition domain. *J. Biol. Chem.* **1998**, *273* (31), 19502-8.
236. Wragg, S.; Drickamer, K., Identification of amino acid residues that determine pH dependence of ligand binding to the asialoglycoprotein receptor during endocytosis. *J. Biol. Chem.* **1999**, *274* (50), 35400-6.
237. Meier, M.; Bider, M. D.; Malashkevich, V. N.; Spiess, M.; Burkhard, P., Crystal structure of the carbohydrate recognition domain of the H1 subunit of the asialoglycoprotein receptor. *J. Mol. Biol.* **2000**, *300* (4), 857-65.
238. Bianucci, A. M.; Chiellini, F., A 3D model for the human hepatic asialoglycoprotein receptor (ASGP-R). *J. Biomol. Struct. Dyn.* **2000**, *18* (3), 435-51.
239. Giddens, J. P.; Lomino, J. V.; Amin, M. N.; Wang, L. X., Endo-F3 Glycosynthase Mutants Enable Chemoenzymatic Synthesis of Core-fucosylated Triantennary Complex Type Glycopeptides and Glycoproteins. *J. Biol. Chem.* **2016**, *291* (17), 9356-70.
240. Ou, C.; Li, C.; Zhang, R.; Yang, Q.; Zong, G.; Dai, Y.; Francis, R. L.; Bournazos, S.; Ravetch, J. V.; Wang, L. X., One-Pot Conversion of Free Sialoglycans to Functionalized Glycan Oxazolines and Efficient Synthesis of Homogeneous Antibody-Drug Conjugates through Site-Specific Chemoenzymatic Glycan Remodeling. *Bioconjug Chem* **2021**, *32* (8), 1888-1897.
241. Green, E. D.; Adelt, G.; Baenziger, J. U.; Wilson, S.; Van Halbeek, H., The asparagine-linked oligosaccharides on bovine fetuin. Structural analysis of N-glycanase-released

- oligosaccharides by 500-megahertz <sup>1</sup>H NMR spectroscopy. *J. Biol. Chem.* **1988**, 263 (34), 18253-68.
242. Bendiak, B.; Harris-Brandts, M.; Michnick, S. W.; Carver, J. P.; Cumming, D. A., Separation of the complex asparagine-linked oligosaccharides of the glycoprotein fetuin and elucidation of three triantennary structures having sialic acids linked only to galactose residues. *Biochemistry* **1989**, 28 (15), 6491-9.
243. Sato, H.; Fukae, K.; Kajihara, Y., 2D selective-TOCSY-DQFCOSY and HSQC-TOCSY NMR experiments for assignment of a homogeneous asparagine-linked triantennary complex type undecasaccharide. *Carbohydr. Res.* **2008**, 343 (8), 1333-45.
244. Ahn, G.; Banik, S. M.; Miller, C. L.; Riley, N. M.; Cochran, J. R.; Bertozzi, C. R., LYTACs that engage the asialoglycoprotein receptor for targeted protein degradation. *Nat Chem Biol* **2021**, 17 (9), 937-946.
245. Bush, B. B.; Ernst, J. T.; Packard, G. K.; Lewis, J. G.; Turtle, E. D. ASGPR cell surface receptor binding compounds and conjugates. WO2022-US37227  
2023288033, 20220714, 2023.
246. Hou, F. S.; Xue, J.; Zhao, Y.; Miao, D. Triptolide conjugates and uses thereof. WO2021-US46802  
2022040487, 20210820, 2022.
247. Astronomo, R. D.; Burton, D. R., Carbohydrate vaccines: developing sweet solutions to sticky situations? *Nat. Rev. Drug Discov.* **2010**, 9 (4), 308-24.
248. Ritter, G.; Boosfeld, E.; Adluri, R.; Calves, M.; Oettgen, H. F.; Old, L. J.; Livingston, P., Antibody response to immunization with ganglioside GD3 and GD3 congeners (lactones, amide and gangliosidol) in patients with malignant melanoma. *Int. J. Cancer* **1991**, 48 (3), 379-85.
249. Krug, L. M.; Ragupathi, G.; Ng, K. K.; Hood, C.; Jennings, H. J.; Guo, Z.; Kris, M. G.; Miller, V.; Pizzo, B.; Tyson, L.; Baez, V.; Livingston, P. O., Vaccination of small cell lung cancer patients with polysialic acid or N-propionylated polysialic acid conjugated to keyhole limpet hemocyanin. *Clin. Cancer Res.* **2004**, 10 (3), 916-23.
250. Trkulja, C. L.; Jungholm, O.; Davidson, M.; Jardemark, K.; Marcus, M. M.; Hägglund, J.; Karlsson, A.; Karlsson, R.; Bruton, J.; Ivarsson, N.; Srinivasa, S. P.; Cavallin, A.; Svensson, P.; Jeffries, G. D. M.; Christakopoulou, M. N.; Reymer, A.; Ashok, A.; Willman, G.; Papadia, D.; Johnsson, E.; Orwar, O., Rational antibody design for undruggable targets using kinetically controlled biomolecular probes. *Sci. Adv.* **2021**, 7 (16), eabe6397.